UNITED STATES
DEPARTMENT OF
COMMERCE
PUBLICATION

SECTION A

JOURNAL OF RESEARCH

of the NATIONAL BUREAU OF STANDARDS

Volume 74A, Number 5 September - October 1970

Physics and Chemistry

U.S.
DEPARTMENT
OF
COMMERCE
National
Bureau of
Standards

UM

Journal of Research

of the

National Bureau of Standards

A. Physics and Chemistry

Sept.–Oct. • 1970

VOLUME • 74A

NUMBER • 5

Editor: C. W. Beckett

Associate Editor: D. D. Wagman

Publication dates:
Feb. 1, Apr. 1, June 1, Aug. 1, Oct. 1, Dec. 1, 1970

J. Res. Nat. Bur. Stand. (U.S.), A
CODEN: JNBAA 74A (5) 617–745 (1970)

JOURNAL OF RESEARCH

The National Bureau of Standards Journal of Research reports research and development in the fields of activity shown at right. Also included from time to time are survey articles on topics closely related to the Bureau's scientific and technical program.

The Journal is published in three separate sections as follows:

A. Physics and Chemistry

Contains papers of interest primarily to scientists working in these fields. Issued six times a year. Annual subscription: domestic, $9.50; foreign $11.75. Single copy, varies.

B. Mathematical Sciences

Presents studies and compilations designed mainly for the mathematician and the theoretical physicist. Issued quarterly. Annual subscription: domestic, $5.00; foreign, $6.25. Single copy, $1.25.

C. Engineering and Instrumentation

Reports research and development results of interest chiefly to the engineer and the applied scientist. Issued quarterly. Annual subscription: domestic, $5.00; foreign, $6.25. Single copy, $1.25.

U.S. DEPARTMENT OF COMMERCE
Maurice H. Stans, Secretary
NATIONAL BUREAU OF STANDARDS
Lewis M. Branscomb, Director

Order all publications from the Superintendent of Documents
U.S. Government Printing Office, Washington, D.C. 20402

Use of funds for printing this publication approved by the Director of the Bureau of the Budget (June 22, 1966).

KUM

JOURNAL OF RESEARCH of the National Bureau of Standards—A. Physics and Chemistry
Vol. 74A, No. 5, September–October 1970

Heat Capacity and Thermodynamic Properties of α-Beryllium Nitride, Be_3N_2, from 20 to 315 K*

George T. Furukawa and Martin L. Reilly

Institute for Basic Standards, National Bureau of Standards, Washington, D.C. 20234

(May 27, 1970)

The heat capacity of α-beryllium nitride, Be_3N_2, was determined from 20 to 315 K and the thermodynamic properties calculated from 0 to 315 K. The entropy at 298.15 K was found to be 34.4 ± 0.3 $J/K \cdot mol$ (8.23 ± 0.08 cal/K·mol). The precision using a calorimeter of a new design is shown to be ± 0.01 percent over most of the temperature range of the measurements.

Key words: α-beryllium nitride; calorimeter; entropy; heat capacity; specific heat; thermodynamic properties.

1. Introduction

The results of heat-capacity measurements of α-beryllium nitride, Be_3N_2, presented between 20 and 315 K in this paper have been obtained in connection with a research program at the National Bureau of Standards to provide thermodynamic data on light-element compounds. In connection with this program, the high-temperature enthalpy measurements have previously been reported by Douglas and Payne [1][1]. Earlier, Satoh [2] reported relative enthalpy measurements at three temperatures in the range 273 to 773 K on a sample of 98.13 weight percent purity, the impurities being 0.78, 0.87, and 0.22 percent BeO, Fe_2O_3, and SiO_2, respectively. Recently Justice [3] reported measurements in the range 25 to 310 K on a sample of 96.7 weight percent purity.

2. Apparatus and Method

The low-temperature heat-capacity measurements were made from about 20 to 315 K in an adiabatic calorimeter of a design similar in principle to that described previously [4]. Many design changes have been incorporated in calorimeters that have since been constructed. Although results of heat-capacity measurements obtained with them have been published, e.g., references [5, 6, 7, 8], no detailed descriptions of the calorimeters have been reported at their successive stages of development. Changes have been made to facilitate the assembly of the calorimeter, to achieve better temperature control of the electrical leads, and to improve the quality of automatic control of the adiabatic shield. In the design of the new calorimeter used for the measurements on beryllium nitride, a provision was made for the calibration, whenever required, of the resistance thermometer attached to the calorimeter vessel during the heat-capacity measurements. Thus, samples of a wide range of sizes and shapes can be investigated in the calorimeter provided that a resistance thermometer and a thermocouple can be attached in good thermal contact with the sample or the sample "holder." Although the new calorimeter is considered already "obsolete" in some respects, its description is given in this paper for purposes of a record of a stage in calorimeter development.

Figure 1 shows a schematic drawing of the calorimeter. Briefly, the double-walled sample vessel containing a resistance thermometer and heater is suspended in a vacuum space by means of a nylon cord. The vessel is thermally shielded from radiation by a thin gold-plated copper "jacket" maintained at the same temperature as the same vessel. The heat conduction along the electrical lead wires to the sample vessel is controlled separately at the "thermometer-heater lead control," which also contains the reference platinum resistance thermometer. The thermometer in the sample vessel is calibrated against the reference thermometer in the "thermometer-heater lead control," which is maintained at the same temperature as the sample vessel. For the measurements with beryllium nitride, on which the performance of the calorimeter was tested, a calibrated platinum resistance thermometer was incorporated in the sample vessel to test the "calibration method." The results of the "calibration" are given in section 2.5.1.

The calorimeter system was cooled by immersing in a suitable refrigerant as described previously [4] and shown schematically in figure 1.

*This work was supported by the Advanced Research Projects Agency, Department of Defense, under Order No. 20 and by the Air Force Office of Scientific Research, Office of Aerospace Research, United States Air Force under AFOSR Contract No. ISSA 68-0004.

[1] Figures in brackets indicate the literature references at the end of this paper.

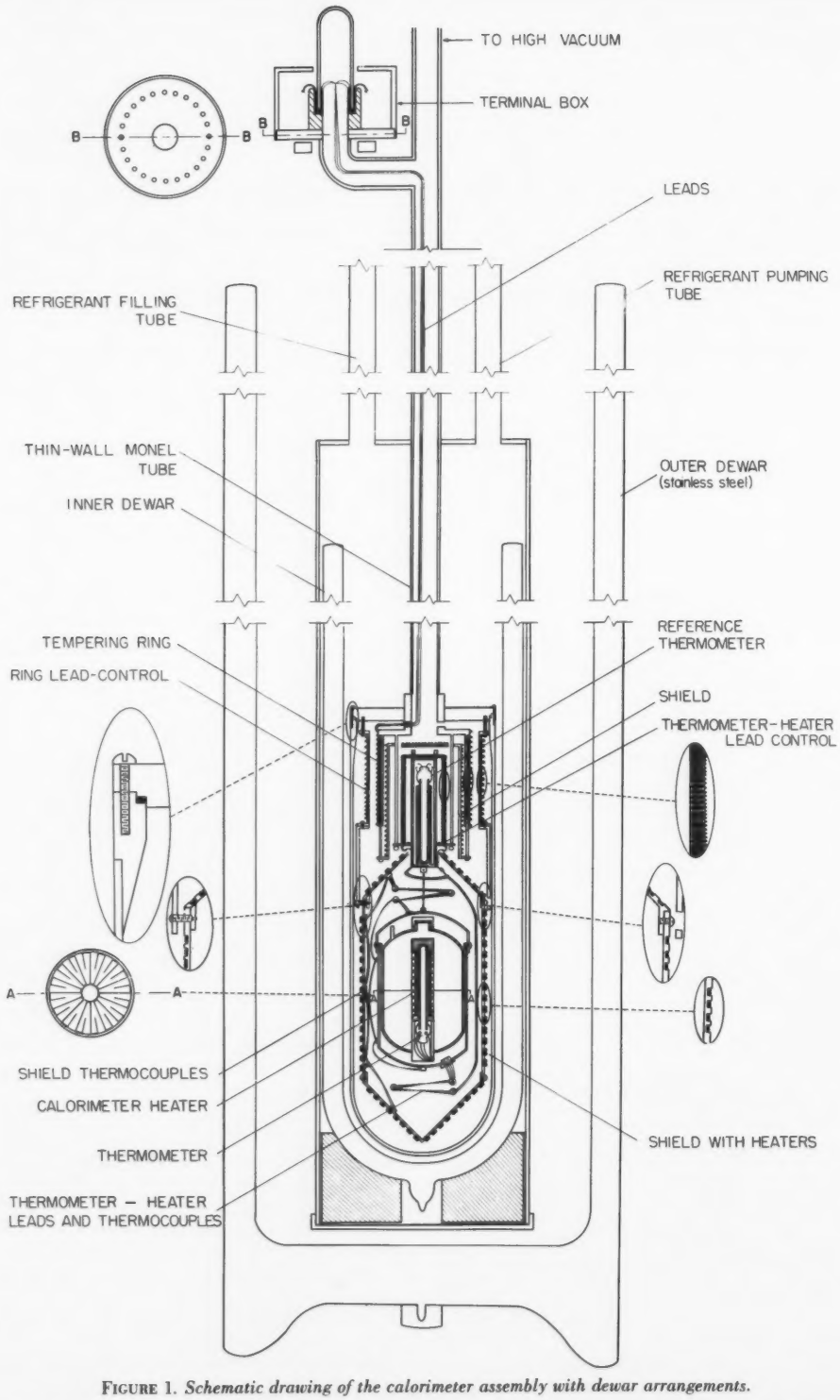

FIGURE 1. *Schematic drawing of the calorimeter assembly with dewar arrangements.*

The inner dewar system is employed with the following refrigerants: liquid hydrogen, pumped liquid or solid hydrogen, or pumped liquid or solid nitrogen.

Details of the calorimeter design and construction are described in the following sections. *Reference to trade names is made only for identification and simplification of description and does not imply in any way the endorsement of the products by the National Bureau of Standards.*

2.1. Cement

The adhesive used for cementing the wires and thermocouple assembly for thermal contact was exclusively Glyptal lacquer at full strength or diluted with xylene. After application, the lacquer was air dried at 130 °C for 6 hr.

2.2. Wires

2.2.1. Electric Lead Wires

The electric lead wires were all 0.160-mm-diam (AWG No. 34) copper, insulated with a heavy coating of Formvar enamel and double silk wrap. Before using the wire, a dilute solution of lacquer (1 part lacquer to 5 parts xylene) was applied to improve the bonding and abrasion resistance of the silk insulation. The outside diameter of the insulated wire was about 0.280 mm.

2.2.2. Thermocouple Wires

The thermocouple wires (0.127 mm diam) were constantan and Chromel-P insulated with double silk wrap. A dilute solution of lacquer was also applied to the wires to improve the bonding and abrasion resistance of the silk insulation.

Three methods were used to attach the thermocouples for sensing temperatures. In the first method, the two thermocouple wires were soldered to thin copper disks (5 mm diam × 0.051 mm thick) with a "clearance hole" at the center for a screw. The disks in turn were attached to temperature-sensing points ("threaded holes") with screws using thin mica disks (0.013 mm thick) for electrical insulation. A thin layer of lacquer was applied between the surfaces to improve the thermal contact. This method was used to sense the temperature on the "thermometer-heater lead control" and its shield, "ring lead control," and "tempering ring."

In the second method, the two thermocouple wires were soldered to thin copper strips (3 mm wide × 20 mm long × 0.051 mm thick). The strips were in turn cemented with lacquer to temperature-sensing points using thin mica sheets (0.013 mm thick) for electrical insulation. This method was used on the "thermometer-heater lead control" to sense its temperature relative to the sample vessel. The strips were arranged parallel to the axis and around the cylindrical surface of the "thermometer-heater lead control" and a double silk insulated copper wire (0.079 mm diam) was wound tightly over the strips to improve the thermal contact and mechanical strength. A dilute solution of lacquer (1 part lacquer to 3 parts xylene) was applied over the assembly.

FIGURE 2. *Calorimeter assembly with vacuum can and sample vessel removed.*

In the third method, the two thermocouple wires were soldered together and placed between two mica sheets (0.025 mm thick); then a gold-plated copper sheath (0.20 mm thick) was crimped over them. A thin layer of lacquer was applied between the layers before crimping the copper sheath. These sheathed thermocouples were used with rather broad "M-shaped" holders silver soldered on the radiation shield and on the sample vessel. (Figs. 2 and 3 show the sheathed thermocouples both before and after being wedged into the tightly sprung M-shaped holders). A very thin layer of stopcock grease was applied to the sheathed thermocouples used on the sample vessel to improve the thermal contact. The total mass of grease was less than 0.1 mg.

2.2.3. Heater Wires

Approximately 75 percent Ni–20 percent Cr alloy was used for the "calorimeter heater" because of its small change in resistance (less than 1 percent) over the temperature range of measurements [10]. The insulation on the wire was double glass-fiber wrap with silicone enamel as the binder. The heater resistance was 100 Ω.

The heater wires (0.160 mm diam) used for temperature control on the adiabatic shields and "electrical lead controls" were copper-nickel alloys insulated with double glass-fiber wrap with silicone enamel as binder. The outside diameter of the insulated wires

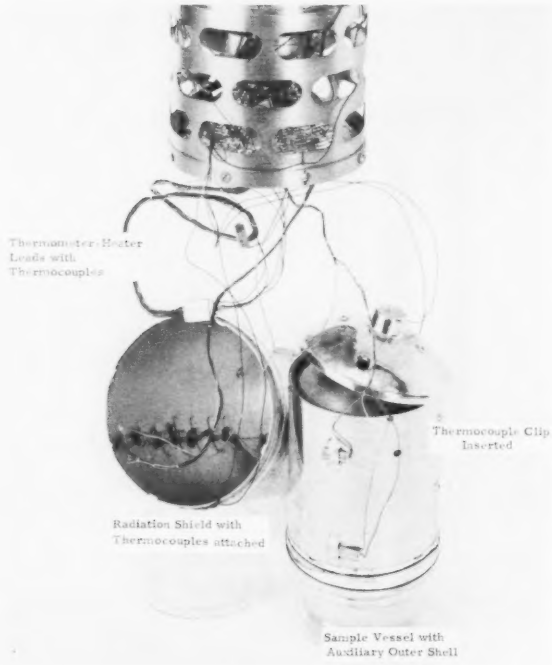

FIGURE 3. *Interior view of radiation shield for sample vessel and sample vessel with auxiliary outer shell.*

was about 0.340 mm. Alloy wires of different Cu-Ni compositions were selected to yield a total resistance of about 200 Ω for each of the control heaters.

2.3. Adiabatic Shields

The calorimeter sample vessel was "adiabatically shielded" by a combination of a radiation shield, a high vacuum (10^{-5} torr or better) to minimize gaseous heat conduction, and temperature control of electrical leads to the sample vessel. The temperature of the radiation shield surrounding the sample vessel was controlled independently from that of the electrical leads to the vessel. The details of the design used in the radiation shields and for the control of electrical lead temperature will be given separately.

2.3.1. Temperature Control and Tempering of Electrical Lead Wires

a. Temperature control of electrical lead wires. All electrical leads entered the calorimeter through the Apiezon W wax seal at the terminal box and traversed the length of the high vacuum pump-out tube. (See fig. 1.) The leads were then attached to the "tempering ring" and later attached to the "ring lead-control." After the "ring lead-control" the lead wires were attached to the "thermometer-heater lead-control." before going to the sample vessel. At each of the above locations some of the wires branched out to thermocouples and to heaters.

At the "tempering ring," the electrical leads were brought to the temperature of the refrigerant in which the calorimeter was immersed. At the "ring lead-control," the temperature of the leads was raised close to that of the "thermometer-heater lead control." At the "thermometer-heater lead control" the leads were maintained at the same temperature as that of the sample vessel.

b. Tempering of electric lead wires. The copper lead wires (0.280 mm diam including insulation) were tempered by individually cementing them with lacquer (full strength) into separate, tightly fitting grooves (0.254 mm wide × 0.254 mm deep) machined "along" the cylindrical copper surface parallel to its axis.[2] The heater wires were tightly wound (helically) over the copper wires and cemented. The "ring lead-control" and "thermometer-heater lead control" were wired in this manner. (See insert of fig. 1). On the "tempering ring," where heating was not needed, insulated copper wire was wound over the lead wires to improve the thermal contact and mechanical strength. A dilute solution of lacquer (1 part lacquer to 3 parts xylene) was applied over the wires.

2.3.2. Radiation Shields

a. *Shield for the calorimeter vessel.* This radiation shield was essentially a thin copper shell of 0.810 mm thickness consisting of three sections, a cylinder and two end cones (90°). Screws held the two cones to the cylinder. A thin film of grease was used between the surfaces that were in contact. For the heater wire, an evenly spaced groove (0.620 mm wide × 0.310 mm deep) was machined helically on the cylinder and "spirally" on the cones. The distribution of the heater wire grooves was made very nearly the same over the entire shield surface to yield even heating. The M-shaped thermocouple holders were silver-soldered on the inner surface of the shield. The shield was gold-plated.

A pair of heater wires was wound into the tightly fitting groove of the shield. The procedure for winding the heater wire was first to paint the groove with lacquer (full strength) and to press the wire pair into the groove before the lacquer dried. In the process the excess lacquer was pushed out. Additional lacquer (1 part lacquer to 3 parts xylene) was applied over the wire and copper shield. The heater wires on the cones and on the cylinder were connected in series.

The sheathed thermocouples for sensing the shield temperature relative to that of the sample vessel surface were inserted into the tightly fitting M-shaped holders. A thin layer of lacquer was applied to these surfaces to improve the thermal contact. (See figs. 1 and 3). Thermocouples were attached at five locations on the radiation shield: three on the cylindrical portion and one on each conical ends. The corresponding four locations on the sample vessel were: one at each end and two on the side.

[2] A blunt tool was run through the grooves to eliminate any machining "burrs" and to provide a very smooth surface for the insulated wires. To date after six years of use, no wire has become grounded or "shorted" to another one.

b. *Radiation shield for the "thermometer-heater lead control."* This shield was designed to be used only when the thermometer in the sample vessel is being calibrated relative to the reference thermometer installed in the "thermometer-heater lead control." During heat-capacity measurements no electric power is applied to the shield, i.e., the temperature of the shield is not controlled. When the thermometer is being calibrated, the shield and the "ring lead-control" are controlled to be at the same temperature as that of the "thermometer-heater lead control." Under such operating conditions no electric power is needed to maintain the "thermometer-heater lead control" at the same temperature as that of the sample vessel. As explained later, a more satisfactory thermometer calibration is achieved by avoiding the small fluctuations which would otherwise occur in the reference thermometer resistance with any change in the electrical power to the "thermometer-heater lead control." (See section 2.5.1.)

The radiation shield was a thin (0.810 mm thickness) copper cylinder with one end closed with a copper disk of the same thickness. The shield was gold plated and polished. There were no grooves on this shield.

The shield heater wire was wound helically, without overlapping, on the cylindrical portion of the shield using lacquer for cement. A flat heater was cemented on the flat end. The flat heater was prepared by spirally winding the heater wire, wet with lacquer, between two Teflon disks spaced at the thickness of the wire. The heater was removed from between the Teflon disks after drying and cemented to the shield.

2.3.3. Thermocouples

The number of constantan-Chromel-P thermocouple junctions in series between temperature control points was as follows:

a. between "ring lead-control" and "thermometer-heater lead control": 3;
b. between "thermometer-heater lead control" and sample vessel: 6;
c. between sample vessel and its radiation shield: 4;
d. between "thermometer-heater lead control" and its radiation shield: 3.

In addition to the above thermocouples, copper-constantan thermocouples were used to check the temperature of the "ring lead-control," the radiation shields, and the "thermometer-heater lead control" relative to that of the "tempering ring." To achieve temperature control the "tempering ring" was always colder than any of the other "points."

2.3.4. Temperature Control of the Adiabatic Shields

The temperatures of the "ring lead control," "thermometer-heater lead control," and the radiation shields were controlled by adjusting the electric current in the heater wires wound on them. An automatic control system combining electronic and electromechanical equipment was used in conjunction with the differential thermocouples to adjust the heater currents [11].

2.4. Sample Vessel

The cross-sectional views of the sample vessel are shown in figure 1. The vessel was essentially all copper construction with outer surfaces gold plated. The parts of the vessel were assembled with "silver solder." The inner container surface was covered with a thin layer of tin which served also to "solder" the vanes in place. The auxiliary outer thin copper shell served to achieve more reproducible surface temperatures between the vessel plus sample and empty vessel measurements. The thermometer and calorimeter heater were centrally located in a re-entrant well of the inner vessel.

The thermocouple junctions (six) for sensing the temperature difference between the sample vessel and the thermometer-heater leads were enclosed in a single large sheath and inserted in an M-shaped holder at the base of the auxiliary shell. A very thin film of stopcock grease was used to improve the thermal contact. The thermometer and heater leads were also enclosed in the same sheath. Thus, the thermocouples sensed the temperature of the "thermometer-heater lead control" relative to that of the electrical leads at the sample vessel where the thermocouple sheath was in thermal contact. One of the "voltage taps" for the calorimeter vessel heater was located in the thermocouple sheath and the other at the "thermometer-heater lead control." (See fig. 1.)

2.5. Measurement Instruments and Procedures

2.5.1. Temperature Measurements

The platinum resistance thermometers (laboratory designations: 1057849 in the sample vessel and 1066759 in the "thermometer-heater lead control") used in the measurements were calibrated in accordance with the International Practical Temperature Scale of 1968 [12]. The temperatures in T given in this paper are equivalent to the International Practical Kelvin Temperature Scale expressed as T_{68} in reference [12].

The measurements of thermometer resistance were made to the nearest 0.00001 Ω. Initially a manual Mueller bridge was used and later an automatic Mueller bridge. The resistance-time observations with the automatic Mueller bridge were obtained on punched cards and were analyzed by means of a computer to calculate the "initial" and "final" thermometer resistances associated with each experimental point. The observations with the manually operated bridge were processed by means of a desk calculator.

As mentioned previously in section 2, the thermometer calibration method was tested by intercomparing the temperature indications of the calibrated platinum resistance thermometers in the sample vessel and in the "thermometer-heater lead control." The calorimeter used in the measurements with beryllium nitride presented in this paper did not have the radiation shield for the "thermometer-heater lead control." (See sec. 2.3.2(b).) Hence, electric power

was introduced also during thermometer calibration into "thermometer-heater lead control" to maintain its temperature as close as possible to that of the sample vessel. Small temperature fluctuations (corresponding to about 0.2 or 0.5 mK) occurred in the "thermometer-heater lead control" from the control adjustments of the electric power, necessitating many rapid measurements to obtain a suitable average. The results of the "calibration" at a few selected temperatures are summarized in table 1. The maximum spread is 4 mK. The thermometer in the "thermometer-heater lead control" indicated more often higher temperatures than the thermometer in the sample vessel, but this deviation may be partially due to the difference in the temperature interpolation of the thermometers [9]. The degree of agreement in the temperature scale is satisfactory for heat-capacity measurements, particularly since the calibration data at many temperature points will be fitted by the method of least squares to equations in $R(T)$ and the temperature changes corresponding to the observed sample vessel thermometer resistances calculated from the equations.

TABLE 1. *Comparison of the temperatures of platinum resistance thermometers in the calorimeter sample vessel and the "thermometer-heater lead control" under adiabatic control*

Thermometer No. 1057849 in Calorimeter Sample Vessel	Thermometer No. 1066759 in "Thermometer-Heater Lead Control"	Temperature Difference No. 1057849–No. 1066759
T, K	*T*, K	*mK*
91.123	91.123	0
113.690	113.692	−2
137.255	137.258	−3
194.267	194.264	3
220.230	220.232	−2
251.932	251.930	2
267.055	267.059	−4
301.052	301.054	−2

In another calorimeter [21], identical in every respect to that used with beryllium nitride, a radiation shield was added around the "thermometer-heater lead control" to be used during thermometer calibration. When this radiation shield and the "ring lead-control" were controlled to be at the same temperature as that of the "thermometer-heater lead control," no electric power was needed to maintain the "thermometer-heater lead control" at the same temperature as that of the sample vessel. This added feature eliminated the small fluctuations in the "thermometer-heater lead control" that occurred with the control current adjustments. The calibration results obtained were comparable to those given in table 1, except that the measurements were more uniform and were obtainable more leisurely. Figure 1 shows the location of this auxiliary radiation shield and the calorimeter description given earlier in this paper includes this shield.

2.5.2. Electric Power and Time Interval Measurements

The calorimeter heater circuit employed was similar to that previously described [11]. The electrical energy, ΔQ, introduced into the calorimeter was determined from the product of the average calorimeter heater voltage, $\bar{e}$, the current, $\bar{\imath}$, and the time interval, τ, of electric power input:

$$\Delta Q = \bar{e}\bar{\imath}\tau. \tag{1}$$

The average $\bar{e}$ and $\bar{\imath}$ were obtained from a series of voltage observations made at equally spaced times during the heating period. A Wenner potentiometer in conjunction with a volt box, standard resistors, and saturated standard cells was used in the measurements. The standard resistors and the standard cells were calibrated at the National Bureau of Standards in terms of the national standards. A constant current supply, stable to about 2 parts per million (ppm), was the source of power for the calorimeter heater. By using the constant current supply in conjunction with the Ni-Cr alloy wire of low temperature-coefficient of resistance for the calorimeter heater, the heater voltage did not change during the heating period by more than 0.01 percent per minute over the entire temperature range of the heat-capacity measurements. Thus, the relatively slowly changing voltage was read quite conveniently, and with ease, to the five- to six-figure capability of the Wenner potentiometer.

The duration of each heating period τ was measured by means of a high-precision interval timer operated on the 60-Hz frequency standard provided at the National Bureau of Standards. The 60-Hz frequency standard is based on a 100-kHz quartz oscillator which is stable to 0.5 ppm. As a check, an electronic counter based on a thermostated 1-MHz quartz oscillator was used simultaneously in the measurement of the heating period. The electronic counter was checked periodically with a 100-kHz frequency standard wired into the laboratory. The estimated uncertainty in the determination of the heating interval was not greater than ± 0.01 s for any heating period, none of which was less than 2 min in these experiments.

3. Sample

The Be_3N_2 sample was specially prepared for the measurements by the Brush Beryllium Company, Cleveland, Ohio, by reacting pure nitrogen and beryllium powder at elevated temperatures and crushing the product to particle sizes between 20 and 50 mesh (0.8 and 0.3 mm sieve openings, respectively). The material received was thoroughly mixed in a controlled-atmosphere box containing dry argon (dew-point: − 70 °C) and samples were apportioned for chemical analysis, for the high-temperature relative enthalpy measurements [1], and for the low-temperature heat-capacity measurements described in this paper. The samples for the chemical analysis and the high-temperature enthalpy measurements were sealed in test tubes under dry argon. The sample that was poured into the low-temperature calorimeter

vessel weighed 97.415 g. The calorimeter vessel containing the sample was pumped at high vacuum and purged with dry helium gas several times and finally, helium gas at a pressure of 9300N/m² (70 torr) was sealed in the container with the sample.[3] After completion of the measurements, the calorimeter vessel was opened in the controlled-atmosphere box and the sample was divided and sealed in polyethylene bags for chemical analysis. The sealed polyethylene bags were placed individually in screwcap jars which were in turn placed in desiccators, the whole operation being done in the controlled-atmosphere box.

The results of spectrochemical analysis of the sample obtained by the NBS Spectrochemical Analysis Section are summarized in table 2. Only the impurity elements that were detected are listed. The results of the chemical analyses on the material obtained by the Microchemical Analysis Section of the Bureau before and after the calorimetric measurements are given in table 3. For the nitrogen and total beryllium analyses, about 0.3-g samples were first dissolved in dilute hydrochloric acid and the solution diluted to 250 cm³ in a volumetric flask. A 10-cm³ aliquot was analyzed for nitrogen using the Kjeldahl method, the ammonia being titrated with 0.01 *N* hydrochloric acid that had been standardized against ammonium dihydrogen phosphate by means of the Kjeldahl procedure. The total beryllium was determined by precipitating the beryllium hydroxide in a 10-cm³ aliquot with ammonium hydroxide. The beryllium hydroxide was filtered, ignited, and weighed as BeO. The free beryllium was determined by dissolving 2-g samples in hydrochloric acid. The hydrogen formed was dried, converted to water, and weighed. No analysis was made for beryllium carbide, Be_2C. The analysis for free beryllium would include Be_2C, which forms methane and then water under the conditions of the analysis. The apparently low free beryllium analysis indicates very little Be_2C, if any.

TABLE 2. *Summary of spectrochemical analysis of the sample of α-beryllium nitride,* Be_3N_2*—impurity elements that were detected*

Element	Wt %	Element	Wt %
Al	0.001−0.01	Mg	0.001−0.01
Ca	<0.001	Mn	<0.001
Cr	0.001−0.01	Ni	0.001−0.01
Cu	<0.001	Si	0.01 −0.1
Fe	0.01 −0.1	Ti	0.001−0.01

Analysis by Elizabeth K. Hubbard, NBS Spectrochemical Analysis Section

The analysis for water represents all forms of hydrogen present in the sample. Samples (20 mg) were heated at 1050 °C in a carbon-hydrogen-nitrogen analyzer and the amount of water driven off was determined. The oxygen was determined by a nondestructive 14-Mev neutron activation technique. Five determinations were made using 6-g samples.

[3] The pressure was observed in mm Hg and converted to mm Hg at 0°C and standard gravitational acceleration of 980.665 cm/s² for the processing of the data. The conversion to N/m² was made using the definition: normal atmosphere = 101,325 N/m² = 760 torr (mm Hg at 0 °C and standard gravity[13].

TABLE 3. *Chemical analysis of the sample of α-beryllium nitride,* Be_3N_2

Element	wt %	Element	wt %
Original Sample			
Be (total)	49.06	N	49.45
	49.09		49.52
			49.84
mean . . .	49.08	mean . . .	49.60
Be (free)	0.09		
	0.11	Cl	< 0.02
	0.09	F	< 0.01
mean . . .	0.10		
Sample Removed from Calorimeter Vessel			
Be (total)	48.72	N	48.97
	48.68		48.89
mean . . .	48.70	mean . . .	48.93
Be (free)	0.04	H_2O	1.16
	0.04		1.12
mean . . .	0.04	mean . . .	1.14
O	2.38 (average of 5 determinations)		

Chemical analysis by R. A. Paulson, NBS Microchemical Analysis Section

Oxygen analysis by activation method, S. Nargolwalla, NBS Activation Analysis Section

The results of the chemical analysis were found to be inconsistent and unexpected. The decrease in the free beryllium content in the samples before and after the measurements cannot be attributed to chemical reactions at temperatures of the measurements. (Small heat effects were observed above about 320 K. See later parts of this section for further details). The difference is probably due to nonhomogeneity in the material, although relatively large samples (2 g) were used in this determination.

The decrease in the total beryllium content because of a chemical reaction during the heat measurements does not seem possible. If the observed heat effects resulted from a chemical reaction within the sample, the expected reaction would be:

$$3\,Be(OH)_2 + Be_3N_2 \rightarrow 6BeO + 2NH_3. \qquad (2)$$

This should lead to an increase in the apparent beryllium content, since the ammonia would be lost on opening the sample vessel.

For the material removed from the calorimeter

vessel after the heat measurements, the mass balance for beryllium found is not consistent in terms of the analyses obtained. The analyses for N, O, and total Be sum to 100.01 percent and the addition of H (0.13 percent) found as water makes the total weight percent 100.14. This is within the expected limits of accuracy of the chemical analyses. However, inconsistencies arise when these analyses are used to obtain mass balance among the chemical species that are expected to be present (Be_3N_2, BeO, $Be(OH)_2$, and Be metal). On the basis of the results of the oxygen and water analyses (2.38 and 1.14 percent, respectively), the percentage of beryllium as BeO and $Be(OH)_2$ sums to 0.77 percent. When the Be metal (0.04 percent) and beryllium (47.22 percent) as Be_3N_2, based on the nitrogen analysis, are added to 0.77 percent, the total beryllium becomes 48.03 percent. This is considerably lower than the total beryllium (48.70 percent) from the chemical analysis. The masses of the substances present also sum to considerably less than 100 percent (96.15%-Be_3N_2, 2.72%-$Be(OH)_2$, 0.56%-BeO, and 0.04%-Be metal; 99.47%-total mass). These inconsistencies can be resolved if the Be metal analysis were higher (about 0.7 percent), but this is not possible since the estimated error in the chemical analysis for Be metal is much less than this value.

On the other hand, if the analysis shown in table 3 for water is ignored, the remaining analyses would become consistent on the basis that the substances present are only Be_3N_2, BeO, and Be metal. All of the oxygen (2.38 percent) would then be taken to be present as BeO, which corresponds to 3.73 percent BeO or 1.34 percent Be. When the percentages of Be as Be_3N_2 and as Be metal are added to 1.34 percent, the total "calculated" Be is 48.61 percent. This is within the limits of chemical analysis found for total Be (48.70 percent). When the 96.15 percent Be_3N_2, based on the nitrogen analysis, is added to the percentages of BeO and Be metal, the total weight percent is 99.92 percent. The analyses for total beryllium, nitrogen, and oxygen, as mentioned earlier, sum to 100.01 percent. These values are all within the limits of the chemical analysis.

The source of heat effects observed during the measurements (to be described later) can not be explained in terms of the known possible chemical reaction within the sample. The possible chemical reaction depicted by eq (2), in which the water from $Be(OH)_2$ reacts with Be_3N_2 to form BeO and NH_3, is not consistent with the chemical analyses. The reaction is obviously not possible if the water is securely held at the temperatures of the heat measurements. Duval and Duval [14] interpreted their thermal gravimetric analysis work to indicate that the decomposition of $Be(OH)_2$ starts around 150 °C and that complete decomposition of $Be(OH)_2$ to BeO and H_2O occurs only on heating to 951 °C. The observed loss in mass at temperatures below 150 °C was attributed to adsorbed water in their sample. If any moisture were present in the sample that was used in the work reported here, it was adsorbed between the times the sample was removed from the furnace and received from the supplier.

After careful consideration of the various possibilities that could be selected on the basis of the chemical analyses and the estimated uncertainties that would arise from them, the choice was made to ignore the analysis obtained for water in the reduction of the heat-capacity measurements. The sample was taken to be 96.23 percent Be_3N_2, 3.73 percent BeO, and 0.04 percent Be metal and corrections were applied to the observed values of heat capacity for BeO [15] and Be metal [16].

Two crystalline modifications of Be_3N_2 have been reported, the $\alpha-Be_3N_2$ of bcc lattice with anti-Mn_2O_3 structure [17, 18] and the $\beta-Be_3N_2$ of hexagonal structure [18]. The $\alpha-Be_3N_2$ transforms into the $\beta-Be_3N_2$ form at 1400 °C [18]. The x-ray examination by the NBS Crystallography Section of the sample after the heat-capacity measurements showed only the $\alpha-Be_3N_2$ form within the limits of analysis of the method.

4. Results and Method of Data Reduction

Two series of measurements were made, one on the calorimeter vessel with sample (gross) and the other on the empty vessel (tare). Briefly, the measured energy increments (ΔQ) and the corresponding thermometer resistances (R) before and after heating for the two series of measurements were analyzed on the high-speed digital computer to obtain dQ/dR of the sample as a function of the thermometer resistance [19]. After adjusting for the helium exchange gas used with the Be_3N_2 sample, the values of heat capacity (dQ/dT) of the sample were then calculated at even temperatures from the dR/dT and the $R-T$ calibration for the thermometer using the relation:

$$dQ/dT = (dQ/dR)\,(dR/dT). \tag{3}$$

In greater detail, the analysis procedure was to obtain first the best polynomial equation of the form

$$dQ/dR = \sum a_n R^n \tag{4}$$

to represent the experimental data on the empty calorimeter vessel (tare) [20]. The polynomial equation for tare measurements was then evaluated at the thermometer resistances observed for the gross measurements in order to obtain the energy increments for sample only (net) from the observations on the calorimeter vessel plus sample experiments, i.e.,

$$\Delta Q_R(\text{sample}) = \Delta Q_R(\text{gross}) - \Delta Q_R(\text{tare}). \tag{5}$$

(Hereafter, ΔQ_R(sample) will also be referred to as observed data on the sample and the corresponding quantity $\Delta Q/\Delta T$(sample) as observed sample heat capacity). The best polynomial equation giving dQ/dR for the sample only was then obtained and dQ/dT calculated according to eq (3) above.

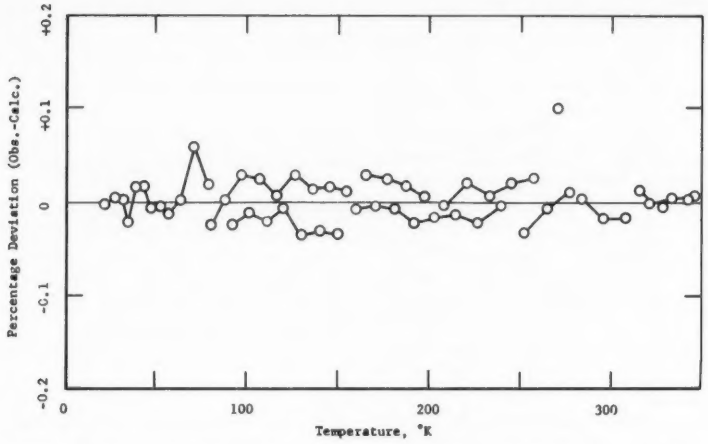

FIGURE 4. *Percentage deviation of the empty sample vessel heat capacities from the polynomial equation:*

$$dQ/dR = \sum_{n=-4}^{+10} a_n R^n.$$

Consecutive measurements obtained during the day are connected by lines.

Figure 4 shows the deviation of the experimental data on the empty container from corresponding values calculated from the polynomial equation fitted by the method of least squares to the energy-resistance observations. The range of the polynomial was from $n=-4$ to $n=+10$ (see eq (4)). The root-mean-square (rms) of the percentage deviation of all data from the polynomial equation was 0.02 percent. For the final reduction of the data the two poor points shown in figure 4 were not considered; the rms of the percentage deviation of the remaining data was 0.008 percent.

Due to increasingly poorer precision at the lowest experimental temperatures the sample data were fitted with two overlapping equations. Figure 5 shows the deviation of the sample data from the polynomial (n ranging from 0 to 4) fitted to the data over the temperature range 20 to 110 K and figure 6 the deviation of the data from the polynomial (n ranging from -2 to $+10$) fitted over the temperature range 60 to 315 K. Heat capacity values calculated from the two equations agreed within 0.02 percent over the temperature range 80 to 100 K. The heat capacity values obtained from the two equations were joined at 90 K. The rms of the percentage deviation of the observed sample heat capacity from the polynomial equations is 0.06 percent above 50 K. The deviation increases below 50 K.

Figures 5 and 6 show the precision of the gross measurements; the boundary curves represent the effect on the final smooth values of a change of 0.025 percent in the values of the heat-capacity measurements for the empty and filled sample vessel; e.g., at 100 K (fig. 6), a change in the heat capacity of 0.025 percent of the empty vessel causes slightly less than 0.1 percent change on the sample while a similar change of the gross measurements causes about 0.12 percent change on the sample. Figures 5 and 6 show

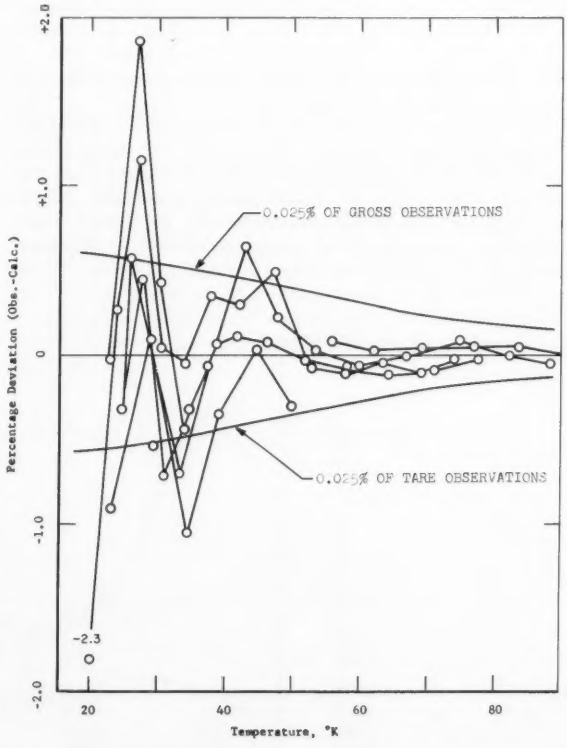

FIGURE 5. *Percentage deviation of the α-beryllium nitride sample heat capacities from the polynomial equation:*

$$dQ/dR = \sum_{n=0}^{+4} a_n R^n.$$

Consecutive measurements obtained during the day are connected by lines.

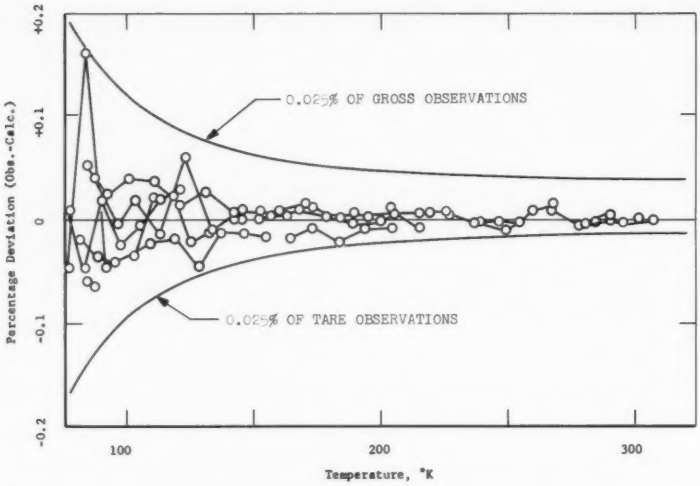

FIGURE 6. *Percentage deviation of the α-beryllium nitride sample heat capacities from the polynomial equation:*

$$dQ/dR = \sum_{n=-2}^{+10} a_n R^n.$$

Consecutive measurements obtained during the day are connected by lines.

that above 50 K the precision of the gross measurements is about ± 0.01 percent.

As mentioned earlier, heat effects were observed during the measurements of the heat capacity above about 320 K. The final results that are presented are based on the data obtained between 20 and 315 K subsequent to heating above 320 K. In figure 7 are shown values of heat capacity initially obtained between 80 and 315 K prior to heating above 320 K. The base line (zero line) of the figure corresponds to the final smoothed values. Above 150 K, the values of the initial measurements and those after heating above 320 K are shown to be essentially the same. Below 150 K, the values of the initial measurements are somewhat higher. Since no data were obtained initially below 80 K, no comparison could be made below 80 K between the values before and after heating above 320 K. In the range 80 to 315 K, however,

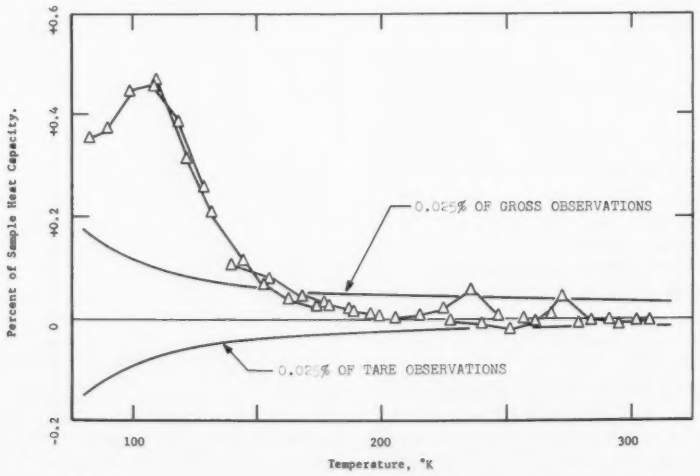

FIGURE 7. *Percentage deviation of initial measurements from the final selected α-beryllium nitride sample heat capacities.*

Consecutive measurements obtained during the day are connected by lines.

the heating above 320 K did not make a large change in the heat capacity of the sample, at the most about 0.5 percent at 100 K. The comparison shows that the heat capacity of the sample was not affected grossly when heated above 320 K.

The values of heat capacity of Be_3N_2 that were generated at evenly spaced temperatures from dQ/dR in accordance with eq (2) were corrected for BeO [15] and Be metal [16] and converted to molal basis. The molecular weight was taken to be 55.05 g, based on the 1961 atomic weight scale [22]. These molal values were analyzed further for extrapolation to 0 K. The final selected values below 20 K are based on the extrapolation of the experimental heat capacity using the heat-capacity function:

$$C = 1943.73(705/T)^{-3} \quad \text{J/K·mol.} \tag{6}$$

The final smoothed values of heat capacity have a relatively large uncertainty arising from the possible impurities in the sample. Above 100 K the estimated uncertainty is 0.5 percent and below this temperature 1 percent.[4]

The values of heat capacity from 0 to 315 K were applied in the usual thermodynamic relations:

$$H_T - H_0^c = \int_0^T C dT, \tag{7}$$

$$S_T = \int_o^T (C/T) dT, \tag{8}$$

and

$$G_T - H_0^c = (H_T - H_0^c) - TS_T, \tag{9}$$

to obtain the thermodynamic properties. The values are given in table 4.

[4] The uncertainty, as used with the values obtained in this paper and indicated by the symbol ±, is an estimate reached by examining contributions to the inaccuracy from imprecision and possible systematic errors in the measurements. The authors estimate that there is a 50–50 chance that the error is no larger than that indicated.

Justice [3] recently reported heat-capacity measurements on $\alpha-Be_3N_2$ of 96.7 percent purity. The significant impurities were BeO—2.7 percent, Be metal—0.2 percent, C—0.1 percent, and Fe—0.3 percent. The entropy at 298.15 K that Justice [3] reported is 8.170 cal/K · mol, which is in good agreement with that (8.23 ± 0.08 cal/K · mol) found in this investigation. The values of heat capacity obtained also join satisfactorily, in both the magnitude of heat capacity and its slope, with those derived from the high-temperature relative enthalpy measurements reported by Douglas and Payne [1]. (See Douglas and Payne [1] for tables of thermodynamic properties of Be_3N_2 up to 1200 K).

The results presented in this paper (figs. 5, 6, and 7) show that the precision obtained on the empty vessel is ±0.01 percent over the entire temperature range of the measurements, while on the vessel with sample the precision is ±0.01 only above about 50 K. There is no explanation for the precision of the gross measurements to be poorer than that of the tare measurements at the lower temperatures. A large part of the apparently poorer precision of the sample data at the lower temperatures is believed to be caused by the poorer fit of the equation to the sample data. The trends in the deviations shown in figure 5 partially support this belief. A part of the poorer equational fit to the sample data may be caused by the choice of the equation to represent the tare data, resulting in a complex net sample data to be fit by an equation. A high-quality fit of the gross data is also not easily achieved because of the combined contribution of the sample and vessel. Because of the poor quality of the beryllium nitride sample, an intensive experimental study of these questions was considered inadvisable. Also, the uncertainty at these lower temperature contributes very little to the overall uncertainty in S_{298}. Therefore, no further experimental measurements were made on beryllium nitride. The study of these "finer details" is planned when an opportunity arises on a material of high purity.

TABLE 4. *Molal thermodynamic functions for α-beryllium nitride,* (Be_3N_2), *solid phase*

Gram Molecular weight = 55.0500 g Cal = 4.1840 J

T, K = 273.15 + t °C

T	C_P°	$(H_T^\circ - H_0^c)$	$(H_T^\circ - H_0^c)/T$	$(S_T^\circ - S_0^c)$	$-(G_T^\circ - H_0^c)$	$-(G_T^\circ - H_0^c)/T$
K	J/K	J	J/K	J/K	J	J/K
0.00	0.0000	0.0000	0.00000	0.00000	0.00000	0.00000
5.00	.0007	.0009	.00017	.00023	.00029	.00006
10.00	.0055	.0139	.00139	.00185	.00462	.00046
15.00	.0187	.0702	.00468	.00624	.0234	.00156
20.00	.0444	.222	.0111	.0148	.0740	.00370
25.00	.0863	.541	.0217	.0289	.181	.00722
30.00	.147	1.116	.0372	.0497	.374	.0125
35.00	.230	2.048	.0585	.0782	.690	.0197
40.00	.339	3.459	.0865	.116	1.171	.0293
45.00	.480	5.492	.122	.163	1.865	.0414

TABLE 4. *Molal thermodynamic functions for α-beryllium nitride, (Be_3N_2), solid phase*—Continued

Gram Molecular weight = 55.0500 g

Cal = 4.1840 J

T, K = 273.15 + t °C

T	C_p°	$(H_T^\circ - H_0^C)$	$(H_T^\circ - H_0^C)/T$	$(S_T^\circ - S_0^C)$	$-(G_T^\circ - H_0^C)$	$-(G_T^\circ - H_0^C)/T$
K	J/K	J	J/K	J/K	J	J/K
50.00	.660	8.323	.166	.223	2.826	.0565
55.00	.888	12.170	.221	.296	4.117	.0749
60.00	1.172	17.294	.288	.385	5.813	.0969
65.00	1.522	24.000	.369	.492	7.999	.123
70.00	1.944	32.634	.466	.620	10.771	.154
75.00	2.446	43.575	.581	.771	14.238	.190
80.00	3.029	57.226	.715	.947	18.521	.232
85.00	3.697	74.005	.871	1.150	23.752	.279
90.00	4.451	94.338	1.048	1.382	30.070	.334
95.00	5.292	118.66	1.249	1.645	37.626	.396
100.00	6.218	147.40	1.474	1.940	46.574	.466
105.00	7.227	180.98	1.724	2.267	57.078	.544
110.00	8.314	219.80	1.998	2.628	69.302	.630
115.00	9.473	264.24	2.298	3.023	83.416	.725
120.00	10.701	314.65	2.622	3.452	99.590	.830
125.00	11.993	371.35	2.971	3.915	117.99	.944
130.00	13.343	434.67	3.344	4.411	138.79	1.068
135.00	14.747	504.87	3.740	4.941	162.16	1.201
140.00	16.201	582.23	4.159	5.503	188.26	1.345
145.00	17.699	666.96	4.600	6.098	217.25	1.498
150.00	19.236	759.28	5.062	6.724	249.29	1.662
155.00	20.807	859.37	5.544	7.380	284.54	1.836
160.00	22.406	967.40	6.046	8.066	323.14	2.020
165.00	24.030	1083.5	6.567	8.780	365.24	2.214
170.00	25.671	1207.7	7.104	9.522	410.99	2.418
175.00	27.326	1340.2	7.658	10.290	460.51	2.631
180.00	28.990	1481.0	8.228	11.083	513.93	2.855
185.00	30.659	1630.1	8.811	11.900	571.37	3.089
190.00	32.328	1787.6	9.408	12.740	632.96	3.331
195.00	33.994	1953.4	10.017	13.601	698.81	3.584
200.00	35.655	2127.5	10.638	14.483	769.01	3.845
205.00	37.307	2309.9	11.268	15.383	843.67	4.115
210.00	38.949	2500.6	11.907	16.302	922.87	4.395
215.00	40.579	2699.4	12.555	17.238	1006.7	4.682
220.00	42.195	2906.3	13.211	18.189	1095.3	4.979
225.00	43.796	3121.3	13.873	19.155	1188.6	5.283
230.00	45.381	3344.3	14.540	20.135	1286.9	5.595
235.00	46.948	3575.1	15.213	21.128	1390.0	5.915
240.00	48.496	3813.7	15.890	22.133	1498.2	6.242
245.00	50.024	4060.0	16.572	23.148	1611.4	6.577
250.00	51.531	4313.9	17.256	24.174	1729.7	6.919
255.00	53.015	4575.3	17.942	25.209	1853.1	7.267
260.00	54.475	4844.0	18.631	26.253	1981.8	7.622
265.00	55.911	5120.0	19.321	27.304	2115.7	7.984
270.00	57.321	5403.1	20.011	28.363	2254.8	8.351
273.15	58.197	5585.0	20.447	29.033	2345.2	8.586
275.00	58.707	5693.2	20.702	29.427	2399.3	8.725
280.00	60.067	5990.1	21.393	30.497	2549.1	9.104
285.00	61.404	6293.8	22.084	31.572	2704.3	9.489
290.00	62.717	6604.1	22.773	32.652	2864.8	9.879
295.00	64.008	6920.9	23.461	33.735	3030.8	10.274
298.15	64.811	7123.8	23.893	34.419	3138.1	10.525
300.00	65.278	7244.2	24.147	34.821	3202.2	10.674
305.00	66.522	7573.7	24.832	35.910	3379.0	11.079
310.00	67.735	7909.3	25.514	37.002	3561.3	11.488
315.00	68.905	8251.0	26.194	38.095	3749.0	11.902

H_0^C and S_0^C apply to the reference state of the solid at 0 K.

5. References

[1] Douglas, T. B., and Payne, W. H., J. Res. Nat. Bur. Stand. (U.S.), **73A** (Phys. and Chem.), 471 (1969).

[2] Satoh, S., Sci. Papers Inst. Phys. Chem. Research (Tokyo) **34**, 888 (1938).

[3] Justice, B. H., J. Chem. Eng. Data **14**, 384 (1969).

[4] Scott, R. B., Meyers, C. H., Rands, R. D., Jr., Brickwedde, F. G., and Bekkedahl, N., J. Res. Nat. Bur. Stand. (U.S.), **35**, 39 (1945), RP1661.

[5] Furukawa, G. T., Reilly, M. L., and Piccirelli, J. H., J. Res. Nat. Bur. Stand. (U.S.), **68A** (Phys. and Chem.), 381 (1964).

[6] Furukawa, G. T., Reilly, M. L., and Piccirelli, J. H., J. Res. Nat. Bur. Stand. (U.S.), **68A** (Phys. and Chem.), 651 (1964).

[7] Furukawa, G. T., and Saba, W. G., J. Res. Nat. Bur. Stand. (U.S.), **69A** (Phys. and Chem.), 13 (1965).

[8] Furukawa, G. T., and Saba, W. G., J. Res. Nat. Bur. Stand. (U.S.), **71A** (Phys. and Chem.), 3 (1967).

[9] Hoge, H. J., and Brickwedde, F. G., J. Res. Nat. Bur. Stand. (U.S.), **28**, 217 (1942) RP1454.

[10] Furukawa, G. T., Reilly, M. L., and Saba, W. G., Rev. Sci. Instr. **35**, 113 (1964).

[11] Westrum, E. F., Jr., Furukawa, G. T., and McCullough, J. P., Adiabatic low-temperature calorimetry, in Experimental Thermodynamics, Calorimetry of Non-Reacting Systems, Vol. 1, pp. 133–214 (Butterworths, London, 1968).

[12] The International Practical Temperature Scale of 1968, adopted by the Comité International des Poids et Mesures, Metrologia **5**, 35 (1969).

[13] United States Department of Commerce, Nat. Bur. Stand. (U.S.), Handb. 102, ASTM Metric Practice Guide (1967) 46 pp.

[14] Duval, T., and Duval, C., Anal. Chim. Acta **2**, 53 (1948).

[15] Furukawa, G. T., and Reilly, M. L., unpublished measurements on BeO.

[16] Furukawa, G. T., and Reilly, M. L., unreported results of analysis of literature heat-capacity data on beryllium metal.

[17] Stackelberg, M. V., and Paulus, R., Z. physik. Chem. **22B**, 305 (1933).

[18] Eckerlin, P., and Rabenau, A., Z. anorg. allgem. Chem. **304**, 218 (1960).

[19] Furukawa, G. T., and Reilly, M. L., J. Res. Nat. Bur. Stand. (U.S.), **69A** (Phys. and Chem.) 5 (1965).

[20] Walsh, P., Comm. ACM **5**, 511 (1962).

[21] Furukawa, G. T., Saba, W. G., and Ford, J. C., J. Res. Nat. Bur. Stand. (U.S.), **74A** (Phys. and Chem.), No. 5, 631–639. (Sept.–Oct. 1970).

[22] Cameron, A. E., and Wichers, E., J. Am. Chem. Soc. **84**, 4175 (1962).

(Paper 74A5–625)

JOURNAL OF RESEARCH of the National Bureau of Standards—A. Physics and Chemistry
Vol. 74A, No. 5, September–October 1970

Heat Capacity and Thermodynamic Properties of β-Lithium Hexafluoroaluminate, Li_3AlF_6, from 15 to 380 K*

George T. Furukawa, William G. Saba, and James C. Ford*****

Institute for Basic Standards, National Bureau of Standards, Washington, D.C. 20234

(May 27,1970)

The heat capacity of β-lithium hexafluoroaluminate, Li_3AlF_6, was determined from 15 to 380 K and the thermodynamic properties calculated from the results. The entropy at 298.15 K was found to be 187.88 ± 0.38 J/K · mol (44.904 ± 0.090 cal/K · mol).

Key words: Calorimetry; entropy; heat capacity; β-lithium hexafluoroaluminate; thermodynamic properties.

1. Introduction

The heat-capacity measurements on β-lithium hexafluoroaluminate, Li_3AlF_6, have been obtained between 15 and 380 K as a part of the research program at the National Bureau of Standards to provide accurate thermodynamic data on light-element compounds. The specimen employed in the measurements was a portion of the same Li_3AlF_6 preparation from which the sample had been taken for the previously reported relative enthalpy measurements between 273.15 and 1073.15 K by Douglas and Neufer [1].[1]

The phase diagram of the lithium fluoride–aluminum fluoride binary system shows one congruent melting compound, lithium hexafluoroaluminate, Li_3AlF_6 [2, 3]. As observed in other compounds of composition M_3AlF_6 of the alkali fluoride–aluminum fluoride system [4], the Li_3AlF_6 also exhibits polymorphism. Five crystalline forms have been reported between room temperature and the melting point (1056 K) [5, 6, 7]. When γ–Li_3AlF_6 is cooled slowly to room temperature from about 600 °C, β–Li_3AlF_6 is obtained; when the sample is quenched from about 600 °C to room temperature, α–Li_3AlF_6 is obtained [5]. The α form seems to be stable up to 225 °C; but when heated above this temperature, the β form slowly appears. The reverse transformation has not been observed [7]. From x-ray powder pattern data, Garton and Wanklyn [5] have indexed α- and β-Li_3AlF_6 on the basis of hexagonal unit cell; more recently Burns et al. [21] indexed α-Li_3AlF_6 on the basis of orthorhombic unit cell.

*This work was supported by the Advanced Research Projects Agency, Department of Defense, under Order No. 20 and by the Air Force Office of Scientific Research, Office of Aerospace Research, United States Air Force, under AFOSR Contract No. ISSA 68–0004.

**U.S. Patent Office, Crystal Plaza, 2021 Jefferson Davis Highway, Arlington, Va. 22202.
***203 Aronomink Drive, Newark, Del. 19711.

[1] Figures in brackets indicate the literature references at the end of this paper.

2. Sample

The Li_3AlF_6 sample, furnished by the Oak Ridge National Laboratory (ORNL) through the courtesy of R. E. Thoma and G. M. Hebert, had been prepared by fusing stoichiometric proportions of LiF and anhydrous AlF_3 in a graphite crucible. The product was stated to be single phase by x-ray diffractometric and petrographic (microscopic) examinations and to contain 0.04 percent of water and 0.06 percent of oxygen from other oxygen-containing compounds. The sample was received in the form of a fused lump. The results of chemical analysis of a piece broken off the lump are summarized in table 1.

The analysis procedure for aluminum and lithium involved the dissolving of about a 0.2-g sample in sulfuric acid and heating to remove the fluorine as hydrogen fluoride. Aluminum was precipitated from the resulting solution as aluminum hydroxide with NH_4OH. The precipitate was filtered, ignited, and weighed as Al_2O_3. The filtrate was evaporated to dryness with H_2SO_4 and the residue weighed as Li_2SO_4 and Na_2SO_4. The sodium was determined by flame photometry and the lithium was determined by difference.

The analysis for fluorine was similar to the procedure described by Hoffman and Lundell [8]. About 0.2 g of the sample was fused with anhydrous sodium carbonate and the cooled material transferred to a Claissen flask and dropping funnel system assembled for distillation. The fused material was dissolved in sulfuric acid (1–1 mixture) added from the dropping funnel. The solution was boiled at about 160 °C, adding small amounts of water through the dropping funnel whenever the temperature rose to about 170 °C. The distillate, containing the fluorine as fluorosilicic acid, was collected in a

TABLE 1. *Chemical analysis of β-lithium hexafluoroaluminate*, Li_3AlF_6*

Element	Percentage by Weight		
	Analysis		
	Individual	Mean	Theoretical
Li	12.8_7 12.9_4 12.9_5	12.9_2	12.87
Na	0.12 0.07	0.10	0
Al	16.68 16.79	16.74	16.68
F	70.29 70.56	70.42	70.45
Sum		100.18	100.00

*Analyzed by E. June Maienthal and R. A. Paulson, NBS Applied Analytical Research Section.

solution of sodium hydroxide. The solution was evaporated to about 250 cm^3 and the fluoride was precipitated as PbClF from the solution. Next, the PbClF precipitate was dissolved in dilute nitric acid and the chlorine determined by the Volhard method. The amount of fluorine was computed from the corresponding chlorine equivalence.

The fused sample as received from ORNL had some outer areas of black coloration. Most of the black surface material was removed by scraping and the remaining sample was crushed to particle sizes between 0.5 to 2 mm on the edge and thoroughly mixed (all of the handling being done in an argon-atmosphere dry box with the dew point at about −80 °C). Only minute amounts of black flecks remained in the sample. Of the original sample of about 200 g, 162.6555 g were used for the low-temperature heat-capacity measurements. The remainder, packaged in 1-g or 10-g units sealed in polyethylene bags, was reserved for high-temperature relative enthalpy measurements and for any additional analyses. The samples sealed in polyethylene bags were in turn placed in separate jars sealed with polyethylene snap-caps and stored in a desiccator containing magnesium perchlorate.

X-ray diffractometric examination of one of the 1-g samples was made by H. E. Swanson of the Crystallography Section of the National Bureau of Standards. The diffraction pattern was found to correspond to the low-temperature β-Li_3AlF_6 phase reported by Garton and Wanklyn [5]; no characteristic strong lines of α-Li_3AlF_6 were observed. X-ray examination of the material after the heat-capacity measurements showed no change in the diffraction pattern.

The sample was analyzed spectrochemically after the heat-capacity measurements. The results of the analysis are summarized in table 2.

TABLE 2. *Spectrochemical analysis of β-lithium hexafluoroaluminate*, Li_3AlF_6 *

Element	Percentage Limits By Weight	Element	Percentage Limits By Weight
Ag	< 0.001	Mg	0.001 − 0.01
Ba	< 0.001	Mn	< 0.001
Be	< 0.001	Na	0.1 − 1
Ca	0.001 − 0.01	Ni	[a] 0.1 − 1
Cr	0.001 − 0.01	Pb	< 0.001
Cs	< 0.001	Rb	< 0.001
Cu	< 0.001	Si	< 0.001
Fe	0.01 − 0.1	Sn	< 0.001
Ga	0.001 − 0.01	Ti	0.001 − 0.01
K	< 0.001		

*Analyzed by Virginia C. Stewart, NBS Spectrochemical Analysis Section.

[a] A second spectrochemical analysis showed 0.01 to 0.1 percent nickel; chemical analysis showed 0.04 percent nickel.

The high nickel impurity content was unexpected and was considered highly improbable to have been introduced anywhere during the crushing and other handling processes employed in preparing the sample for the measurements. Since the original chemical analysis for lithium as Li_2SO_4 could have included $NiSO_4$, a separate chemical analysis was made for nickel. Two Li_3AlF_6 samples of about 0.6 g each were dissolved in water and perchloric acid. As a control, 0.500 mg of nickel was added to one of the samples. The nickel content of the solution was then determined spectrophotometrically using the dimethylglyoxime color reaction. The nickel found was 0.04 weight percent. Since the first spectrochemical analysis was on a small sample, a second spectrochemical analysis was made on a portion of a large Li_3AlF_6 sample throughly mixed by grinding. The nickel analysis was 0.01 to 0.1 percent.

These analyses for nickel indicate that the Li_3AlF_6 sample could be somewhat inhomogeneous. Since the crushed sample was thoroughly mixed and the sample size used in the chemical analysis was relatively large, the nickel content found by chemical analysis is considered most likely to be representative of the sample. Except for the small amount of sodium found in the sample, the analyses obtained agree with the theoretical values within the precision of the analytical procedure. Since the sodium content is low and is most likely present as Na_3AlF_6, the sample was taken to be 100 percent β−Li_3AlF_6 and no correction was made to the observed values of heat capacity for composition.

3. Apparatus and Method

The measurements were made using the calorimeter to be described in the paper on beryllium nitride (Be_3N_2) [9]. Since a calibrated thermometer was used in the sample vessel, the thermometer-calibration feature built into the calorimeter was not used in the measurements.

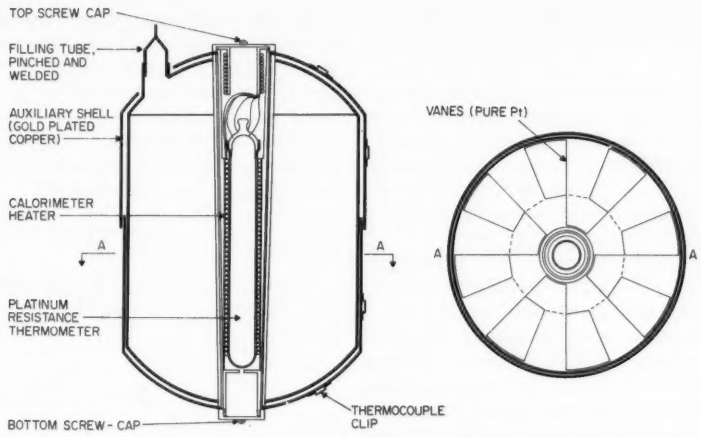

FIGURE 1. *Calorimeter sample vessel system with platinum-iridium alloy vessel, central removable platinum resistance thermometer-heater assembly, and auxiliary outer copper shells.*

A platinum-iridium alloy vessel, with pure platinum vanes to enhance temperature equilibrium, contained the Li_3AlF_6 sample. Figure 1 shows a schematic representation of the calorimeter vessel system. The vertical platinum vanes, shown bent and arranged radially in the figure, were spot-welded at numerous places along the wall and the central tapered tube. The "floating" portion of the vanes was confined by bending the upper and lower half sections in opposite directions, shown by the alternate solid and dashed lines, respectively. The internal taper of the central tube was "finished" after the welding by reaming and lapping to a high polish.

The removable platinum-thermometer–heater assembly had a taper that closely matched the taper of the central tube. The calorimeter heater (100 Ω), wound tightly on the platinum thermometer and cemented with epoxy resin, was a nickel-chromium alloy wire of low temperature-coefficient of resistance [10]. The combination was encased in a thin layer of tin-lead eutectic solder within the stainless steel tapered insert. The heater was "centrally" located in the insert so that its two ends would be nearly equally heated. The gold-plated outer auxiliary shells of copper were clamped to the vessel at the top and bottom with screwcaps as shown; the shells telescoped within each other at the middle. The calorimeter vessel system was suspended within the adiabatic shield of the calorimeter by means of a nylon cord [9]. Tests during the heating periods showed that the average temperatures of the two auxiliary shells differed at most about 0.02 K.

The following steps were taken in assembling the calorimeter vessel system: A thin layer of stopcock grease was applied to the parts of the tapered insert, calorimeter vessel, auxiliary shells, and screwcaps that were to be in mechanical contact. The lower auxiliary shell was first clamped to the vessel with the bottom screwcap, drawing the tapered thermometer-heater assembly tightly into the tapered central tube of the vessel. The upper auxiliary shell was then clamped to the vessel with the top screwcap.

The same order was followed in the disassembly of the vessel system. After removing the lower auxiliary shell and the bottom screwcap, the top screwcap was tightened to loosen the tapered thermometer–heater assembly from the vessel. The upper auxiliary shell and thermometer-heater assembly were removed as a unit and could be later separated by loosening the screwcap. Actually, the upper auxiliary shell and the thermometer–heater insert were left intact and the top screwcap loosened when the insert was being reinstalled in the tapered tube of the calorimeter vessel.

The sample was introduced through a platinum filling tube (about 0.6 cm i.d.) gold-soldered into an auxiliary tubular opening on the vessel. The filling was done in a dry box (argon atmosphere; dew-point: about −80 °C). After filling, the sample was pumped and purged several times with helium gas through the filling tube and finally sealed by pinching a 2-cm section of the platinum tube (previously annealed) flat, then simultaneously severing and sealing the tube at the middle of the flattened portion with an acetylene torch. A small amount [2] (8770 N/m²) of helium gas was sealed in the vessel with the sample to help achieve rapid thermal equilibrium.

The platinum resistance thermometer (laboratory designation: 1066756) employed in the measurements was calibrated in accordance with the International Practical Temperature Scale of 1968 [12]. The temperatures T given in this paper correspond identically to the International Practical Kelvin Temperatures referred to with the symbol T_{68} in the above reference in kelvin units (symbol K).

The thermometer resistance measurements were made to the nearest 0.00001 Ω using initially a manual

[2] The observed pressure was initially expressed and the heat data processed in terms of mm Hg at 0 °C and standard gravitational acceleration of 980.665 cm/s². The conversion to N/m² was made using the definition: 1 normal atmosphere = 101,325 N/m² = 760 torr (mm Hg at 0 °C and 980.665 cm/s²) [11].

389-821 O - 70 - 2

and later an automatic Mueller bridge. The observations with the automatic Mueller bridge [13, 14] were recorded automatically on punched cards and processed on a high-speed digital computer. In both manual and automatic methods the platinum thermometer resistances R_i and R_f were obtained, corresponding to before and after the introduction of a measured energy increment ΔQ. The process used to reduce these observations to values of heat capacity at evenly spaced integral temperatures will be described later.

The electrical power introduced into the calorimeter heater was determined by manual measurements, using a Wenner potentiometer in conjunction with a volt box, standard resistor, and saturated standard cells, which were all calibrated at the National Bureau of Standards. A constant current source stable to about 2 ppm or better minimized current fluctuations. By using the Ni-Cr alloy wire mentioned earlier for the calorimeter heater, the total change of the heater voltage was not more than 0.05 percent during any heating period; for most of the measurements the total change was about 0.02 percent.

The heating interval was determined by means of a high-precision interval timer operated on the 60-Hz frequency standard provided at the National Bureau of Standards and stable to 0.5 ppm. As a check, an electronic counter containing a temperature-controlled 1-MHz calibrated quartz oscillator was also simultaneously employed in the measurement of the heating time interval. The estimated uncertainty in the determination of the heating time interval was not greater than ± 0.01 s for any heating period, none of which was less than 2 min in these experiments.

The calorimeter heater circuit was the same as that previously described [15]. Because of the short time constant of the constant current supply system, a make-before-break action was used in the calorimeter heater–dummy heater switch [14]. The energy increment (ΔQ), introduced during the heating period, was determined as the product ($ei\tau$) of the heating time interval (τ), the average voltage drop (e) across the calorimeter heater, and the current flow (i) through the heater [15]. The average e and i were obtained from the observations, made at equally spaced time intervals (1 or 0.5 min) during the heating period. As mentioned earlier, the observed values of i were essentially constant and e usually changed about 0.02 percent during the heating period.

The 1961 atomic weights based on carbon 12 were used to convert the mass of Li_3AlF_6 investigated to gram formula weight basis [16]. The energy measurements were made in terms of the mksa unit of energy, the joule. Whenever conversion to calorie was made, the following relation was used: 1 calorie = 4.1840 J.

4. Results

Two series of measurements were made: one on the calorimeter vessel with sample (gross) and the other on the empty vessel (tare). The method of data reduction (to obtain smoothed values of heat capacity of Li_3AlF_6 from the measured energy increments ΔQ and the corresponding thermometer resistances R_i and R_f before and after heating, respectively) was similar to that described previously [17]. In principle, the procedure was to obtain dQ/dR of the sample (net) as a function of the thermometer resistance R. From the R versus T calibration and dR/dT for the thermometer, the heat capacity dQ/dT was calculated according to the relation:

$$dQ/dT = (dQ/dR)\,(dR/dT). \tag{1}$$

Briefly, the steps in the procedure were as follows: The measurements on the empty vessel represented by

$$\Delta Q = \int_{R_i}^{R_f} f(R)\,dR \tag{2}$$

were analyzed on a high-speed digital computer to obtain

$$dQ/dR = f(R). \tag{3}$$

The function $f(R)$ used in analyzing the present measurements was a polynomial in $(\ln R)/R$, i.e.,

$$f(R) = \sum_{n=0}^{N} a_n\,((\ln R)/R)^n. \tag{4}$$

The coefficients of eq (4) were obtained by the method of least squares using double precision calculations (16 to 17 figure accuracy). Experimental data obtained between about 15 and 380 K on the empty vessel are shown in figure 2 to be, except for a few points, within about ± 0.04 percent of the fifteenth-degree polynomial equation (eq (4), $n=0$ to $n=15$) fitted to the data (92 observations).

The polynomial equation for the measurements on the empty vessel was then evaluated to obtain values of ΔQ (tare) corresponding to the thermometer resistance intervals (R_i and R_f) observed for the gross measurements in order to obtain the energy increments for sample only, i.e.,

$$\Delta Q(\text{sample}) = \Delta Q(\text{gross}) - \Delta Q(\text{tare}). \tag{5}$$

The values of ΔQ (sample and their corresponding values of R_i and R_f were fitted by the method of least squares to a polynomial equation of the form given also by eq (4). Figure 3 shows the deviation of the sample data (182 observations) from the final smoothed values based on a seventeenth-degree polynomial equation (eq (4), $n=0$ to $n=17$). The values of heat dQ/dT for the sample were calculated using eq (1), from dQ/dR evaluated from the polynomial equation at values of R corresponding to integral values of temperature T and from dR/dT of the platinum resistance thermometer. The values of dQ/dT were calculated from 15 to 380 K at 5 K intervals. (These values of dQ/dT will hereafter be referred to as experimental values).

In all of these calculations the second and third derivatives of the polynomial equations were examined

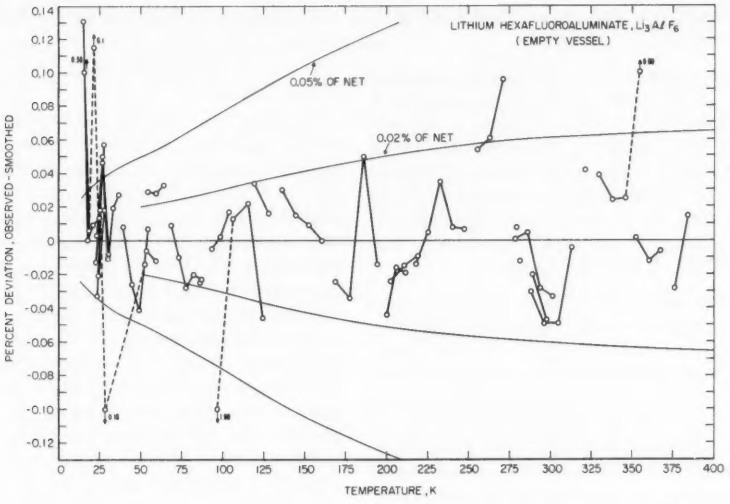

FIGURE 2. *Deviation of empty-vessel measurements from polynomial equation:*

$$dQ/dR = \sum_{n=0}^{15} a_n((\ln R)/R)^n,$$

fitted to the data.

Consecutive measurements obtained during the day are connected by lines.

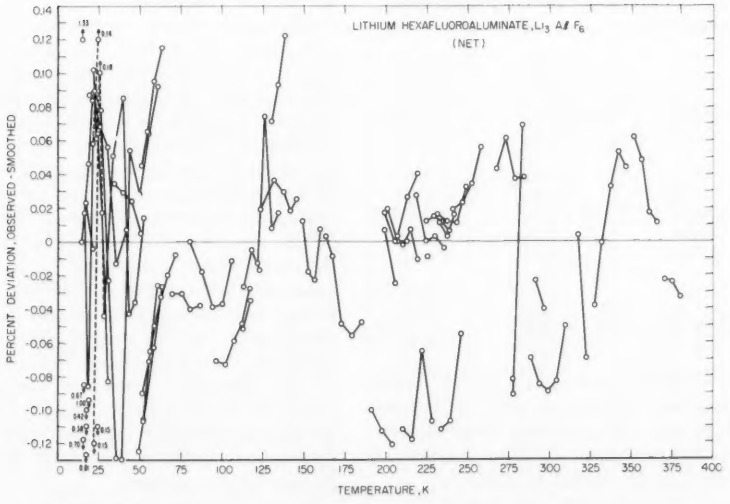

FIGURE 3. *Deviation of the sample data (net) from polynomial equation:*

$$dQ/dR = \sum_{n=0}^{17} a_n((\ln R)/R)^n,$$

fitted to the data.

Consecutive measurements obtained during the day are connected by lines.

closely to ascertain that the equations "behave" in a manner expected of $dQ/dR = f(R)$ [17].

The values of heat capacity below the experimental range (lower limit = 15 K) were obtained by graphical extrapolation to 0 K of C/T^3 versus T plot of experimental values between 15 and 50 K. A slight adjustment (0.1 percent) was made to the experimental values around 20 to 25 K in order that the values of heat capacity between 0 and 50 K be smooth. The adjustment is within the scatter of the data (fig. 3) and the uncertainty in the dR/dT of the thermometer.

Considering the precision of the measurements, the possible systematic errors, and impurities in the sample, the estimated uncertainty[3] of the final smoothed values of heat capacity is 0.2 percent above 100 K. Below 100 K, because of the diminution in the thermometer sensitivity and in the relative fraction of the net over the gross heat capacity, the estimated uncertainty is 1 percent at the lower temperature limit (15 K) of the measurements. Because of the relatively poor thermal conductivity of platinum-iridium alloy as compared with copper, the time for "temperature equilibrium" was, with helium gas sealed in the vessel, about 30 to 40 min after the termination of heating. About one-half the time is required with all-copper vessels.

The smoothed values of heat capacity from 0 to 380 K were then used to calculate the thermodynamic properties using the relations:

$$H_T - H_0^\circ = \int_0^T C dT, \tag{6}$$

$$S_T = \int_0^T (C/T) dT, \tag{7}$$

and

$$G_T = H_0^\circ = (H_T - H_0^\circ) - TS_T. \tag{8}$$

The values of $(H_T - H_0)/T$ and $(G_T - H_0^\circ)/T$ were obtained by dividing the values of $(H_T - H_0^\circ)$ and $(G_T - H_0^\circ)$ obtained in eqs (6) and (8), respectively, by the appropriate temperature T. The values of thermodynamic properties are listed in table 3.

Greene, Gross, and Hayman [7] calculated $S_{298} = 45$ cal/K · mol for α-Li_3AlF_6 from the results of their heats of reaction measurements combined with vapor-equilibrium data and the relative enthalpy data reported by Douglas and Neufer [1]. The value agrees very favorably with the more accurate result 44.904 ±0.090 cal/K · mol obtained in the present work. (Mixture of α and β phases of Li_3AlF_6 were obtained in the chemical combination reaction of LiF and AlF_3 studies by Greene et al. Because of the slowness of conversion from α to β phase, the heat of reaction was taken by Greene et al. to be equally applicable to either phase).

Douglas and Neufer [1] reported enthalpy measurements (relative to 0 °C) up to 800 °C on the same Li_3AlF_6 sample. In table 4, their measurements at 323.15 K (50 °C) and 373.15 K (100 °C) are compared with the corresponding values given in table 3 based on the heat-capacity measurements obtained in the present work. The deviations of the values of enthalpy increments calculated using the enthalpy equation, derived by Douglas and Neufer [1] from their experimental data between 273.15 and 743.15 K, are in good agreement with the values from the heat-capacity measurements; the deviations of their mean observed values are, however, almost an order of magnitude greater and are of opposite signs. The good agreement between the present work and the values from the enthalpy equation based on the data between 273.15 and 743.15 K seems, therefore, somewhat fortuitous. The individual observations reported by Douglas and Neufer [1] also show wide scatter, probably because of varying amounts of α- and β-Li_3AlF_6 being formed in the "drop" experiments.

The heat capacities of the mixed metal oxide compounds $BeO \cdot Al_2O_3$ [18] and $BeO \cdot 3Al_2O_3$ [19] were found to exhibit positive deviation from those obtained by simple addition of heat capacities of the oxide components. In the region from 200 to 400 K the deviation from "additivity" is only 1 or 2 percent. At the lower temperatures, the deviation increases with decreasing temperature. At room temperature, only where enough data were available for comparison, the deviation from additivity of the heat capacities was found to be analogous to the deviation from additivity of the molal volumes of the oxides [19].

Figure 4 shows a positive deviation from additivity of the heat capacity of Li_3AlF_6. For Na_3AlF_6, the deviation from additivity is found to be only ±0.1 percent between 180 and 360 K, the negative deviation being between 200 and 260 K [20]. The estimated uncertainty of the data in the temperature range is, however, ±0.3 or ±0.4 percent. The general shape of the deviation curves is similar to those found for $BeO \cdot Al_2O_3$ and $BeO \cdot 3Al_2O_3$ [18, 19]. The minimum in the deviation is around 220 K for Li_3AlF_6, while those for $BeO \cdot Al_2O_3$ and $BeO \cdot 3Al_2O_3$ occur at higher temperatures.

At room temperature, the deviation from additivity of the molal volume of Li_3AlF_6 is about 5.6 percent and of the heat capacity about 1 percent, and of Na_3AlF_6 about 5 and 0.05 percent, respectively. The deviation from additivity of the molal volume of $BeO \cdot Al_2O_3$ is about 1.2 percent and of $BeO \cdot 3Al_2O_3$ about 4 percent, with the deviation from additivity of the heat capacity being about 1 percent for both mixed metal oxides.

These results seem to indicate that the additivity of heat capacities and molal volumes of mixed metal oxides and fluorides behave similarly. Additional data are needed to determine whether this relation holds over a broader range of temperatures.

[3] The uncertainty as used in this paper is an estimate reached by examining contributions to the inaccuracy from imprecision and possible systematic errors in the measurements. The authors estimate that there is a fifty-fifty chance that the error is no larger than that indicated.

TABLE 3. *Thermodynamic functions for β-lithium hexafluoroaluminate* (Li_3AlF_6) *solid phase*

1 Mole = 0.1617889 Kg $TK = 273.15 + t$ °C

T	C_p^c	$H_T^\circ - H_0^c$	$(H_T^\circ - H_0^c)/T$	S_T°	$-(G_T^\circ - H_0^c)$	$-(G_T^\circ - H_0^c)/T$
K	*J/K-mol*	*J/mol*	*J/K-mol*	*J/K-mol*	*J/mol*	*J/K-mol*
0.00	0.000	0.000	0.000	0.000	0.000	0.000
5.00	.019	.024	.005	.006	.008	.002
10.00	.160	.391	.039	.052	.128	.013
15.00	.604	2.116	.141	.186	.673	.045
20.00	1.664	7.458	.373	.486	2.263	.113
25.00	3.577	20.201	.808	1.047	5.970	.239
30.00	6.275	44.542	1.485	1.927	13.267	.442
35.00	9.573	83.947	2.398	3.135	25.789	.737
40.00	13.307	141.00	3.525	4.653	45.137	1.128
45.00	17.355	217.54	4.834	6.452	72.789	1.618
50.00	21.654	314.97	6.299	8.501	110.07	2.201
55.00	26.146	434.40	7.898	10.774	158.17	2.876
60.00	30.782	576.67	9.611	13.247	218.14	3.636
65.00	35.542	742.43	11.422	15.898	290.94	4.476
70.00	40.414	932.27	13.318	18.709	377.39	5.391
75.00	45.387	1146.7	15.290	21.667	478.27	6.377
80.00	50.444	1386.3	17.329	24.757	594.28	7.429
85.00	55.560	1651.3	19.427	27.968	726.05	8.542
90.00	60.712	1941.9	21.577	31.290	874.15	9.713
95.00	65.875	2258.4	23.773	34.711	1039.1	10.938
100.00	71.031	2600.7	26.007	38.221	1221.4	12.214
105.00	76.157	2968.7	28.273	41.811	1421.5	13.538
110.00	81.234	3362.2	30.565	45.471	1639.6	14.906
115.00	86.249	3780.9	32.877	49.193	1876.3	16.315
120.00	91.191	4224.5	35.205	52.968	2131.6	17.764
125.00	96.049	4692.7	37.541	56.790	2406.0	19.248
130.00	100.82	5184.9	39.884	60.650	2699.6	20.766
135.00	105.49	5700.7	42.227	64.543	3012.6	22.315
140.00	110.05	6239.6	44.568	68.462	3345.1	23.893
145.00	114.51	6801.0	46.904	72.402	3697.2	25.498
150.00	118.87	7384.5	49.230	76.358	4069.1	27.127
155.00	123.10	7989.5	51.545	80.325	4460.8	28.779
160.00	127.23	8615.4	53.846	84.298	4872.4	30.452
165.00	131.24	9261.6	56.131	88.275	5303.8	32.144
170.00	135.14	9927.6	58.398	92.251	5755.1	33.854
175.00	138.93	10612.	60.645	96.224	6226.3	35.579
180.00	142.60	11316.	62.871	100.19	6717.4	37.319
185.00	146.16	12038.	65.074	104.15	7228.2	39.071
190.00	149.61	12778.	67.253	108.09	7758.8	40.836
195.00	152.95	13534.	69.408	112.02	8309.1	42.611
200.00	156.18	14307.	71.57	115.93	8878.9	44.395
205.00	159.31	15096.	73.640	119.83	9468.4	46.187
210.00	162.35	15900.	75.716	123.70	10077.	47.987
215.00	165.28	16719.	77.765	127.56	10705.	49.792
220.00	168.12	17553.	79.786	131.39	11352.	51.603
225.00	170.87	18400.	81.780	135.20	12019.	53.419
230.00	173.53	19261.	83.746	138.98	12704.	55.238
235.00	176.10	20135.	85.684	142.74	13409.	57.060
240.00	178.60	21022.	87.593	146.48	14132.	58.884
245.00	181.01	21921.	89.475	150.18	14873.	60.709
250.00	183.35	22832.	91.330	153.87	15633.	62.535
255.00	185.62	23754.	93.156	157.52	16412.	64.362
260.00	187.82	24688.	94.956	161.14	17209.	66.188
265.00	189.95	25632.	96.728	164.74	18023.	68.014
270.00	192.01	26587.	98.474	168.31	18856.	69.838

TABLE 3. *Thermodynamic functions for β-lithium hexafluoroaluminate* (Li_3AlF_6) *solid phase*—Continued

T	C_p°	$H_T^\circ - H_0^\circ$	$(H_T^\circ - H_0^\circ)/T$	S_T°	$-(G_T^\circ - H_0^\circ)$	$-(G_T^\circ - H_0^\circ)/T$
273.15	193.28	27194.	99.560	170.55	19390.	70.987
275.00	194.01	27553.	100.19	171.85	19706.	71.661
280.00	195.96	28527.	101.89	175.37	20574.	73.482
285.00	197.84	29512.	103.55	178.85	21460.	75.300
290.00	199.66	30506.	105.19	182.31	22363.	77.115
295.00	201.44	31509.	106.81	185.74	23283.	78.927
298.15	202.53	32145.	107.82	187.88	23871.	80.067
300.00	203.16	32520.	108.40	189.14	24220.	80.736
305.00	204.84	33540.	109.97	192.51	25174.	82.540
310.00	206.47	34568.	111.51	195.85	26145.	84.341
315.00	208.06	35605.	113.03	199.17	27133.	86.137
320.00	209.61	36649.	114.53	202.46	28137.	87.929
325.00	211.12	37701.	116.00	205.72	29157.	89.716
330.00	212.59	38760.	117.46	208.95	30194.	91.499
335.00	214.03	39827.	118.89	212.16	31247.	93.276
340.00	215.43	40900.	120.30	215.34	32316.	95.047
345.00	216.80	41981.	121.69	218.50	33400.	96.814
350.00	218.14	43068.	123.05	221.63	34501.	98.574
355.00	219.45	44162.	124.40	224.73	35617.	100.33
360.00	220.74	45263.	125.73	227.81	36748.	102.08
365.00	222.00	46370.	127.04	230.86	37895.	103.82
370.00	223.23	47483.	128.33	233.89	39056.	105.56
373.15	223.99	48187.	129.14	235.79	39796.	106.65
375.00	224.44	48602.	129.61	236.90	40233.	107.29
380.00	225.62	49727.	130.86	239.88	41425.	109.02

H_0° and S_0° apply to the reference state of the solid at zero K.

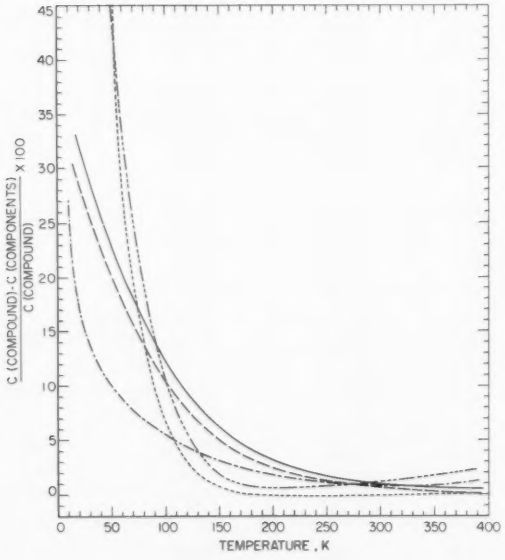

FIGURE 4. *Comparison of the additivity of heat capacities.*

—— $BeO \cdot 3Al_2O_3$ versus $BeO + 3Al_2O_3$
— — $BeO \cdot 3Al_2O_3$ versus $BeO \cdot Al_2O_3 + 2Al_2O_3$
– – – $BeO \cdot Al_2O_3$ versus $BeO + Al_2O_3$
– – – – Li_3AlF_6 versus $3LiF + AlF_3$
– – – – Na_3AlF_6 versus $3NaF + AlF_3$

TABLE 4. *Comparison of enthalpy differences obtained on β-lithium hexafluoroaluminate,* Li_3AlF_6

Temperature interval	This work	Douglas and Neufer [1]	
		Mean observed	Equation [a]
K	*J/mole*	*J/mole*	*J/mole*
273.15 to 323.15	10117	10156	10124
273.15 to 373.15	20994	20964	20996

[a] These values are from an enthalpy equation derived by Douglas and Neufer [1]:

$$H_T^\circ - H_{273.15\,K}^\circ = 64.1398T + 0.0070246T^2 - 13653.13 \log_{10} T + 15{,}220.6 \text{ in cal/mole for the interval 273.15 to 743.15 K.}$$

The authors are grateful to R. E. Thoma and G. M. Hebert of the Oak Ridge National Laboratory for the preparation of the lithium hexafluoroaluminate sample. A number of staff members at the National Bureau of Standards have contributed toward the characterization of the sample. Grateful acknowledgment is made to V. C. Stewart for the spectrochemical analysis, to E. J. Maienthal and P. A. Paulson for the chemical analysis, and to H. E. Swanson for the x-ray analysis.

5. References

[1] Douglas, T. B., and Neufer, J. E., Solid Li_3AlF_6: Thermodynamic Functions from 298° to 1000 °K based on recent measurements of its relative enthalpy at the National Bureau of Standards, Preliminary Report on the Thermodynamic Properties of Selected Light-Element and Some Related Compounds, unpublished report.

[2] Fedotieff, P. P., and Timofeeff, K., Z. anorg. allg. Chem. **206,** 263 (1932).

[3] Rolin, M., and Muhlethaler, R., Bull. Soc. Chim. France, 2593 (1964).

[4] Holm, J. L., Acta Chem. Scand. **19,** 261 (1965).

[5] Garton, G., and Wanklyn, B. M., J. Inorg, Nucl. Chem. **27,** 2466 (1965).

[6] Holm, J. L., Acta Chem. Scand. **20,** 1167 (1966).

[7] Greene, P. D., Gross, P., and Hayman, C., Trans. Faraday Soc. **64,** 633 (1968).

[8] Hoffman, J. I., and Lundell, G. E. F., J. Res. Nat. Bur. Stand. (U.S.), **20,** 607 (1938).

[9] Furukawa, G. T., and Reilly, M. L., J. Res. Nat. Bur. Stand. (U.S.), 74A (Phys. and Chem.), No. 5, 617–629 (Sept.-Oct. 1970).

[10] Furukawa, G. T., Reilly, M. L., and Saba, W. G., Rev. Sci. Instr. **35,** 113 (1964).

[11] United States Department of Commerce, Nat. Bur. Stand. (U.S.), Handb. 102, ASTM Metric Practice Guide (1967) 46 pp.

[12] The International Practical Temperature Scale of 1968, Adopted by the Comité International des Poids et Mesures, Metrologia **5,** 35 (1969).

[13] Williams, A. J., Jr., and Mergner, G. C., IEEE Trans. Instr. Meas. **IM–15,** 121 (1966).

[14] Furukawa, G. T., Automation problems in thermometry and calorimetry, in Netsu, Ondo Sokutei, to Shisanetsu Bunseki, 1969, ed. Y. Otsubo, H. Kanbe, and S. Seki, pp. 1–35, (Kagaku Gijutsu-Sha, Tokyo, 1969).

[15] Westrum, E. F., Jr., Furukawa, G. T., McCullough, J. P., Adiabatic low-temperature calorimetry in Experimental Thermodynamics, Vol. I, Calorimetry of Non-Reacting Systems, ed. J. P. McCullough and D. W. Scott, pp. 133–214 (Butterworths, London, 1968).

[16] Cameron, A. E., and Wichers, E., J. Am. Chem. Soc. **84,** 4192 (1962).

[17] Furukawa, G. T., and Reilly, M. L., J. Res. Nat. Bur. Stand. (U.S.), **69A** (Phys. and Chem.), 5 (1965).

[18] Furukawa, G. T., and Saba, W. G., J. Res. Nat. Bur. Stand. (U.S.), **69A** (Phys. and Chem.), 13 (1965).

[19] Furukawa, G. T., and Saba, W. G., J. Res. Nat. Bur. Stand. (U.S.), **71A** (Phys. and Chem.), 3 (1967).

[20] Furukawa, G. T., and Reilly, M. L., from unpublished tables of thermodynamic properties of LiF, NaF, and AlF_3 based on analysis of literature data.

[21] Burns, J. H., Tennissen, A. C., and Brunton, G. D., Acta Cryst. **B24,** 225 (1968).

(Paper 74A5–626)

JOURNAL OF RESEARCH of the National Bureau of Standards—A. Physics and Chemistry
Vol. 74A, No. 5, September–October 1970

Thermodynamics of Hydrochloric Acid in 80 Weight Percent 2-Methoxyethanol and 20 Weight Percent Water From 10 to 50 °C

Harry P. Thun*, Bert R. Staples, and Roger G. Bates**

Institute for Materials Research, National Bureau of Standards, Washington, D.C. 20234

(June 4, 1970)

Electromotive-force measurements of cells of the type Pt, H_2|HCl(m) in 2-methoxyethanol + H_2O|AgCl, Ag at nine temperatures ranging from 10 to 50 °C were used to derive (a) the standard emf of the cell in 80 weight percent 2-methoxyethanol (methylcellosolve), (b) the activity coefficient of HCl, (c) the relative partial molal enthalpy and heat capacity of HCl, and (d) the thermodynamic constants for the transfer of HCl from water to 80 weight percent methylcellosolve. The molality of the acid ranged from 0.006 to 0.106 mol kg^{-1}. To obtain the standard emf it was necessary to correct for ion-pair formation and to use the extended terms of the Debye-Hückel theory. The standard emf varied with temperature (t, °C) according to the equation $E_t^\circ = 0.14382 - 1.517 \times 10^{-3} t - 3.8317 \times 10^{-6} t^2 - 2.3838 \times 10^{-9} t^3$. Vapor pressures and dielectric constants for this mixture were measured over the temperature range. At 25 °C the solvent has a vapor pressure of 2506.5 Nm^{-2} (18.8 mm Hg) and a dielectric constant of 31.5.

Key words: Activity coefficients; non-aqueous emf; standard emf; thermodynamic constants for HCl transfer.

1. Introduction

As a possible solvent for the determination of stability constants of metal ion complexes, 2-methoxyethanol (methylcellosolve) can be considered as very promising. It not only dissolves numerous organic compounds but also many inorganic salts such as several of the metal perchlorates including sodium perchlorate and the lanthanide perchlorates. Unfortunately, the pure solvent has a rather low dielectric constant (about 2.3 at 25 °C), and it therefore seemed preferable to examine a suitable mixture with water.

Simon et al. [1, 2][1] have already carried out an impressive number of pK determinations for organic acids and bases in a mixture containing 80 wt % 2-methoxyethanol and 20 wt % water. A pH cell with glass electrode and calomel electrode was used. The pH scale in this medium has not been standardized, and consequently the measurements of Simon and his coworkers were based on the aqueous standard buffer solutions. In order to obtain unambiguous results in future electromotive-force studies on complex stabilities and pK values in 80 wt % methylcellosolve, it is necessary to establish a pH scale in this medium. The present study on the thermodynamics of HCl was carried out as a first step toward the establishment of a standard acidity scale in a solvent containing 80 wt % 2-methoxyethanol and 20 wt % water.

Measurements of the emf of the cell

Pt; H_2(g), HCl(m) in 80 wt % 2-methoxyethanol, AgCl; Ag

were made from 10 to 50 °C at intervals of 5 °C and for six molalities of hydrochloric acid in the nominal range of 0.006 to 0.1 mol kg^{-1}. In order to correct the observed emf to the standard 1 atm partial pressure of hydrogen, it was necessary to measure the vapor pressure of the mixed solvent. The evaluation of the standard emf of the cell at each temperature further necessitated measurements of the dielectric constant ϵ and the density ρ_0 of the solvent. The procedure followed for the analysis of the emf data was very similar to the one adopted by Pool and Bates [3].

2. Experimental Procedure

The 2-methoxyethanol was obtained commercially, and gas chromatographic analysis showed the water content to be less than 0.03 percent. No other volatile impurities could be detected, and no further purification was attempted. The mixed solvent was prepared by weighing distilled water and the 2-methoxyethanol.

*On leave 1968–69 from Laboratory for Analytical Chemistry, J. Plateaustraat, 22, Gent, Belgium, 9000.

**Present address: Dept. of Chemistry, University of Florida, Gainesville, Florida 32601.

[1] Figures in brackets indicate the literature references at the end of this paper.

The dielectric constant of the mixed solvent was measured at 10, 25, and 50 °C, using freshly distilled water and spectro-grade acetone as reference materials. The Multi-Dekameter instrument [2] was used for these measurements. The temperature of the cell was adjusted to within 0.1 °C of the nominal temperature of circulating water from a constant-temperature bath. The results are given in table 1.

TABLE 1. *Dielectric constants of the 80 wt % 2-methoxyethanol solvent*

t	ϵ
(°C)	
10	34.7
25	31.5
50	27.8

For the vapor pressure measurements, a flask containing the solvent was immersed in a water bath, the temperature of which was controlled to ±0.01 °C. The flask was connected to a U-tube mercury manometer and the pumping system, which included a mercury diffusion pump. Because 2-methoxyethanol attacks the high-vacuum grease, Teflon stopcocks had to be used.

Before the flask was connected to the vacuum line, the temperature of the solvent was lowered to −72 °C in an ethanol–solid carbon dioxide mixture, so that the evacuation of the system would not cause any change in the composition of the liquid. To avoid condensation of vapors in the manometer, the latter was placed in a controlled air bath with a transparent plastic panel. In this way, the manometer could be kept at 56 °C throughout the measurements. The rest of the apparatus, except for the flask, was wrapped with heating tape and kept at a temperature well above 50 °C. Before starting the measurements, the pressure in the apparatus was reduced below 1 μm Hg. The readings were taken with a cathetometer giving a precision of 0.05 mm Hg.

The measured values for the vapor pressure of the 80 wt percent 2-methoxyethanol solvent under study in the temperature range 10 to 50 °C are given in table 2. They were fitted to the following equation

TABLE 2. *Vapor pressures of the 80 wt % 2-methoxyethanol solvent*

t	Pressure		σ
°C	Nm^{-2}	mm Hg	mm Hg
10	973.3	(7.3)	(0.1)
15	1346.6	(10.1)	(0.2)
20	1813.2	(13.6)	(0.2)
25	2506.5	(18.8)	(0.3)
30	3373.1	(25.3)	(0.2)
35	4479.6	(33.6)	(0.1)
40	5919.5	(44.4)	(0.2)
45	7732.7	(58.0)	(0.4)
50	10052.	(75.4)	(0.6)

[2] Multi-Dekameter, Type MDK–06, Wiss. Techn. Werkstätten, Weilheim, Obb., Germany. Reference to trade name is made only for identification and does not imply in any way the endorsement of the product by the National Bureau of Standards.

$$\log p = 9.061 - \frac{2321.7}{T} \tag{1}$$

by the method of least squares. In this equation, T is the thermodynamic temperature $t(°C) + 273.15$.

The densities of the mixed solvent were measured with a pycnometer. The results are presented in table 3.

TABLE 3. *Density of the 80 wt % 2-methoxyethanol solvent*

t	Density
°C	$g\ cm^{-3}$
10	0.9997
15	.9955
20	.9910
25	.9868
30	.9824
35	.9781
40	.9739
45	.9693
50	.9647

High-purity hydrochloric acid was used to make a stock solution, of molality approximately 0.1 mol kg^{-1}, in the mixed solvent. The hydrochloric acid was tested for the presence of bromide and found to be satisfactory (< 0.002 mole percent). Solutions of six different molalities m were prepared by weighing the stock solution and diluting it with a weighed amount of the mixed solvent.

The design of the cells, preparation of electrodes, purification of the hydrogen gas, and other experimental details have been described previously [4, 5].

The values of the emf were corrected to 1 atm partial pressure of hydrogen and are given in table 4. Each entry in the table represents the average of three replicate cells prepared for each molality of hydrochloric acid. Each cell was measured at all nine temperatures. The lowest and highest emf values for replicate cells differed, at most, by 0.1 mV. The emf at 25 °C was recorded three times, namely, at the beginning, middle, and end of the run. The three values usually agreed within 0.05 mV.

3. Standard Emf of the Cell

The standard emf ($E°$) of the cell used is derived from the measured emf (E) by the Nernst equation:

$$E° = E + (2RT/F) \ln (m\gamma_{\pm}) = E + (2RT/F) \ln (m'\gamma'_{\pm}) \tag{2}$$

where m and $\gamma_{\pm}$ are the stoichiometric molality and mean molal activity coefficient of HCl in the solvent under study, and m' and $\gamma'_{\pm}$ are the actual molality of ionized HCl and the true mean activity coefficient. In a first attempt to derive $E°, \gamma_{\pm}$ was calculated by a form of the Debye-Hückel equation

$$-\log \gamma_{\pm} = \frac{A(m\rho_0)^{1/2}}{1 + B\mathring{a}(m\rho_0)^{1/2}} \tag{3}$$

TABLE 4. *Emf (in volts) of the cell* Pt; H_2 (*g, 1 atm*), HCl (*m*) *in 80 wt % 2-methoxyethanol,* AgCl; Ag

m	Temperature, °C								
	10	15	20	25	30	35	40	45	50
mol kg^{-1}									
0.006012	0.39176	0.38873	0.38550	0.38212	0.37840	0.37471	0.37086	0.36674	0.36240
.010897	.36671	.36333	.35976	.35614	.35221	.34823	.34425	.33991	.33557
.02183	.33804	.33432	.33045	.32650	.32231	.31807	.31365	.30897	.30448
.04213	.31188	.30768	.30353	.29928	.29486	.29028	.28564	.28073	.27575
.07855	.28714	.28283	.27834	.27370	.26888	.26408	.25921	.25411	.24902
.10620	.27509	.27063	.26596	.26131	.25647	.25150	.24641	.24111	.23591

where ρ_0 is the solvent density, $\mathring{a}$ is the ion-size parameter, and the Debye-Hückel constants A and B took into account the temperature and dielectric constant of the solvent. From these $\gamma_\pm$ values, the apparent $E°$ was calculated according to

$$E°' = E° + \beta m = E + (2RT/F) \ln (m\gamma_\pm). \quad (4)$$

Least squares treatment of $E°$ as a function of m permitted extrapolation to zero ionic strength and yielded preliminary values for $E°$. However, straight lines could not be obtained, suggesting that the hydrochloric acid was not completely ionized in the medium under investigation. There were no results available for the ion-pair dissociation constant K_d for HCl in this medium, so an empirical treatment had to be used, as was the case in earlier work in 95 percent ethanol [3].

The following procedure was used. The mean activity coefficient $\gamma_\pm$ was derived from eq (3) and values of m' were calculated for each stoichiometric molality (m) by the equation

$$K_d = \frac{(m'\gamma_\pm)^2}{(m-m')}. \quad (5)$$

A reasonable value of K_d in the range 0.01 to 1.0 was chosen. With these estimates of m', the true molality of dissociated HCl, new values for the $\gamma'_\pm$ "true" activity coefficient were calculated by an extended form of eq (3):

$$-\log \gamma'_\pm = \frac{A(m'\rho_0)^{1/2}}{1 + B\mathring{a}(m'\rho_0)^{1/2}} + \log (1 + 0.002m'\bar{M}) \quad (6)$$

where $\bar{M}$ is the mean molar mass of the mixed solvent (46.273 g mol^{-1}). The $\gamma'_\pm$ so obtained was substituted in a modified form of eq (5)

$$K_d = \frac{(m'\gamma'_\pm)^{1/2}}{(m-m')} \quad (7)$$

and used to obtain a new m'. This iterative procedure was repeated n times, until the difference

$$|\gamma'_{\pm_n} - \gamma'_{\pm_{n-1}}| \leqslant 10^{-5}.$$

From these values of $\gamma_\pm$ and m', $E°$ was calculated by the method of least squares from $E°'$ defined by

$$E°' = E° + \beta m' = E + (2RT/F) \ln (m'\gamma'_\pm). \quad (8)$$

For each value of K_d chosen, a set of $\mathring{a}$ values was used to calculate m', $\gamma'_\pm$, and $E°'$. Decreasing ranges of both K_d and $\mathring{a}$ were selected until values were found that produced the minimum standard deviation of $E°'$ values from a linear function of m'. These were taken to be the true values of K_d and $\mathring{a}$. The resulting intercept ($E°$) of the plot of $E°'$ as a function of m' seemed to vary only a few hundredths of a millivolt with changes in K_d of 0.005 and changes in $\mathring{a}$ of 0.05 Å. The final $E°$ at each temperature is given together with the "best" values of K_d and $\mathring{a}$. Ion-pairing seems to be less extensive in 80 wt % methylcellosolve ($K_d = 0.204$) than in 95 percent ethanol ($K_d = 0.033$ [3]). This conclusion is consistent with the slightly higher dielectric constant and the considerably larger amount of water in the methylcellosolve-water solvent. The standard emf can be represented by the equation

$$E°_t = 0.14382 - 0.001517t - 3.8317 \times 10^{-6}t^2 - 2.3838 \times 10^{-9}t^3 \quad (9)$$

where t is the temperature in °C. Values of $E°$ calculated by eq (9) are also compared with the experimental values in table 5.

TABLE 5. *Summary of results for the standard emf* (E°) *of the cell in 80 wt % 2-methoxyethanol solvent*

t	K_d	($\mathring{a}$)	$E°$	[a]σ_d	$E°$ calc.[b]	$\Delta E°$
°C			*V*	*mV*		*mV*
10	0.366	4.59	0.12822	0.04	0.12827	0.05
15	.306	4.79	.12027	.04	.12019	.08
20	.227	4.73	.11192	.03	.11193	.01
25	.204	4.60	.10353	.04	.10344	.09
30	.130	4.60	.09466	.08	.09479	.13
35	.116	4.37	.08589	.08	.08592	.03
40	.089	4.36	.07693	.10	.07685	.08
45	.071	4.41	.06763	.10	.06757	.05
50	.058	4.21	.05804	.17	.05808	.04

[a] Standard deviation of $E°$.
[b] By eq (9).

TABLE 6. *Stoichiometric mean activity coefficient ($\gamma_\pm$) of hydrochloric acid in 80 wt % 2-methoxyethanol from 10 to 50 °C*

t	m(HCl), mol kg^{-1}					
	0.006012	0.010897	0.02183	0.04213	0.07855	0.10620
°C						
10	0.751	0.692	0.621	0.551	0.490	0.464
15	.747	.687	.615	.545	.482	.456
20	.740	.679	.606	.535	.472	.446
25	.735	.672	.598	.526	.464	.437
30	.728	.663	.587	.514	.454	.425
35	.723	.656	.578	.506	.444	.416
40	.717	.648	.570	.496	.434	.407
45	.711	.640	.561	.487	.424	.398
50	.704	.629	.548	.476	.413	.386

4. Thermodynamic Properties of Hydrochloric Acid

With the aid of eq (2) and the stoichiometric molalities, the stoichiometric activity coefficients $\gamma_\pm$ were derived from $E°$ and the measured values of E. These values are shown in table 6. For each molality, log $\gamma_\pm$ was fitted to a power series of the form

$$-\log \gamma_\pm = A + BT + CT^2 \qquad (10)$$

where T is the thermodynamic temperature, t(°C) +273.15.

The constants of this equation are given in table 7, together with the standard deviations of the calculated values of log $\gamma_\pm$.

TABLE 7. *Constants of the eqation* $-\log \gamma_\pm = A + BT + CT^2$

m	A	$B \times 10^3$	$C \times 10^6$	$\sigma \times 10^3$
mol kg^{-1}				
0.006012	0.195708	−1.0828	2.9359	0.5
.010897	.518064	−3.2864	7.1346	.4
.02183	.41377	−2.5559	6.4359	.9
.04213	.409875	−2.4130	6.6281	1.0
.07855	.675343	−4.0528	9.7507	0.5
.10620	.402071	−2.2042	6.9208	.8

The relative partial molal enthalpy $\bar{L}_2$ and the relative partial molal heat capacity $\bar{J}_2$ of hydrochloric acid in the medium studied were calculated from the constants B and C of eq (10) by the following formulas:

$$\bar{L}_2 = (2RT^2 \ln 10)(B + 2CT) \qquad (11)$$

and

$$\bar{J}_2 = (4RT \ln 10)(B + 3CT). \qquad (12)$$

The values obtained for $\bar{L}_2$ at 10, 25, and 50 °C and for $\bar{J}_2$ at 25 °C are summarized in table 8.

The standard thermodynamic quantities for the transfer process

TABLE 8. *Relative partial molal enthalpy ($\bar{L}_2$) and relative partial molal heat capacity ($\bar{J}_2$) of hydrochloric acid in 80 wt % 2-methoxyethanol*

t	m (HCl), mol kg^{-1}					
	0.006012	0.010897	0.02183	0.04213	0.07855	0.1062
	$\bar{L}_2$, J mol^{-1}					
10	1780	2315	3342	4115	4509	5121
25	2273	3295	4363	5239	5995	6519
50	3257	5297	6412	7480	8992	9307
	$\bar{J}_2$, J K^{-1} mol^{-1}					
25	35	71	73	80	107	100

HCl (in H_2O) = HCl (in 80 wt % 2-methoxyethanol-20 wt % water)

can be derived from the standard emf ($E°$) of the cell in water [6] and in 80 wt % 2-methoxyethanol together with the variation of $E°$ with temperature. From eq (9) the standard Gibbs energy of transfer ($\Delta G_t°$) is found to be

$$\Delta G_t° = -31338.1 + 254.465T - 0.607549T^2 + 7.90581 \times 10^{-4}T^3 \qquad (13)$$

and

$$\Delta S_t° = +254.465 - 1.21510T + 2.37174 \times 10^{-3}T^2 \qquad (14)$$

while

$$\Delta H_t° = \Delta G_t + T\Delta S_t°. \qquad (15)$$

For 25 °C the thermodynamic functions for the transfer of HCl have the following values:

$$\Delta G_t° = 11477.0 \text{ J mol}^{-1}$$

$$\Delta S_t° = -103.0 \text{ JK}^{-1} \text{ mol}^{-1}$$

$$\Delta H_t° = -19237.0 \text{ J mol}^{-1}$$

The large positive value for the transfer free energy suggests that the affinity of 2-methoxyethanol for HCl is less than that of water, or, in other words, that water is the more basic component of the solvent mixture. In view of the structural changes characteristic of alcohol-water mixtures [7], however, judgments of this sort must be made with caution.

5. References

[1] Simon, W., Meuche, D., and Heilbronner, E., Helv. Chim. Acta **39**, 290 (1956).

[2] Simon, W., Mörikofer, A., and Heilbronner, E., Helv. Chim. Acta **40**, 1918 (1957).

[3] Pool, K. H., and Bates, R. G., J. Chem. Thermodynamics **1**, 21 (1969).

[4] Bates, R. G., Determination of *pH*, Ch. 9 and Appendix (John Wiley & Sons, New York, N.Y., 1964).

[5] Gary, R., Bates, R. G., and Robinson, R. A., J. Phys. Chem. **68**, 1186 (1964).

[6] Bates, R. G., and Bower, V. E., J. Res. Nat. Bur. Stand. (U.S.) **53**, 283 (1954).

[7] Franks, F., and Ives, D. J., Quart. Rev. **20**, 1 (1966).

(Paper 74A5–627)

JOURNAL OF RESEARCH of the National Bureau of Standards—A. Physics and Chemistry
Vol. 74A, No. 5, September–October 1970

Vapor Pressure and Heat of Sublimation of Platinum

E. R. Plante, A. B. Sessoms, and K. R. Fitch

Institute for Materials Research, National Bureau of Standards, Washington, D.C. 20234

(May 21, 1970)

The vapor pressure of platinum was measured by the Langmuir method in the temperature range 1700–2000 K using a vacuum microbalance. Eight series of data gave concordant results and an average third-law heat of sublimation of 564.49 kJ mol^{-1} with an estimated overall uncertainty of 2.1 kJ mol^{-1} (134.92 ± 0.5 kcal mol^{-1}). Three out of eight second-law heats agreed with the third-law heats within one standard error but there was a tendency for second-law heats to be low. This was attributed to small systematic errors in the measurements. A vapor-pressure equation representing the data is $\log P(\text{atm}) = -29020/T + 7.502$, based on our third-law heat and tabulated entropies evaluated at 1800 K. Our data agree well with several previous Langmuir determinations but significantly decrease the error in the heat previously accepted.

Inability to obtain saturation pressures at lower temperatures, previously reported in the literature, was confirmed. It was shown that microgram quantities of carbon are capable of blocking the sublimation reaction.

Key words: Heat of sublimation; Langmuir vaporization; platinum; rate of vaporization; vapor pressure.

1. Introduction

This study was undertaken as part of an NBS contribution to a program involving the measurement of vapor pressures of selected standard materials in various cooperating laboratories. The object of these measurements is to determine reliable standard vapor pressure data and to reveal, if possible, any systematic differences in vapor pressures which might be attributable to different methods of measurement. Data leading to vapor pressures or heats of sublimation of platinum have been reported by a number of investigators [1–10][1] using several methods of measurement over a wide temperature range. Results from some of these data are listed in table 2 and comments on these studies are reserved for section 4 of this paper.

2. Experimental Method

Data were obtained by Langmuir rate of sublimation measurements using a vacuum microbalance. Techniques and procedures were similar to those used previously [11]. Vacuum in the range of 10^{-7} to 10^{-9} torr was maintained and indicated by a commercial sputter-ion pump. Preliminary data were obtained using Standard Reference Material, SRM 680, but this material is not generally available in a convenient form for Langmuir measurements. Later measurements were made on SRM 747 stock which will be certified as a vapor-pressure standard. Samples were machined from the stock materials, both of about five 9's purity, into right circular cylinders having nominal diameters of 0.25 or 0.20 cm and lengths of 1.9 cm. A hole 0.1 cm in diameter and 1.5 cm long, assumed to represent blackbody conditions, was drilled along the cylinder axis and a suspension hole 0.025 cm in diameter was drilled along a diameter about 0.20 cm from the other end. Machining was accomplished by ordinary machining methods using oil cutting fluid on the 0.25-cm-diam samples except that designated SRM 747–17, which was machined using oil-free tools and trichloroethylene cutting fluid. The blackbody hole of the 0.20-cm sample was machined by arc erosion. Samples machined using oil cutting fluids were rinsed in acetone or ethanol to remove any residual traces of oil. However, this procedure was not effective, as two of the three samples treated in this way gave evidence of contamination as discussed later.

The sample was suspended from one arm of an equal-arm quartz beam microbalance by a chain of 0.025-cm-diam sapphire or quartz rods connected together by V-shaped hooks made by heating and bending the rods. The lower 10 cm of the suspension was 0.0075-cm platinum wire, which passed through the suspension hole in the samples and over the hook on the lowest suspension rod.

The appendage of the vacuum chamber in which the sample hung was a 22-mm o.d. Vycor[2] tube made with a fused silica window at the bottom. The window could be protected during sublimation experiments with a magnetically actuated shutter. The shutter was used to

[1] Figures in brackets indicate the literature references at the end of this paper.

[2] Reference to trade names is made only for completeness of description and does not imply in any way the endorsement of the product by the National Bureau of Standards.

protect the window during the first three experiments but was not used during the remaining five. For our experimental arrangement it was found that the increase in the window correction factor was not significantly greater when the shutter was not used than when it was. This is because the shutter must be kept open for a large fraction of the time during short experiments when the rate of sublimation is highest. Data were designated as belonging to a new experimental series when new window and/or mirror correction values were determined, when a different observer made temperature measurements, when the sample was changed, or when a combination of these changes was made.

Prior to experiments, a thin platinum coating which did not heat inductively was deposited on the interior surface of the Vycor tube and a grounding device consisting of a split circular stainless steel ring, about 1 cm wide and having a magnetically actuated wire hinge, was inserted into the Vycor tube so that it made contact with the platinum coating. The Vycor tube was connected to the system by means of a standard taper joint using Apiezon W sealant. A wire connected the grounding device to an electrical ground. With the sample in place, the hinge of the grounding device could be magnetically deflected until it made contact with the wire supporting the sample. This allowed for removal of any static charge generated during the high-temperature heating. Heating was accomplished by induction at 450 kHz. The metal sample served as its own susceptor.

Temperatures were measured with an NBS-calibrated optical pyrometer through a calibrated window and mirror. Calibration corrections for the window and mirror were determined in separate experiments using a band lamp. Corrections were determined in terms of "A" values where $A = (1/T) - (1/T_w)$; T is the brightness temperature in Kelvins of the source; and T_w is the brightness temperature of the source with the window or mirror in the optical path. Window corrections were determined before and after each series of measurements and the average value accepted. Mirror corrections were determined less frequently; an average of two independent sets of determinations was used.

In obtaining each datum point the following sequence of operations was followed: (1) the rest point of the balance was determined, (2) the sample was heated to a temperature about 100 K below the lowest temperature where vapor pressure measurements were practicable, (3) the power of the oscillator was adjusted to a predetermined setting and held constant, (4) the power was turned off, (5) the sample and platinum coating on the Vycor sleeve were grounded, and (6) the rest point of the balance was redetermined.

The mass change of the sample was determined from the displacement of the beam of the microbalance and the previously determined sensitivity, which was about 0.5 μg/μm. The change in sensitivity with load is sufficiently small so that the weight change during a series of experiments (about 2 mg) has negligible effect on it. Data during these experiments were obtained with two different but similar balances. One was gold plated and had been used for previous experiments. The second was unplated and had slightly higher sensitivity. Both balances exhibited excellent zero-point stability in contrast to some previous drift problems [11]. This is attributed to a more nearly constant ambient temperature at our new NBS facility, use of a narrower slot on the kinematic table which supported the gold-plated balance, and the grounding procedure which eliminates static charge on the sample and its surroundings.

Initial time for an experiment was taken when the brightness of the blackbody hole matched the preset brightness of the pyrometer filament set for a temperature 50 K or so below the expected temperature for a particular power setting. Final time was taken as the time the power was turned off. The first temperature measurement was usually obtained within the first minute of the experiment, at which time the sample had attained its ultimate temperature. This method of determining the duration of the experiment represents a slight change from our previous practice and was made because the rate of heating is slower than the rate of cooling. Qualitatively, the time required to heat from the base temperature to the operating temperature is inversely proportional to the temperature difference between them. For low-temperature runs the length of time to go from the base temperature to 50 K below the operating temperature would be about 15 s, while for high-temperature runs about 3 s would be required. We believe that systematic error resulting from this approximation is small.

Some difficulties were encountered in achieving linear log P versus $1/T$ relationships in two of the platinum samples which had been exposed to oil during the machining process. These samples exhibited the same type of behavior as described by Hampson and Walker [4] with platinum and by Carrera et al. with ruthenium [12]; that is, below about 1800 K the apparent vapor pressure deviated negatively from the normal curve. This behavior is apparently due to carbon contamination as a result of pyrolysis of oil residue introduced during machining, since a sample of the same reference material did not exhibit this behavior when machined using trichloroethylene cutting fluid. In addition, after the sample showing abnormal behavior was heated in air it gave normal vapor-pressure measurements. Finally, after the vapor-pressure measurements were completed, the 0.25-cm sample 747–15, which weighed 1.74 g, was heated in contact with graphite powder at 1735 K for half an hour. During this process it gained 72 μg. Microscopic examination of the sample at 75× showed a uniform darkening of the surface. Attempts at measuring the vapor pressure of this sample showed complete blocking of the vaporization process at temperatures up to 1860 K, while at 1900 K and above, the vaporization rate was normal. Measurements in the transition range were not very satisfactory because the sample temperature tended to increase or decrease at constant power setting. This behavior differs greatly from that of a pure sample, whose temperature would remain constant within a few degrees. These observations would seem to indi-

cate that the carbon contamination stays close to the surface of the sample and that the extent of diffusion into the sample during the measurements is negligible. We can speculate that above the transition temperature the rate of sublimation is normal because the carbon is dissolved by the platinum and the rate of platinum diffusion through the solution is high, while below the transition temperature, the carbon would precipitate, and the rate of platinum diffusion through the carbon would be low.

3. Data and Thermodynamic Treatment

Vapor pressures were calculated using the equation [3]

$$P=\frac{m}{\alpha a t}\left(\frac{2\pi RT}{M}\right)^{1/2} \tag{1}$$

where m is the mass of material sublimed, t is the duration of the experiment, a is the projected surface area of the sample, T is the absolute temperature on the 1968 IPTS [13], R is the gas constant, M is the atomic weight of the vaporizing species, monatomic platinum, and α is the vaporization coefficient which we assumed is equal to unity. The value of the sample area at temperature, A_T, was calculated using the equation

$$A_T=A_R[1+2\beta(T-300)]$$

where A_R is the area calculated from measurements made at room temperature and β is the linear thermal expansion coefficient. For platinum, β was taken to be 11.3×10^{-6} K^{-1}. This correction amounts to an increase in the surface area at temperature of 2 to 4 percent.

Sample areas at room temperature for the various samples were 1.60 cm^2, 1.64 cm^2, 1.64 cm^2, and 1.27 cm^2 for the platinum SRM 747 I through IV series, respectively, and 1.64 cm^2 for the platinum SRM 680 data.

A linear equation was fitted to the data by least squares solution of the approximate integrated form of the Clausius-Clapeyron equation

$$\log P(\text{atm})=-\frac{\Delta H^\circ}{R'T}+\frac{\Delta S^\circ}{R'} \tag{2}$$

where ΔH° and ΔS° are the heat and entropy changes at an average temperature and R' is $R\ln 10$.

In addition, third-law heats of sublimation were calculated using the equation

$$\Delta H^\circ_{298}=T\left[\Delta-\left(\frac{G^\circ_T-H^\circ_{298}}{T}\right)-R\ln P(\text{atm})\right] \tag{3}$$

where $\Delta-\left(\frac{G^\circ_T-H^\circ_{298}}{T}\right)$ is the difference in free-energy functions of product and reactant. Free-energy function data for platinum were from Hultgren et al. [14]. Finally, accurate second-law heats and entropies were obtained using a method suggested by Horton [15] which is similar to Cubicciotti's method [16]. This consists of fitting by least squares $\Delta-\left(\frac{G^\circ_T-H^\circ_{298}}{T}\right)-R\ln P$ versus $1/T$ and allowing for non-zero intercept. The slope corresponds to an accurately adjusted second-law heat, while the intercept corresponds to ΔS°_{298} (3d law) $-\Delta S^\circ_{298}$ (2d law). To show this, add and subtract each of the quantities $\Delta(H^\circ_T-H^\circ_{298})/T$ and $\Delta(S^\circ_T-S^\circ_{298})$ from the negative of eq (2). Combining appropriate terms, the result is

$$-R\ln P=\frac{\Delta H^\circ_{298}(2)}{T}+\Delta\left(\frac{H^\circ_T-H^\circ_{298}}{T}\right)-\Delta S^\circ_{298}(2)-\Delta(S^\circ_T-S^\circ_{298}), \tag{4}$$

which is equivalent to Cubicciotti's [16] eq (4) or Horton's [15] eq (22). Here, the (2)'s and (3)'s following heats or entropies are used to designate second-law or third-law values. The quantity $\Delta(S^\circ_T-S^\circ_{298})-\Delta(H^\circ_T-H^\circ_{298})/T$ equals $\Delta-(G^\circ_T-H^\circ_{298})/T-\Delta S^\circ_{298}(3)$. Therefore, collecting temperature-dependent terms, we can write

$$-R\ln P+\Delta-\left(\frac{G^\circ_T-H^\circ_{298}}{T}\right)=\Delta S^\circ_{298}(3)-\Delta S^\circ_{298}(2)+\frac{\Delta H^\circ_{298}(2)}{T}. \tag{5}$$

By subtracting the intercept from $\Delta-(G^\circ_{298}-H^\circ_{298})/T=\Delta S^\circ_{298}$ (3d law), we can also obtain ΔS°_{298} (2d law). The convenience of this method results from the fact that the $\Delta-(G^\circ_T-H^\circ_{298})/T-R'\log P$ terms are used in evaluating the third-law heats so that the data necessary for calculating an accurate second-law heat are already available. This method gives the same results as that described by Cubicciotti [16]. We should note also that the difference between the third-law entropy and the second-law entropy is a constant and is independent of temperature. The second-law entropy can, therefore, be determined at any temperature by subtracting the intercept from ΔS°_T (3d law). We have, however, chosen to evaluate the second-law entropy at 298 K for convenience.

4. Results

Basic data used in the calculation, the vapor pressures, and individual third-law heats are listed in table 1. Table 2 lists the average second-law heat and entropy change at 298.15 K and their standard errors, the coefficients of eq (2) and their standard errors, the standard deviation in the pressure in log units, and the average third-law heat and its standard error for each series of data. The mean third-law heat, calculated as the average of the means for each run, is 564.49 kJ mol^{-1} (134.92 kcal mol^{-1}).

The overall uncertainty in this value is estimated to be ±2100 J mol^{-1} (±0.5 kcal mol^{-1}). This is calculated using an uncertainty in the pyrometer calibration

[3] Values of constants used in the equation were: $R=8.3143$ J mol^{-1} K^{-1} or 1.98717 cal mol^{-1} K^{-1}, atomic weight of platinum = 195.09; one standard atmosphere = 101.325 Nm^{-2}

389-821 O - 70 - 3

TABLE 1. *Compilation of platinum data* [a]

VAPOR PRESSURE OF PLATINUM SRM 680 .25 CM. SAMPLE SERIES I

Temp.	Time	Wgt. loss	Pressure		ΔH°_{298}	ΔH°_{298}
Kelvins	*seconds*	*micrograms*	*atmospheres*		*cal/mol*	*J/mol*
1809	1500	112	2.98	E−9	134796	563987
1781	2100	74.2	1.40	E−9	135416	566580
1866	900	168	7.57	E−9	135521	567018
1735	6600	95	5.64	E−10	135106	565285
1835	1200	133	4.46	E−9	135234	565817
1777	3000	102	1.35	E−9	135245	565865
1852	900	130	5.84	E−9	135475	566826
1821	1200	97.6	3.26	E−9	135352	566312
1704	7200	54.6	2.95	E−10	134922	564515
1675	10800	38.5	1.37	E−10	135210	565718
1909	300	135	1.84	E−8	135221	565767
1902	240	83.8	1.43	E−8	135688	567719
1807	1500	93.6	2.49	E−9	135294	566072
1978	180	210	4.86	E−8	136192	569826
1978	180	284	6.57	E−8	135007	564868
1759	3600	73.7	8.08	E−10	135690	567729
1945	210	190	3.74	E−8	134979	564751
1930	210	148	2.90	E−8	134935	564566
1752	4800	104	8.53	E−10	134970	564714
1802	1800	113	2.50	E−9	134911	564469
1697	9000	68.1	2.94	E−10	134387	562276
1875	600	136	9.21	E−9	135433	566652
1748	4800	81.3	6.66	E−10	135526	567041
1951	210	194	3.82	E−8	135305	566114

VAPOR PRESSURE OF PLATINUM SRM 680 .25 CM. SAMPLE SERIES II

1823	1200	111	3.71	E−9	135030	564964
1949	150	182	5.02	E−8	134111	561119
1755	2400	57.1	9.38	E−10	134866	564281
1879	600	162	1.10	E−8	135054	565067
1700	9000	65.3	2.82	E−10	134762	563846
1790	1800	89.3	1.97	E−9	134875	564315
1838	900	116	5.19	E−9	134898	564411
1727	7200	88.4	4.80	E−10	135046	565033
1908	240	115	1.96	E−8	134912	564474

VAPOR PRESSURE OF PLATINUM SRM 680 .25 CM. SAMPLE SERIES III

1833	1200	139	4.66	E−9	134929	564541
1882	600	163	1.11	E−8	135232	565813
1906	240	105	1.79	E−8	135117	565331
1939	210	169	3.32	E−8	135030	564965
1841	900	128	5.73	E−9	134752	563803
1827	1200	105	3.51	E−9	135523	567027
1692	9000	56.8	2.45	E−10	134610	563207
1781	2100	83.6	1.58	E−9	134988	564789
1732	7200	102	5.55	E−10	134932	564554

VAPOR PRESSURE OF PLATINUM SRM 680 .25 CM. SAMPLE SERIES IV

1933	180	130	2.98	E−8	135036	564989
1833	1200	132	4.42	E−9	135121	565347
1903	300	132	1.80	E−8	134888	564371
1822	2400	246	4.11	E−9	134586	563108
1753	3600	86.5	9.46	E−10	134685	563524
1699	10800	70.5	2.53	E−10	135051	565052
1873	900	256	1.16	E−8	134432	562464
1817	1500	130	3.47	E−9	134834	564143
1797	2400	153	2.54	E−9	134486	562690
1733	7200	108	5.88	E−10	134810	564043

TABLE 1. *Compliation of platinum data* [a] — Continued

VAPOR PRESSURE OF PLATINUM SRM 747–15 .25 CM. SAMPLE SERIES I

1864	600	114	7.89	E–9	135224	565778
1912	240	114	2.00	E–8	135113	565313
1806	1800	121	2.75	E–9	134864	564272
1698	10800	70.9	2.61	E–10	134867	564284
1750	4800	96.8	8.14	E–10	134981	564760
1932	180	130	3.05	E–8	134878	564329
1837	1200	158	5.43	E–9	134660	563419
1781	2700	116	1.75	E–9	134626	563276
1726	7200	94.4	5.26	E–10	134655	563398
1890	300	107	1.49	E–8	134692	563552

VAPOR PRESSURE OF PLATINUM SRM 747–17 .25 CM SAMPLE SERIES II

1936	180	164	3.76	E–8	134346	562105
1854	1200	216	7.28	E–9	134807	564031
1823	1800	176	3.92	E–9	134830	564130
1794	2700	150	2.21	E–9	134761	563841
1889	480	174	1.48	E–8	134647	563365
1726	7200	88.5	4.81	E–10	134962	564681
1780	3600	150	1.65	E–9	134760	563836
1748	5400	113	8.23	E–10	134791	563965
1932	180	120	2.75	E–8	135275	565993
1706	10800	89.4	3.22	E–10	134781	563926
1930	180	139	3.18	E–8	134581	563087

VAPOR PRESSURE OF PLATINUM SRM 747–17 .25 CM. SAMPLE SERIES III

1869	600	143	9.67	E–9	134826	564110
1836	1200	159	5.33	E–9	134656	563400
1731	5400	78.7	5.71	E–10	134757	563824
1924	180	117	2.67	E–8	134839	564168
1781	2700	113	1.66	E–9	134813	564058
1807	1800	123	2.73	E–9	134964	564689
1701	10800	93.4	3.36	E–10	134248	561695
1903	300	139	1.90	E–8	134683	563516
1963	120	156	5.39	E–8	134777	563905
1753	3600	80.7	8.83	E–10	134925	564528

VAPOR PRESSURE OF PLATINUM SRM 747–15 .20 CM. SAMPLE SERIES IV

1925	240	111	2.46	E–8	135221	565767
1830	1800	150	4.32	E–9	134987	564784
1876	600	115	1.01	E–8	135160	565510
1780	3000	93.6	1.60	E–9	134869	564291
1945	180	119	3.52	E–8	135202	565686
1800	1800	87.8	2.51	E–9	134749	563792
1894	360	104	1.52	E–8	134898	564411
1708	10800	67.1	3.12	E–10	135044	565025
1746	7200	112	7.90	E–10	134781	563924
1858	900	127	7.37	E–9	135048	565039

[a] Data are listed in experimental sequence.

of ±5 K, an uncertainty in the window and prism correction of ±4 K, and three standard errors in the mean third-law heat. This estimation neglects two possible sources of systematic error about which little is known; namely, deviation of the blackbody hole from blackbody conditions, and temperature inhomogeneity of the sample. Error in the third-law heat resulting from errors in the free-energy function data is considered negligible.

The average third-law heats for each series of measurements are reasonably consistent within the expected error limits. There is a tendency for second-law heats and entropies to be lower than the respective third-law values, but the significance of this is questionable.

TABLE 2. *Derived quantities for platinum* [a]

Source	Second-Law Values									Third-Law Values	
	ΔH°_{298}	[b] S.E.	[c] ΔS°_{298}	S.E.	$-\Delta H^\circ_T/R'$	S.E.	$\Delta S^\circ_T/R'$	S.E.	[b] S.D. (log P)	ΔH°_{298}	S.E.
	kJ mol^{-1}	*kJ mol*$^{-1}$	*J mol*$^{-1}$*K*$^{-1}$	*J mol*$^{-1}$*K*$^{-1}$	*K*	*K*				*kJ mol*$^{-1}$	*kJ mol*$^{-1}$
SRM 680 I	555.20	6.16	144.85	3.38	28520	321	7.189	0.176	0.042	565.85	0.31
SRM 680 II	553.82	4.77	144.66	2.63	28457	254	7.184	.140	.018	564.78	.26
SRM 680 III	552.48	5.09	144.07	2.79	28393	264	7.156	.145	.018	564.56	.27
SRM 680 IV	564.76	8.62	151.11	4.76	29034	454	7.524	.250	.031	563.97	.32
SRM 747–15 I	558.56	6.41	147.56	3.53	28710	335	7.338	.185	.025	564.24	.27
SRM 747–17 II	568.25	6.39	153.06	3.50	29208	334	7.621	.183	.027	563.91	.29
SRM 747–17 III	557.23	6.11	147.09	3.35	28629	316	7.307	.174	.025	563.79	.26
SRM 747–15 IV	554.95	4.67	145.30	2.55	28514	247	7.216	.135	.017	564.82	.22
Mean, This Work										564.49	.24
Jones et al. [2]	537.51	26.37	135.99	14.12	27564	1385	6.708	.742	.131	565.13	1.71
D & M [3]	606.45	32.31	173.95	18.81	31285	1683	8.759	.980	.118	566.38	1.36
H & W [4]	539.54	23.40	137.60	11.71	27571	1220	6.742	.611	.051	565.71	0.46
NSB [6]	536.97	17.20	.....	.....	27518	896	.....	.....	.....	.....	.....
P & A [7] (s)	536.29	25.15	133.53	12.69	27411	1311	6.534	.662	.040	570.30	.45
P & A [7] (l)	582.93	14.56	156.14	6.56	28684	760	7.147	.342	.039	570.79	.44
Koch et al., 1 [9]	617.04	26.95	176.74	11.97	30433	1406	8.208	.624	.094	558.11	1.64
Koch et al., 1A [9]	601.94	23.32	169.01	10.46	29653	1219	7.808	.547	.119	560.87	1.43

[a] All temperatures were converted to the 1968 IPTS.
[b] S.E.=standard error: S.D.= standard deviation.
[c] Based on tabulated data, $\Delta S^\circ_{298} = 150.68$ J mol^{-1}K^{-1}.

This could be understood in terms of a non-unit evaporation coefficient or error in the free energy function data for $Pt(s)$, but it is more likely that small systematic errors in our measurements are responsible. Specifically, the method of establishing the duration of each experiment could lead to larger negative deviations in the observed pressure as the time of an experiment is shortened. However, such systematic error, if it occurred, cannot be seen in the present data, possibly because of insufficient precision.

One set of data, series I on SRM 747, shows a trend in the third-law heats and residuals with order of experiment which could be indicative of a changing "A" value of the window during the series. However, measurements showed a "normal" increase of about 10 percent in the "A" value, which corresponds to a change in temperature of about 1° at 1800 K. To remove the trend in residuals, the "A" value would have had to change systematically by about 70 percent during the experiments. Several other possibilities to account for trend could be put forward but discussion of this point seems futile. The data for this series are normal in that they give heats and entropies in good agreement with the other series but are abnormal because of the trend in third-law heats and residuals.

Below the melting point, the vapor pressure of platinum can be adequately represented by the equation

$$\log P(\text{atm}) = -\frac{29020}{T} + 7.502,$$

which is based on our mean third-law heat and tabulated entropies evaluated at 1800 K. At 1500 K, an accurately calculated vapor pressure will deviate from the pressure predicted by this equation by only 3 percent. The poorest agreement with this equation occurs in the SRM 680 III data. At 1600 and 2000 K, the approximate temperature extremes for this series, the least squares equation representing the SRM 680 III data gives pressures deviating by + 10 percent and − 10 percent, respectively. In terms of temperature this corresponds to an error of +5° at 1600 and −5° at 2000 K.

Table 2 also contains some derived quantities obtained from other studies. These data were reevaluated after conversion of temperature scales to the 1968 IPTS. This increased the average third-law heats by approximately 800 J and had negligible effect on second-law heats. Data rejected by the original authors were also rejected in our calculations. Second-law heats based on the data of Dreger and Margrave [3] and Norman, Staley, and Bell [6] differed significantly from those reported. However, it was not clear that their reported second-law heats were evaluated by least squares.

Data obtained by Langmuir sublimation studies include the original work of Langmuir and Mackay [1] corrected by Jones, Langmuir, and Mackay [2]; Dreger and Margrave [3]; and Hampson and Walker [4]. A preliminary analysis of Hampson and Walker's data was also published by Diamond et al. [5]. These three studies give average third-law heats in substantial agreement with our data. Some mass spectrometric Knudsen effusion data were presented by Norman, Staley, and Bell [6], who reported a second-law heat in fair agreement with the Langmuir data. Peleg and Alcock [7] carried out some torsion Langmuir and torsion Knudsen experiments. Their data were

published only in graphical form but evaluation of the graphical data indicates pressures lower by roughly 40 percent at 2000 K than those obtained in the classical Langmuir experiments. This difference was attributed by Peleg and Alcock to errors arising in determining the duration of the experiment in the classical Langmuir experiments. They argue that weight losses occurring during the preheating and cooling cycles, as well as outgassing of the sample during the experiment, lead to high pressures. However, errors of this magnitude resulting from measurement of the duration of the experiment or outgassing are unlikely. A systematic difference in temperature measurement of about 20 K would account for the difference in measured pressures. Errors of this magnitude are frequently encountered and the arrangement used by Peleg and Alcock, which consisted of sighting an optical pyrometer on the surface of a specimen heated by radiation, can lead to significant errors in either direction depending on the geometric relationship of heater to specimen and the emittance of the specimen. Very high temperature measurements in the range 3400 to 3900 K were reported by Falk [8], who used a shock tube technique. These measurements yielded pressures agreeing within a factor of two with extrapolated pressures based on the classical Langmuir experiments. This agreement is excellent considering the length of the extrapolation, the extremely high temperatures, and the complexity of the experimental method. However, these data are subject to greater interpretive error than those of the simpler experiments and no attempt has been made to derive thermodynamic quantities from them. Recent Langmuir measurements carried out on molten platinum by Koch et al. [9] by a novel technique give average third-law heats somewhat below our average third-law heat. However, lack of knowledge of the emittance of molten platinum as a function of temperatures makes their result relatively unreliable. Finally, some rate of vaporization data by Rytvin and Ulybysheva [10] were noted but were too fragmentary to be considered further.

In summary, our data give good agreement with those of three previous Langmuir determinations. The major contribution of our data is that they significantly decrease the error in the heat previously accepted, primarily because of improved precision. Unanswered questions remain concerning the effect and importance of temperature gradients in our sample, extent of deviation from blackbody conditions in the blackbody sight hole, and whether or not apparent systematic errors are experimental artifacts or are properties of platinum. Questions of this sort can be answered only by systematic studies which yield improved precision.

5. References

[1] Langmuir, I., and Mackay, G. M. J., Phys. Rev. **4**, 377 (1914).
[2] Jones, H. A., Langmuir, I., and Mackay, G. M. J., Phys. Rev. **30**, 201 (1927).
[3] Dreger, L. H., and Margrave, J. L., J. Phys. Chem. **64**, 1323 (1960).
[4] Hampson, R. F., Jr., and Walker, R. F., J. Res. Nat. Bur. Stand. (U.S.), **65A** (Phys. and Chem.), 289 (1961).
[5] Diamond, J. J., Efimenko, J., Hampson, R. F., and Walker, R. F., Reactivity of Solids, Proc. Fourth Intern. Symp. Reactivity of Solids, Amsterdam, 1960, J. H. deBoer et al., eds. (Elsevier Publ. Co., Amsterdam, The Netherlands).
[6] Norman, J. H., Staley, H. G., and Bell, W. E., J. Phys. Chem. **71**, 3686 (1967).
[7] Peleg, M., and Alcock, C. B., J. Sci. Inst. **43**, 558 (1966). For a larger graph of the Pt data see also Bulletin de la Societé Française de Ceramique Nr. 72 (1966).
[8] Falk, T. J., J. Chem. Phys. **49**, 3727 (1968); also, J. Chem. Phys. **48**, 3305 (1968).
[9] Koch, R. K., Calvert, E. D., Thomas, C. R., and Beall, R. A., U.S. Bur. Mines RI 7271 (1969).
[10] Rytvin, E. I., and Ulybysheva, L. P., Izv. Akad. Nauk SSSR, Metal [1], 247 (1969).
[11] Plante, E. R., and Szwarc, R., J. Res. Nat. Bur. Stand. (U.S.), **70A** (Phys. and Chem.), 175 (1966).
[12] Carrera, N. J., Walker, R. F., and Plante, E. R., J. Res. Nat. Bur. Stand. (U.S.), **68A** (Phys. and Chem.), 325 (1964).
[13] The International Temperature Scale of 1968, Metrologia **5**, 35 (1969).
[14] Hultgren, R., Orr, R. L., Anderson, P. D., and Kelley, K. K., Selected Values of Thermodynamic Properties of Metals and Alloys, p. 221 (John Wiley & Sons, Inc., New York, N.Y., 1963).
[15] Horton, W. S., J. Res. Nat. Bur. Stand. (U.S.), **70A** (Phys. and Chem.), 533 (1966).
[16] Cubicciotti, D., J. Phys. Chem. **70**, 2410 (1966).

(Paper 74A5–628)

JOURNAL OF RESEARCH of the National Bureau of Standards—A. Physics and Chemistry
Vol. 74A, No. 5, September–October 1970

Thermophysical Properties of Methane: Virial Coefficients, Vapor and Melting Pressures*

Robert D. Goodwin**

Institute for Basic Standards, National Bureau of Standards, Boulder, Colorado 80302

(June 1, 1970)

For use in the computation of thermodynamic properties in gaseous and liquid states at $T < 300$ K there are given concise descriptions of the properties named in the title. Numerous published data on methane are combined with some new analytical expressions which give more acceptable behavior than previously could have been achieved.

Key words: Melting pressures; methane; thermophysical properties; vapor pressures; virial coefficients.

List of Symbols

Subscripts c and t refer to critical and triple points.

$a, b, c, d,$	coefficients for eq (4).
$A, B,$	coefficients for eq (6).
$B_i, C_i,$	coefficients for eqs (2, 3).
$B(\tau), C(\tau),$	the "virial coefficients."
$d,$	density
$\Delta,$	any relative deviation, $(y/y_{calc}-1)$.
$\epsilon,$	exponent in various expressions.
J,	the Joule.
l,	the liter.
mol,	16.042 g of methane.
$P,$	pressure, 1 atm = 0.101325 MN/m^2.
$R,$	the gas constant, 8.3143 J/(mol K).
$\sigma,$	d/d_c, density reduced at d_c.
$T,$	temperature, K on the IPTS (1968).
$\tau,$	T/T_c, temperature reduced at T_c.
$v,$	$1/d$, molal volume.
$x,$	defined argument in various equations.
$Y,$	dependent variable in eq (6).
$Z,$	Pv/RT, the "compressibility factor."

1. Introduction

It appears likely that many technological processes will increasingly involve the liquefaction, storage, and pumping of methane either as a pure fluid or as the major component of liquefied natural gas. Hence our ultimate objective is the determination of accurate thermodynamic properties for this fluid from room temperature down to the solid-liquid boundary, with emphasis on the saturated and compressed liquid states.

Analytical description of physical properties is a practical necessity for the tedious computations which must be performed to obtain a network of thermodynamic functions. In the present report we select some published properties data and place them in analytical form directly useful for thermal computations. This work is appropriate because more data are available for methane than for any fluid previously studied experimentally at this laboratory. Data from different sources on a given property seldom are completely consistent. With the increase of available data we often suffer a decrease of precision. Our new analytical descriptions, however, are powerful tools for examining raw data because they are constrained to accepted fluids behavior, especially at the critical point [1, 2][1]. Their use provides a principal justification for reexamining data on methane.

Our particular objective in this and a following report is to describe the coexistence regions, because they are boundaries for *PVT* behavior in the one-phase domain. The virial equation of state (valid at densities below one half the critical density) is treated first, however, because it will be used to estimate some coexistence data. It also provides low-density *PVT* "data" not available through our high-density experimental techniques.

Temperatures in this report have been converted from the 1948 to the 1968 IPTS [3] via an interpolation program provided by Rolf Prydz.

The values of fixed-point constants selected for present work are given on the first two lines of table 1. Temperatures are on the IPTS–1968. In a following

*This work was conducted at NBS under sponsorship of The American Gas Association.
**Cryogenics Division, National Bureau of Standards, Boulder, Colorado 80302.

[1] Figures in brackets indicate the literature references at the end of this paper.

report on the orthobaric densities we had found $T_c = 190.5 \pm 0.1$ K. We then discovered two new investigations of the critical region [24, 25]. Values from these publications are given on the last two lines of table 1. Temperatures have been increased by 0.032 K to bring them onto IPTS–1968. To avoid proliferation of published critical-point constants we have adopted $T_c = 190.53$ K from [25]. Our critical-point pressure is given by the vapor pressure equation of the present report. Our critical-point density is obtained from our rectilinear diameter.

TABLE 1. *Fixed-point constants for methane*

Fixed point	T	P	d
	K	*atm*	*mol/l*
Triple point	90.66 [11]	0.1151	28.0536*
Critical point	190.53	45.346	10.15
C.P. [24]	190.58 ± 0.05	.....	10.35 ± 0.13
C.P. [25]	190.530	45.346	10.1475

*Density of liquid at T_t.

2. The Virial Coefficients

It is convenient for correlation in corresponding states to define reduced variables $\tau \equiv T/T_c$, $\sigma \equiv d/d_c$. The truncated virial equation used here then is

$$Z = 1 + B(\tau)\cdot\sigma + C(\tau)\cdot\sigma^2. \qquad (1)$$

The second and third virial coefficients $B(\tau)$, $C(\tau)$ are dimensionless.

Data for $B(\tau)$ have been selected from four sources [4, 5, 6, 7]. Representation of these data, needed for computations, is given by the same type of expansion as was used for hydrogen [8],

$$B(\tau) = \sum_{i=1}^{6} B_i \cdot (1/\tau)^{(2i-1)/4}. \qquad (2)$$

Data were eliminated, however, if they diverged more than 1 percent. We are left with the set of points plotted on figure 1. The line is calculated from (2) with coefficients

$B_1 = 16.67\ 707$, $B_4 = -203.22\ 428$,

$B_2 = -87.41\ 490$, $B_5 = 108.55\ 0470$,

$B_3 = 187.43\ 954$, $B_6 = -23.21\ 3116$.

The rms relative deviation for 25 points is 0.31 percent. Individual deviations, $\Delta \equiv (B/B_{calc} - 1)$, are given in percent on figure 2. Equation (2) may not be accurate for $\tau \geq 2$ with above coefficients.

Calculated data for $B(\tau)$ will be published by Sengers, Klein, and Gallagher using an intermolecular potential function adjusted to the experimental data

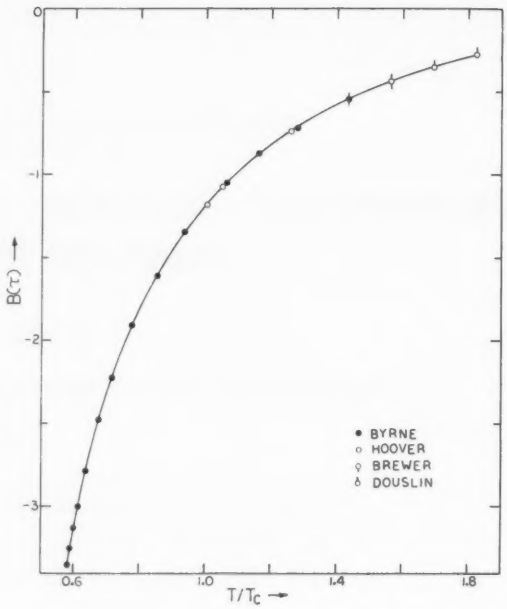

FIGURE 1. *Second virial coefficient* $B(\tau)$ *for methane.*

These data are represented by eq (2).

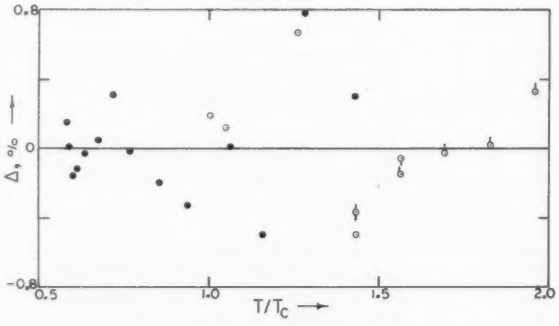

FIGURE 2. *Relative deviations of second virial coefficient data from eq* (2).

Points are identified as on figure 1.

[26]. For thermal computations this has the very important advantage that the temperature dependence is theoretically based, as compared with a polynomial adjusted to imprecise experimental data only. To see how drastic this may be, compare coefficients of eq (2) given above with values given below for data of [26] in the range $110 \leq T \leq 450$ K,

$B_1 = 2.109\ 914$, $B_4 = -16.022\ 404$,

$B_2 = -7.268\ 397$, $B_5 = 9.450\ 4285$,

$B_3 = 13.088\ 869$, $B_6 = -2.532\ 2231$.

The rms relative deviation for 47 data is 0.051 percent. There is no clear indication that the deviations are systematic. At $T \leq 200$ K no deviation exceeds 0.02

percent. At $T > 200$ K no deviation exceeds 0.17 percent.

For $C(\tau)$ few data are available at low temperatures. Figure 3 gives data of [5] at $\tau < 1.5$, and data of [7] at $\tau > 1.5$. We had devised a form for describing data on hydrogen [8], which later was modified [9], and now is further changed to obtain a better representation of these methane data,

$$C(\tau) = [C_1/\tau^{1/2} + C_2/\tau^5] \cdot [1 - \exp\,(1 - C_3 \cdot \tau^2)]. \quad (3)$$

The line on figure 3 is calculated from (3) with constants,

$$C_1 = 0.23844, \qquad C_2 = 0.56243, \qquad C_3 = 1.90.$$

The behavior given by (3) is quite similar to that of recent precise data on oxygen [10] for which a maximum value of $C(\tau) = 0.50$ occurs at $\tau = 0.9$. The root for oxygen is near $\tau_0 = 0.70$, whereas C_3 was selected for methane to shift this root to a slightly higher value.

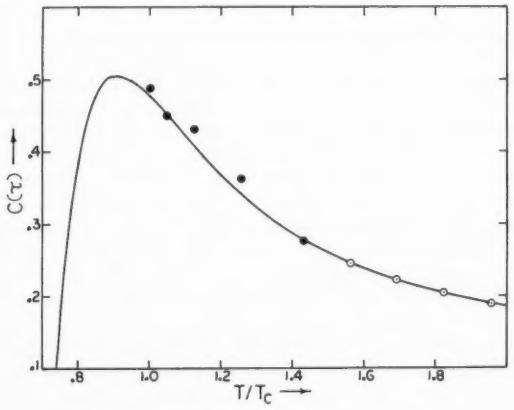

FIGURE 3. *Third virial coefficient* C(τ) *for methane.*

At $T/T_c < 1.5$, the data are from [5]; above 1.5 they are from [7]. The line is calculated with eq (3).

3. The Vapor Pressures

The vapor pressures of liquid methane have been observed by numerous authors, giving roughly 200 $P-T$ pairs [11, . . ., 16]. Some data differ by several percent from the smoothed behavior of all data. Only by use of a reliable form of vapor-pressure equation with a minimum of arbitrary constants does it appear possible to attack this mass of data with relative confidence [1]. Our independent variable is

$$x(T) \equiv (1 - T_t/T)/(1 - T_t/T_c)$$

and the new equation is

$$\log_e (P/P_t) = a \cdot x + b \cdot x^2 + c \cdot x^3 + d \cdot x \cdot (1-x)^\epsilon. \quad (4)$$

Exponent ϵ has been established at this laboratory through examination of more precise data on other substances: $\epsilon = 1.433$ for fluorine [17] and $\epsilon = 1.45 \pm 0.05$ for oxygen (Rolf Prydz); and $\epsilon = 1.45$ for nitrogen [27].

We take $\epsilon = 1.45$ for methane. At first we allowed the triple-point pressure in (4) to appear on the right as a least-squares coefficient, finding a value in agreement with [11], table 1. Thereafter we used (4) as written, constrained to the triple point. By use of (4) as a reliable smoothing function we successively eliminated inconsistent data, ending with 161 points and an rms relative deviation of 0.27 percent by use of coefficients,

$$a = \;\; 4.470\;3915, \qquad c = -0.744\;4619,$$

$$b = \;\; 2.250\;3526, \qquad d = \;\; 1.601\;7258.$$

Deviations are plotted on figure 4. Filled circles are 47 smoothed data recommended by Armstrong [11]. The remaining 114 points (N pts) and their ranges are

Author	N pts	Range, T, K
Bloomer [15]	17	111.4 − 190.4
Grigor [16]	32	98.2 − 188.9
Hestermans [14]	16	117.3 − 189.6
Itterbeek [12]	20	149.8 − 190.3
Vennix [13]	29	133.7 − 190.2

4. The Melting Pressures

Melting pressures $P(T)$ for coexisting solid and liquid methane have been observed to $P = 156$ [18] and in the range $970 \leq P \leq 2700$ atm [19]. Another three points at $P < 46$ [20] agree well with [18]. The latter authors gave methane vapor pressures at their melting temperatures. We have used temperatures derived from these vapor pressures via (4). They are at most 0.03 K higher than those given in [18].

To examine the melting pressures we plot $Y(P, T) \equiv (P - P_t)/(T - T_t)$ versus $x \equiv T/T_t$ as recommended in [21], figure 5. Solidly filled circles represent data from [19] used with triple-point constants of table 1.

For the data of [18] alone, the Simon melting equation

$$(P - P_t) = P_0 \cdot (x^\epsilon - 1) \quad (5)$$

yields an exponent ϵ in excess of 3.0, much greater than found for many other fluids [21]. The authors [19] found $\epsilon = 1.01$ and rounded the triple-point temperature to $T_t = 89$ K, making three adjusted constants. It is possible that their methane was insufficiently pure for present purposes. By adding 2 K to all of their temperatures, the points of figure 5 move down and to the right (large, open circles).

We now examine for comparison a possibly similar substance, argon, for which precise, independent data are available: from [22] to $P = 1500$; and from [23] at $970 \leq P \leq 6000$ atm. Figure 6 gives these argon data in the same range covered by the methane data. The

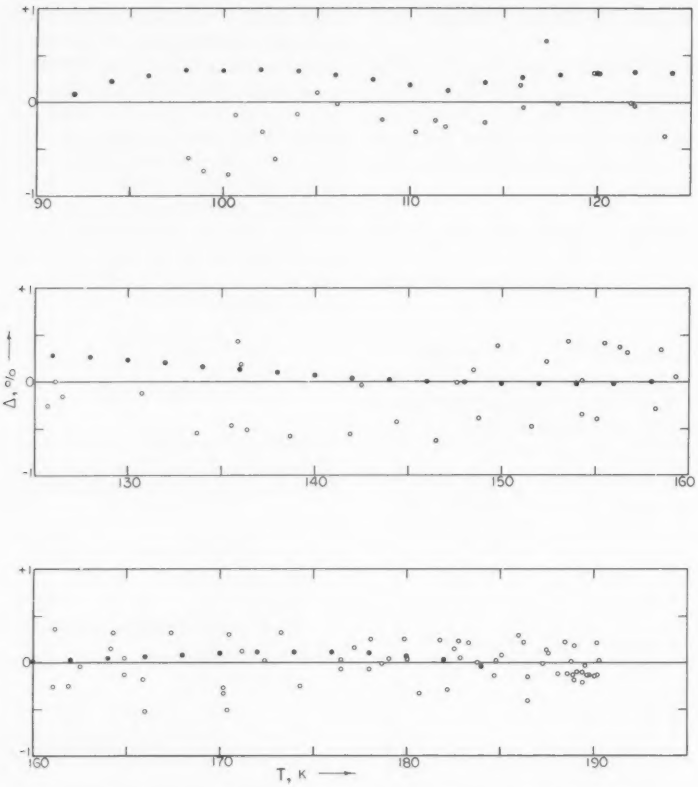

FIGURE 4. *Relative deviations of methane vapor pressures from eq (4).*

Filled circles are from [11].

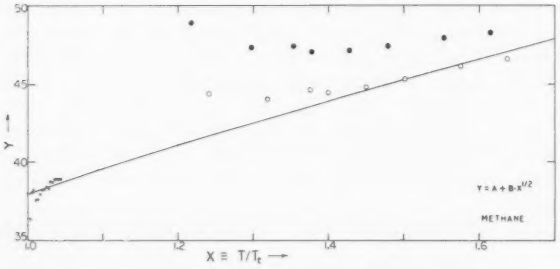

FIGURE 5. *The melting function* $Y \equiv (P-P_t)/(T-T_t)$ *for methane.*

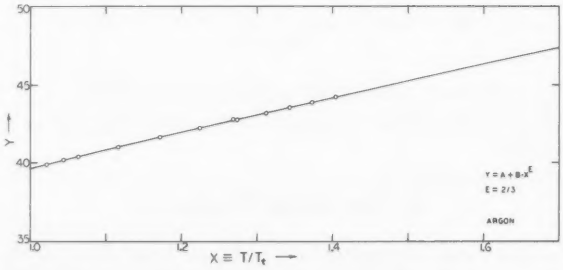

FIGURE 6. *The melting function* $Y \equiv (P-P_t)/(T-T_t)$ *for argon.*

16 argon pressures are represented with an rms relative deviation of 0.091 percent by the expression

$$Y(P, T) = A + B \cdot x^{\epsilon}, \tag{6}$$

$$A = 21.4192, \qquad B = 18.1926, \qquad \epsilon = 2/3,$$

which was used to draw the line on figure 6.

For methane on figure 5 we see that a greater curvature at the origin (than used for argon) should give a better representation. We arbitrarily take $\epsilon = 1/2$, to give the provisional melting pressure equation (6) for methane with constants

$$A = 5.318, \qquad B = 32.635, \qquad \epsilon = 1/2$$

The line on figure 5 was calculated with these constants.

Melting pressures beyond our present range of interest have been observed to 24,000 atm [28]. To complete our reporting, however, we give these data on figure 7.

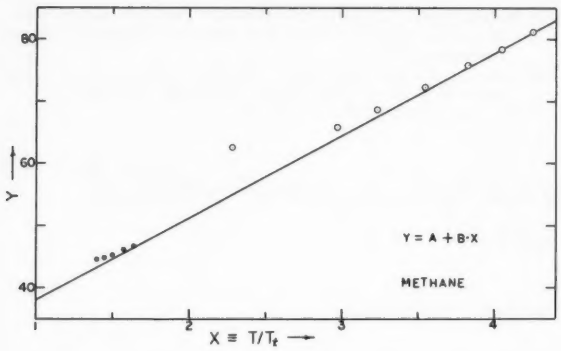

FIGURE 7. *The melting function* $Y \equiv (P-P_t)/(T-T_t)$ *for methane up to* $P=24{,}000$ *atm.*

Small circles are from [19]; large circles from [28]. The line is $Y = 24.75 + 13.25 \cdot x$.

5. Conclusions

This correlation has been undertaken to evaluate the quality of existing physical properties measurements on compressed gaseous and liquid methane, to reveal significant gaps or inconsistencies in existing measurements, and to provide accurate analytical representations of selected data for preliminary thermodynamic computations. Selected data for the second virial coefficient at temperatures down to the normal boiling point are of good quality, but few if any consistent data exist for lower temperatures. Further results for the third virial coefficient are needed at low temperatures. For the vapor pressures, the rms deviation of 0.3 percent found here could be reduced one order of magnitude through self-consistent measurements of high accuracy [17]. New determinations of the melting pressures to about 300 atm clearly are needed. Available analytical expressions are capable of representing all of the properties we have examined within the precision of the measurements.

6. References

General Surveys

[G1] Matthews, C. S., and Hurd, C. O., Thermodynamic properties of methane, Trans. Am. Inst. Chem. Engrs. **42,** 55 (1946).

[G2] Din, F., ed., Thermodynamic Functions of Gases, Vol. **3,** Ethane, Methane, Nitrogen (Butterworths Scientific Publications, London, 1961).

[G3] Edmister, W. C., Applied Hydrocarbon Thermodynamics, Vol. **1,** (Gulf Publ. Co., Houston, Texas, 1961).

[G4] Guereca, R. A., Richardson, H. P., Gordon, J. L., et al., Thermophysical Properties of Selected Gases Below 300 Degrees K, Inform. Circ. No. 8317, Helium Research Center, Bureau of Mines (Amarillo, Texas, 1967).

[G5] Hall, Louise A., A Bibliography of Thermophysical Properties of Methane from 0 to 300 °K, Nat. Bur. Stand. (U.S.), Tech. Note 367 (U.S. Gov't. Printing Office, Washington, D.C. 20402, May 1968).

Mr. William J. Hall generously provided the essential least-squares and iteration programs used throughout this and earlier work by the author. Dwain E. Diller kindly made improvements in this manuscript.

Specific References

[1] Goodwin, R. D., Nonanalytic vapor pressure equation with data for nitrogen and oxygen, J. Res. Nat. Bur. Stand. (U.S.), **73A** (Phys. and Chem.), No. 5, 487 (1969).

[2] Goodwin, R. D., Estimation of critical constants T_c, ρ_c from the $\rho(T)$ and $T(\rho)$ relations at coexistence, J. Res. Nat. Bur. Stand. (U.S.), **74A** (Phys. and Chem.), No. 2, 221 (1970).

[3] The international practical temperature scale of 1968, Metrologia **5,** No. 2, 35–49 (1969).

[4] Byrne, M. A., Jones, M. R., and Staveley, L. A. K., Second virial coefficients of argon, krypton and methane and their binary mixtures at low temperatures, Trans. Faraday Soc. **64,** No. 7, 1747 (1968).

[5] Hoover, A. E., Nagata, I., Leland, T. W., and Kobayashi, R., Virial coefficients of methane, ethane, and their mixtures at low temperatures, J. Chem. Phys. **48,** No. 6, 2633 (1968).

[6] Brewer, Jerome, Determination of Mixed Virial Coefficients, Midwest Research Institute, Kansas City, Missouri 64110, (Dec., 1967), Defense Documentation Center No. AD–663 448.

[7] Douslin, D. R., Harrison, R. H., Moore, R. T., and McCullough, J. P., P–V–T Relations for methane, J. Chem. and Eng. Data **9,** No. 3, 358 (1964).

[8] Goodwin, R. D., Diller, D. E., Roder, H. M., and Weber, L. A., Second and third virial coefficients for hydrogen, J. Res. Nat. Bur. Stand. (U.S.), **68A** (Phys. and Chem.), No. 1, 121 (1964).

[9] Chueh, P. L., and Prausnitz, J. M., Third virial coefficients of nonpolar gases and their mixtures, Am. Inst. Chem. Eng. J. **13** (5), 869 (1967).

[10] Weber, Lloyd A., $P-V-T$, thermodynamic and related properties of oxygen from the triple point to 300 K at pressures to 33 MN/m², J. Res. Nat. Bur. Stand. (U.S.), **74A** (Phys. and Chem.), No. 1, 93–129 (1970).

[11] Armstrong, G. T., Brickwedde, F. G., & Scott, R. B., Vapor pressures of the methanes, J. Res. Nat. Bur. Stand. (U.S.) **55,** No. 1, 39–52 (1955).

[12] Van Itterbeek, A., Staes, K., Verbeke, O., and Theeuwes, F., Vapour pressure of saturated liquid methane, Physica **30,** 1896 (1964).

[13] Vennix, Alan John, Low Temperature Volumetric Properties and the Development of an Equation of State for Methane, Thesis, Dept. of Chem. Engrn'g., Rice University, Houston, Texas, April, 1965.

[14] Hestermans, P., and White, David, The vapor pressure, heat of vaporization and heat capacity of methane from the boiling point to the critical temperature, J. Phys. Chem. **65,** 362 (Feb., 1961).

[15] Bloomer, O. T., and Parent, J. D., Liquid-vapor phase behavior of the methane-nitrogen system, Chem. Eng. Prog. Symposium Ser. 6, **49,** 11–24 (1952).

[16] Grigor, Anthony F., The Measurement and Correlation of Some Physical Properties of Methane and Per-deuteromethane, Thesis, Dept. of Chem., Pennsylvania State Univ., December 1966; J. Chem. Phys. **48**(3), 1032 (1968).

[17] Prydz, Rolf, Straty, G. C., and Timmerhaus, K. D., Properties of fluorine along the vapor-liquid coexistence boundary, submitted to J. Chem. Phys., 1970.

[18] Clusius, K., and Weigand, K., Die Schmelzkurven der Gase A, Kr, X, CH_4, CH_3D, CD_4, C_2H_4, C_2H_6, COS, und PH_3 bis 200 Atm. Druck, Z. physik. Chem. **B46,** No. 1, 1–37 (1940).

[19] Stryland, J. C., Crawford, J. E., and Mastoor, M. A., Melting temperatures of krypton, xenon, and methane at pressures up to 3000 atm, Can. J. Phys. **38,** 1546 (1960).

[20] Freeth, F. A., and Verschoyle, T. T. H., Physical constants of the system methane-hydrogen, Proc. Roy. Soc. (London) **130A,** 453 (1931).

[21] Goodwin, R. D., and Weber, L. A., A comparison of two melting-pressure equations constrained to the triple point using data for eleven gases and three metals, Nat. Bur. Stand. (U.S.), Tech. Note 183, October 6, 1963. U.S. Gov't. Printing Office, Washington, D.C. 20402.

[22] Michels, A., and Prins, C., The melting lines of argon, krypton, and xenon up to 1500 atm; representation of the results by a law of corresponding states, Physica **28,** 101 (1962).

[23] Bridgman, P. W., The melting curves and compressibilities of nitrogen and argon, Proc. Am. Acad. Arts Sci. **70,** 1 (1935).

[24] Ricci, F. P., and Scafè, E., Orthobaric density of CH_4 in the critical region, Phys. Letters **29A,** (No. 11), 650 (1969).
[25] Jansoone, V., Gielen, H., DeBoelpaep, J., and Verbeke, O. B., The pressure-temperature-volume relationship of methane near the critical point, Physica **46,** 213 (1970).
[26] Sengers, J. M. H. L., Klein, Max, and Gallagher, J. S., Pressure-volume-temperature relationships of gases: Virial coefficients, to appear in a forthcoming edition of The American Institute of Physics Handbook.
[27] Weber, Lloyd A., Some vapor pressure and PVT data on nitrogen in the range 65–140 K, The Journal of Chemical Thermodynamics (1970).
[28] Grace, J. D., and Kennedy, G. C., The melting curves of five gases to 30 kb, J. Phys. Chem. Solids **28,** 977 (1967).

(Paper 74A5–629)

JOURNAL OF RESEARCH of the National Bureau of Standards—A. Physics and Chemistry
Vol. 74A, No. 5, September–October 1970

Specific Heats, C_v, of Compressed Liquid and Gaseous Fluorine*

Rolf Prydz and Robert D. Goodwin****

Institute for Basic Standards, National Bureau of Standards, Boulder, Colo. 80302

(May 11, 1970)

Experimental specific heats at constant volume for compressed gaseous and liquid fluorine are reported from 80 K to 300 K at pressures to about 23 MN/m².

Key words: Compressed gas; compressed liquid; fluorine; heat capacities; specific heats.

List of Symbols

$C_b(T)$	heat capacity of empty bomb
$C_v^\circ(T)$	ideal gas specific heat
$C_v(\rho, T)$	specific heat at constant volume
C_x	work done to expand calorimeter bomb
N	total g moles of fluid in closed system
N_c	g moles of fluid in capillary tube
P	pressure, 1 MN/m² = 9.86923 atm
Q	calorimeter heat input
ρ	density
T	temperature, K, on the IPTS (1968)
T_1, T_2	temperature at start and end of heating interval
T_a	average temperature in ΔT
$\Delta T \equiv$	$T_2 - T_1$, calorimetric temperature increment
$v \equiv$	$1/\rho$, molal volume
V_b	volume of calorimeter bomb.

1. Introduction

These specific heat measurements and the reported specific heat data along the vapor-liquid coexistence boundary [1][1] are part of a program in this laboratory to determine the thermodynamic properties of compressed gaseous and liquid fluorine. Since no single-phase specific heat data of either liquid or gaseous fluorine have been published previously, it is the purpose of this paper to report new such measurements at constant volume, C_v, from just below the normal boiling point (85 K) to 300 K at pressures to 23 MN/m² (1 MN/m² = 9.86923 atm). These data supplement recent PVT measurements of fluorine in this laboratory for the computation of the thermodynamic properties of this fluid.

2. Experimental Apparatus

The calorimeter and the cryostat used for these experiments are the same as the ones used for oxygen [2, 3], though the valves in the system were modified for compatibility with high-pressure fluorine [4]. Briefly, the calorimeter is a thin, spherical stainless steel shell, 5 cm in diameter, surrounded by adiabatic shields automatically controlled at the temperature of the calorimeter. This temperature is measured using a platinum resistance thermometer calibrated by NBS on the IPTS 1968 temperature scale. Fluorine filling pressures are measured by referencing to oil pressure derived from an oil dead-weight gage through an intermediate nitrogen system (the nitrogen system is a safety precaution to reduce the possibility of direct contact between the fluorine and the dead-weight gage oil, a catastrophic situation).

A separate fluorine filling and recovery system was constructed consisting of a 10-liter stainless steel storage cylinder, a thermal pressure booster assembly, and a hydrogen fluoride (HF) absorber. The fluorine is kept in the storage cylinder at a pressure of about 1.5 MN/m². Calorimeter filling pressures are generated by the thermal booster, which is surrounded by a liquid nitrogen bath. Sodium fluoride pellets in the HF absorber serve to remove any traces of hydrogen fluoride in the fluorine before it is condensed in the booster.

A cabinet surrounding the cryostat and the supply system is maintained at a slightly reduced pressure, relative to ambient pressure, by an exhaust fan located outside the laboratory. This reduces the probability of venting the extremely toxic fluorine fumes into the laboratory if a leak should develop in the system. In

*This work was carried out at the National Bureau of Standards under the sponsorship of the United States Air Force (MIPR No. FO4611-70-X-0001).
**Cryogenics Division, National Bureau of Standards, Boulder, Colo. 80302.
[1] Figures in brackets indicate the literature references at the end of this paper.

the case of a system failure, however, provisions have been made for emergency venting of the fluorine through charcoal reactors outside the laboratory. Detailed description of materials that may be used for construction of fluorine handling systems and apparatuses is given by reference [5].

3. Procedures

The specific heat, C_v, of a substance is determined from the energy input, Q, to raise the temperature of a unit mass by ΔT. Experimental specific heats are obtained in the following way. The energy input to the calorimeter, Q, is obtained from simultaneous readings of potential and current as the heating time interval is measured by an electronic counter. The electric power input is obtained by averaging three pairs of potential and current readings. Five temperatures are measured immediately preceding a heating interval and are then extrapolated linearly to obtain the temperature, T_1, of the calorimeter at the mid-time of the heating period as if no heat had been added. At the end of the heating interval the temperature of the calorimeter may increase for about 20 min before a very slow cooling begins (imperfect adiabatic shielding). Five new temperatures are then measured and again linearly extrapolated to the mid-time of the heating interval to obtain T_2. Assigned to that particular specific heat observation is the average temperature $T_a=(T_1+T_2)/2$. The temperature increase of the calorimeter is $\Delta T=T_2-T_1$.

Calorimeter filling pressures are measured by the dead-weight gage and are corrected for the hydrostatic head of fluorine in the capillary tube leading down to the calorimeter bomb. From this pressure and the filling temperature, a one-phase density is calculated with an uncertainty of about 0.1 percent from an equation of state of the type previously applied to deuterium [6]. The fluorine mass in the calorimeter is then calculated from the known volume, V_b, of the calorimeter (uncertainty of about 0.1 percent) [2]. The number of moles of sample in the capillary volume ($0.0002 \cdot V_b$) is computed from an estimated temperature distribution [2] and the equation of state. Thus, the total mass of sample in the closed system is known to an uncertainty of about 0.2 percent.

To obtain the density, ρ, at each specific heat observation, corrections must be made for the expansion of the calorimeter bomb and the amount of fluorine in the capillary tube by calculating the pressures at T_1 and T_2. The application of a double iteration method to adjust for the relative change of the mass of sample in the capillary tube, N_c, and the combined effect of temperature and pressure expansion of the stainless steel calorimeter, has been discussed by Goodwin and Weber [3]. Thus, the expression for density is

$$\rho=[N-N_c(P, T)]/V_b(P, T) \qquad (1)$$

where N is the total number of g moles in the closed system. The densities ρ_1, ρ_2 obtained in this manner at T_1, T_2 may be used to compute the adjustment in the heat capacity, C_x, due to the work done to expand the calorimeter bomb as

$$\Delta v=1/\rho_2-1/\rho_1$$

and

$$C_x=[T_2(\partial P/\partial T)_2-\Delta P/2]\cdot\Delta v/\Delta T. \qquad (2)$$

Using this expression, the experimental specific heats are calculated from

$$C_v=[Q/\Delta T-C_b]/[N-N_c]-C_x \qquad (3)$$

where Q is the total energy input and C_b is the heat capacity of the empty calorimeter bomb from [1]. The heat capacity adjustment, C_x, is largest for the highest densities, being of the order of 1.2 percent of the total heat capacity, $Q/\Delta T$, for run No. 8.

The purity of the fluorine sample used for these measurements was 99.99 percent as determined from residual gas analysis after reaction of the fluorine with mercury.

4. Experimental Results

The location of all experimental C_v data on the PVT surface is given in figure 1. Also indicated in this

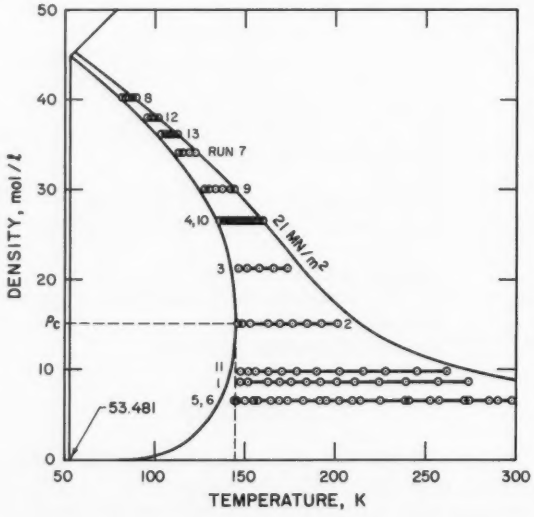

FIGURE 1. *Locus of* C_v *data on* $\rho-T$ *surface.*

figure is the critical point ($\rho_c=15.10$ mole/l; $T_c=144.31$ K), which helps to give the relative location of each experimental run. Upper limits of 300 K in temperature and 21 MN/m² in pressure bound the range of the data together with the vapor-liquid coexistence boundary. Table 1 gives the filling conditions of the calorimeter bomb for each run as determined by the temperature-pressure conditions of the first two columns of this table. Next is the calculated volume of the calorimeter and the density calculated from the equation of state. N is the total number of g moles

TABLE 1. *Loading conditions for the samples*

Run	T	P	V_b	D	N
	K	MN/m^2	cm^3	mol/l	mol
1	174.825	8.4244	73.014	8.709	0.6360
2	166.789	10.4272	73.008	15.184	1.1087
3	175.609	18.6026	73.114	21.245	1.5535
4	155.918	17.4279	73.040	26.238	1.9167
5	193.408	8.3099	73.071	6.551	0.4787
6	195.075	8.6601	73.079	6.770	0.4948
7	116.282	8.8620	72.850	34.098	2.4843
8	84.845	8.6315	72.774	40.123	2.9202
9	133.421	9.4309	72.901	29.905	2.1803
10	147.833	12.6624	72.972	26.611	1.9420
11	188.588	10.8379	73.080	9.807	0.7168
12	98.066	10.6331	72.819	37.922	2.7617
13	108.200	12.6513	72.860	36.220	2.6392

as obtained from the density and the calorimeter and capillary volumes.

The experimental results are given in table 2. Identification in the first column is the run number followed by two digits for the data point of that run. Next are the observed temperature, the estimated pressure, the calorimeter bomb volume, V_b, and the calculated density at these conditions. Further, the ΔT column is the temperature increment of the heating period. The following columns have the total heat capacity $Q/\Delta T$, the heat capacity of the empty calorimeter, and the adjusted specific heat of the fluorine sample as calculated from eq (3). These specific heat values also include curvature adjustments as discussed by Goodwin and Weber [2]. However, the adjustments changed only the two first points (points No. 215, 216) of run No. 2 which is closest to the critical density. The estimated maximum

TABLE 2. *Specific heats of fluorine*

ID	T_a	P	V_b	D	ΔT	$Q/\Delta T$	Tare	C_v	Error in C_v
	K	MN/m^2	cm^3	mol/l	K	J/K	J/K	$J/mol\ K$	%
115	147.552	5.380	72.905	8.723	3.394	85.994	65.724	31.77	1.37
116	152.783	5.985	72.926	8.720	7.150	85.764	66.936	29.50	1.11
117	162.897	7.122	72.966	8.715	7.083	86.406	69.066	27.16	1.21
118	169.884	7.888	72.994	8.712	7.023	87.170	70.396	26.26	1.26
119	176.795	8.636	73.022	8.708	6.951	88.028	71.613	25.69	1.30
120	184.349	9.443	73.053	8.704	8.321	89.004	72.845	25.28	1.27
121	192.537	10.314	73.088	8.700	8.225	90.032	74.078	24.96	1.30
122	201.228	11.230	73.125	8.696	9.643	91.099	75.285	24.73	1.28
123	211.965	12.355	73.171	8.690	12.101	92.340	76.653	24.52	1.24
124	225.285	13.739	73.230	8.683	14.820	93.804	78.188	24.40	1.22
125	240.581	15.316	73.298	8.675	16.052	95.418	79.769	24.44	1.22
126	257.055	16.999	73.373	8.666	17.250	96.938	81.293	24.42	1.23
127	275.383	18.851	73.457	8.656	19.832	98.526	82.811	24.52	1.22
215	145.586	5.509	72.901	15.207	1.592	116.052	65.248	44.63	1.17
216	148.230	6.116	72.914	15.204	3.738	106.091	65.886	35.76	0.86
217	153.049	7.229	72.938	15.199	5.966	102.260	66.995	31.65	.79
218	162.488	9.422	72.986	15.189	5.989	100.533	68.985	28.28	.86
219	169.101	10.969	73.021	15.181	7.341	100.628	70.252	27.21	.84
220	176.346	12.671	73.060	15.173	7.265	101.105	71.537	26.47	.86
221	184.279	14.535	73.103	15.164	8.736	101.761	72.834	25.88	.85
222	192.861	16.551	73.151	15.154	8.587	102.574	74.125	25.44	.87
223	201.351	18.538	73.199	15.144	8.576	103.543	75.301	25.24	.88
316	146.736	6.508	72.913	21.305	4.342	112.663	65.528	30.10	.75
317	151.590	8.466	72.945	21.295	5.439	111.336	66.667	28.49	.72
318	158.187	11.202	72.990	21.282	7.844	110.993	68.107	27.31	.67
319	165.967	14.489	73.044	21.265	7.819	111.295	69.664	26.48	.70
320	173.700	17.787	73.100	21.249	7.769	112.027	71.079	26.01	.71
401	138.316	5.515	72.880	26.298	4.171	117.573	63.374	27.84	.72
402	142.452	8.307	72.917	26.284	4.148	117.631	64.462	27.28	.73
403	146.560	11.092	72.954	26.270	4.130	118.010	65.485	26.93	.74
404	150.651	13.867	72.991	26.256	4.113	118.570	66.452	26.70	.76
405	154.652	16.575	73.028	26.243	4.098	118.889	67.349	26.38	.77
406	158.702	19.294	73.066	26.229	4.076	119.551	68.214	26.26	.78
407	162.321	21.709	73.100	26.216	3.241	120.014	68.952	26.11	.86
408	136.840	4.521	72.868	26.303	2.434	117.418	62.970	27.99	.90
409	140.138	6.741	72.896	26.292	4.197	117.547	63.860	27.56	.72
410	144.283	9.548	72.933	26.278	4.137	117.849	64.925	27.15	.74
411	148.395	12.338	72.971	26.264	4.129	118.233	65.925	26.81	.75
412	152.431	15.071	73.008	26.250	4.106	118.646	66.857	26.52	.76
413	156.495	17.813	73.046	26.236	4.088	119.232	67.748	26.35	.77
414	160.539	20.522	73.084	26.223	4.067	119.780	68.592	26.18	.78

TABLE 2. *Specific heats of fluorine*—Continued

ID	T_a	P	V_b	D	ΔT	$Q/\Delta T$	Tare	C_v	Error in C_v
	K	MN/m^2	cm^3	*mol/l*	*K*	*J/K*	*J/K*	*J/mol K*	%
501	143.968	4.531	72.887	6.568	6.264	78.966	64.846	29.41	1.39
502	150.160	5.035	72.909	6.566	6.193	79.565	66.338	27.54	1.50
503	157.025	5.576	72.934	6.563	7.630	**80.543**	67.861	26.40	1.48
504	164.958	6.186	72.963	6.561	8.344	81.731	69.470	25.52	1.51
505	173.561	6.837	72.995	6.558	9.010	83.033	71.055	24.92	1.54
506	182.850	7.530	73.030	6.554	9.728	84.443	72.608	24.62	1.55
507	192.588	8.249	73.068	6.551	10.269	85.684	74.085	24.12	1.58
508	203.140	9.021	73.109	6.547	**11.047**	**87.039**	**75.538**	23.91	1.59
509	214.436	9.841	73.154	6.543	11.777	88.433	76.950	23.86	1.60
510	226.887	10.738	73.204	6.539	13.401	89.815	78.362	23.79	1.58
511	241.823	11.806	73.265	6.533	16.807	91.380	79.890	23.86	1.55
512	258.287	12.975	73.333	6.527	16.518	92.961	81.400	24.00	1.57
513	274.496	14.114	73.401	6.521	16.373	94.356	82.741	24.10	1.59
514	290.482	15.228	73.469	6.515	16.164	95.605	83.946	24.18	1.60
612	146.154	4.772	72.896	6.788	**11.929**	79.850	65.387	29.14	1.17
613	157.907	5.751	72.938	6.784	**11.696**	81.181	68.048	26.45	1.30
614	169.905	6.709	72.983	6.779	12.437	82.937	70.400	25.24	1.37
615	182.617	7.701	73.031	6.775	13.158	84.761	72.571	24.53	1.42
616	196.025	8.731	73.083	6.770	13.861	86.567	74.574	24.12	1.46
617	210.026	9.795	73.139	6.765	14.402	88.329	76.415	23.96	1.48
618	224.468	10.883	73.197	6.759	15.194	89.981	78.098	23.88	1.50
619	239.344	11.994	73.258	6.754	14.932	91.523	79.647	23.86	1.53
620	**253.945**	13.075	73.319	6.748	14.696	92.969	81.017	24.00	1.55
621	271.674	14.377	73.394	6.741	15.897	94.492	82.517	24.04	1.55
622	285.815	15.406	73.455	6.735	12.963	95.630	83.605	24.13	1.62
623	298.381	16.315	73.509	6.730	12.775	96.617	84.503	24.30	1.63
708	113.159	4.271	72.804	34.121	2.987	128.246	55.210	28.37	0.73
709	116.127	8.617	72.848	34.100	2.960	128.856	56.333	28.18	.74
710	119.070	12.839	72.891	34.079	2.944	129.683	57.400	**28.08**	.75
711	121.991	16.927	72.934	34.058	2.916	130.538	58.415	28.04	.75
801	82.992	3.711	72.733	40.147	1.886	138.288	40.657	31.67	0.80
802	84.877	8.707	72.775	40.123	1.884	138.887	41.750	31.59	.81
803	86.751	13.555	72.815	40.100	1.866	139.729	42.811	31.51	.82
804	**88.610**	18.265	72.856	40.077	1.851	140.624	43.839	31.50	.82
805	90.459	22.835	72.895	40.055	1.847	141.300	44.836	31.41	.83
901	127.307	3.459	72.833	29.935	3.060	126.035	60.157	29.56	0.74
902	130.410	6.500	72.867	29.920	3.174	122.094	61.114	27.30	.77
903	133.766	9.761	72.905	29.904	3.573	122.720	62.103	27.12	.74
904	137.312	13.159	72.945	29.887	3.557	123.401	**63.100**	26.97	.75
905	141.435	17.057	72.992	29.867	2.324	123.929	64.200	26.70	.92
906	143.738	19.203	73.018	29.856	2.338	124.410	64.788	26.64	.92
1001	136.731	4.878	72.870	26.649	2.432	117.889	62.940	27.84	.90
1002	139.557	6.853	72.896	26.639	3.269	118.034	63.707	27.51	.79
1003	143.010	9.275	72.927	26.628	3.687	118.156	**64.604**	27.09	.77
1004	146.658	11.838	72.961	26.615	3.678	118.586	65.509	26.83	.78
1005	150.301	14.391	72.995	26.602	3.661	119.050	66.371	26.61	.79
1006	146.130	11.467	72.956	26.617	3.671	118.316	65.381	26.76	.78
1007	149.750	14.006	72.990	26.604	3.640	119.403	**66.243**	26.86	.78
1008	153.359	16.526	73.024	26.591	3.625	119.840	67.064	26.65	.79
1009	156.935	19.004	73.058	26.579	3.600	120.339	67.842	26.50	.80
1101	147.346	5.524	72.906	9.831	4.494	89.746	65.675	33.47	1.08
1102	151.817	6.133	72.924	9.829	4.528	88.710	66.718	30.56	1.16
1103	156.825	6.799	72.945	9.826	5.565	88.556	67.819	28.81	1.13
1104	163.000	7.603	72.971	9.822	6.890	88.838	69.087	27.43	1.11
1105	170.484	8.562	73.002	9.818	8.202	89.572	70.506	26.47	1.10
1106	179.341	9.681	73.040	9.813	9.833	90.590	72.039	25.75	1.09
1107	189.770	10.984	73.086	9.807	11.191	91.825	73.672	25.18	1.10
1108	201.740	12.466	73.139	9.799	12.942	93.192	75.353	24.74	1.10
1109	215.428	14.147	73.201	9.791	14.702	94.770	77.068	24.54	1.10
1110	230.571	15.991	73.271	9.781	15.862	96.420	78.754	24.47	1.11
1111	246.166	17.873	73.345	9.772	15.683	97.942	**80.304**	24.42	1.13
1112	262.176	19.784	73.421	9.761	16.772	99.494	81.734	24.58	1.13

TABLE 2. *Specific heats of fluorine*—Continued

ID	T_a	P	V_b	D	ΔT	$Q/\Delta T$	Tare	C_v	Error in C_v
	K	*MN/m²*	*cm³*	*mol/l*	*K*	*J/K*	*J/K*	*J/mol K*	%
1202	95.454	5.079	72.769	37.949	2.217	134.275	47.411	29.99	.78
1203	97.662	9.778	72.811	37.926	2.205	135.029	48.495	29.89	.79
1204	99.850	14.308	72.853	37.904	2.189	135.863	49.535	29.87	.79
1205	102.024	18.690	72.893	37.882	2.173	136.779	50.538	29.84	.80
1301	103.424	4.095	72.779	36.261	2.241	131.406	51.168	29.13	0.80
1302	105.653	8.130	72.817	36.242	2.233	131.819	52.144	28.95	.81
1303	107.863	12.051	72.855	36.222	2.206	132.602	53.082	28.89	.82
1304	110.062	15.860	72.892	36.204	2.211	133.243	53.986	28.83	.82
1305	112.247	19.560	72.928	36.185	2.185	133.987	54.856	28.78	.83

uncertainty in the C_v measurements is given in the last column. This uncertainty should rapidly increase with diminishing temperature intervals, ΔT, and with diminishing mass of sample, N. It is based on the following estimated uncertainties in the different variables:

N, 0.2%	Q, 0.05%	ΔT, 0.1%
C_b, 0.1%	ΔP, 0.1%	dP/dT, 1.0%.

The number of significant figures given in table 2 is not justified on the basis of the uncertainty of the data, but is presented to maintain internal consistency.

No single-phase specific heat data of fluorine are available for comparison with the new measurements. However, the general behavior of the data is illustrated in figure 2. For a wide range of densities about the critical isochore, the specific heat increases sharply as the temperature approaches the two-phase envelope, which is to be expected. At densities far removed from the critical, the temperature dependence is relatively weak. Data obtained earlier with this apparatus for oxygen [2, 3] indicated that the deviations from other published oxygen values were within the accuracy of the specific heat measurements as given in the last column of table 2.

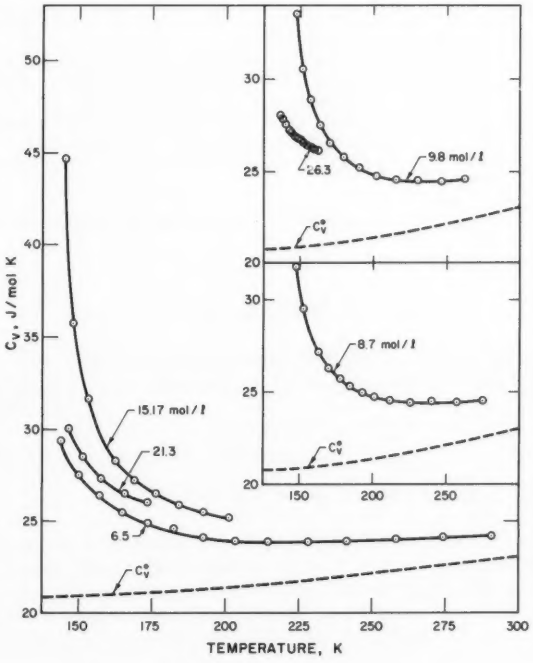

FIGURE 2. *Selected isochores of* C_v *data.*

The authors acknowledge the support of the Air Force Rocket Propulsion Laboratory, Edwards, California. Also, thanks are due to G. K. Johnson of Argonne National Laboratory for supplying the purified fluorine used for these experiments.

5. References

[1] Goodwin, R. D., and Prydz, R., Specific heats of fluorine at coexistence, J. Res. Nat. Bur. Stand. (U.S.), 74A (Phys. and Chem.), No. 4, 499–505 (July–Aug. 1970).

[2] Goodwin, R. D., and Weber, L. A., Specific heats of oxygen at coexistence, J. Research Nat. Bur. Stand. (U.S.), **73A**, (Phys. and Chem.), No. 1, 1–13 (Jan.–Feb. 1969).

[3] Goodwin, R. D., and Weber, L. A., Specific heats C_v of fluid oxygen from the triple point to 300 K at pressures to 350 atmospheres, J. Research Nat. Bur. Stand. (U.S.), **73A** (Phys. and Chem.), No. 1, 15–24 (Jan.–Feb. 1969).

[4] Straty, G. C., Bellow-sealed valve for reactive gases at moderately high pressures, Rev. Sci. Instr. **40**, No. 2, 378–79 (1969).

[5] Straty, G. C., and Prydz, R., Fluorine compatible apparatus for accurate *PVT* measurements, Rev. Sci. Instr. 41, No. 8, 1223–27 (1970).

[6] Prydz, R., Timmerhaus, K. D., and Stewart, R. B., The thermodynamic properties of deuterium, Advances in Cryogenic Engineering, Vol. **13**, 384–96 (1967).

(Paper 74A5–630)

389-821 O - 70 - 4

JOURNAL OF RESEARCH of the National Bureau of Standards—A. Physics and Chemistry
Vol. 74A, No. 5, September–October 1970

Acidic Dissociation of Diprotonated Piperazine in Methanol-Water Solvents From 10 to 40 °C

Maya Paabo and Roger G. Bates*

Institute for Materials Research, National Bureau of Standards, Washington, D.C. 20234

(May 6, 1970)

The first dissociation constant of piperazinium ion has been determined by the emf method in five methanol-water solvents (10 to 70 wt % MeOH) at 25 °C and in three solvents (10, 20, and 50 wt % MeOH) from 10 to 40 °C. From the variation of the dissociation constant with temperature, the changes of enthalpy, entropy, and heat capacity were derived and compared with similar data for piperazinium ion in water. The variation of pK, $\Delta S°$, and $\Delta C_p°$ have been used to interpret the effect of the double positive charge on the solute-solvent interactions as compared to the effect exhibited by a single positive or a negative charge.

Key words: Dissociation constant; ionization constant; methanol; mixed solvents; piperzaine; pK; thermodynamics.

1. Introduction

The piperazinium ion dissociates in two stages:

$$PzH_2^{++} + H_2O \leftrightarrows H_3O^+ + PzH^+, \quad K_1$$

$$PzH^+ + H_2O \leftrightarrows H_3O^+ + Pz, \quad K_2$$

where Pz represents the neutral base piperazine,

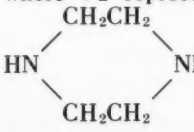

about 25,000 times as large as the second, so the two equilibria can conveniently be studied separately.

In elucidating the role of ionic charge in ion-solvent interactions, the influence of changing solvent composition on an equilibrium such as the first stage in the dissociation of diprotonated piperazinium ion is of unusual interest. Although considerable attention has been devoted to the nature of solvent effects on the dissociation and related thermodynamic behavior of neutral and singly charged acids, it appears that no similar investigation of the dissociation of a doubly charged cation acid has been made. It is the purpose of this paper to report the results of a study of the first dissociation of piperazinium ion in five methanol-water solvents containing 10, 20, 33.4, 50, and 70 wt percent methanol.

2. Method

The p_sK_1 of piperazinium ion in methanol-water mixtures was determined by measuring the emf of the cell

Pt; H_2(g, 1 atm), Pz · 2HCl(m),

Pz · HCl(m) in X wt % methanol, AgCl; Ag

where m is molality and X is 10, 20, 33.4, 50, or 70 wt percent. The measurements in 33.4 and 70 wt percent methanol were made at 25 °C and those in 10, 20, and 50 wt percent methanol from 10 to 40 °C.

The p_sK_1 was calculated by the equation

$$p_sK_1 = \frac{(E - {}_sE°)F}{RT \ln 10} + \log m_{Cl^-} + \log \frac{m_{PzH_2^{++}}}{m_{PzH^+}} + \log \left({}_s\frac{\gamma_{PzH_2^{++}} \cdot \gamma_{Cl^-}}{\gamma_{PzH^+}} \right) \quad (1)$$

where ${}_sE°$ is the standard potential of the silver-silver chloride electrode in methanol-water mixtures [1–4].[1]

The activity coefficients of each ionic species i was estimated with the aid of the Debye-Hückel equation

$$-\log {}_s\gamma_i = \frac{A\sqrt{I}\sqrt{d_0}}{1 + B\mathring{a}\sqrt{I}\sqrt{d_0}} \quad (2)$$

*Present address: Department of Chemistry, University of Florida, Gainsville, Florida 32601.

[1] Figures in brackets indicate the literature references at the end of this paper.

where A and B are the constants of the Debye-Hückel theory, dependent only on the temperature and dielectric constant of the solvent, d_0 is the density of the solvent, I is the total ionic strength, and $\mathring{a}$ is the ion-size parameter. The values of $A\sqrt{d_0}$ and $B\sqrt{d_0}$ for the solvent mixtures have been given elsewhere [3, 5, 6].

A small correction for the ionization of the PzH_2^{++} ion was made by estimating the molality of hydrogen ion formed with the aid of the approximation

$$-\log m_H = p_s(a_H\gamma_{Cl}) + \log {}_s(\gamma_H\gamma_{Cl}) = p_s(a_H\gamma_{Cl}) - \frac{2A\sqrt{I}\sqrt{d_0}}{1+B\mathring{a}\sqrt{I}\sqrt{d_0}}. \quad (3)$$

The acidity function $p_s(a_H\gamma_{Cl})$ was derived from the experimental data by the equation

$$p_s(a_H\gamma_{Cl}) = \frac{(E - {}_sE^\circ)F}{RT\ln 10} + \log m_{Cl^-}. \quad (4)$$

The "approximate" dissociation constant p_sK_1' was then defined as follows:

$$p_sK_1' \equiv \frac{(E - {}_sE^\circ)F}{RT\ln 10} + \log m_{Cl^-} + \log \frac{m - m_{H^+}}{m + m_{H^+}} - \frac{4A\sqrt{I}\sqrt{d_0}}{1+B\mathring{a}^\circ\sqrt{I}\sqrt{d_0}} = p_sK_1 - \beta I \quad (5)$$

where β is the slope parameter. The p_sK_1' varies linearly with I when the proper value of $\mathring{a}$ is chosen; its value at infinite dilution is p_sK_1. The method of least squares with the OMNITAB computer program was used to calculate the values of p_sK_1, β, and $\mathring{a}$. The "true" values of p_sK_1, β, and $\mathring{a}$ were assumed to be those which gave the smallest standard deviation of regression.

3. Experimental Procedure

The general experimental procedures closely followed those used previously in methanol-water

TABLE 1. *Electromotive force of the cell:* Pt; $H_2(g, 1\ atm)$, *Piperazine* · 2HCl (m), *Piperazine* · HCl (m), AgCl; Ag *in water-methanol mixtures from 10 to 40 °C (in volts)*

m	10°	15°	20°	25°	30°	35°	40°
			10 Wt % Methanol				
0.002689	0.66092	0.66031	0.65949	0.65844	0.65713	0.65564	0.65397
.005166	.64872	.64792	.64689	.64563	.64417	.64248	.64058
.007367	.64245	.64155	.64043	.63908	.63751	.63573	.63375
.009903	.63747	.63652	.63532	.63389	.63226	.63041	.62835
.01218	.63415	.63314	.63189	.63041	.62873	.62683	.62473
.01471	.63112	.63006	.62877	.62725	.62553	.62360	.62145
.01746	.62851	.62741	.62608	.62451	.62277	.62078	.61862
.01981	.62653	.62532	.62401	.62244	.62062	.61853	.61644
.02226	.62482	.62366	.62227	.62067	.61885	.61682	.61461
.02463	.62332	.62215	.62073	.61910	.61728	.61524	.61299
.03761	.61742	.61615	.61465	.61293	.61101	.60889	.60658
.04970	.61364	.61230	.61073	.60897	.60700	.60484	.60247
			20 Wt % Methanol				
0.003242	0.64453	0.64354	0.64234	0.64090	0.63928	0.63741	0.63545
.006150	.63318	.63203	.63066	.62906	.62727	.62528	.62305
.008753	.62734	.62610	.62465	.62295	.62110	.61904	.61675
.01204	.62226	.62094	.61941	.61766	.61573	.61358	.61122
.01513	.61884	.61748	.61591	.61410	.61211	.60993	.60752
.01781	.61651	.61511	.61350	.61167	.60967	.60745	.60502
.02146	.61382	.61238	.61073	.60886	.60682	.60457	.60210
.02382	.61242	.61096	.60930	.60741	.60536	.60309	.60061
.02714	.61062	.60914	.60745	.60553	.60345	.60117	.59867
.03270	.60812	.60658	.60486	.60292	.60082	.59849	.59597
.04548	.60395	.60237	.60057	.59855	.59641	.59405	.59148
.04863	.60308	.60147	.59967	.59767	.59550	.59312	.59055
			50 Wt % Methanol				
0.002483	0.61288	0.61033	0.60773	0.60490	0.60189	0.59882	0.59559
.005169	.60115	.59846	.59568	.59271	.58953	.58618	.58280
.007478	.59609	.59336	.59051	.58747	.58425	.58090	.57746
.009872	.59211	.58933	.58647	.58339	.58015	.57673	.57326
.01198	.58983	.58699	.58407	.58100	.57780	.57439	.57088
.01501	.58688	.58407	.58115	.57803	.57469	.57133	.56784
.01728	.58540	.58258	.57966	.57653	.57325	.56982	.56630
.01996	.58360	.58076	.57781	.57469	.57142	.56795	.56445
.02213	.58262	.57980	.57685	.57371	.57041	.56698	.56344
.02501	.58113	.57826	.57532	.57216	.56888	.56542	.56190
.04988	.57446	.57156	.56857	.56541	.56210	.55864	.55511

system [3] and applied to a determination of the dissociation constants of piperazinium ion in water [7]. The cells used were of the improved type described elsewhere [8].

A stock solution containing equal moles of piperazine mono- and dihydrochloride was prepared by dissolving the required weight of free piperazine in standard aqueous hydrochloric acid. Weight dilutions with additional water and methanol were made to achieve the desired molality and solvent composition.

Methanol (spectro grade) was used as obtained commercially without further purification. Hydrochloric acid for the preparation of solutions was distilled twice and standardized by gravimetric determination of chloride. The piperazine was a portion of the same material used for the study in water [7].

4. Results

The emf data, corrected to 1 atm hydrogen pressure, are summarized in tables 1 and 2. The values of p_sK_1 and $\mathring{a}$ derived from the experimental data are listed in table 3. The estimated uncertainties in p_sK_1 are given in the last column of table 3. They represent two standard deviation limits.

The experimental p_sK_1 values were fitted to the Harned-Robinson equation [9], where T is the thermodynamic temperature,

$$pK = A/T + B + CT \qquad (6)$$

by the method of least squares using the OMNITAB computer program. The constants A, B, and C are given in table 4. The residual standard deviation of the fit to the Harned-Robinson equation was less than 0.001 in all three methanol-water mixtures.

5. Thermodynamic Functions

The standard thermodynamic quantities for the acidic dissociation of piperazinium ion in three methanol-water mixtures were calculated by the usual thermodynamic formulas from the constants of eq (6) given in table 4. The values for 10, 25, and 40 °C are listed in table 5. The estimated uncertainties in these values at 25 °C are given in parentheses. They again represent two standard deviation limits as obtained by variance analysis.

6. Discussion

The effect of changing solvent composition on the acidic dissociation constant of diprotonated piperazinium ion and the associated thermodynamic constants for the dissociation process are summarized in table 6. As is the case for singly charged cation acids, enrichment of the solvent with methanol increases the degree of dissociation. Unlike most of the singly charged cation acids, however, the pK of diprotonated piperazinium ion appears not to have reached a minimum at a solvent composition of 70 wt percent methanol. With the decrease in pK there is a small regular increase in the enthalpy of dissociation. Much more striking, however, are the changes in the entropy and heat capacity of dissociation when the percentage of methanol in the solvent is increased. The entropy change becomes rapidly more positive, while the

TABLE 2. *Electromotive force of the cell:* Pt; H_2(*g*, *1 atm*), *Piperazine* ·2HCl (*m*), *Piperazine* · HCl (*m*), AgCl; Ag *in water-methanol mixtures at 25 °C* (*in volts*)

Wt % Methanol			
33.4		70	
m	*E*	*m*	*E*
0.002375	0.62944	0.002457	0.57070
.004876	.61584	.005206	.56024
.007578	.60842	.009058	.55410
.009933	.60416	.01009	.55289
.01261	.60060	.01241	.55097
.01495	.59817	.01456	.54940
.01762	.59588	.01844	.54744
.02032	.59396	.01976	.54682
.02253	.59255	.02388	.54534
.02516	.59114	.02458	.54508
.03744	.58620	.03653	.54222
.05018	.58279		

TABLE 3. *The first dissociation constant of piperazinium ion in five water-methanol solvent mixtures from 10 to 40 °C*

Wt % Methanol	*t*	p_sK_1	*a*	Estimated uncertainty
	°C		(Å)	
10	10	5.496	3.1	0.001
	15	5.390	3.1	.001
	20	5.288	3.1	.001
	25	5.190	3.2	.001
	30	5.095	3.2	.001
	35	5.002	3.3	.001
	40	4.911	3.3	.001
20	10	5.372	2.8	.001
	15	5.260	2.9	.001
	20	5.152	2.9	.001
	25	5.048	2.9	.001
	30	4.949	3.0	.001
	35	4.851	3.0	.001
	40	4.756	3.1	.001
33.4	25	4.854	3.0	.001
50	10	4.916	2.1	.003
	15	4.798	2.0	.003
	20	4.690	2.1	.003
	25	4.583	2.1	.003
	30	4.481	2.1	.003
	35	4.384	2.1	.003
	40	4.291	2.1	.003
70	25	4.293	0	.005

TABLE 4. *Values of the constants for the temperature variation of the dissociation constant*

Wt % Methanol	*A*	*B*	*C*
10	1534.587	0.6891	−0.00216628
20	1890.389	−1.5377	.000824178
50	2353.773	−5.0240	.00574370

change in heat capacity, which has a large positive value in the aqueous solvent, decreases sharply, reaching a value of -66 J K^{-1} mol^{-1} when half of the mass of the water solvent has been replaced by methanol.

The contrary variation of $\Delta S°$ and $\Delta C_p°$ as the molecular structure of the acid is modified progressively by substitution or as the composition of the solvent is progressively altered has long been observed but is not completely understood. Electrostatic interactions between simple ions and dipolar solvent molecules would be expected to alter the entropy and heat capacity of the system in the same direction. Indeed, orientation of solvent molecules in the neighborhood of the ions should lead to a decrease in both quantities. The fact that methanol is less polar than water is therefore consistent with the observation that $\Delta S°$ for the dissociation of diprotonated piperazinium ion increases as methanol is added to the solvent.

Everett and his coworkers [10–12] have suggested that the variation of heat capacity effects in the opposite sense to entropy effects may be caused by "hydrophobic interactions" between neutral molecules and the solvent structure. Although the locus of charge on the monoprotonated piperazinium ion presumably is surrounded by a hydration shell, there remains a considerable length of hydrocarbon chain beyond the influence of the charge. This portion of the structure can interact with the solvent in the same way as a neutral molecule [11]. In the diprotonated ion, however, the two charges at opposite ends of the ring assure, through their cooperative influence, that hydrophobic interactions with the solvent are of little importance.

Solvent effects on the pK of weak acids in methanol-water solvents are strongly dependent on the charge type of the dissociation process [6]. In figure 1, the change in pK, namely $p({}_sK) - p({}_wK)$, as methanol is added to the aqueous solvent is plotted for acids of four charge types. These acids are dihydrogen phosphate ion [13, 14], acetic acid [15], ammonium ion [5], and the doubly charged piperazinium cation, PzH_2^{++}. Although some individual variations are to be expected, the strong interactions between bivalent ions and the solvent molecules are reflected in the sign and magnitude of the solvent effect.

TABLE 5. *Standard thermodynamic quantities for the acidic dissociation of* PzH_2^{++} *ion in water-methanol solvent mixtures*

Wt % Methanol	*t*	$\Delta H°$	$\Delta S°$	$\Delta C_p°$
	°C	*J mol*$^{-1}$ [a]	*J K*$^{-1}$ *mol*$^{-1}$ [a]	*J K*$^{-1}$ *mol*$^{-1}$ [a]
10	10	32,706	10.3	23
	25	33,068 (69)	11.5 (0.2)	25 (16)
	40	33,448	12.8	26
20	10	34,928	20.5	−9
	25	34,790 (118)	20.0 (0.4)	−9 (27)
	40	34,645	19.6	−10
50	10	36,248	33.9	−62
	25	35,289 (97)	30.6 (0.3)	−66 (22)
	40	34,281	27.3	−69

[a] 4.184 J = 1 cal.

TABLE 6. *Solvent effect on the thermodynamic quantities for the acidic dissociation of* PzH_2^{++} *ion in water-methanol solvents at 25 °C*

Wt % Methanol	*pK*	$\Delta H°$	$\Delta S°$	$\Delta C_p°$
		J mol^{-1}	*J K*$^{-1}$ *mol*$^{-1}$	*J K*$^{-1}$ *mol*$^{-1}$
[a]0	5.333	31,080	2.2	86
10	5.190	33,068	11.5	25
20	5.048	34,790	20.0	−9
33.4	4.854	.....	.....	.....
50	4.583	35.289	30.6	−66
70	4.293	.....	.....	.....

[a] Reference [7].

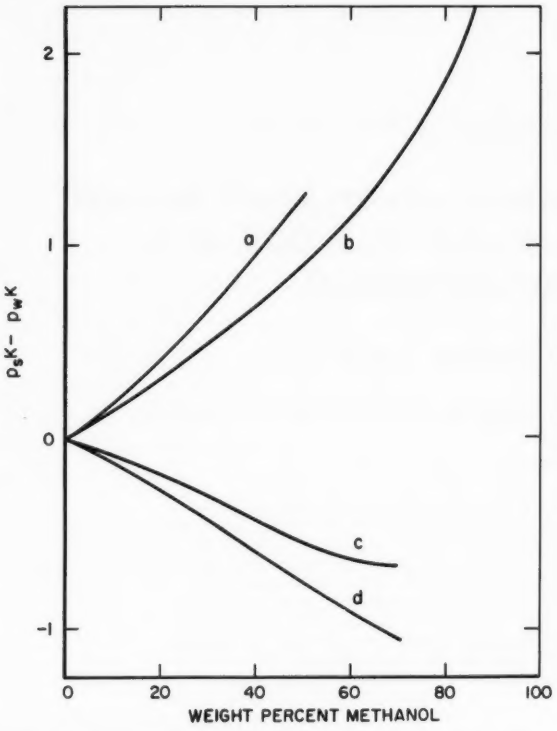

FIGURE 1. *Change of* pK *with solvent composition for weak acids of four different charge types:* (a) *dihydrogen phosphate ion;* (b) *acetic acid;* (c) *ammonium ion;* (d) *diprotonated piperazinium ion.*

7. References

[1] Harned, H. S., and Thomas, H. C., J. Am. Chem. Soc. **57,** 1666 (1935); **58,** 761 (1936). The $_sE°$ values of Harned and Thomas at 25 °C have been recalculated (see ref. [4]). The $_sE°$ values at other temperatures have been corrected in the same ratio.

[2] Bates, R. G., and Rosenthal, D., J. Phys. Chem. **67,** 1088 (1963).

[3] Paabo, M., Robinson, R. A., and Bates, R. G., J. Chem. Eng. Data **9,** 374 (1964).

[4] Paabo, M., Bates, R. G., and Robinson, R. A., Anal. Chem. **37,** 462 (1965).

[5] Paabo, M., Bates, R. G., and Robinson, R. A., J. Phys. Chem. **70,** 247 (1966).

[6] Bates, R. G., and Robinson, R. A., Acid-base behavior in methanol-water solutions, in Chemical Physics of Ionic Solutions, B. E. Conway and R. G. Barradas, eds. (John Wiley & Sons, Inc., New York, N.Y., 1966).

[7] Hetzer, H. B., Robinson, R. A., and Bates, R. G., J. Phys. Chem. **72,** 2081 (1968).

[8] Gary, R., Bates, R. G., and Robinson, R. A., J. Phys. Chem. **68,** 1186 (1964).

[9] Harned, H. S., and Robinson, R. A., Trans. Faraday Soc. **36,** 973 (1940).

[10] Everett, D. H., Landsman, D. A., and Pinsent, B. R. W., Proc. Roy. Soc. **A215,** 403 (1952).

[11] Cox, M. C., Everett, D. H., Landsman, D. A., and Munn, R. J., J. Chem. Soc. (B), 1373 (1968).

[12] Timimi, B. A., and Everett, D. H., *ibid.*, 1380 (1968).

[13] Ender, F., Teltschik, W., and Schafer, K., Z. Elektrochem. **61,** 775 (1957).

[14] Paabo, M., Robinson, R. A., and Bates, R. G., J. Am. Chem. Soc. **87,** 415 (1965).

[15] Shedlovsky, T., and Kay, R. L., J. Phys. Chem. **60,** 151 (1956).

(Paper 74A5–631)

JOURNAL OF RESEARCH of the National Bureau of Standards—A. Physics and Chemistry
Vol. 74A, No. 5, September–October 1970

Thermal Conductivity Standard Reference Materials From 4 to 300 K. I. Armco Iron: Including Apparatus Description and Error Analysis*

J. G. Hust,** Robert L. Powell,** and D. H. Weitzel**

Institute for Basic Standards, National Bureau of Standards, Boulder, Colorado 80302

(May 15, 1970)

An apparatus for the measurement of thermal conductivity, electrical resistivity, and thermopower of solids from 4 to 300 K is described. This apparatus, a modified version of the one used earlier in this laboratory, utilizes the steady-state, axial heat flow method. Included is a detailed discussion of the limitations of the apparatus, probable errors, and data analysis methods.

Thermal conductivity, electrical resistivity, Lorenz ratio, and thermopower data are reported for several specimens of Armco iron for temperatures from 4 to 300 K. At low temperatures the electrical resistivity and thermal conductivity vary from specimen to specimen by more than 10 percent. However, the Lorenz ratios of these specimens differ by less than 2.5 percent; and the intrinsic resistivities calculated by using Matthiessen's rule differ by less than 0.5 percent of the total resistivities. Thus, Armco iron specimens can be used as standards by measuring the residual resistivities and utilizing the Lorenz ratio reported here.

Key words: Cryogenics; equipment; electrical resistivity; error analysis; iron; Lorenz ratio; Seebeck effect; thermal conductivity; transport properties.

Contents

	Page
1. Introduction	674
2. Experimental apparatus	674
2.1. Specimen assembly and thermocouples	675
2.2. Temperature controls	676
2.3. Thermal tempering of wires	677
2.4. Measuring system	677
3. Specimen preparation and measurement techniques	677
4. Calculations and data analysis	678
4.1. Thermal conductivity	678
4.1.1. Difference method	678
4.1.2. Semi-continuous method	678
4.1.3. Continuous method	678
4.2. Electrical resistivity	679
4.2.1. Mean temperature method	679
4.2.2. Approximate integral method	679
4.3. Thermopower	679
4.4. Lorenz ratio	680
5. Error analysis	680
5.1. Temperature measurement errors	680
5.1.1. Reference block temperature	681
5.1.2. Specimen temperatures	681
5.2. Heat flow errors	681
5.2.1. Conduction losses	682
5.2.2. Radiation losses	682
5.2.3. Temperature drift effects	682
5.3. Dimensional and measuring system errors	683
5.4. Precision, accuracy, and uncertainty	683
6. Specimen characterization	684
7. Results	685
8. Discussion	686
9. References	689

*This work was carried out at the National Bureau of Standards under the sponsorship of the NASA(SNPO–C), Contract R–45.
**Cryogenics Division, National Bureau of Standards, Boulder, Colo. 80302.

1. Introduction

The development of new structural materials and renewed interest in existing materials by the aerospace industry is creating a demand for thermal and electrical property measurements on these materials. Such data are needed for the selection of suitable construction materials and the prediction of operating characteristics of low-temperature systems. To help satisfy the immediate needs for these data, an apparatus has been built to measure the thermal conductivity, electrical resistivity, and thermopower of solids. This apparatus is designed to measure samples with thermal conductivities varying from 0.1 to 5,000 W/mK at temperatures from 4 to 300 K.

Thermal conductivitity data of technically important solids accurate to 5 percent satisfy current demands. However, future demands will likely be more stringent. For this reason the present program is directed toward the acquisition of thermal conductivity data which are accurate to within 1 percent. Thermal conductivity data accurate to within 1 percent are difficult to determine, especially for poor conductors or at temperatures above about 120 K, because of the difficulty of maintaining thermal losses at a sufficiently low level.

Measurements have been made on several aerospace alloys, Hust et al. [1].[1] Another phase of this program, to establish standard reference data on several reference materials (or specimens), has begun. We intend to measure several specimens of materials which appear to be useful as standards. For some materials, material variability may be so great that only standard reference specimens, i.e., measured specimens (not standard materials), will be useful. Standard reference specimens or materials are useful for intercomparison of existing apparatus, for debugging new apparatus, and for calibration of comparative apparatus. The apparent large differences between the results of various investigators for a given material (50% is not unheard of) are evidence of the need for intercomparisons, calibrations, and standardization. The availability of standard reference materials will result in more accurate and more permanent transport property data for technically important solids.

This paper contains the results of our measurements on the transport properties of Armco iron.[2] Armco iron was investigated at low temperatures primarily because of its extensive use as a thermal conductivity standard at higher temperatures by R. W. Powell[3] and others [2]. Also included are a complete description of the apparatus, data analysis methods, and uncertainty analysis of the results. This apparatus is similar to that described by R. L. Powell et al. [3]; however, a sufficient number of modifications have been made to warrant a complete new description.

[1] Figures in brackets indicate the literature references at the end of this paper.

[2] The use in this paper of trade names of specific products is essential to a proper understanding of the work presented. Their use in no way implies any approval, endorsement, or recommendation by the National Bureau of Standards. Armco iron is a registered trade name of a commercially pure iron produced by Armco Steel Corporation.

[3] Two authors in this field have the same surname. R. W. Powell has done most of his research above room temperature. For many years he was at the National Physical Laboratory in England; he is now at the Thermophysical Properties Research Center of Purdue University.

2. Experimental Apparatus

Of the many methods described in the literature for the measurement of thermal conductivity, probably the simplest both conceptually and mechanically is the axial heat flow method. In this configuration the specimen is in the form of a rod with constant cross-sectional area and the heat flow is along the axis of the rod. This configuration is also convenient for the simultaneous measurement of the electrical resistance and the Seebeck voltage. Accurate measurements can be obtained by this method as long as radiation and other radial losses can be limited to a reasonable value. Above 300 K this is difficult to do except for good conductors. The temperature range of interest in this work is below 300 K; thus the axial heat flow method was chosen to obtain the most accurate data. The apparatus is shown in figure 1.

The cryostat consists of concentrically mounted specimen, specimen shield (filled with glass fiber), vacuum can, and glass cryogen dewar. The glass dewar is supported by a stainless steel container soldered to the top plate to create a closed system. This system is immersed in a nitrogen-filled stainless steel dewar. For temperatures up to about 200 K, the inner glass dewar

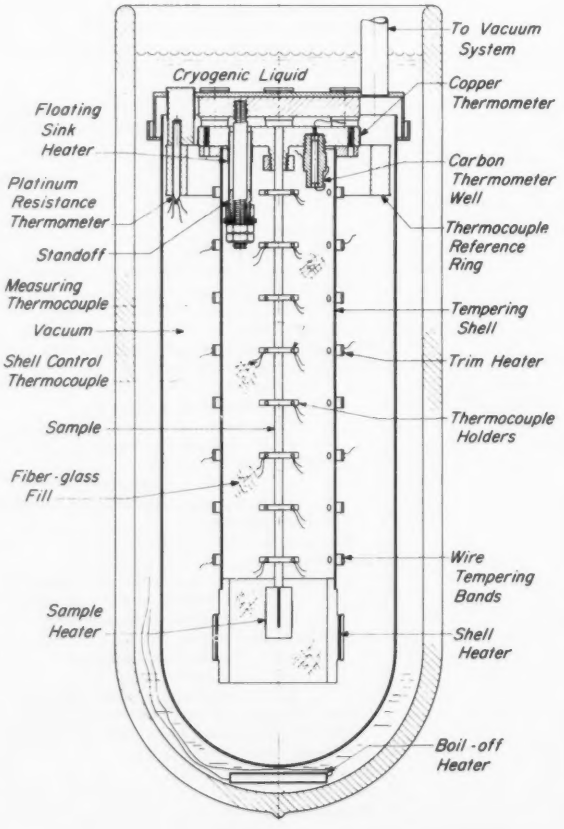

FIGURE 1. *Thermal conductivity apparatus.*

is filled with liquid helium, hydrogen, or nitrogen depending on the temperature range desired. The outer dewar is filled with liquid nitrogen to reduce the boil-off rate of the liquid in the inner dewar. The pressure above the liquid in the inner dewar is controlled with a manostat to isolate the bath from atmospheric pressure variations which in turn would create temperature variations of the bath. To obtain measurements in the range of 200 to 300 K, the outer stainless steel dewar is removed and the inner dewar is filled with either a dry ice–alcohol bath or an ice-water bath.

The top end of the specimen is clamped to a temperature-controlled copper heat sink (floating sink). A heater is attached to the bottom end of the specimen. The temperature of the specimen is determined at eight equally spaced positions along its length by thermocouples fastened to knife-edged thermocouple holders. Heat losses from the specimen are minimized by evacuating the specimen chamber, surrounding the specimen with a temperature-controlled cylindrical shell, and filling the space between the specimen and shell with glass fiber. The upper end of the shell surrounding the specimen is attached to the floating sink. The shell temperature distribution is controlled by means of a main heater at the bottom of the shell and three trim heaters equally spaced along the shell. The temperature differences between the specimen and shell are determined by differential thermocouples located at the heater positions.

The floating sink is attached to the lid of the vacuum can by means of three replaceable standoff bolts and sleeves. An electrical heater is wrapped on the sleeves to allow temperature control of the floating sink and thus the upper end of the specimen and surrounding shield.

A heavy copper ring (about 10 cm diam, 1 cm thick, and 2.5 cm long) is attached to and in good thermal contact with the lid of the vacuum chamber. This lid in turn is in direct contact with the pressure-controlled cryogenic liquid. The copper ring serves as the temperature reference for all of the thermocouples in the system. Mounted in the copper ring is a platinum resistance thermometer to determine the reference temperature for temperatures above 20 K. The reference temperature at helium temperatures is determined by the vapor pressure of the liquid helium.

The electrical resistance of the specimen is determined by passing an electrical current through it and measuring the potential drop between thermocouple holders number one and eight. Forward and reverse readings are taken to eliminate the Seebeck voltage from this measurement. The Seebeck voltage (thermovoltage) is determined from the difference in forward and reverse readings and is also measured directly with zero electrical current. These determinations of the Seebeck voltage agree with one another to within the noise of the null detector system ($\pm 0.01\ \mu V$). The Seebeck voltage is measured with respect to "normal" Ag wire (Ag–0.37 at % Au).

The differences between this apparatus and that described earlier by R. L. Powell et al. [3] are (1) the addition of the floating sink and its associated control circuitry, (2) two additional trim heaters along the shell surrounding the specimen, (3) use of glass fiber radiation shielding around the specimen necessary for extending measurements above 120 K, (4) pressure control on the space above the cryogenic liquid, (5) use of thermocouples with a higher sensitivity and stability at low temperatures, and (6) use of more advanced electronic control circuitry and measuring apparatus.

2.1. Specimen Assembly and Thermocouples

The specimen is clamped at its upper and lower ends to the floating sink and specimen heater, respectively. To improve the thermal contact at these clamps, a low vapor pressure thermal contact grease is applied. Better contact has been obtained using an alloy of indium and gallium (liquid at room temperature). However, it was found that this material reacts with aluminum, for example, and probably diffuses quite rapidly with other samples. Its use was discontinued until more of its characteristics are understood.

The specimens are 23-cm-long cylinders. The cross-sectional area of each is based on the thermal conductivity of that specimen. The best conductors have the smallest cross-sectional area (0.1 cm^2), while the poorest conductors have the largest cross-sectional area (1 cm^2). The diameter of each specimen is measured to within ± 0.0001 cm at several points along its length. The maximum diameter variation of each specimen is about ± 0.0003 cm from the mean diameter.

The thermocouples are attached to the thermocouple holders via epoxy cement, a metal cylinder, and a coating of low vapor pressure thermal contact grease. This assembly is shown in figure 2. The knife edge on each thermocouple holder fits into a machined groove (0.05 mm deep) on the specimen. These grooves are machined at a spacing of 2.540 ± 0.003 cm. The actual spacing is determined with a goniometric microscope to ± 0.0001 cm.

The temperature measuring and differential thermocouples are ISA Type KP versus Au-Fe (Au-0.07 at % Fe). These thermocouples were fabricated from single rolls of type KP and Au-Fe wires. Segments

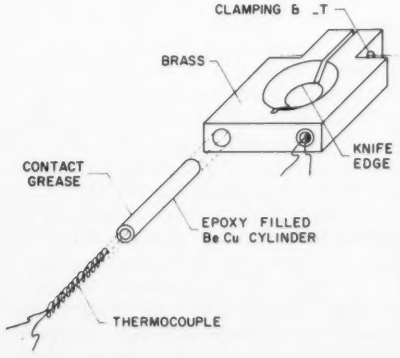

FIGURE 2. *Thermocouple mount.*

of wire from the beginning and end of these rolls were spot calibrated in the range 4 to 300 K using the boiling points of liquid helium, liquid hydrogen, and liquid nitrogen, the sublimation point of CO_2, and the triple point of water. These spot calibrations were compared with the standard table (as established at this laboratory by Sparks et al. [4], and a new table was established for these thermocouples. The differences between thermocouples from the same roll were negligible, i.e., the emf of a thermocouple constructed from the opposite ends of the Au-Fe wire used in this apparatus was less than 1 μV with one junction in liquid helium and the other junction in ice. This represents a change in the mean thermopower of less than 1 part in 5000. One of the thermocouples in the apparatus was also intercompared with a germanium-resistance-thermometer from 4 to 30 K. In this range no difference could be measured, to within 1 μV, between this thermocouple and those fabricated for spot calibration. The thermopower of the standard thermocouple is illustrated in figure 3. The emf differences between the thermocouples used in this apparatus and the standard calibration table are shown in figure 4.

The standard table for these thermocouples presented by Sparks et al. [4] is based on the temperature scale IPTS–68 above 20 K and on the NBS P2–20 (1965) scale below 20 K. The IPTS–68 is the present best estimate of the thermodynamic temperature scale. The gradient along the specimen as determined from these thermocouples and used for calculating thermal conductivity is thus based on these scales.

2.2. Temperature Controls

High-precision temperature controllers are used on the floating sink, the shell surrounding the specimen, and the cryogenic liquid surrounding the specimen chamber. The first two are electronic while the latter

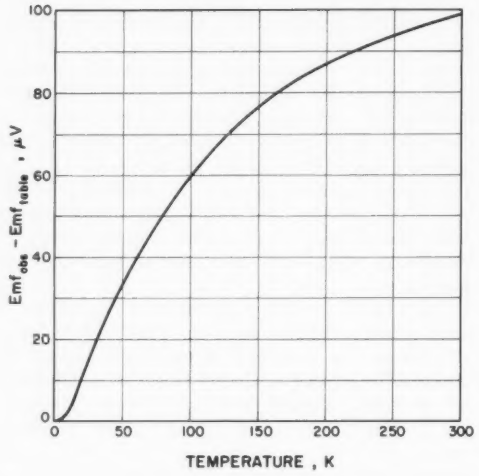

FIGURE 4. *Emf differences between the thermocouples used in this apparatus and the standard calibration table.*

is mechanical. The heart of the electronic controllers is a dc proportional and integral amplifier capable of 1 mK control when used in conjunction with a dc bridge, differential thermocouples, and conventional low-level (microvolt) amplifiers. This unit was developed by J. C. Jellison and N. C. Winchester of the NBS Cryogenics Division. The control circuit for the floating sink is shown in figure 5. The sensing resistor is a copper wire resistor for temperatures above about 30 K and a conventional carbon resistor for temperatures below about 30 K. The dummy leads shown are leads from the instrumentation rack to the cryostat paralleling those to the sensing resistor. This is to compensate for temperature drift effects on the sensing resistor leads. This circuit is capable of controlling the floating sink temperatures, and therefore

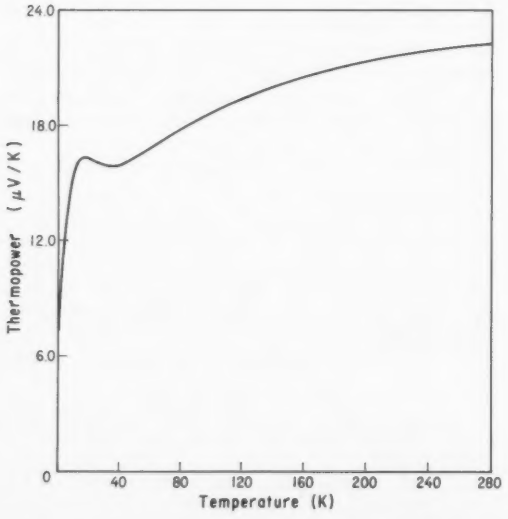

FIGURE 3. *Thermopower of chromel versus* Au-Fe (Au-*0.7 at* % Fe).

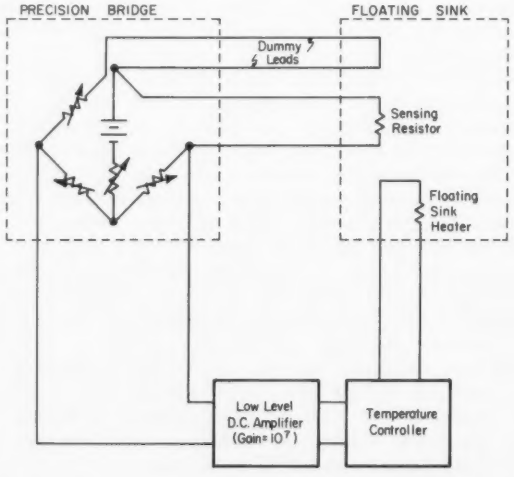

FIGURE 5. *Control circuit for floating sink.*

the upper end of the specimen, to better than 1 mK.

The shell-to-specimen difference temperature is controlled with a similar circuit, but the sensing elements are the differential thermocouples between the shell and specimen. This circuit is capable of maintaining the shell temperature within 1 mK of the specimen temperature at the control point. The bottom (main) heater and the three trim heaters on the shell are automatically controlled.

The mechanical pressure control (manostat) on the cryogenic liquid surrounding the cryostat is capable of controlling the vapor pressure of the liquid to about 0.1 torr. This manostat is similar to one described by Cataland et al. [5]. For liquid nitrogen, hydrogen, and helium at their normal boiling points this corresponds to temperature control of 1, 0.3, and 0.1 mK, respectively. At the triple point of nitrogen a pressure variation of 0.1 torr corresponds to a temperature variation of 5 mK. These numbers are somewhat unrealistic, since undoubtedly there is some stratification in the liquid. Thus, as the liquid level drops due to boil-off, the temperature at a fixed point in the dewar changes slightly even though the pressure at the surface remains constant.

2.3. Thermal Tempering of Wires

All of the leads attached to the specimen assembly are brought horizontally to the shell, then up the shell, and finally to the reference temperature block. On the reference temperature block the wires are all soldered to small copper wires which are taken out of the vacuum system via stainless steel tubes and wax seals at room temperature. It is important that the wires are brought into near thermal equilibrium with the shell and reference block respectively. To accomplish this, a calculated length of wire is cemented to an isothermal region of each of these components. The length calculation has been performed (with a safety factor of about 5) as described by Hust [6] to assure a temperature difference of less than 1 mK. Bringing about such equilibrium is here referred to as thermal tempering or just tempering.

It is obvious in the case of the reference temperature block that these wires must be tempered to the reference block. Any errors which are present due to poor thermal tempering will appear directly in the apparent temperature of the sample. The differential thermocouples used to control the sample-to-shell temperature differences must also be well tempered to the proper isothermal region on the shell. To create isothermal regions on the shell, copper bands are attached to the stainless steel shell at each measuring position. Again the length of wire required to temper to within 1 mK has been used. All leads from the specimen are thermally tempered to the shell at the appropriate location to minimize the conduction heat loss along these leads.

All of the copper leads going from the reference temperature block to room temperature are thermally tempered to a copper block in contact with the liquid nitrogen in the outer dewar. This is to reduce heat flow to the reference block and also to reduce the boil-off rate during liquid helium tests.

2.4. Measuring System

To determine the thermal conductivity, electrical resistivity, and thermopower as a function of temperature we need to determine the temperature of the reference block, the temperature distribution of the specimen, the specimen heater power, the specimen resistance, the Seebeck emf, and the dimensions of the specimen. The emfs are measured with a seven-dial potentiometer-null detector system. The temperature of the reference block is determined from the resistance of a platinum resistance thermometer (No. 1037903) calibrated from 10 to 90 K on the NBS–55 scale and above 90 K on the IPTS (1948) scale. Corrections as compiled by Hust [7] have been applied to convert both of these to the IPTS–68. The 1958 He^4 vapor pressure scale [8] is used to establish the reference block temperature for the liquid helium tests.

The specimen heater power is determined by measuring the electrical current and voltage across the specimen heater. The voltage-measuring leads are connected so as to include one-half of the power generated in the current leads between the specimen and shell. This is based on the assumption that about one-half of the heat generated in these leads flows to the specimen heater while the other half flows to the shell. The electrical resistance of the wire from specimen-to-shell is about 0.2 percent of the total heater resistance. This connecting wire was selected as a compromise to satisfy two conflicting criteria: (a) small electrical resistance compared to the heater resistance, (b) large thermal resistance to minimize heat conduction from specimen-to-shell.

A strip chart recorder is part of the measuring system to facilitate observation of drift rates and other fluctuations in any of the measured voltages. This is used to indicate the degree of steady state achieved.

3. Specimen Preparation and Measurement Techniques

The specimens are machined and ground to specified nominal dimensions, after which they are accurately measured in a temperature-controlled measurement lab. Without further mechanical or thermal abuse, each specimen is fitted with thermocouple holders and heater. The specimen assembly is installed in the cryostat, the space between the shell and specimen is packed with glass fiber, and the vacuum can is soldered into place. The cryostat is evacuated to better than 10^{-5} torr and is subsequently cooled with the desired cryogenic liquid. The specimen is brought into equilibrium with the bath temperature (helium exchange gas at about 0.1 to 0.5 torr is generally introduced into the vacuum space to speed the approach to equilibrium). With all power to the specimen and shield heaters off, the zero emfs of the thermocouples are read. These zero corrections, caused by various inhomogeneities in the circuit, are considered to be constant throughout the run with each different cryogenic bath.

Data on a given run are taken only after thermal steady state has been established with a vacuum of better than 10^{-5} torr. Thermal steady state is considered established after systematic drift of the indicated thermocouple temperatures are below the detectability or controlability limit, approximately 1 mK per hour.

Isothermal resistivity data are obtained at the same time that the zero emfs are recorded. Also, to obtain further isothermal resistivity data and information regarding the differences between the eight measuring thermocouples, data are taken with the floating sink above the temperature of the surrounding bath but with no heat input to the specimen. The thermocouples thus indicate the temperature difference from the specimen to the reference block. If the specimen is at equilibrium with the floating sink, all eight thermocouples should produce the same emf. The scatter in these recorded emfs is an indication of the validity of using a single calibration table for all eight thermocouples. These measurements indicate that the thermocouple sensitivities are the same to within to 0.1 percent.

4. Calculations and Data Analysis

4.1. Thermal Conductivity

The defining equation for one-dimensional heat flow is

$$\dot{Q} = -\lambda(T) A \frac{dT}{dX} \tag{1}$$

where $\dot{Q}$ is the rate of heat flow through the rod, $\lambda(T)$ is the thermal conductivity of the rod at temperature T, A is the cross-sectional area of the rod, and dT/dX is the temperature gradient along the rod at temperature T.

Solving for $\lambda(T)$ we obtain

$$\lambda(T) = -\frac{\dot{Q}}{A}\frac{dX}{dT}. \tag{2}$$

Several methods can be used to obtain λ values from the experimental data.

4.1.1. Difference Method

Values of $\lambda(T)$ can be obtained from the measured values of X_i, T_i by equating the derivative dX/dT to the ratio of increments $\Delta X/\Delta T$ (ΔX and ΔT are the distances and temperature differences, respectively, between adjacent measuring positions on the specimen).

$$\lambda(\bar{T}) \approx -\frac{\dot{Q}}{A}\frac{\Delta X}{\Delta T} \tag{3}$$

This method results in seven values of $\lambda(\bar{T})$ for each run; $\bar{T}$ is the mean temperature between each adjacent pair of thermocouples.

4.1.2. Semi-Continuous Method

One could also represent functionally the X_i, T_i data by a least squares fit to obtain the parameters, A_1, A_2, . . . A_m,

$$X = X(T, A_1, A_2, \ldots A_m). \tag{4}$$

Then upon differentiation with respect to T to obtain $X' = dX/dT$, we have

$$\lambda(T) = -\frac{\dot{Q}}{A} X', \tag{5}$$

which yields a continuous set of values of λ over the temperature range of each run. Of course, since each run is treated separately one would end up with a set of discontinuous curves.

4.1.3. Continuous Method

It would be more desirable to represent the measured data for all of the runs simultaneously. This would have the advantage of resulting in a $\lambda(T)$ function continuous over the entire range of measurement. It is also more desirable because the statistics of the least squares fit are then based upon $8n$ points (n is the number of runs) instead of just 8 points. This can be accomplished in the following manner. In the absence of experimental errors, it is clear that one should obtain identical values of λ (from overlapping runs) at a given temperature regardless of the value of $\dot{Q}$, A, or X. For two overlapping runs these variables may be different at the given temperature. Thus if we rewrite eq (2) in the form

$$\lambda(T) = -\frac{dZ}{dT}, \qquad \text{where } Z = \frac{\dot{Q}X}{A}, \tag{6}$$

we see that

$$Z = Z(T, A_1, A_2, \ldots A_m) \tag{7}$$

can differ from run to run only by a constant. Thus in general we have

$$Z = Z_j(T, A_1, A_2, \ldots A_m) + b_j. \tag{8}$$

The b_j, called shift factors, serve only to account for the discontinuous shifts which occur in the Z versus T values from run to run, and do not appear directly in the function dZ/dT. Thus we can fit the $8n$ data points to determine the m parameters, $A_1, A_2, \ldots A_m$, and the n-1 shift factors, $b_2, b_3, \ldots b_n$. Note that the first shift factor may be arbitrarily set equal to zero. The number of degrees of freedom of the fit in the absence of other conditions is therefore $7n - m + 1$. In this experiment we have eight thermocouple measuring stations and the temperature differences between adjacent positions is generally smaller than about 10 K, sometimes less than 1 K. Because of these small temperature differences the results from eqs (3), (5), and (6) should be quite similar.

4.2. Electrical Resistivity

The measurement of current through and voltage across the specimen determines the specimen resistance, R, between measuring stations 1 and 8. Most of the measurements are made with a thermal gradient on the specimen and, since the measurement is across the entire specimen, the total span of temperature may be quite large (over 100 K). Thus resistivity, ρ, as a function of temperature, T, must be obtained from measured resistances of a nonisothermal specimen. The defining equation for resistivity is

$$R = \int_{x_1}^{x_2} \frac{\rho(T)\,dX}{A}. \tag{9}$$

4.2.1. Mean Temperature Method

The approach generally taken is to assume that $\rho(T)$ and dX/dT are slowly varying functions over the specimen, which results in

$$\rho(\bar{T}) \approx \bar{\rho}_x = \frac{RA}{x_2 - x_1}, \qquad \text{where } \bar{T} = \frac{T_2 + T_1}{2}, \tag{10}$$

and $\bar{\rho}_x$ is the average resistivity over the specimen.

It is noted that, if large gradients exist in the specimen, eq (10) may be significantly in error. In this experiment we have measured temperatures at eight positions along the specimen thus we can compensate partially for this error by computing $\bar{T}$ from eq (11)

$$\bar{T} \equiv \frac{\int_{x_1}^{x_2} T\,dX}{\int_{x_1}^{x_2} dX} \approx \frac{\sum_{i=1}^{7} \bar{T}_i \Delta X_i}{\sum_{i=1}^{7} \Delta X_i} \tag{11}$$

where the summation extends over the seven measured segments and $\bar{T}_i$ is the mean temperature of the ith segment. One can check the assumptions after obtaining the $\rho(\bar{T})$ curve. The $\rho(\bar{T})$ values are inserted into eq (9) and compared to the experimental data for each run. This calculation is done numerically with

$$R \approx \sum_{i=1}^{7} \frac{\rho(\bar{T}_i)\Delta X_i}{A}. \tag{12}$$

The differences between values calculated from eq (12) and measured resistances will indicate whether systematic errors exist in the data representation.

4.2.2. Approximate Integral Method

One can use the more correct but also more complicated procedure as follows. From eq (9) we obtain

$$RA = \int_{x_1}^{x_2} \rho(T)\,dx \approx \sum_{i=1}^{7} \rho(\bar{T}_i)\Delta X_i \tag{13}$$

where $\bar{T}_i$ is the mean temperature of the ith segment.

Now we assume a functional form for the resistivity versus temperature equation over the temperature range of all the measurements.

$$\rho(T) = a_1 f_1(T) + a_2 f_2(T) + \ldots a_m f_m(T) \tag{14}$$

where $a_1, a_2 \ldots a_m$ are parameters and $f_1, f_2 \ldots f_m$ are specified functions of temperature. Substituting (14) into (13) we obtain

$$RA = a_1 \sum_{i=1}^{7} f_1(\bar{T}_i)\Delta X_i + a_2 \sum_{i=1}^{7} f_2(\bar{T}_i)\Delta X_i + \ldots + a_m \sum_{i=1}^{7} f_m(\bar{T}_i)\Delta X_i. \tag{15}$$

With the n experimental values of $R (n \geq m)$ we may perform a least squares fit of (15) to determine the m parameters, $a_1, a_2 \ldots a_m$.

Some of the electrical resistivity measurements are carried out under isothermal conditions. For these measurements one obtains from (9) and (14)

$$RA = \frac{\rho(T)}{X_2 - X_1} = \frac{a_1 f_1(T)}{X_2 - X_1} + \frac{a_2 f_2(T)}{X_2 - X_1} + \ldots + \frac{a_m f_m(T)}{X_2 - X_1} \tag{16}$$

where T is measured. Thus (15) and (16) can be used simultaneously to determine the parameters.

4.3. Thermopower

The problem of determining the thermopower of a specimen is similar to that for determining the electrical resistivity. The quantity measured is the Seebeck voltage, V_s, over the temperature interval T_1 to T_2. The thermopower, S, is defined by

$$V_s = \int_{T_1}^{T_2} S\,dT = \bar{S}(T_2 - T_1). \tag{17}$$

For small gradients the equation (difference method)

$$\bar{S}(T) \approx \frac{V_s}{T_2 - T_1} \tag{18}$$

yields a relatively accurate estimation of the thermopower at temperature $\bar{T}$. However, as the gradients become larger, if S varies with T, this approximation becomes progressively worse. An approach which allows one to circumvent this difficulty is based on the following integral method. Assume a functional form for S,

$$S = b_1 g_1'(T) + b_2 g_2'(T) + \ldots + b_m g_m'(T), \qquad \text{where } g_i' = \frac{dg_i}{dT}. \tag{19}$$

Performing the integration in (17) we obtain

$$V_2 = b_1[g_1(T_2) - g_1(T_1)] + b_2[g_2(T_2) - g_2(T_1)] + \ldots + b_m[g_m(T_2) - g_m(T_1)]. \quad (20)$$

Equation (20) is dependent upon the measured variables V_s, T_2, T_1, and the parameters b_1, b_2, . . ., b_m. The m parameters can be determined by least squares fitting of $n \geq m$ sets of measurements.

4.4. Lorenz Ratio

The Lorenz ratio, L, is defined as the product of the total thermal conductivity, λ, and electrical resistivity, ρ, divided by temperature, T,

$$L = \frac{\rho\lambda}{T}. \quad (21)$$

Methods have been described to obtain λ and ρ as a function of temperature. These functions may be used directly to obtain the lorenz ratio as a function of temperature.

5. Error Analysis

Terms such as accuracy, uncertainty, imprecision, etc., are used with various meanings by different authors. This is due, at least in part, to the lack of rigorous definitions for some of these terms. To avoid this confusion a brief discussion of such terms is included here. This discussion is generally consistent with papers by Eisenhart [9], Natrella [10], ASTM [11], and Ku [12].

In this paper the words *accuracy* and *precision* will refer to a measurement process, while the word *uncertainty* will refer to the reported values obtained from such a process. The uncertainty of a reported value is indicated by giving credible limits within which the "true" value is to be found. There is, of course, a certain amount of risk that the true value will fall outside of these limits. The reporter's estimate of the magnitude of this risk is generally not made clear. Some authors will give limits which allow essentially no risk (100% confidence); others will allow large risk (say less than 50% confidence). In this paper we will consider the risk to be relatively small (about 95% confidence). The total uncertainty of a reported value is determined partly by the estimated accuracy (strickly, *in*accuracy) of a measurement process, partly by how well the inaccuracy is known, and, finally, by the number of times the process is repeated.

The accuracy of a given measurement process is determined by both the random and systematic (bias) errors inherent in the measurement process. The magnitude of the total random error determines the precision (strictly, the *im*precision) of the measurement. *Precision* thus concerns the closeness together or repeatability of measurements; while *accuracy* concerns closeness to what was to be measured. This implies that one must also very carefully state that which is to be measured. The usual basis of an index of precision is the standard deviation of the statistical distribution of the random errors of measurement. Unfortunately, a single comprehensive measure of accuracy (or inaccuracy), analgous to the standard deviation as a measure of imprecision, does not exist. To characterize one's knowledge of the accuracy of a measurement process it is necessary to indicate (a) limits to the systematic error or bias and the degree of confidence of the writer, and (b) the precision, using a well-defined index of precision. It is noted that the statistically precise concept of a family of confidence intervals associated with a definite confidence level is applicable only when the data are based on an adequate sampling of the total range of circumstances. It follows that these concepts are not strictly applicable when systematic errors are a significant part of the inaccuracy of the measurement process. In many experiments, including this one, it is highly impractical to accomplish an adequate sampling of the total range of circumstances, and thus a subjective estimate of the magnitude of systematic errors is necessary to describe completely the uncertainty of the results presented. It is, of course, desirable that these subjective estimates be based, as much as possible, on experimental evidence gathered under similar circumstances.

To characterize the uncertainty of a reported value, we will use the same approach as in characterizing the accuracy of a measurement process: (1) indicate limits to the probable *systematic* error in the final result at a subjectively estimated 95 percent confidence, (2) indicate the uncertainty of the final result due to *random* error by giving the 95 percent confidence interval for the mean. Note that this interval is dependent upon the number of measurements, while the standard deviation of the measurement process is not.

The total uncertainty of a reported value will be indicated by a single number obtained from the bias estimator (95% confidence) and the equivalent 95 percent confidence level confidence interval based on the imprecision of the measurements. We have chosen to take the root-mean-square value of these independent quantities as the uncertainty of the reported data with a 95 percent confidence.

The experimental errors in this work are classed generally as temperature measurement errors and heat flow errors. Each of these can be further subdivided into systematic and random errors. Both of these affect the overall uncertainty of the results but the latter determinines the imprecision of the measurement process. Some of these errors are systematic errors on a single run but tend to become randomized over the entire sequence of measurements on a single specimen. It is desirable to randomize as many as possible of the potential systematic errors (i.e., make measurements over a larger range of circumstances) to get a better measure of the probable data uncertainty from the imprecision of the measurement process.

5.1. Temperature Measurement Errors

In the determination of the uncertainty of thermal conductivity and thermopower both temperature and

temperature difference errors must be considered. In the measurement of electrical resistivity, however, only the temperature measurement errors contribute to the total uncertainty. This distinction should be noted in the following discussion.

5.1.1. Reference Block Temperature

The reference junction for each of the thermocouples is on the reference block. Thus any error in the temperature determination of the reference block will appear in all other measured temperatures. The reference block temperature is determined with a platinum resistance thermometer (PRT) for each of the runs except the liquid helium runs. The PRT measurements are uncertain by 0.01 K below 90 K and 0.002 K above 90 K. The PRT measurement uncertainty is caused primarily by thermally and electrically induced noise. This PRT was calibrated in 1953 by NBS, Washington. In 1966 its calibration was checked by L. L. Sparks of the NBS Cryogenics Division, Boulder, Colo. The differences found at 20, 75, and 273 K were -0.00057, 0.00007, and 0.0002 Ω, respectively. These differences were plotted and interpolations were performed on the resulting curve to obtain a new calibration for this PRT. The interpolation is uncertain to about 5 mK in the 20 to 90 K range and 1 mK in the 100 to 723 K range.

The reference block temperatures for the liquid helium runs are determined using the 1958 He^4 vapor pressure scale [8]. The temperatures obtained from the He^4 vapor pressure determinations are uncertain by 0.01 K. Neither the measurement of vapor pressure nor the temperature-pressure relation contribute a significant error. However the reference ring temperature may be slightly higher than the liquid helium temperature because of heat flow across the interface between the specimen chamber lid and the liquid helium. Also there may be a temperature discontinuity at the liquid-gas surface and some stratification in the liquid resulting in actual temperatures slightly different (possibly as much as 0.01 K) than the measured temperatures. Neither of these effects produces a systematic error in the case of the PRT measurements at higher temperatures, since the PRT is mounted directly on the reference block.

The thermal tempering calculations indicate that the thermocouple reference junctions are within 1 mK of the reference block.

5.1.2. Specimen Temperatures

The measured specimen temperatures may be in error for several reasons. Thermocouple calibration errors, specimen temperature disturbances caused by the attachment of thermocouples, thermocouple contact resistance, extraneous thermal emfs, and reference block temperature measurement errors are contributing factors to the total specimen temperature error. As pointed out in section 2.1, the thermocouple calibration is determined from the standard table as modified by spot calibrations for these specific spools of wire. The calibration uncertainties of the standard table are reported by Sparks et al. [4] as less than 0.015 K. The interpolation-calibration uncertainty of the subsequent spool calibration is somewhat larger. The deviations between the spool calibration and the standard table are shown in figure 4. Interpolations from figure 4 are uncertain by 1 μV between 4 and 20 K and 2 μV between the higher temperature calibration points. The interpolation error will be greatest midway between the calibration points. This corresponds to a maximum absolute temperature uncertainty of about 0.1 K and a relative temperature difference uncertainty of 0.5 percent between 4 and 20 K, 0.2 percent between 20 and 76 K, and 0.1 percent above 76 K. Another source of error is present since all thermocouples are represented by a single calibration table. Real differences undoubtedly exist between these thermocouples; however, as indicated previously, these differences are less than 1 μV, even for a temperature interval from 4 to 300 K.

The magnitude of the temperature disturbance caused by the thermocouple attachment will be small if the shell temperature is adjusted to minimize heat flow along the thermocouples to the sample. This adjustment also minimizes the problem introduced by thermal contact resistance between the specimen and the thermocouples. It is difficult to assess the effect of these errors separately. Errors caused by these effects, combined with conduction and radiation losses, are considered in a later section.

Extraneous thermal emf in the thermocouple leads is in part eliminated by considering the isothermal zero readings previously mentioned. Experimentally these zero readings are found to consist of a fixed component and a smaller variable component. The former is probably caused by the general environment of the apparatus and the latter by short-term temperature fluctuations in the apparatus. The fixed component of the zero readings is eliminated by subtracting it from the experimental data in the presence of a gradient. The variable component contributes about 0.01 K to experimental imprecision in the temperature differences.

The total uncertainty in temperature and temperature difference is taken as the root mean square of the above components. This method of propagating errors is valid for independent errors [12]. The possible error in temperature, primarily of a systematic nature, may be as high as 0.10 K above 20 K and 0.5 percent of temperature below 20 K. The uncertainty in temperature differences contains both systematic and random components. The systematic errors in ΔT may approach 0.5 percent of ΔT between 4 and 20 K, 0.2 percent of ΔT between 20 and 76 K, and 0.1 percent of ΔT above 76 K. The uncertainty in ΔT due to random error is about 0.01 K.

5.2. Heat Flow Errors

The rate of heat generated by the heater at the bottom of the specimen is calculated from potentiometric measurements of voltage and current. Not all of this heat flows up the specimen. Some is lost, by conduction, through connecting leads, glass fiber

389-821 O - 70 - 5

packing, and gas. Some is lost, by radiation, to the shell and other components in the specimen chamber. Some heat is also effectively lost or gained due to temperature drift and the associated enthalpy changes of the specimen assembly.

5.2.1. Conduction Losses

The heat lost by conduction has been directly measured at low temperatures where radiation losses are negligible. These measurements, accomplished by heating up the shell a known amount with respect to the specimen, indicate a loss or gain of about 0.01 mW per degree difference between shell and specimen. These losses increase with temperature due to the increase of the thermal conductivity of the connecting components. This measured value agrees with the calculated value to within the combined uncertainty of both values (50%). It has been found experimentally that this heat loss amounts to a small fraction ($< 0.1\%$) of the total heat flow for a typical gradient and specimen-to-shell temperature difference which are 1 mK at the bottom of the specimen and 0.1 K at the top.

5.2.2. Radiation Losses

An upper limit has been established for the radiation loss from the specimen. This calculation is based upon a knowledge of the thermal conductivity (including radiation transfer) of the glass fiber packing. The thermal conductivity of glass fiber as a function of packing density was reported by Christiansen et al. [13, 14]. They determined room temperature (300 K) conductivities of 0.0065 and 0.0011 $Wm^{-1}K^{-1}$ at fiber densities of 1/2 and 15 lb/ft^3 (8.1 to 243 kg/m^3) respectively. At 190 K the measured values were 0.0048 and 0.00056 $Wm^{-1}K^{-1}$ at 8.1 and 243 kg/m^3 respectively. However the measurements at 190 K were done with an enclosure emissivity of about 0.9 while at 300 K the emissivity was 0.2. Thus the decrease in thermal conductivity from 300 to 190 K was not as great as if the emissivities had been the same in both cases. The fiber density in this thermal conductivity apparatus was about 5 kg/m^3 during the earlier measurements. By varying the shell-to-specimen temperature, data was obtained which resulted in a rough measure of the thermal conductivity of the glass fiber at 300 K. The value obtained, 0.008 $Wm^{-1}K^{-1}$, is in reasonable agreement with the data by Christiansen et al. [13, 14]. In later measurements the packing density was increased to about 50 kg/m^3. The radiation losses that exist due to temperature differences between the specimen and shell are on the order of 1 mW per degree difference at 300 K. However, if the shell is maintained at nearly the same temperature distribution as the specimen, we need not be concerned about this. We do need to consider the radiation loss through the glass fiber parallel to the specimen, part of which comes from the specimen assembly and part from the shell. Assuming that the ratio of these heat losses is proportional to the ratios of the areas of each part we can establish an upper limit to the percentage heat loss of the specimen as a function of the product λA of the specimen at 300 K and at 190 K. Table 1 contains these upper limits at fiber densities of 8.1 and 243 kg/m^3. The ratio of shell-to-specimen surface areas (including specimen heater, thermocouple holders, and leads) is taken as constant at 4:1.

TABLE 1. *Radiation losses*

Specimen $\lambda A(WmK^{-1})$	Percent radiation loss*			
	190 K		300 K	
	8.1 kg/m^3	243 kg/m^3	8.1 kg/m^3	243 kg/m^3
1×10^{-4}	1.6	0.2	13.0	1.6
2	0.8	.1	6.4	0.8
4	.4	.05	3.2	.4
6	.25	.03	2.0	.3
8	.20	.025	1.6	.2
10×10^{-4}	.15	.020	1.2	.2

*These values are based on data reported by Christiansen et al. [13, 14], enclosure emissivity = 0.9

The value of λA for the measurements reported here is 8×10^{-4} WmK^{-1} at 300 K. Thus the radiation error with a packing density of 50 kg/m^3 is estimated to be less than 2 percent at 300 K. At 200 K this error is less than 0.2 percent.

5.2.3. Temperature Drift Effects

As the temperature of the specimen assembly varies, the heat content or enthalpy of the assembly changes. These enthalpy variations represent corresponding changes in the rate of heat flow at a given point in the specimen. The obvious solution to this problem is to obtain true steady state conditions. Of course it is experimentally impossible to do this exactly and so one must design the system such that the effect of maximum temperature drift rates at "steady state" is tolerable. The amount of heat per unit time, $\dot{Q}_{\text{drift}}$, absorbed or liberated by the specimen assembly due to a temperature drift of dT/dt can be estimated from

$$\dot{Q}_{\text{drift}} = \sum \left(Cm \frac{dT}{dt} \right) = \left(Cm \frac{dT}{dt} \right)_{\substack{\text{heater} \\ \text{block}}} + \left(Cm \frac{dT}{dt} \right)_{\text{sample}} + \left(Cm \frac{dT}{dt} \right)_{\substack{\text{thermo-} \\ \text{couple} \\ \text{holders}}}$$

where C is specific heat and m is mass. The specific heat of these materials changes greatly between 4 and 300 K. The largest specific heats occur at 300 K and thus the severest restriction on the tolerable dT/dt will be seen at 300 K. The mass of the aluminum heater block is 15 g. The mass of the eight thermocouple holders varies from 15 to 45 g depending on specimen size. The cross-sectional areas of the various specimens are adjusted in accordance to their relative conductivities so that the rate of heat flow is about the same for a given temperature and temperature gradient. However specimens larger than about 2 cm diameter cannot be used in this apparatus. A specimen of a

low-conductivity alloy represents the worst case, i.e., smallest heat flow for a given gradient and largest heat capacity. The rate of heat flow to produce a small (say 10 K) temperature difference across this entire sample at 300 K is 0.04 W. The mass of a low-conductivity specimen is about 200 g. To insure that enthalpy changes of the specimen assembly are less than say 0.5 percent of 0.04 W we obtain

$$\frac{dT}{dt} \leq .0015 \text{ K/hr}$$

or for type KP versus Au-Fe thermocouples

$$\frac{dE}{dt} \leq 0.03 \ \mu\text{V/hr}.$$

Thus the control system on the floating sink must be stable to within about 0.0015 K/hr and the measuring instrumentation must be capable of detecting changes in thermocouple emfs of 0.03 μV/hr. In each case this represents approximately the limitation of these systems.

In summary, we can say that at low temperature (below 100 K) the uncertainty in the amount of heat flowing in the specimen is negligible ($< 0.1\%$) if the temperature of the specimen is steady to within the limitations of this instrumentation (0.0015 K/hr) and if the shell-to-specimen temperature difference is less than 0.1 K. Above 100 K radiation heat transfer parallel to the specimen becomes important. For Inconel 718 the radiation heat loss may be as much as as 2 percent even if the shell temperature matches the specimen temperature. If a shell-to-specimen mismatch occurs, radiation perpendicular to the specimen will introduce a heat loss of about 20 mW per degree difference.

5.3. Dimensional and Measuring System Errors

The errors in measuring cross-sectional area and thermocouple position are relatively small. The uncertainty in the diameter determinations is less than 0.0001 cm, which for the smallest specimen measured (0.1 cm^2 cross-sectional area) corresponds to 0.03 percent. The position of the thermocouples is measured to within 0.0001 cm. The separation between adjacent thermocouples (2.54 cm) is therefore accurate to within 0.004 percent. The properties presented in this paper are with respect to the room temperature dimensions of the specimen. If the properties at the true dimensions are desired, small corrections must be applied for contraction of the specimens upon cooling. This correction is on the order of 0.1 percent at 4 K for these specimens. The uncertainties introduced by the measuring instruments are also in general negligible compared to other uncertainties in the system. The thermocouple and specimen resistance voltages are measured to within 0.01 μV. The specimen heater voltage and current are measured to better than 0.01 percent. The PRT voltages and currents are measured to better than 0.01 percent, except near 20 K where the uncertainty in PRT voltages is 0.1 percent. The limitations in these measurements is caused primarily by electrical noise in the system.

5.4. Precision, Accuracy, and Uncertainty

The primary objective of the preceding error analysis is to obtain estimates of limits to the probable systematic errors in this measurement process. The expected imprecision of the measurement process also may be estimated from this analysis; however, a more reliable estimate of the imprecision is obtained from a statistical analysis of the experimental results. The estimated systematic errors of the properties reported here are obtained through the use of error propagation formulas [12] and the estimated systematic errors in the measured variables. Considerable experimental effort has been directed toward assessing the validity of these estimates. Runs have been repeated; runs have been conducted with overlapping temperature ranges at a given reference block temperature and also with different reference block temperatures; in some cases the specimen has been measured, removed, reassembled, and remeasured; the effect of shell-to-specimen temperature differences has been investigated; to randomize systematic thermocouple calibration errors, eight thermocouples were used along the specimen instead of only two or three; the effect of specimen temperature drift has been experimentally investigated. These investigations and the design of the apparatus result in a high degree of confidence in our error estimates.

The estimated limit to systematic error in thermal conductivity, caused primarily by error in determination of heat flow and temperature difference, is 2 percent at 300 K decreasing to 0.2 percent at 200 K, 0.2 percent from 200 K to 50 K increasing to 1 percent at 4 K. The estimated systematic error in electrical resistivity is 0.05 percent below 30 K and 0.1 percent at higher temperatures. At low temperatures the electrical resistivity becomes essentially independent of temperature and thus the systematic errors are primarily due to dimensional errors.

The limit to systematic error in thermopower with respect to the reference material (normal silver) is estimated to be less than 0.5 percent + 0.01 μV/K at 4 K, falling to 0.2 percent + 0.01 μV/K at 30 K, and to 0.1 percent + 0.01 μV/K above 76 K.

Estimates of the standard deviations of the measurement processes for thermal conductivity, electrical resistivity, and thermovoltage are obtained from all of the data obtained at this time. The standard deviation of the measurement process is computed from the variance of the least squares fit, i.e., the sum of the squares of the residuals divided by the degrees of freedom. The standard deviation of the thermal conductivity measurement is 1.0 percent of the conductivity based on values ranging from 0.7 to 1.7 percent for various specimens. The standard deviation of the electrical resistance measurement depends strongly on the resistivity of the specimens. The standard deviation for the better conductors is about 0.1 percent. For the poorer conductors the standard deviation of

the electrical resistance measurement is about 0.01 percent. The larger deviations can be reduced somewhat by using a larger electrical current through the good conductors; however, care must be exercised to avoid transient heating effects caused by the power dissipation in the small connecting leads. The standard deviation of the thermovoltage measurements is 0.1 μV based on values ranging from 0.04 to 0.14 μV for the various specimens.

Estimates of the standard errors of the reported calculated values for thermal conductivity, electrical resistivity, and thermopower are calculated from the variance-covariance matrix of the parameters determined by least squares fit for each of the data sets. The method of calculation is given by Natrella [10] (Standard deviation of a predicted point, pp. 6–12). The computed values are temperature dependent and vary from specimen to specimen; average values of the standard error are 0.25 percent for thermal conductivity and 0.1 percent for electrical resistivity at low temperatures and 0.05 percent at high temperatures. The standard error for thermopower varies from 0.1 μV/K at the lower temperatures to 0.003 μV/K at the higher temperatures.

Based on these estimates of limits to systematic bias and standard error, we estimate (with 95% confidence) the uncertainty in thermal conductivity to be 2.5 percent at 300 K, decreasing to 0.70 percent at 200 K, 0.70 percent from 200 K to 50 K, increasing to 1.5 percent at 4K. The uncertainty in electrcial resistivity is 0.25 percent. Thermopower uncertainty is estimated as 0.5 percent + 0.2μV/K at 4 K, 0.2 percent + 0.05 $\mu V/K$ *at* 30 K, and 0.1 percent + 0.03 μV/K above 76 K.

6. Specimen Characterization

An Armco iron rod (2.54 cm diam and 35.6 cm long) was obtained from Battelle Memorial Institute. This rod is from the same lot of stock as the specimens measured at several other laboratories [15, 20]. We did not redetermine the composition of this rod in view of the repeated determinations by other investigators [15, 18, 19, 20]. The composition, given by R. W. Powell [18], of Armco iron in weight percent is: 0.02 C, 0.03 Mn, 0.006 P, 0.023 S, 0.004 Si, 0.08 Cu, 0.08 Ni, and 99.8 Fe. This rod was annealed by the supplier as follows: 1/2 hr at 870 °C in a gas-heated air muffle, and then in a quartz capsule at 1×10^{-6} torr for $1\frac{1}{2}$ hr, at 875 °C, furnace cooled to 150 °C, held at 150 °C for 24 hr, and furnace cooled to room temperature. We cut the rod into quarters along its axis and cut a 5-cm-long piece from each end of each quadrant. These eight pieces were used for electrical residual resistivity ratio, hardness, and grain size measurements. Two of the center 25-cm sections were measured in the thermal conductivity apparatus. These specimens were chosen on the basis of the electrical resistivity measurements to maximize the difference between them. The division of the rod and the labeling of specimens are shown in figure 6.

The hardness of these specimens, after machining, was B–40.0. The specimens were subsequently re-

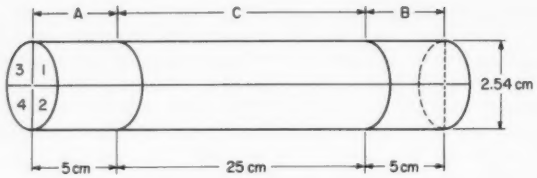

FIGURE 6. *Division of Armco iron rod.*
Each of the 12 pieces shown was machined into a circular cylinder for measurement.

annealed using the same procedure indicated by the supplier. The hardness after anneal was B–37.1. The grain size approximated from ASTM Chart E112, plate 1 was 0.053 mm and 0.064 mm after machining and after reannealing, respectively.

The electrical residual resistivity ratios, ρ_{273K}/ρ_{4K} of the eight specimens (1A . . . 4A, 1B . . . 4B) after machining and of two of these specimens after reannealing are recorded in table 2. These ratios, obtained from electrical resistance measurements at 273 K and 4 K in a specially fabricated dip probe, are estimated to be accurate to about 0.5 percent. Table 2 also contains the resistivity ratios of specimens 2C and 4C. The data marked with asterisks were obtained from the thermal conductivity apparatus.

C. F. Lucks of Battelle Memorial Institute performed similar measurements on another bar of Armco iron [21]. The spread of his results on six specimens is $\pm$ 8.5 percent of the mean while the spread of our 10 specimens is $\pm$ 6.5 percent. The mean value of the residual resistivity ratio (13.65) determined from our data is 5.5 percent below the mean value measured by Lucks. It is noted from table 1 that the residual resistivity ratios are lower after annealing. This is probably caused by diffusion of impurities from the grain boundaries upon heat treatment. Impurities in solution are more effective electron scatterers than impurity precipitates at grain boundaries. Residual resistivity ratios reported by other investigators are also included in table 2.

TABLE 2. *Residual resistivity ratio* (ρ_{273K}/ρ_{4K}) *of Armco iron*

Specimen	After machining	After annealing
1A	14.12	
2A	13.81	
3A	14.13	
4A	12.99	
1B	13.81	
2B	14.51	12.88
3B	14.09	
4B	12.77	11.52
2C	13.86, 13.93*	12.57*
4C	12.44, 12.53*	

*These values were determined from measurements using the thermal conductivity apparatus.

Source	ρ_{273K}/ρ_{4K}
Lucks [21]	12.5 to 14.7
Fulkerson et al. [15]	9.8, 10.0
Shanks et al. [19]	12.6

7. Results

The transport properties of specimens 2C and 4C were measured in the thermal conductivity apparatus. Specimen 2C was subsequently annealed (same annealing procedure as described before) and remeasured.

The data analysis methods used, of those described in section 4, are (a) the difference method for thermal conductivity, (b) the approximate integral method for electrical resistivity, and (c) the integral method for thermopower. The other methods described were also tried; but for various reasons they were discarded in favor of those indicated above. The experimental data were functionally represented with the following arbitrarily chosen equations:

$$\ln \lambda = \sum_{i=1}^{n} a_i [\ln T]^{i+1} \tag{22}$$

$$\rho = \sum_{i=1}^{m} b_i [\ln T]^{i-1} \tag{23}$$

$$S = \sum_{i=1}^{l} c_i [\ln T']^i / T'; \quad T' = \frac{T}{10} + 1 \tag{24}$$

where λ = thermal conductivity, ρ = electrical resistivity, S = thermopower, and T = temperature. Temperatures are based on the IPTS–68 scale above 20 K and the NBS P2–20 (1965) scale below 20 K. The parameters, a_i, b_i, and c_i, determined by least squares, are presented in tables 3, 4, and 5. The number of terms used to represent each of the data sets is optimized, through the use of orthonormal functions, so that none of the precision of the data is lost by "underfitting" nor are any necessary oscillations introduced by "overfitting."

The following is a brief description of the method used. The overdetermined set of equations is formed from the experimental data and by the appropriate equations (22, 23, or 24), using 16 terms in each equation. This set of equations was converted to an orthonormal system according to the Bjorck modification of the Gram-Schmidt orthogonalization procedure [22]. The 16 orthonormal coefficients for these orthonormal functions are then obtained for the best fit of the data.

TABLE 3. *Parameters in equations (22), (23), and (24) for Armco iron, specimen 2C*

i	Thermal conductivity coefficients	Electrical resistivity coefficients	Thermopower coefficients
1	4.51614994	-4.95025810×10^{-7}	-3.44881675×10^{2}
2	-4.13926935	1.65473929×10^{-6}	2.37913833×10^{3}
3	2.07599685	-2.37099406×10^{-6}	-6.68364762×10^{3}
4	-8.61606749×10^{-1}	1.93668635×10^{-6}	9.99411766×10^{3}
5	3.39315321×10^{-1}	-9.93191337×10^{-7}	-8.67747098×10^{3}
6	-9.99896812×10^{-2}	3.31399468×10^{-7}	4.46376537×10^{3}
7	1.79360964×10^{-2}	-7.18946332×10^{-8}	-1.32173829×10^{3}
8	-1.71155124×10^{-3}	9.77121499×10^{-9}	2.08103179×10^{2}
9	6.66070951×10^{-5}	$-7.54546890\times10^{-10}$	-1.35462989×10^{1}
10		2.52377946×10^{-11}	

TABLE 4. *Parameters in equations (22), (23), and (24) for Armco iron, specimen 2C after annealing*

i	Thermal conductivity coefficients	Electrical resistivity coefficients	Thermopower coefficients
1	7.43890940	-4.20510751×10^{-7}	-5.10933863×10^{2}
2	-1.14675555×10^{1}	1.45081937×10^{-6}	3.36812410×10^{3}
3	9.73124560	-2.12826875×10^{-6}	-9.06609424×10^{3}
4	-5.28250471	1.77366602×10^{-6}	1.30552541×10^{4}
5	1.89245802	-9.25249389×10^{-7}	-1.09917641×10^{4}
6	-4.41102771×10^{-1}	3.13228379×10^{-7}	5.52800895×10^{3}
7	6.37973455×10^{-2}	-6.87884712×10^{-8}	-1.61455399×10^{3}
8	-5.17020759×10^{-3}	9.44600166×10^{-9}	2.52389423×10^{2}
9	1.78835874×10^{-4}	$-7.35822503\times10^{-10}$	-1.63749922×10^{1}
10		2.47951038×10^{-11}	

TABLE 5. *Parameters in equations (22), (23), and (24) for Armco iron, specimen 4C*

i	Thermal conductivity coefficients	Electrical resistivity coefficients	Thermopower coefficients
1	8.21226100	-5.03088441×10^{-7}	-6.42943844×10^{2}
2	-1.32577224×10^{1}	1.69059561×10^{-6}	4.14540857×10^{3}
3	1.14738701×10^{1}	-2.42733181×10^{-6}	-1.09289158×10^{4}
4	-6.21776147	1.98402296×10^{-6}	1.54381788×10^{4}
5	2.19527810	-1.01722378×10^{-6}	-1.27838650×10^{4}
6	-5.01619108×10^{-1}	3.39158569×10^{-7}	6.34295244×10^{3}
7	7.10720281×10^{-2}	-7.35034919×10^{-8}	-1.83456286×10^{3}
8	-5.64940725×10^{-3}	9.97927431×10^{-9}	2.84809534×10^{2}
9	1.91995267×10^{-4}	$-7.69854134\times10^{-10}$	-1.83820643×10^{1}
10		2.57278514×10^{-11}	

The absolute magnitude of each coefficient is indicative of the relative significance of the corresponding term and also directly indicates the average absolute magnitude of that term. This is so since the sum of squares of each orthonormal function is unity over the data set. A plot of the absolute magnitudes of orthonormal coefficients versus the term number will usually exhibit a generally decreasing character until the noise level of the data is reached, and then fluctuate about that value. The point at which the noise level is reached indicates the number of terms one should retain in the function in order to best fit the data with this function. This test procedure is similar to, but more straightforward and more intuitively desirable than, a statistical test such as the F-test. From these orthonormal coefficients and functions one obtains the coefficients (parameters) of the original equation. In this work the original equation is also fitted to the data using the more common procedure in which one establishes the so-called normal equations and obtains the least squares coefficients by the Gauss-Jordan matrix inversion routine [23]. Since the coefficients for a least squares fit must be unique, disagreement between these two independently obtained sets of coefficients is used to detect the presence of significant round-off error. Round-off error is absent to nine significant figures in the coefficients presented here.

Values of λ, ρ, L, and S are given in tables 6, 7, and 8 as computed from eqs (22), (23), and (24). A complete

listing of all raw experimental data is contained in an NBS report for future reference.

8. Discussion

The thermal conductivities of these three Armco iron specimens cut from one rod differ by as much as 10 percent at low temperatures; the differences observed in electrical resistivity are similar. The thermal conductivity deviations of the three sets of values are shown in figure 7. In figure 7, $\bar{\lambda}$ is the mean thermal conductivity for the three specimens at temperature, T. These data seem to indicate that Armco iron is a poor thermal conductivity standard material at low temperatures. Since Armco iron is already in extensive use as a high-temperature standard reference material [2], it would be desirable to make use of it at low temperatures as well. The following analysis is given to indicate how Armco iron may be useful at low temperatures.

The Lorenz ratio, $\rho\lambda/T$, computed from these measurements is much less variable from specimen to specimen at low temperatures than either ρ or λ. This is expected for materials which are primarily electronic thermal conductors. Figure 8 illustrates the deviations of the Lorenz ratios for each specimen from the mean values. Since these deviations are not appreciably larger than the uncertainty in the computed Lorenz ratio, the Lorenz ratio is assumed to be essentially invariant from specimen to specimen. Thus, one can compute the thermal conductivity of a particular specimen of Armco iron from its electrical resistivity and the Lorenz ratios reported here.

TABLE 6. *Transport properties of Armco iron, specimen 2C*

Temperature	Thermal conductivity	Electrical resistivity	Lorenz ratio × 10^8	Thermopower
K	$Wm^{-1}K^{-1}$	$\mu\Omega m$	V^2/K^2	$\mu V/K$
6	21.7	0.006905	2.49	0.02
7	25.6	.006903	2.52	.06
8	29.2	.006911	2.53	.07
9	32.8	.006920	2.53	.06
10	36.4	.006926	2.52	.07
12	43.5	.006929	2.51	.13
14	50.7	.006932	2.51	.22
16	57.9	.006941	2.51	.32
18	65.0	.006957	2.51	.43
20	71.8	.006981	2.50	.54
25	87.0	.007067	2.46	.82
30	98.9	.007196	2.37	1.18
35	107	.007386	2.26	1.67
40	113	.007664	2.16	2.28
45	115	.008051	2.06	3.00
50	116	.008562	1.99	3.79
55	115	.009202	1.93	4.63
60	114	.009976	1.89	5.51
65	112	.01088	1.87	6.38
70	110	.01191	1.87	7.24
75	107	.01306	1.87	8.07
80	105	.01432	1.88	8.86
85	103	.01568	1.89	9.60
90	100	.01713	1.91	10.30
95	98.4	.01867	1.93	10.95
100	96.6	.02028	1.96	11.54
110	93.4	.02371	2.01	12.58
120	90.8	.02736	2.07	13.44
130	88.7	.03119	2.13	14.13
140	87.1	.03516	2.19	14.67
150	85.8	.03923	2.24	15.07
160	84.7	.04340	2.30	15.37
170	83.9	.04765	2.35	15.57
180	83.1	.05196	2.40	15.69
190	82.4	.05633	2.44	15.74
200	81.8	.06077	2.48	15.73
220	80.5	.06983	2.55	15.56
240	79.1	.07918	2.61	15.23
260	77.5	.08888	2.65	14.77
280	75.9	.09903	2.68	14.19
300	74.3	.10970	2.72	13.51

TABLE 7. *Transport properties of Armco iron, specimen 2C, after annealing*

Temperature	Thermal conductivity	Electrical resistivity	Lorenz ratio × 10^8	Thermopower
K	$Wm^{-1}K^{-1}$	$\mu\Omega m$	V^2/K^2	$\mu V/K$
6	19.7	0.007645	2.52	−0.02
7	23.2	.007645	2.53	.08
8	26.6	.007658	2.54	.11
9	29.9	.007669	2.55	.11
10	33.2	.007674	2.55	.11
12	39.8	.007676	2.54	.15
14	46.4	.007676	2.54	.23
16	52.9	.007685	2.54	.33
18	59.4	.007702	2.54	.44
20	65.6	.007726	2.53	.56
25	79.8	.007812	2.49	.87
30	91.2	.007936	2.41	1.25
35	99.6	.008119	2.31	1.75
40	105	.008388	2.21	2.37
45	108	.008766	2.11	3.09
50	110	.009268	2.04	3.87
55	110	.009902	1.98	4.72
60	109	.01067	1.94	5.58
65	108	.01157	1.92	6.45
70	106	.01259	1.91	7.30
75	104	.01374	1.91	8.12
80	102	.01500	1.91	8.91
85	100	.01635	1.93	9.65
90	98.4	.01781	1.95	10.34
95	96.7	.01934	1.97	10.97
100	95.1	.02096	1.99	11.56
110	92.3	.02438	2.05	12.59
120	90.1	.02803	2.10	13.43
130	88.3	.03185	2.16	14.10
140	86.9	.03581	2.22	14.63
150	85.7	.03988	2.28	15.02
160	84.7	.04404	2.33	15.31
170	83.8	.04827	2.38	15.50
180	83.0	.05258	2.42	15.62
190	82.2	.05694	2.46	15.67
200	81.4	.06137	2.50	15.66
220	79.8	.07042	2.56	15.50
240	78.2	.07978	2.60	15.18
260	76.6	.08952	2.64	14.72
280	75.3	.09971	2.68	14.14

TABLE 8. *Transport properties of Armco iron, specimen 4C*

Temperature	Thermal conductivity	Electrical resistivity	Lorenz ratio × 10^8	Thermopower
K	$W m^{-1} K^{-1}$	$\mu\Omega m$	V^2/K^2	$\mu V/K$
6	19.6	0.007675	2.51	−0.07
7	23.0	.007664	2.52	.07
8	26.3	.007673	2.52	.11
9	29.6	.007685	2.53	.11
10	32.9	.007694	2.53	.11
12	39.4	.007702	2.53	.13
14	46.0	.007706	2.53	.19
16	52.5	.007715	2.53	.28
18	58.9	.007730	2.53	.39
20	65.1	.007752	2.52	.50
25	79.1	.007834	2.48	.80
30	90.5	.007960	2.40	1.18
35	98.9	.008149	2.30	1.66
40	105	.008427	2.20	2.27
45	108	.008814	2.11	2.97
50	109	.009324	2.04	3.74
55	110	.009965	1.98	4.58
60	109	.01074	1.95	5.44
65	107	.01164	1.92	6.30
70	106	.01267	1.91	7.15
75	104	.01382	1.91	7.98
80	102	.01507	1.92	8.77
85	99.8	.01643	1.93	9.51
90	97.9	.01789	1.95	10.20
95	96.2	.01942	1.97	10.85
100	94.6	.02104	1.99	11.44
110	91.8	.02446	2.04	12.47
120	89.6	.02811	2.10	13.31
130	87.9	.03193	2.16	13.99
140	86.5	.03589	2.22	14.51
150	85.4	.03996	2.28	14.91
160	84.5	.04412	2.33	15.20
170	83.8	.04836	2.38	15.39
180	83.1	.05267	2.43	15.51
190	82.4	.05704	2.47	15.56
200	81.8	.06146	2.51	15.55
220	80.4	.07052	2.58	15.39
240	78.8	.07986	2.62	15.07
260	77.0	.08957	2.65	14.62
280	75.3	.09973	2.68	14.05
300	73.8	.11040	2.71	13.36

TABLE 9. *The Lorenz ratio and intrinsic electrical resistivity of Armco iron*

(Average of the results from specimens 2C, 2C (after annealing), and 4C)

Temperature	Lorenz ratio × 10^8	Intrinsic electrical resistivity
K	V^2/K^2	$\mu\Omega m$
4	2.263	0.0000
5	2.455	.0000
6	2.505	.0000
7	2.523	.0000
8	2.531	.0000
9	2.533	.0000
10	2.532	.0000
12	2.529	.0000
14	2.528	.0000
16	2.528	.0000
18	2.527	.0001
20	2.521	.0001
25	2.477	.0002
30	2.395	.0003
35	2.292	.0005
40	2.188	.0008
45	2.096	.0011
50	2.021	.0016
55	1.965	.0023
60	1.927	.0030
65	1.905	.0040
70	1.895	.0050
75	1.895	.0061
80	1.903	.0074
85	1.917	.0087
90	1.935	.0102
95	1.956	.0117
100	1.980	.0134
110	2.034	.0168
120	2.091	.0204
130	2.150	.0242
140	2.209	.0282
150	2.266	.0323
160	2.320	.0364
170	2.371	.0407
180	2.418	.0450
190	2.461	.0494
200	2.499	.0538
220	2.562	.0628
240	2.610	.0722
260	2.647	.0819
280	2.682	.0921
300	2.724	.1028

In order for the above procedure to be practical, one needs a relatively quick method of generating a ρ versus T curve for a particular specimen from relatively few measurements. Matthiessen's rule indicates that $\rho = \rho_0 + \rho_i$, where ρ_0 is the residual resistivity of the specimen and ρ_i is the intrinsic resistivity of the material. It is known that this rule is not satisfied exactly and that a correction term $\Delta(\rho_0, \rho_i)$ exists. However, if this correction term is sufficiently small one can construct a sufficiently accurate ρ versus T curve for a given specimen from ρ_i, assumed to be the same for all specimens, and the value of ρ_0 as measured for each specimen. To investigate this possibility, ρ_i was computed for each of the three specimens using Matthiessen's rule. The relative deviations of the computed values of ρ_i from the mean of three sets is shown in figure 9. This plot shows that ρ_i values for these three specimens, as computed from Matthiessen's rule, differ from the mean by less than 0.3 percent of the total resistivity. This deviation is only slightly larger than the estimated uncertainty of the measurements. It is not unreasonable to assume that ρ_i for other specimens is within a few tenths of a percent of the mean values of these three specimens. Thus, characterized Armco iron specimens may be used as low-temperature standards. The thermal conductivity,

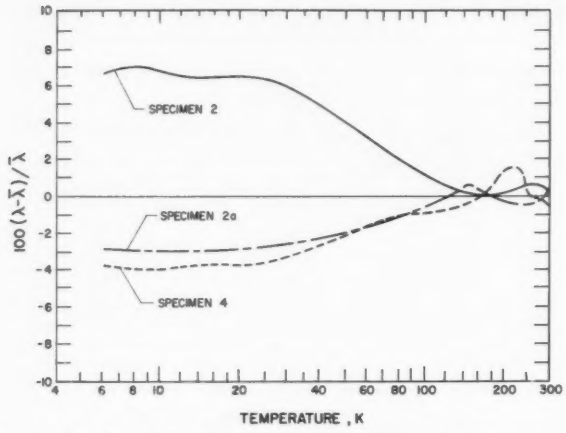

FIGURE 7. *Deviations of the thermal conductivities of each specimen from the mean values.*

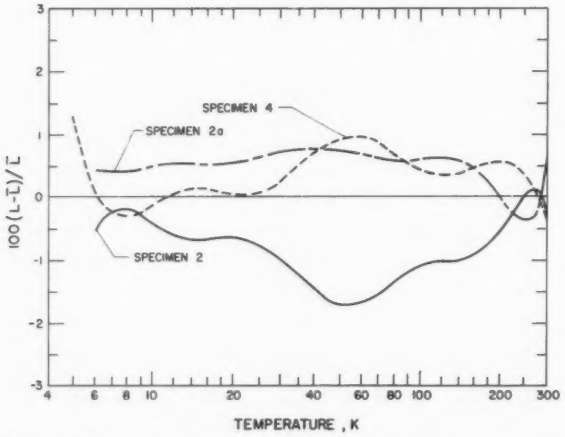

FIGURE 8. *Deviations of the Lorenz ratios of each specimen from the mean values.*

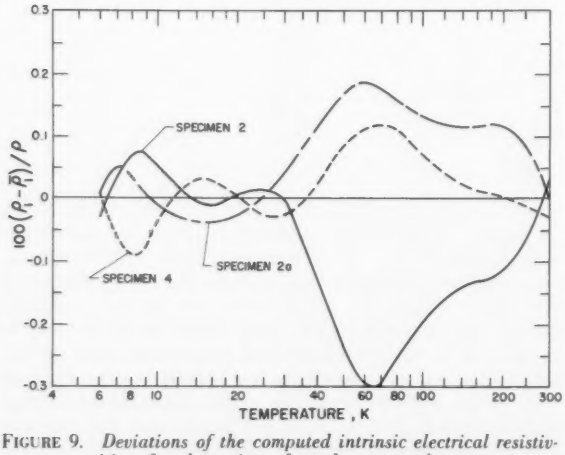

FIGURE 9. *Deviations of the computed intrinsic electrical resistivities of each specimen from the mean values.*

λ, of a standard reference specimen of Armco iron according to these results may be computed from

$$\lambda = \frac{LT}{\rho} = \frac{LT}{\rho_i + \rho_0} \tag{25}$$

where L and ρ_i are given in table 9 and ρ_0 is determined by a relatively simple measurement.

Numerous thermal conductivity and electrical resistivity measurements on Armco iron have been reported; some of these measurements extend to temperatures as low as −200 °C. R. W. Powell [2] reviewed the data published prior to 1962; this review indicates that the only low-temperature data at that time were those of Lucks and Deem [24]. Since that time low-temperature data have been reported by Fulkerson et al. [15]. Larsen et al. [25], R. W. Powell et al. [18], Shanks et al. [19], and Watson et al. [20]. These and other high-temperature measurements have been done as a result of a proposal by C. F. Lucks (Battelle Memorial Institute) to carry out a round-robin experiment on Armco iron. Reported data on these specimens can be interpreted to show (1) experimental differences between laboratories (assuming insignificant material variability), (2) material variability in a given lot of Armco iron (assuming insignificant experimental errors), or (3) a combination of (1) and (2) of comparable proportions. Not surprisingly, the latter seems to be the result of these measurements, as is indicated in the following discussion.

The electrical resistivity measurements are generally reported to be accurate to better than 1 percent. Thermal conductivity data are generally reported to be accurate to better than 3 percent. Thus, the uncertainty in Lorenz ratios caused by experimental measurement errors is expected to be less than 4 percent. The ice-point electrical resistivities measured by several investigators [15, 16, 18, 19, 20, 25] range from 0.09 $\mu\Omega$m to 0.104 $\mu\Omega$m; this range (14 nΩm) is significantly larger than the expected uncertainty of the measurements. This is a larger material variation than we would expect on the following basis: Matthiessen's rule is expected to be reasonably correct, as confirmed by our measurements; and, thus, the same absolute variation observed in electrical resistivity at the ice point should also be observed in the residual resistivity. However the measured residual resistivities ranged only from 6.1 to 10.6 nΩm (a range of 4.5 nΩm).

Some investigators [15, 19, 20] have measured the electrical resistivity of several specimens to investigate the effect of heat treatment; their results show possible differences of several percent but it seems unlikely that at room temperature the real material differences exceed about 5 percent.

Since the electronic component of thermal conductivity is the major conductivity component in Armco iron, the specimen-to-specimen variation in electrical resistivity must be reflected in the thermal conductivity. However, since the experimental measurement uncertainty is not significantly smaller than the probable material variability, it is difficult to determine material differences. The variation in reported thermal

conductivities from all sources near the ice point is about 6 percent, not unreasonable according to the previous comments.

As indicated previously, the Lorenz ratio should be more invariant from specimen to specimen than either electrical resistivity or thermal conductivity. Comparison of all the reported Lorenz ratios at 0 °C shows a variation of about 2.5 percent. Considering the previously estimated uncertainty of 4 percent, this is considered excellent agreement. However, it would appear that this agreement is fortuitous. Upon careful examination of the methods used by the various investigators, it is noted that the electrical resistivity and thermal conductivity measurements were performed either on different specimens or at different times. In the latter case the specimen was invariably either machined or heat treated between the two types of measurements. Since we know that specimen-to-specimen variations exist and, since we know that mechanical strain or heat treatment changes the transport properties, it follows that the Lorenz ratio should be calculated from nearly simultaneous measurements of electrical resistivity and thermal conductivity on the same specimen. This apparent operational discrepancy may explain the larger Lorenz ratio variation at low temperatures. For example, at −150 and −200 °C the differences between the extreme values of Lorenz ratio are about 12 percent. As pointed out previously, the specimen-to-specimen percentage variation in electrical resistivity and thermal conductivity is greater at low temperatures.

Although our purpose is primarily investigation at low temperatures, it seems that a comment regarding the use of Armco iron as a high-temperature reference material is in order. It is clear that variations from specimen to specimen and variations caused by heat treatment are several percent. Under these circumstances it is prudent to make "in place" calibrations by electrical resistivity measurements whenever Armco iron is used at high temperatures. At low temperatures it is probably sufficient to make a residual resistivity measurement for calibration purposes as previously described.

In conclusion, it appears that the available data neither confirm nor contradict our previous estimate of the invariance of the Lorenz ratio and the intrinsic electrical resistivity. However, since the specimens we used had a rather limited range of residual resistivity (6.7 to 7.6 nΩm) compared to the high value observed by Fulkerson et al. [15] (10.0 nΩm), it would be desirable to make additional thermal and electrical measurements on a specimen having a higher residual resistivity.

The absolute thermopowers of these three specimens are compared in figure 10. The deviations between specimens are only slightly larger than the uncertainty in the tabulated values; thus no significant difference between specimens can be detected from this property. The thermopower values tabulated are absolute values although our measurements were carried out with respect to normal silver wire. The absolute thermopowers of normal silver reported by Borelius et al. [26] were used to convert the experimental data to the absolute scale.

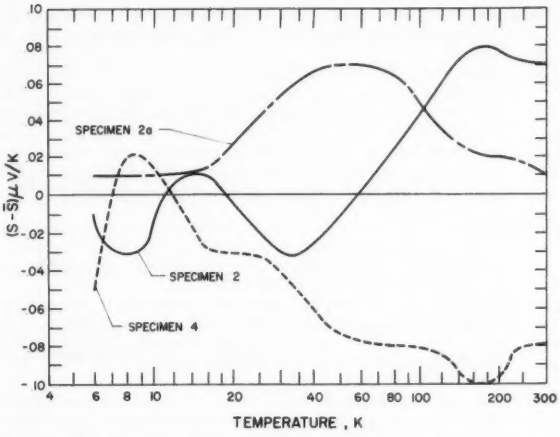

FIGURE 10. *Deviations of the thermopowers of three specimens from the mean values.*

We wish to thank C. F. Lucks of Battelle Memorial Institute for supplying the Armco iron rod and information regarding annealing. R. P. Reed and R. L. Durcholz of this laboratory did the hardness and grain size testing.

9. References

[1] Hust, J. G., and R. L. Powell, Thermal conductivity of aerospace alloys at cryogenic temperatures, Proc. Eight Conf. Thermal Conductivity (eds. C. Y. Ho and R. E. Taylor, Plenum Press, New York, N.Y., 1969), pp. 197–208.

[2] Powell, R. W., Armco iron as a thermal conductivity standard, Review of published data, Progress in International Research on Thermodynamics and Transport Properties (eds. J. F. Masi and D. H. Tsai, Academic Press, New York, N.Y., 1962), pp. 454–465.

[3] Powell, R. L., Rogers, W. M., and Coffin, D. O., An apparatus for measurement of thermal conductivity of solids at low Temperatures, J. Res. Nat. Bur. Stand. (U.S.) **59**, 349–355 (1957).

[4] Sparks, L. L., Powell, R. L., and Hall, W. J., Progress on cryogenic thermocouples, Advances in Cryogenic Engineering (ed. K. D. Timmerhaus, Plenum Press, New York, N.Y., 1969), Vol. **14**, pp. 316–321. (Also to be published in more detail as an NBS Monograph.)

[5] Cataland, G., Edlow, M. H., and Plumb, H. H., Liquid helium vapor pressure regulator, Rev. Sci. Instr. **32**, No. 8, 980–981 (1961).

[6] Hust, J. G., Thermal anchoring of wires in cryogenic apparatus, Rev. Sci. Instr. 41, 622–624 (1970).

[7] Hust, J. G., A compilation and historical review of temperature scale differences, Cryogenics 9, 443–455 (1969).

[8] Brickwedde, F. G., Durieux, M., Clement, J. R., and Logan, J. K., The 1958 He^4 scale of temperature, J. Res. Nat. Bur. Stand. (U.S.), **64A** (Phys. and Chem.), No. 1, 1–17 (1960).

[9] Eisenhart, C., Realistic evaluation of the precision and accuracy of instrument calibration systems, J. Res. Nat. Bur. Stand. (U.S.), **67C** (Eng. and Instr.), No. 2, 161–187 (1963).

[10] Natrella, M. G., Experimental Statistics, Nat. Bur. Stand (U.S.), Handb. 91, (U.S. Government Printing Office, Washington, D.C., 1963).

[11] ASTM (1961), Use of the Terms Precision and Accuracy as Applied to Measurement of a Property of a Material, ASTM Designation E177–61T, ASTM Standards, Pt. 11, pp. 1758–1766.

[12] Ku, H. H., Notes on the use of propagation of error formulas, J. Res. Nat. Bur. Stand. (U.S.), **70C** (Eng. and Instr.), No. 4 (1966).
[13] Christiansen, R. M., and Hollingsworth, Jr., M., The performance of glass fiber insulation under high vacuum, Advances in Cryogenic Engineering (ed. K. D. Timmerhaus, Plenum Press, New York, N.Y., 1960), Vol. **4**, p. 141.
[14] Christiansen, R. M., and Marsh, H. N., Jr., Low temperature insulating systems, Advances in Cryogenic Engineering (ed. K. D. Timmerhaus, Plenum Press, New York, N.Y., 1960), Vol. **5**, p. 171.
[15] Fulkerson, W., Moore, J. P., and McElroy, D. L., Comparison of the thermal conductivity, electrical resistivity, and Seebeck coefficient of a high-purity iron and an Armco iron to 1000 °C, J. Appl. Phys. **37**, 2639–2653 (1966).
[16] Laubitz, M. J., Thermal and electrical properties of Armco iron at high temperatures, Can. J. Phys. **38**, 887–907 (1960).
[17] Laubitz, M. J., The unmatched guard method of measuring thermal conductivity at high temperatures, Can. J. Phys. **41**, 1663–1678 (1963).
[18] Powell, R. W., Hickman, M. J., Tye, R. P., and Woodman, M. J., Armco iron as a thermal conductivity standard; New determinations at the National Physical Laboratory, Progress in International Research on Thermodynamics and Transport Properties, (ASME, Academic Press, New York, N.Y., 1962), pp. 466–473.
[19] Shanks, H. R., Klein, A. H., and Danielson, G. C., Thermal properties of Armco iron, J. Appl. Phys. **38**, 2885–2892 (1967).
[20] Watson, T. W., Flynn, D. R., and Robinson, H. E., Thermal conductivity and electrical resistivity of Armco iron, J. Res. Nat. Bur. Stand. (U.S.), **71C** (Eng. and Instr.) 285–291 (1967).
[21] Lucks, C. F., Private communication.
[22] Bjorck, A., Solving linear least squares problems by Gram-Schmidt orthogonalization, BIT **7**, 1–21 (1967).
[23] Golden, J. T., FORTRAN IV—Programming and Computing (Prentice-Hall, Inc., Englewood Cliffs, N.J., 1965).
[24] Lucks, C. F., and Deem, H. W., Thermal properties of thirteen metals, ASME Spec. Tech. Publ. No. 227 (Feb. 1958).
[25] Larsen, D. C., Powell, R. W., and Dewitt, D. P., The thermal conductivity and electrical resistivity of a round-robin Armco iron sample, initial measurements from 50 to 300 °C, Proc. Eighth Thermal Conductivity Conf. (eds. C. Y. Ho and R. E. Taylor, TPRC, Plenum Press, N.Y., 1969), pp. 675–686.
[26] Borelius, G., Keesom, W. H., Johansson, C. H., and Linde, J. O., Establishment of an Absolute Scale for the Thermoelectric Force, Proc. Kon. Akad. Amsterdam **35**, 10 (1932).

(Paper 74A5–632)

JOURNAL OF RESEARCH of the National Bureau of Standards—A. Physics and Chemistry
Vol. 74A, No. 5, September–October 1970

Mössbauer Spectrometer Calibration Using TiFe*

L. J. Swartzendruber and L. H. Bennett

**Institute for Materials Research,
National Bureau of Standards, Washington, D.C. 20234**

(May 4, 1970)

The splitting of the ^{57}Fe Mössbauer spectrum in TiFe has been carefully measured in a magnetic field and compared with the zero-field quadrupolar splitting of sodium nitroprusside. The comparison gives a value of 1.699 mm/s at 295 K for the sodium nitroprusside splitting. This determination makes use of the known Knight shift of Fe in TiFe and is independent of any velocity measurement. Comparison is made with the splitting of the inner two lines of a pure Fe spectrum.

Key words: Calibration; chemical shift; iron; Knight shift; Mössbauer effect; sodium nitroprusside; TiFe.

1. Introduction

The recent discovery [1][1] of the ^{57}Fe nuclear magnetic resonance in the non-ferromagnetic intermetallic compound TiFe makes this material useful as a reference material for use in Mössbauer effect spectroscopy.

The Mössbauer effect of TiFe in the absence of an external field gives a single resonance line. Applying a known external field splits this line and the separation of the resulting lines can be used to calibrate the Mössbauer effect spectrometer in magnetic field units, energy units, and velocity units. Conversely, if the velocity calibration is known, the TiFe spectrum can be used to determine the applied magnetic field. This is possible because the Knight shift of ^{57}Fe in TiFe is accurately known [1], and because TiFe has an ordered CsCl structure which places each Fe in a cubic site, giving a Mössbauer resonance with no resultant distortion due to the ^{57}Fe excited state electric quadrupole moment. Also the Knight shift of TiFe has the advantage that it is only weakly temperature dependent. By varying the applied field, the TiFe line splitting can be varied. Thus this material is useful for calibration over a wide range of velocities and for checking spectrometer linearity.

In this paper we present data comparing Mössbauer effect spectra of TiFe in a magnetic field of about[2] 50 kG and spectra of sodium nitroprusside (SNP) in zero field. Using this comparison we obtain a calibration for the quadrupole split lines of sodium nitroprusside. Although intrinsically no more precise than a direct velocity determination, this calibration is of interest because it is independent of any velocity measurement. Values quoted in the literature [2–7] for the room-temperature quadrupole splitting of sodium nitroprusside determined by direct velocity measurement vary from 1.65 to 1.85 mm/s. Several of the more precise of these determinations are compared in figure 1. The results obtained by the method used here are in close agreement with the direct velocity determinations of references [2] and [7].

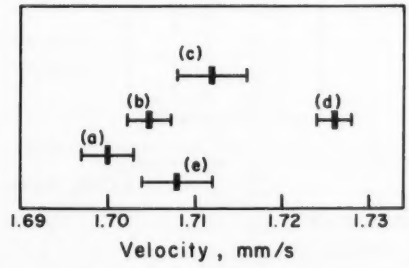

FIGURE 1. *Comparison of various results on the quadrupole splitting of sodium nitroprusside.*

(a) this work.
(b) reference [2].
(c) reference [4].
(d) reference [3].
(e) reference [7].

We have been informed that with new direct velocity measurements, Drs. J. R. DeVoe, J. J. Spijkermann, and J. C. Travis have obtained a value above 1.700 mm/s but within our error bar shown in (a).

The sodium nitroprusside calibration is of considerable interest in Mössbauer spectroscopy with ^{57}Fe. It has been issued [3] for use as a standard reference material for calibrating Mössbauer spectrometers and for comparing isomer shifts in iron-containing compounds. As previously noted by a number of authors [4, 8] sodium nitroprusside has several desirable characteristics for use as a standard. The fairly large

*Supported in part by the Office of Saline Water, Department of the Interior.

[1] Figures in brackets indicate the literature references at the end of this paper.

[2] The field value was carefully measured using NMR, as explained in detail later.

quadrupole splitting is only weakly dependent on temperature (on the order [5] of 10^{-4} mm s^{-1} K^{-1} at room temperature). This is combined with an easily available high chemical purity and stability in addition to near natural resonance linewidths.

Using the results presented here, the Knight shifts and chemical shifts [3] of ^{57}Fe in Fe compounds can be measured to better than 0.5 percent by the Mössbauer effect. This is poor accuracy when compared with normal NMR results. However, it still offers the possibility of valuable results, since the NMR of ^{57}Fe in most compounds is much too weak to be measurable.

2. Experimental Procedure

The Mössbauer effect spectrometer-superconducting magnet system has been described in detail elsewhere [9]. A schematic of the experimental arrangement is shown in figure 2. The velocity drive unit was used in the constant acceleration mode and spectra were stored in a multichannel analyzer.

The source was about 100 mCi of ^{57}Co in a Pd matrix. It was prepared [4] by plating the requisite amount of carrier-free ^{57}Co in a 6-mm-diam circle on one side of a 25-μm foil of pure Pd. This was diffused in a hydrogen atmosphere at about 1270 K for 1 hr followed by a water quench.

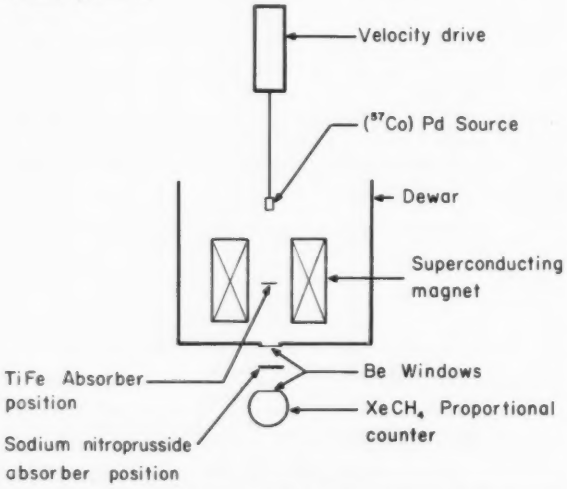

FIGURE 2. *Schematic drawing of the experimental arrangement.*
The source temperature was controlled at 210 K, the TiFe absorber at 120 or 60 K. The sodium nitroprusside temperature was 295 K. The source-to-detector distance was 0.33 m. The γ-ray beam was collimated to a 12-mm diameter at the TiFe absorber position.

The TiFe alloys were prepared by arc melting weighed quantities in an argon atmosphere. The ingots were turned and remelted three times during arc melting. The purity of the starting materials was Ti 99.97 percent and Fe 99.999 percent (no ^{57}Fe enrichment was used). An excess of one atomic percent Ti above the stoichiometric quantity was used. This gives a more perfectly ordered alloy, as evidenced by NMR signal strength [10] and ME line shape [11]. The arc-melted ingot was homogenized at 1470 K for 72 hr and then crushed to a powder. The powder was then annealed by sealing in an evacuated quartz ampoule, heating at 1170 K for 1 hr, then cooling to 870 K by reducing the temperature 30 K/hr. Two samples were prepared from separate melts and the measurements to be reported later detected no significant difference in their ME. (The same annealing procedure was used by Swartz et al. [1] for the TiFe samples in which ^{57}Fe Knight shift measurements were made.) From the annealed powders −200 mesh particles were obtained. These particles were embedded in a lucite disk about 12 mm in diameter and 2 mm thick with enough powder to give 0.02 $\mu g/m^2$ of ^{57}Fe.

The sodium nitroprusside sample [5] was in the form of a 10 mm square cut from a single crystal with the surface parallel to the *ac* plane of the crystal [2]. It was approximately 0.8 mm thick yielding 0.055 $\mu g/m^2$ of ^{57}Fe.

The magnetic field was calibrated by measuring the NMR frequency of Cu at 4.2 K with a super-regenerative detector. Details of this measurement are described more fully in the section on systematic errors.

Runs were made alternately on sodium-nitroprusside and TiFe. A total of eleven sodium nitroprusside spectra and nine TiFe spectra were obtained over a period of about 12 days.

3. Results

A summary of the measurement conditions for each run is given in table 1. The spectrum, $w(x)$, taken with no sample was used to determine the small perturbation introduced by the presence of Fe in the beryllium windows of the magnet dewar and proportional counter. This spectrum is a doublet and was least squares fitted to obtain its position, splitting, and width. Since the sodium nitroprusside is in a small fringing field of several hundred gauss, two runs were taken with the magnet coil de-energized. No significant difference was detected when compared to the spectra taken with the coil energized.

All spectra were least squares fitted using an equation of the form

$$y(x) = a + bx + cx^2 + dw(x) + \sum_{\alpha} h_\alpha D(x, \Delta_\alpha, C_\alpha, \Gamma_\alpha, \epsilon_{h\alpha}, \epsilon_{w\alpha})$$

where

$$D(x, \Delta_\alpha, C_\alpha, \Gamma_\alpha, \epsilon_{h\alpha}, \epsilon_{w\alpha}) = \frac{1+\epsilon_{h\alpha}}{\left[\frac{2}{\Gamma_\alpha(1+\epsilon_{w\alpha})}\right]^2\left(x-\frac{\Delta_\alpha}{2}-C_\alpha\right)^2+1} + \frac{1-\epsilon_{h\alpha}}{\left[\frac{2}{\Gamma_\alpha(1-\epsilon_{w\alpha})}\right]^2\left[x+\frac{\Delta_\alpha}{2}-C_\alpha\right]^2+1}. \quad (1)$$

[3] By chemical shift we mean the NMR frequency shifts often observed in nonmetals. The term chemical shift has sometimes been used to refer to the isomer shift, which is measureable only by ME.

[4] The source preparation was performed by the New England Nuclear Corp., Boston, Mass.

[5] Standard reference material 725; disodium pentacyanonitrosoferrate dihydrate ($Na_2Fe(CN)_5NO \cdot 2H_2O$). Otained from the Office of Standard Reference Materials, National Bureau of Standards, Washington, D.C. in October 1966.

TABLE 1. *Summary of measurement conditions and results obtained*

All runs taken with source at 210 K, magnetic field at 50.131 kG, SNP at 295 K, and TiFe at 120 K, except as noted. The Δ_1 ratios are obtained by averaging the SNP results before and after each TiFe run.

Run No.	Absorber	Δ_1	$\frac{\Delta_1(\text{SNP})}{\Delta_1(\text{TiFe})}$
010970.1	SNP	175.97	
010970.2	TiFe	169.20	1.0403
011070.1	SNP	176.06	
011070.2	TiFe [a]	169.26	1.0396
011170.1	SNP	175.88	
011270.1	SNP [b]	175.73	
011270.2	TiFe	169.03	1.0398
011370.1	SNP	175.80	
011470.1	None [c]		
011470.2	TiFe [a]	168.48	1.0446
011570.1	SNP [b]	176.18	
011570.2	TiFe	169.10	1.0409
011670.1	SNP	175.84	
011670.2	TiFe	168.59	1.0426
011770.1	SNP	175.72	
011770.2	TiFe [d]	168.79	1.0403
011970.1	SNP	175.47	
011970.2	TiFe [d]	168.85	1.0409
012070.1	SNP	176.03	
012070.2	TiFe [d]	168.30	1.0457
012170.1	SNP	175.94	

[a] Second of two samples of TiFe.
[b] No magnetic field.
[c] This run used to obtain window doublet parameters.
[d] TiFe at 60 K.

Here $y(x)$ refers to the amount of resonant absorption as a function of channel No. x. The parameters a, b, and c represent a background parabola arising from the fact that the source-detector distance is varied in the experiment. The doublet due to the presence of Fe in the beryllium windows, determined in the run with no absorber, is represented by $w(x)$ and d is the height of this doublet. For fitting the sodium nitroprusside spectra one doublet is used (see fig. 3) and the summation index α runs over only $\alpha=1$. The TiFe spectra are fitted to two doublets, an outer and a narrowly spaced inner (see fig. 4) and the summation index α runs over $\alpha=1$ and $\alpha=2$. The parameter Δ_α represents the doublet splitting, C_α the center of the doublet, Γ_α the full width at half maximum (FWHM) of each doublet line, $\epsilon_{h\alpha}$ any difference in the height of the two doublet lines, and $\epsilon_{w\alpha}$ any difference in the width of the two doublet lines.

The least squares fit was accomplished by an iterative procedure. The function $y(x)$ was expanded in a Taylor series with only the linear terms retained. Partial derivatives with respect to the various parameters were determined numerically. Initial estimates of a, h_α, C_α, and Γ_α could be made from the raw data to within 5 percent of their final value. The initial estimates for b, c, $\epsilon_{h\alpha}$, and $\epsilon_{w\alpha}$ were taken as zero. The initial estimate for d was determined from a spectrum taken with no absorber. On two of the spectra several least squares fitting procedures were used to determine the effect of deleting various combinations of the background parabola, window doublet, and assymmetry parameters. This is discussed in the next section on systematic errors.

Determination of the splitting of the outer doublet of the TiFe spectrum $\Delta_1(\text{TiFe})$ in a known field calibrates the spectrometer. From the splitting of the sodium nitroprusside doublet in channels $\Delta_1(\text{SNP})$, the splitting in velocity, $v(\text{SNP})$ is given by

$$v(\text{SNP})=\lambda(1+3g_1/g_0)(1+K(T))\left(\frac{\gamma}{2\pi}\right)H\frac{\Delta_1(\text{SNP})}{\Delta_1(\text{TiFe})} \qquad (2)$$

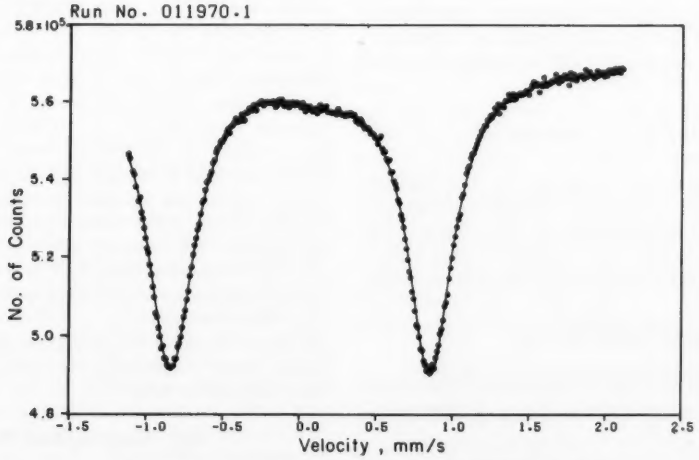

FIGURE 3. *Typical spectrum of sodium nitroprusside.*

Circles are experimental points and the solid line is the least squares fit. The direction of gamma-ray propagation is along the b axis of the crystal. Distortion of background due to Fe in beryllium windows is evident. Velocity zero is taken as the center of the two prominent peaks.

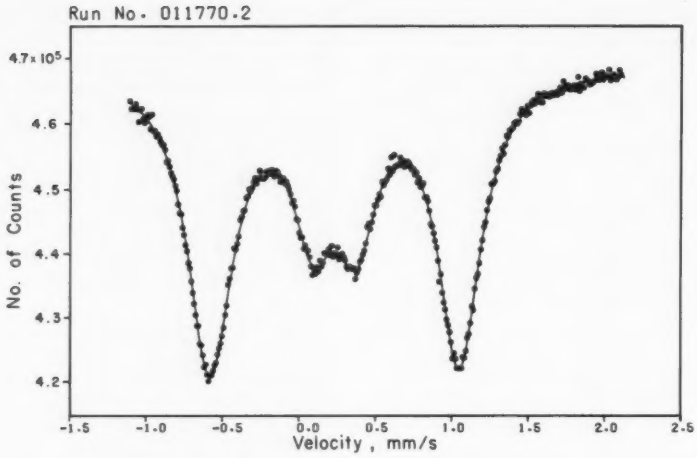

FIGURE 4. *Typical spectrum of* TiFe *in a magnetic field.*

Circles are experimental points and the solid line is the least squares fit. The sample was a polycrystalline powder. Velocity zero the same as for figure 2.

where λ is the wavelength of the Mössbauer effect gamma ray, g_1/g_0 is the ratio of the ^{57}Fe excited state level splitting to ground state splitting, $K(T)$ is the Knight shift of Fe in TiFe, $\gamma/2\pi$ is the gyromagnetic ratio of the ^{57}Fe ground state, and H is the applied field.

In table 1 are listed the 9 values obtained for the ratio $\Delta_1(\text{SNP})/\Delta_1(\text{TiFe})$. For the parameters we adopt

$$\lambda = 0.860231 \text{ Å}^* \text{ [12]}^6$$

$$[1+K(T)]\frac{\gamma}{2\pi} = \begin{cases} 139.37 \text{ Hz/G at T} = 120 \text{ K}^7 \\ 139.42 \text{ Hz/G at T} = 60 \text{ K}^7 \end{cases}$$

$$3g_1/g_0 = 1.714.$$

The selection of these values and their contribution to the systematic error are discussed in the next section. Using these values, and the numbers listed in table 1, we obtain

$$v(\text{SNP}) = 1.6993 \pm 0.0024 \text{ mm/s}$$

as a 90 percent confidence interval[8] for the sodium nitroprusside splitting at 295 K determined as described above. The contribution of the systematic errors are greater than the uncertainty in this value. They are discussed and estimated in the next section.

4. Systematic Errors

Besides the obvious sources of error, the determination of the position of a resonance line to within a few percent of its linewidth presents numerous difficulties. In this section we evaluate the known systematic errors in our determination of the sodium nitroprusside line splitting.

4.1. Magnetic Field Measurement

The magnetic field measurement utilized the ^{63}Cu nuclear magnetic resonance at 4.2 K. The Knight shift of Cu is accurately known [13] (0.232 %) and is nearly temperature independent. A super-regenerative detector of the type described by Rubinstein and Shtrikman [14] was used with a quench frequency of 20 kHz. The ^{63}Cu line was broadened to about 30 kHz by the field inhomogeneity. The accuracy of this method is better than one-half the resonance linewidth and is thus better than about 0.02 percent. No change in resonance frequency was detected when the superconducting magnet was switched to persistent mode. However, there was a field drift of 0.25 percent per hour in the persistent mode. To correct for this, the voltage drop across an 0.001Ω resistor required to give a field of 50.196 kG was measured. During the TiFe runs the field was readjusted every 0.5 hr to this value, giving an average field of 50.131 kG. Measurements of the field were made both before and after taking the ME spectra with no significant change detected. By moving the NMR probe in the magnetic field, the homogeneity of the field was estimated to be better than 0.1 percent over a 12.5-mm sphere. Considering all these factors, we estimate that the magnetic field error could contribute no more than 0.0015 mm/s to the systematic error.

4.2. Gamma-Ray Wavelength

The uncertainty in the value of λ[12] is less than 100 ppm. This is an order of magnitude smaller than the uncertainty of our measurement and will contribute

[6] This value is based on comparison with $\lambda_{WK_\alpha} = 0.2090100$ Å* [12]. Professor J. A. Bearden has kindly informed us that this is his most accurate value at present.

[7] Taken from ref. [1]. These values are based on an effective nuclear moment of ^{39}K in the reference salt (aqueous KI) of 0.39090 μ_N.

[8] Calculated as described by M. G. Natrella in NBS Handbook 91 (U.S. Government Printing Office, 1963) p. 2-2.

less than 0.0002 mm/s to the systematic error in the sodium nitroprusside splitting.

4.3. Knight Shift Values

The uncertainty in the product $[1+K(T)]\gamma/2\pi$ is likewise small and is given [1] as about 300 ppm. Since we use only the product and not $K(T)$ alone, any uncertainty in the ground state nuclear moment of ^{57}Fe does not affect our result. Also, there is no reason to expect a field dependence of the Knight shift of TiFe up to fields much larger than those used here. This view is supported by the fact that there is no detectable change in the TiFe spectra upon lowering the temperature from 120 K to 60 K. The contribution of the Knight shift value to the systematic error is less than 0.0005 mm/s.

4.4. Velocity Drive Linearity

A schematic diagram of the velocity feedback circuit is shown in figure 5. In this experiment we depend critically on the linearity of the reference signal, and the ability of the feedback circuit to reduce the error signal to zero. Throughout the experiment, the error signal was continuously monitored at the output of operational amplifier $A2$. Knowing the parameters of the velocity transducer and the values of R_1, R_2, R_3, and C_1, a correction could be made for the feedback error. However, in no case would this error have exceeded 0.03 channels (out of 175 channels peak separation) and hence it was neglected.

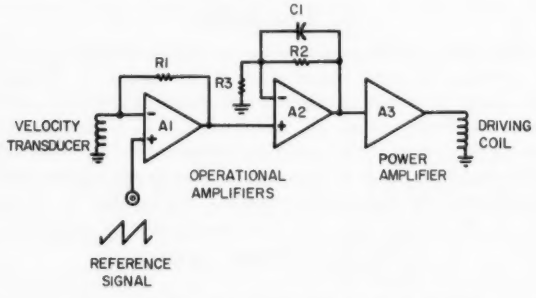

FIGURE 5. *Velocity spectrometer feedback circuit.*
Values of the parameters used were: R1 – 250 kΩ; R2 – 825 kΩ; R3 – 1 kΩ; C1 – 0.047 μF; velocity transducer – 19 kΩ, 2.4 Hr, with 20 vs/m sensitivity.

The channel address voltage of the multichannel analyzer was used to control the reference signal (as described by Ruegg et al. [15]). Operation can be linear only if the reference signal voltage is proportional to the analyzer channel number. This was checked by measuring the reference signal voltage with a precision voltmeter as a function of channel number. A small nonlinearity of ± 0.15 channels over the 332 channels utilized was detected. However, since the TiFe peaks and the sodium nitroprusside peaks fall within 18 channels of each other, the change in Δ_1(SNP)/Δ_1(TiFe) by correcting for this nonlinearity would be only 0.0003 mm/s. This same reasoning applies for any nonlinearity in the velocity transducer. The transducer[9] was a magnetically shielded coil about 180 mm long with an O.D. of 15 mm and with a bar magnet about 110 mm long moving through the inside of the coil. The difference in position of the bar magnet between corresponding peaks of the TiFe and the sodium nitroprusside spectra was only 80 μm. We thus expect the nonlinearity in the velocity transducer to shift the peaks of both TiFe and sodium nitroprusside equally and thus not affect the ratio Δ_1(SNP)/Δ_1(TiFe) significantly. Our estimate of the total systematic error due to velocity drive nonlinearity is 0.0008 mm/s.

4.5. Nuclear Moment Ratio

The ratio of the excited state to the ground state ^{57}Fe moment, $3\ g_1/g_0$, appears in eq (2) and affects the accuracy of the results. (This ratio is actually negative but here we use $3\ g_1/g_0$ to refer to its absolute value.) It cannot be determined accurately from our own spectra because of the reduced intensity and very close spacing of the inner two doublet lines. We therefore use the value of $3\ g_1/g_0$ determined for pure Fe. Several precision measurements of pure Fe Mössbauer spectra have been made. Using an ultrasonic technique, Cranshaw and Reivari [16] obtained $3\ g_1/g_0 = 1.715 \pm 0.003$. Using an interferometer to calibrate their spectrometer, Fritz and Schulze [17] obtained $3\ g_1/g_0 = 1.711 \pm 0.002$. Using Moiré fringes for velocity measurement, DeWaard [18] obtained $3\ g_1/g_0 = 1.713 \pm 0.004$, and using the lead screw of a lathe as a velocity drive, Preston et al. [19] obtained $3\ g_1/g_0 = 1.715 \pm 0.004$. Considering these values we adopt $3\ g_1/g_0 = 1.714 \pm 0.003$. The uncertainty in this value for g_1/g_0 yields an uncertainty of 0.0019 mm/s in the sodium nitroprusside splitting.

We mention the possibility of an anomalous hyperfine field effect [20] which could cause the apparent value of $3\ g_1/g_0$ to be different for ^{57}Fe in TiFe and ^{57}Fe in pure iron. The anomaly arises from the fact that the distribution of magnetic dipole density over the finite nuclear volume may be different for different isotopes or for the ground and excited nuclear states of the same isotope. The effect has been observed, for example, for the Knight shifts of ^{85}Rb and ^{87}Rb in rubidium metal [21] which are, respectively, 0.6527 percent and 0.6502 percent. This anomaly would lead to an error in magnetic field of 0.002 percent using Rb. The anomalous effect is thus expected to be negligible for ^{57}Fe in different materials because it generally decreases with decreasing nuclear size. It has not been detected within the precision of any Fe Mössbauer experiments to date. We therefore feel confident in neglecting it for this experiment.

4.6. Background, Asymmetry, and Vibration

The background for the spectra obtained here were perturbed from an ideal straight line due to the presence of Fe in the Be windows of the dewar and due to

[9] L. V. Syn Model 6LV2, Sanborn Electronics, Waltham, Massachusetts.

source motion. To correct for these perturbations they were included as the parabola and window doublet of eq (1). Also, as indicated in eq (1), the heights and the widths of the doublets were allowed to be asymmetric. The window doublet fraction, d, averaged about 5 percent and the background parabola about 0.5 percent of the total absorption area. The height asymmetry, ϵ_h, averaged about 0.01 and width asymmetry, ϵ_w, about 0.02.

To test the effect of these factors on the results, various fits were made to the data of one TiFe spectrum and one sodium nitroprusside spectrum under various constraints on the parameters of eq (1). The results are shown in table 2.

The Γ_α's obtained for all runs varied from 34 to 36 channels, corresponding to a FWHM of 0.34 ± 0.01 mm/s. This is about 0.07 mm/s larger than the width of 0.27 mm/s exhibited by both the TiFe and the sodium nitroprusside samples under ideal conditions. The excess width is due to vibrations arising from nearby vacuum pumps, building vibrations, etc. The effect of such vibrations is to give the center of the doublets a Gaussian probability distribution. When this assumption is put into eq (1) and a least squares fit made with the parameters Γ_α constrained to correspond to 0.27 mm/s, the results shown in table 2, line (e) are obtained.

A statistical analysis of the various fits shows that the constraints introduced in (b), (c), and (d) of table 2 all result in a statistically significant (5% level or better) increase in the standard deviation of fit. The analysis also shows that the assumptions made in (e) give the best fit to the data. As seen from table 2, the value of $\Delta_1(\text{SNP})/\Delta_1(\text{TiFe})$ is in all cases quite insensitive to the method of fitting the data. The values of Δ_1, though still relatively insensitive, vary considerably more than the ratio $\Delta_1(\text{SNP})/\Delta_1(\text{TiFe})$. When vibrations may be a problem the results shown in table 2 suggest that the most appropriate method would be to fit with a Gaussian distribution of natural-width Lorentzians. The results presented here are quite insensitive to the choice of fitting method since they depend only on the ratio $\Delta_1(\text{SNP})/\Delta_1(\text{TiFe})$.

As seen in table 2, no correction due to background, asymmetry or vibration greater than 0.1 percent is used. We estimate the systematic error due to these factors to be no greater than one-half this correction, 0.0008 mm/s.

The systematic error contributions are summarized in table 3. The result for the sodium nitroprusside splitting is then 1.6993 mm/s with a precision of ± 0.0024 mm/s based on a 90 percent confidence limit for the mean value of all determinations, and with a maximum systematic error of 0.0021 mm/s, not including possible errors in 3 g_1/g_0, λ, and $K(T)$.

TABLE 2. *Effect of constraints on lease squares fitting results for run No. 012070.2* (TiFe) *and run No. 012170.1* (SNP).

Parameters of fit	Δ_1(TiFe)	Δ_1(SNP)	$\frac{\Delta_1(\text{SNP})}{\Delta_1(\text{TiFe})}$	Percent change from [a]	s_{fit} [f]	
					TiFe	SNP
([a])	168.30	175.94	1.0454	.....	0.013	0.012
([b])	168.07	175.77	1.0458	+0.04	.016	.015
([c])	167.88	175.64	1.0462	+.08	.014	.015
([d])	167.90	175.67	1.0463	+.09	.017	.016
([e])	168.19	175.79	1.0452	−.02	.012	.010

[a] Fit to eq (1), no constraints, all parameters allowed to vary independently.
[b] Fit to eq (1), background parabola terms b and c and asymmetry terms ϵ_{bo} and ϵ_{wo} constrained to be zero.
[c] Fit to eq (1), height of window doublet d constrained to be zero.
[d] Fit to eq (1), height of window doublet d, background parabola terms b and c, and asymmetry terms ϵ_{bo} and ϵ_{wo} constrained to be zero.
[e] Fit to eq (1), with h_α given a Gaussian distribution as a function of C_α. Widths Γ_α constrained to 28.0 channels (corresponding to 0.27 mm/s). No other constraints.
[f] Standard deviation of fit, $s_{\text{fit}}^2 = (y - y_{\text{obs}})^2/(N-P)$, where N is the number of data points, P is the number of independent parameters used in the fit, and the data points y_{obs} have been normalized to lie in the range of zero to unity. Both runs had an average of about 5×10^6 counts in each of 330 channels.

TABLE 3. *Contributions to systematic error in this determination of the sodium nitroprusside splitting*

The first four are independently determined constants. The last three are unique with this measurement.

Parameter	Estimated error contribution
	mm/s
γ	0.0002
$K(T)$	.0005
$3\,g_1/g_0$	.0020
Hyperfine field anamoly	.0000
H	.0015
Linearity	.0008
Background, etc	.0008

5. Discussion

The sodium nitroprusside splitting obtained here is compared with other results in figure 1. Within the limit of error, the results compare favorably with those of Grant et al. [2] and Fritz [7]. It is also interesting to compare the splitting obtained for the sodium nitroprusside with a pure iron spectrum. From the results of four runs we estimate

$$\frac{(g_0 - g_1)}{\Delta_1(\text{SNP})} = 0.9886 \pm 0.0010$$

where $(g_0 - g_1)$ is the splitting of the inner two lines of a pure iron spectra. Using this, and the previously quoted value for 3 g_1/g_0 and assuming $\Delta_1(\text{SNP}) = 1.699$ mm/s we obtain $g_0 = 3.918 \pm 0.004$ mm/s and $g_1 = 2.238 \pm 0.004$ mm/s for pure iron at 295 K. These values are compared with previous ME results and with NMR results [22] in table 4. The Mössbauer effect results are in good agreement and give confidence in the correctness of the SNP value. The NMR results are listed for reference. Though inherently more accurate than the ME results, they cannot be directly compared since NMR in ferromagnetic iron measures the splitting for ^{57}Fe atoms in domain walls, whereas the ME measures the splitting for ^{57}Fe atoms within the domains. As described by Schechter et al. [23], the values of g_0 and g_1 are useful for calibrating and checking linearity of spectrometers using pure Fe.

TABLE 4. *Comparison of g_0 and g_1 values obtained for ^{57}Fe in pure Fe at 295 ± 1 K.*

Technique and Ref.	g_0	g_1
	mm/s	*mm/s*
ME, this work	3.918 ± 0.004	2.238 ± 0.004
ME [a] [16]	3.911 ± 0.003	2.236 ± 0.003
ME [17]	3.931 ± 0.003	2.242 ± 0.002
ME [18]	3.916 ± 0.005	2.236 ± 0.006
ME [b] [19]	3.920 ± 0.008	2.240 ± 0.005
NMR [a] [22]	3.909 ± 0.001	

[a] Results given in frequency units, which we have converted to velocity units.
[b] Interpolated between values given for 293 and 298 K.

The results presented for TiFe and sodium nitroprusside make it possible to measure Knight shifts and chemical shifts of Fe in suitable alloys and compounds to about 0.5 percent or better.

To obtain more accurate results, several modifications to the equipment within the state of the art would be useful. This would include an interferometer or Moiré fringe counter for direct velocity measurement while the data are being accumulated. This would allow a check on the internal consistency of the results and, once calibrated, an accurate determination of applied field using TiFe spectra. Higher fields than used here are desirable in order better to resolve the inner two lines of the TiFe applied field spectrum. This would provide a sensitive test for the possible presence of a small hyperfine field anomaly and would allow calibrations of materials such as pure Fe with larger internal field splittings. Also, a more homogeneous and stable magnet would be useful, since the magnet field drift and inhomogeneity gave the largest contribution to the systematic error of this experiment.

The authors wish to thank Dr. J. J. Spijkerman and Dr. J. C. Travis for helpful discussions, Dr. J. Mandel for advice on statistical analysis, and Dr. R. W. Grant for useful comments. We also thank D. P. Fickle for aid with sample preparation and R. D. Robbins and R. L. Parke for technical assistance.

6. References

[1] Swartz, J. C., Swartzendruber, L. J., Bennett, L. H., and Watson, R. E., Phys. Rev. B **1**, 146 (1970).
[2] Grant, R. W., Housley, R. M., and Gonser, U., Phys. Rev. **178**, 523 (1969).
[3] Spijkerman, J. J., Snediker, D. K., Ruegg, F. C., and DeVoe, J. R., Nat. Bur. Stand. (U.S.), Misc. Publ. 260–13 (1967).
[4] Spijkerman, J. J., Ruegg, F. C., and DeVoe, J. R., in Applications of the Mössbauer Effect in Chemistry and Solid-State Physics (International Atomic Energy Agency, Vienna, 1966), p. 254; and Mössbauer Effect Methodology, I. J. Gruverman ed. (Plenum Press Inc., New York, 1965) Vol. 1, p. 115.
[5] Kerler, W., Z. Physik **167**, 194 (1962); W. Kerler and W. Neuwirth, Z. Physik **167**, 176 (1962).
[6] Danon, J., J. Chem. Phys. **41**, 3378 (1964).
[7] Fritz, R., Phys. Letters **31A**, 226 (1970).
[8] Herber, R. H., in Mössbauer Effect Methodology, ed. I. J. Gruverman (Plenum Press Inc., New York, 1965), Vol. 1, p. 3.
[9] Swartzendruber, L. J., Nucl. Instr. and Meth. **69**, 101 (1969).
[10] West, G. W., J. Appl. Phys. **39**, 2213 (1968).
[11] Swartzendruber, L. J., and Bennett, L. H., J. Appl. Phys. **39**, 2215 (1968).
[12] Bearden, J. A., Phys. Rev. **137**, B455 (1965).
[13] Carter, G. C., NBS Alloy Data Center, Gaithersburg, Md., private communication.
[14] Rubinstein, M., and Sktrikman, S., Am. J. Phys. **35**, 945 (1967).
[15] Ruegg, F. C., Spijkerman, J. J., and DeVoe, J. R., Rev. Sci. Instr. **36**, 356 (1965).
[16] Cranshaw, T. E., and Reivari, P., Proc. Phys. Soc. **90**, 1059 (1967).
[17] Fritz, R., and Schulze, D., Nucl. Instr. and Meth. **62**, 317 (1968).
[18] DeWaard, H., Rev. Sci. Instr. **36**, 1728 (1968).
[19] Preston, R. S., Hanna, S. S., and Heberle, J., Phys. Rev. **128**, 2207 (1962).
[20] Bohr, A., and Weisskopf, V. F., Phys. Rev. **77**, 94 (1950).
[21] Blumberg, W. E., Eisinger, J., and Klein, M. P., Phys. Rev. **124**, 206 (1961).
[22] Budnick, J. I., Bruner, L. J., Blume, R. J., and Boyd, E. L., J. Appl. Phys. **32**, 120S (1961).
[23] Shechter, H., Ron, M., Niedzwiedz, S., and Herber, R. H., Nucl. Instr. and Meth. **44**, 268 (1966).

(Paper 74A5–633)

JOURNAL OF RESEARCH of the National Bureau of Standards—A. Physics and Chemistry
Vol. 74A, No. 5, September–October 1970

Energies of $1snl (l \geq 3)$ Configurations in He^4 I as Calculated from Polarization Theory

William C. Martin

Institute for Basic Standards, National Bureau of Standards, Washington, D.C. 20234

(June 14, 1970)

The calculated singlet-triplet mean energies are given for all He^4 I configurations having $3 \leq l \leq n-1$ from $4f$ to $8k$. Since only Stark-shifted transitions have been observed for such configurations with $l \geq 4$, the calculated positions are the most accurate available. The polarization energy (to the quadrupole approximation) for two-electron ions may be evaluated for higher nl or Z from the simple formulas. The calculated and observed positions of the $1snf$ configurations in He^4 I and Li^7 II agree within the experimental uncertainties.

Key words: Atomic energy levels; atomic theory; helium; polarizability.

1. Introduction

In a list of He^4 I energy levels published in 1960 [1],[1] positions were given for several configurations $1s5l$, $6l$, $7l$ ($l \geq 4$) that had been observed only in Stark-effect investigations [2]. An attempt was made to derive the approximate undisplaced positions for these configurations from Foster's measurements [2]. However, Foster [3] had already given a more accurate position for the $5g$ configuration relative to the other levels for $n = 5$. This position was not derived from his observations but from the polarization theory of term defects due to Born and Heisenberg [4] and Waller [5]. (The "term defect" was the difference between the actual term value and the Bohr energy R/n^2.) A simple expression for the polarization defect for $1snl$ configurations for $l \geq 3$ is applied here to obtain positions for several such configurations in He^4 I.

2. Polarization Formulas

Polarization theory [4–9] is now frequently used to describe the deviations of non-penetrating terms T in alkali-like atoms from corresponding hydrogenic term values T_0. For a non-penetrating electron outside a closed-shell core [9]:

$$T - T_0 = \Delta_p = R\alpha_d\langle r^{-4}\rangle + R\alpha_q\langle r^{-6}\rangle \qquad (1)$$

where R is the Rydberg constant and α_d and α_q are the electric dipole and quadrupole polarizabilities of the core in units of a_0^3 and a_0^5, respectively (a_0 is the Bohr radius). The expectation values $\langle r^{-4}\rangle$ and $\langle r^{-6}\rangle$ have been tabulated [8] and Edlén [9] has given a convenient table for use with the expression [2]

$$\Delta_p = A(Z)P(n, l)[1 + k(Z)q(n, l)]. \qquad (2)$$

Here

$$A(Z) = Z_c^4\alpha_d \quad \text{and} \quad k(Z) = Z_c^2\alpha_q/\alpha_d \qquad (3)$$

where Z_c is the net charge of the core; $P(n, l)$ and $q(n, l)$ are the quantities tabulated by Edlén.

The polarization energy for an atom with a core having a partly filled shell will in general contain terms not appearing for the closed-shell core. Bethe [10] gives an expression for the polarization quantum-defect for a two-electron atom ($1snl$) that reduces to the dipole value for large $Z \cdot r$.

It is useful to note that Waller's dipole calculation agrees with the current best observations for $1snf$ in both He^4 I and Li^7 II to within the experimental accuracies. Weiss [11] has now shown that the simple expression (1) is valid for $1snl$ configurations of two-electron ions if $l \geq 3$. In this case T is the arithmetic mean of the singlet and triplet terms for $1snl$. This result allows an accurate calculation of Δ_p for such configurations since the $1s$ core polarizabilities are just the hydrogenic values [5, 7]: $\alpha_d = 9/(2Z^4)$ and $\alpha_q = 15/Z^6$. For helium-like ions $Z_c = Z - 1$, and we have from (3):

$$A(Z) = 9(Z-1)^4/(2Z^4) \qquad (4)$$

$$k(Z) = 10(Z-1)^2/(3Z^2). \qquad (5)$$

[1] Figures in brackets indicate the literature references at the end of this paper.

[2] An expression having similar form was introduced in [6].

389-821 O - 70 - 7

With (4), (5), and (2) the polarization energies for 1*snl* ($l \geq 3$) configurations may be evaluated to the quadrupole approximation for any two-electron ion.

In the case of hydrogenic spectra, T_0 in eq (1) includes the appropriate relativistic correction to the Bohr term [9]. Relativistic corrections for excited states in two-electron ions are not generally available, but calculations for 1*snp* terms ($n=2, 3, 4$) in He I have been reported [12]. The singlet-triplet mean corrections for these terms are of the same order as the relativistic corrections for the corresponding *np* terms in hydrogen. Since the hydrogenic corrections for $l \geq 3$ are less than 0.01 cm^{-1}, the relativistic corrections for He are probably negligible to the accuracies of the calculations given here. Bethe and Salpeter [13] indicate that the mass-polarization correction is negligible for terms having $l \geq 2$ in two-electron ions. Calculations by Mayer and Mayer [6] show that the effect due to penetration of the 1*s* core by the excited wave function would also be negligible to the accuracy needed here. We thus adopt the uncorrected Bohr energy R/n^2 for T_0, the mean of the singlet and triplet terms without the Δ_p correction.

3. Term Defects

An accurate value for the He II ($^2S_{1/2}$) series limit is needed in order to obtain (from calculated terms) the positions of the $l \geq 3$ configurations relative to the *S*, *P*, and *D* levels. Seaton [14] applied a least-squares fitting procedure to several observed series and obtained a weighted mean of 198310.76 ± 0.01 cm^{-1} for the limit (relative to the He^4 I $^1S_0$ ground level at 0.00 ± 0.15 cm^{-1}) [15].[3] His method is a refinement of the usual procedure in that it takes the relation between the quantum defect and the term value explicitly into account in the weighting. He did not, however, give a specific weighting according to the different experimental accuracies. The 3*d*, 4*d*, 5*d* ^1D and 3*d*-6*d* ^3D levels [1, 16] are known to better than 0.01 cm^{-1}, and it should be possible to describe the *D* series with a simple two-parameter formula. If the 3*d*, 4*d*, and 5*d* baricenters are fitted to a Ritz formula $n - n^* = a + \beta T$, a limit of 198310.741 cm^{-1} is obtained. (Here $T = R/n^{*2}$ is the absolute term value, and R for He^4 is taken as 109722.267 cm^{-1}.) Table 1 gives the results of a Ritz-formula fit[4] based on Seaton's value for the limit. Comparison of the observed and calculated baricenters for the accurately known lowest three terms shows them to be consistent with this limit. Seaton's method showed convincingly that the earlier values given for the limit [1, 15] were too high, and his result is adopted here.

TABLE 1. *Term values for the* 1snd (n=*3 to 8*) *baricenters in* He^4 I

Calculated values were determined from a Ritz formula with the constants (see text): $R = 109722.267$ cm^{-1}; $a = 2.6865 \times 10^{-3}$; $\beta = -5.00 \times 10^{-8}$. Observed values are based on levels from Ref. [1] referred to a limit of 198310.76 cm^{-1}.

1*snd*	n^* (calc)	Term (calc)	Term (obs)	O–C
		cm^{-1}	*cm*$^{-1}$	*cm*$^{-1}$
3*d*	2.9979239	12208.254	12208.254	0.000
4*d*	3.9976568	6865.683	6865.679	−.004
5*d*	4.997533	4393.225	4393.228	.003
6*d*	5.997466	3050.417	3050.42	.00
7*d*	6.997426	2240.878	2240.92	.04
8*d*	7.997399	1715.526	1715.49	−.04

Table 2 gives the results of an evaluation of (2) for the He^4 I configurations 1*snl* ($l \geq 3$) to $n = 8$. From (4) and (5) the constants are: $A = 9/32$; $k = 5/6$. The limitation on the principal quantum number is arbitrary and the results may be extended to any 1*snl* configuration with $l \geq 3$. It seems unlikely that the approximations in the method give an error as large as 0.1 cm^{-1} even for 4*f* (the largest value of *T*). The deviations from the observed positions for 5*f* and 6*f* are within the experimental uncertainties. Any reasonable fitting of the *nf* series by one of the usual series formulas shows the observations for the lowest three members to be inconsistent on the scale of ~ 0.1 cm^{-1}.

TABLE 2. *Calculated polarization defects and term values for some configurations in* He^4 I

The term values and positions are singlet-triplet means. $T_0 = (109722.267/n^2)$ cm^{-1}, and $T = T_0 + \Delta_p$.

1*snl*	T_0	Δ_p	T	Position[a]	O–C[b]
	cm^{-1}	*cm*$^{-1}$	*cm*$^{-1}$	*cm*$^{-1}$	*cm*$^{-1}$
4*f*	6857.642	1.168	6858.810	191451.950	−0.01
5*f*	4388.891	0.673	4389.564	193921.196	.14
6*f*	3047.8408	.413	3048.254	195262.506	.08
7*f*	2239.2299	.269	2239.499	196071.261	.00
8*f*	1714.4104	.184	1714.594	196596.166	.00
5*g*	(see	.157	4389.048	193921.712	
6*g*	above)	.101	3047.942	195262.818	
7*g*		.068	2239.298	196071.462	
8*g*		.047	1714.457	196596.303	
6*h*		.032	3047.873	195262.887	
7*h*		.022	2239.252	196071.508	
8*h*		.016	1714.426	196596.334	
7*i*		.009	2239.239	196071.521	
8*i*		.006	1714.416	196596.344	
8*k*		.003	1714.413	196596.347	

[a] Relative to the 1s^2 $^1S_0$ ground level at 0.00 ± 0.15 cm^{-1}. (Position) = 198310.760 cm^{-1} − T; this limit is thought to be accurate to ± 0.01 cm^{-1}.

[b] Difference between the observed [Ref. 1] and calculated positions.

[3] Pekeris calculated a value of 198310.674 ± 0.025 cm^{-1} for the principal ionization energy of He [Phys. Rev. **126**, 1470 (1962)]. If this result is accepted, the $^1S_0$ ground level is at + 0.086 ± 0.025 cm^{-1} relative to the positions as given here and in [1] for all excited configurations. An additional uncertainty that varies from < 0.01 cm^{-1} to > 0.1 cm^{-1} is then associated with the excited levels. The term values calculated here with respect to the limit are not affected by any such change in the ground level.

[4] The series constants (from table 1) give $R\beta/a = -2.04$, quite close to the value −2.00 expected if a and β were entirely due to the dipole polarizability α_d. The *D* terms deviate from the positions predicted by the hydrogenic 1*s* core value for α_d, however, by about 6 percent of the term defects. Weiss [11] finds that the polarization energy for 1*snd* includes terms in addition to the two polarizability terms in eq (1) above. The only available polarization-theory method that will accurately predict the *nd* terms is to fit the low terms by treating the limit, $A(Z)$, and $k(Z)$ as adjustable parameters [9]. Such a fit for the 3*d*, 4*d*, 5*d* baricenters gives $A = 0.27840$ and $k = 0.021$. The calculated limit and all calculated terms then agree to within 0.002 cm^{-1} with corresponding values obtained from fitting the same three terms to the Ritz formula.

It could well be that the $5f$ and $6f$ positions are mainly at fault, as indicated by the deviations in table 2.

The $nf\ ^1F^\circ - ^3F^\circ$ separations obtained from the experimental positions for $4f$ and $5f$ (0.28 and 0.06 cm^{-1}, respectively) [1] are almost surely due to observational error (perhaps including source effects). The calculated separations [17] of only 0.011 and 0.009 cm^{-1}, respectively, should be accurate to much better than an order of magnitude. Thus at least one of the $4f$ terms is in error by more than 0.1 cm^{-1}, and an error of 0.2 cm^{-1} in the mean seems reasonable.

If the various terms are known experimentally to about the same accuracy (in cm^{-1}), the most sensitive comparisons with polarization calculations for $l \geq 3$ are obtained with the lowest nf configurations. The "O–C" results for these configurations in table 2 thus confirm the dipole contribution to the term defect to about 20 percent. They are not accurate enough to check the quadrupole contribution, however, which amounts to only about 2 percent of the dipole correction.

Any errors in T due to the approximations become smaller (in cm^{-1}) for higher values of n. Term values with more than three decimal places would be required in table 2 to give some separations of the higher configurations to the probable accuracy of the method.

The positions (relative to the ground level) previously given by the author [1] for the g, h, and i configurations in He are too high by up to 0.8 cm^{-1} (for $5g$). They are, in fact, unphysical in that they are *above* the corresponding Bohr positions. The best values now available for these configurations, and those of still higher l, are obtained from the polarization theory.

The calculated polarization energy for $l = 3$ is confirmed by the low F terms [18] in Li^7 II to a somewhat better percentage accuracy than the available measurements allow for He^4 I. In table 3 we see that the term defects for Li^7 II nf configurations are about three times the corresponding values for He^4 I. The experimental uncertainty[5] for the lower F terms in Li II is probably about 0.2 cm^{-1}. The calculated and experimental term defects thus agree to within the experimental accuracy, and calculated values different by more than ~ 10 percent would not agree with the observations. The values given for T_0 in table 3 are themselves uncertain by at least 5 percent, because relativistic effects are not included.[6] The total uncertainty in $T_0 - T_{obs}$ for these terms is thus about three times the ~ 4 percent quadrupole contribution to Δ_p.

We see from eq (5) for $k(Z)$ that the quadrupole contribution rises with Z; for high Z, $k(Z) \to 10/3$ and $A(Z) \to 9/2$. The polarization energies for a particular term thus approach asymptotic values with increasing Z. The quadrupole contribution for $4f$ approaches 6.9 percent, and the total polarization defect approaches $(18.37 + 1.28)\ cm^{-1} = 19.65\ cm^{-1}$. However, the realivistic corrections to T_0 are expected to increase as $(Z-1)^4$. These corrections (see footnote 6) are probably already of the same order as the quadrupole energy for $1snf$ in Li II. It appears that verification of the quadrupole term for $1snf$ in two-electron ions would require a calculation of the relativistic effects.

TABLE 3. *Calculated and observed term defects for* 1snf *configurations in* Li^7 II.

The polarization constants for Δ_p are $A = 8/9$ and $k = 40/27$. Term values are singlet-triplet means (see footnote 5). $T_0 = 4R/n^2 = (438914.91/n^2)\ cm^{-1}$.

$1snf$	T_0	T_{obs}	$T_0 - T_{obs}$	Δ_p
	cm^{-1}	cm^{-1}	cm^{-1}	cm^{-1}
$4f$	27432.18	27435.78	3.60	3.74
$5f$	17556.60	17558.69	2.09	2.16
$6f$	12192.08	12193.35	1.27	1.33
$7f$	8957.45	8958.3_2	0.8_7	0.87
$8f$	6858.05	6858.6_8	$.6_3$	.59
$9f$	5418.70	5419.1_8	$.4_8$	.42
$10f$	4389.15	4389.3_3	$.1_8$	.31

Note added in proof: Another effect neglected here is also probably comparable in magnitude to the quadrupole-polarization energy, even in He I. A very recent paper giving polarization energies in He I [C. Deutsch, Phys. Rev. A **2**, 43 (1970)] includes a nonadiabatic correction calculated to be slightly larger than, and opposite in sign to, the quadrupole-polarization contribution.

A. W. Weiss has been very helpful in discussions about two-electron atoms. I am especially grateful for his making available a new derivation that gives a firm theoretical basis for eq (1) as used here. A private letter from William S. Cooper, III, questioning (on the basis of AC Stark-effect observations) the $5g$ position given in [1] stimulated me to examine the accuracy of polarization theory for two-electron atoms.

4. References

[1] Martin, W. C., J. Res. Nat. Bur. Stand. (U.S.), **64A** (Phys. and Chem.), 19 (1960).
[2] Foster, J. S., Phys. Rev. **23,** 667 (1924).
[3] Foster, J. S., Proc. Roy. Soc. (London) **A117,** 137 (1927).
[4] Born, M., and Heisenberg, W., Z. Physik **23,** 338 (1924).
[5] Waller, I., Z. Physik **38,** 635 (1926).
[6] Mayer, J. E., and Mayer, M. G., Phys. Rev. **43,** 605 (1933).
[7] Sternheimer, R. M., Phys. Rev. **96,** 951 (1954).
[8] Bockasten, K., Arkiv Fysik **10,** 567 (1956).
[9] Edlén, B. Atomic Spectra, Secs. 20 and 33, in Encyclopedia of Physics, Flügge, S., ed., Vol. 27 (Springer-Verlag, Berlin, 1964).
[10] Bethe, H. A., Quantenmechanik der Ein- und Zwei-Electronenprobleme, Sec. 15; in Handbuch der Physik, Bd. 24/1 (Springer-Verlag, Berlin, 1933). An expression for the polarization defect for $1snl$ configurations with large n is derived. The evaluations of this expression in table 5 of the article are incorrect for the nF and nG terms.

[5] The calculated singlet-triplet separations of the F terms in Li II are only 0.15 and 0.13 cm^{-1} for $4f$ and $5f$, respectively [17]. These are not observed, being much smaller than the resolved hyperfine splittings of $\sim 1.0\ cm^{-1}$ [18]. On the assumption that the baricenter of the hyperfine structure is also the ^3F, ^1F baricenter, the singlet-triplet means (T_{obs}) in table 3 were made less than the corresponding baricenter term values by small amounts (0.04 cm^{-1} for $4f$ to 0.01 cm^{-1} for $8f$ and $9f$). Term determinations with respect to the limit baricenter were made by using the $2s\ ^2S_1$ baricenter at $134044.19 \pm 0.10\ cm^{-1}$ [18]. An uncertainty of 0.2 cm^{-1} for the lower F terms is probably sufficient to include the additional error due to uncertainty in their positions with respect to $2s\ ^2S_1$.

[6] Relativistic corrections have been calculated for Li II $2p\ ^1P$ [12]. The Li II $1snf$ corrections are probably of the order of the corresponding He II nf corrections, equal to 0.14 cm^{-1} for $4f$.

[11] Weiss, A. W., unpublished calculations.
[12] Schiff, B., Lifson, H., Pekeris, C. L., and Rabinowitz, P., Phys. Rev. **140,** A1104 (1965).
[13] Bethe, H. A., and Salpeter, E. E., Quantum Mechanics of One- and Two-Electron Atoms (Academic Press, New York, 1957), Secs. 37–39.
[14] Seaton, M. J., Proc. Phys. Soc. **88,** 815 (1966).
[15] Herzberg, G., Proc. Roy. Soc. (London) **A248,** 309 (1958).
[16] Martin, W. C., J. Opt. Soc. Am. **50,** 174 (1960).
[17] Heisenberg, W., Z. Physik **39,** 499 (1926). Expressions for the exchange integrals $K_l = G_l(1s, nl)$ are given for $n = l+1$ and $n = l+2$. The approximation made—an assumption of hydrogenic wave functions for 1s and nl—should be very good for 1snf.
[18] Herzberg, G., and Moore, H. R., Can. J. Phys. **37,** 1293 (1959).

(Paper 74A5–634)

JOURNAL OF RESEARCH of the National Bureau of Standards—A. Physics and Chemistry
Vol. 74A, No. 5, September–October 1970

A Theoretical Investigation of the Configurations $(3d+4s)^8 4p$ in Neutral Cobalt (Co I)*

Charles Roth**

(May 28, 1970)

Experimental levels of the configurations $(3d+4s)^8 4p$ were compared with corresponding calculated values. On fitting 154 levels by means of 19 free parameters an rms error of only 164 cm^{-1} was obtained.

Key words: Cobalt; configurations $(3d+4s)^8 4p$; energy levels; g-factors; interactions between configurations.

1. Introduction

Theoretical investigations of odd configurations $3d^n 4p$ for trebly and doubly ionized atoms of the iron group have been published by the author [1, 2][1,2]. In the calculations of doubly ionized Sc, Ti, and V the configurations $3d^{n-1}4s4p$ were added [3], and for Cu II other odd configurations were also included [4].

The configurations $(3d+4s)^3 4p$ were considered previously for the arc spectrum of titanium by Rohrlich [5], as well as by Smith and Siddall [6]. The configurations $3d^9 4s4p$ in Cu I were investigated by Martin and Sugar [7]. Wilson [8] derived from a Hartree-Fock procedure a set of radial parameters for Cu I $3d^9 4s4p$, which predicted satisfactorily the positions of seventeen low levels of Cu I. The configurations $(3d+4s)^n 4p$ were investigated for the arc spectra of calcium, scandium, titanium, vanadium, chromium, manganese, and iron by the author [9–13].

For the configurations $(3d+4s)^3 4p$ of Ti I, Rohrlich obtained an rms error of 1109 cm^{-1} before the advent of high-speed computers. He found it necessary to reject several terms which, however, fit very nicely in the recent investigations of Ti I, [6], [9]. Smith and Siddall obtained an rms error of 355 cm^{-1}, whereas in the author's investigation the rms error was further reduced to 261 cm^{-1}. One main reason for this considerable improvement is due to the fact that the author was able to identify experimental levels of the configuration $3d4s^2 4p$ and thus consider explicitly the interactions of this configuration with the configurations $3d^2 4s4p$ and $3d^3 4p$. Secondly, Smith and Siddall restricted their analysis to the electrostatic approximation, whereas the author included the spin-orbit interactions.

The configurations $(d+s)^8 p$ comprise 165 terms splitting into 438 levels. In AEL [14], 50 terms splitting into 139 levels are assigned to the configurations $3d^8 4p + 3d^7 4s4p$, 8 terms splitting into 19 levels are given without configuration assignments, and in addition, there are 37 undesignated odd levels.

Since only the parameters[3] B', C, C', and α vary monotonically from Ca I to Fe I, only the initial values of these parameters were obtained by linear extrapolation. Then, neglecting C and α for Sc I we obtain initially:

$$\begin{aligned} B' &= 1{,}000 \\ C &= 3{,}660 \\ C' &= 3{,}770 \\ \alpha' &= \alpha = 85 \end{aligned} \tag{1}$$

The initial values of the other parameters were assumed to be equal to the final values for Fe I [13].

The initial value for the height of the configuration $3d^7 4s4p$ can be obtained either from $^6F_{C.G.}$ or $^6G_{C.G.}$ (they differ only by $4F_2'$). Then, from the electrostatic matrix of ^6F [15],

$$^6F_{C.G.} = A' - 15B' - 3G_{ds}' - 3F_2' - G_{ps}' + 12\alpha' = 24180 \tag{2}$$

and

$$A' = 50800 \tag{3}$$

The initial value for the height of $3d^8 4p$ was obtained from the terms ^2D of $3d^8 4p$. By using the fact that the

*An invited paper. The work described in this paper was supported in part by the National Bureau of Standards and the National Research Council of Canada.

**Present address: Department of Mathematics, McGill University, Montreal 110, Canada.

[1] Figures in brackets indicate literature references at the end of this paper.

[2] The reader is referred to these papers for an explanation of the method used, notation, and significance of the various parameters.

The numerical values of all levels and parameters are in cm^{-1}.

[3] Unprimed parameters refer to the configuration $3d^8 4p$, primed parameters to $3d^7 4s4p$ and doubly primed to $3d^6 4s^2 4p$.

trace of a matrix equals the sum of its eigenvalues we obtain, [16, 14]

$$3A-4B+2C+4F_2+10G_3+20\alpha = 3d^8(a\,^3\mathrm{F})4p\,y\,^2\mathrm{D}_{\mathrm{C.G.}} + 3d^8(^1\mathrm{D})4p\,x\,^2\mathrm{D}_{\mathrm{C.G.}} + 3d^8(^3\mathrm{P})4p\,x\,^2\mathrm{D}_{\mathrm{C.G.}} = 126318 \quad (4)$$

From the previously determined values of the other parameters, we obtain

$$A = 39790 \quad (5)$$

Racah and Shadmi [17], found that the parameter D'', the difference between the weighted averages of the terms $3d^{n-2}4s^2$ and $3d^{n-1}4s$ in the second spectra of the iron group, was a linear function of the atomic number with a quadratic correction. By assuming that $D''[(d+s)^n p]$ in the first spectra obeys a similar relationship as a function of atomic number, a parabola is drawn to pass through the points determined by D''(Sc I), D''(Ti I) [9] and D''(Fe I) [13], and extrapolated for Co I, (Sc I and Fe I have experimental levels belonging to $3d^{n-2}4s^24p$, whereas in Ti I, eigenfunctions of some of the higher levels to which experimental levels are assigned contain considerable contributions of $3d4s^24p$ so that the standard deviation in A'' was only 234).

By substituting into eqs (8) and (9) of reference [12] the final values of the parameters for Fe I [13], and adding $-10G_1''-35G_3''$ to eq (9) (see ref. [12]) since the matrices of d^6s^2p, i.e., d^6p, on tape are those calculated by Ishidzu and Obi [18], who did not use the convention that for the case of an almost complete shell and an electron outside the shell, one subtracts from the energy matrix the interaction of the outer electron with the closed shell (see section 3, [19]), we obtain

$$D''(\mathrm{Fe}) = 36420 \quad (6)$$

By using the values of D''(Ti) and D''(Sc) given by eqs (11) and (14) of reference [10], with the above value for D''(Fe) to obtain the parabola through these three points, and extrapolating

$$D''(\mathrm{Co}) = 42410 \quad (7)$$

From eqs (8) and (9) of reference [12] and again adding $-10G_1''-35G_3''$ to eq (9), reference [12], we obtain

$$A'' = 87980 \quad (8)$$

2. Discussion and Results

Although the configuration $3d^64s^24p$ is very high, it markedly influences the results. In the calculations of $3d^84p+3d^74s4p$ the rms error was 209 cm^{-1}, whereas the inclusion of $3d^64s^24p$ reduced the rms error in the uniform treatment[4] to 164 cm^{-1}. Furthermore, the terms obtained from $(4F)+{}^1\mathrm{P}^5$ had very high deviations when considering only $3d^84p+3d^74s4p$. In particular, in $3d^84p+3d^74s4p$ the mean deviation of the term $^4\mathrm{F}(^1\mathrm{P})x\,^4\mathrm{D}$ was -643, whereas with the three configurations the mean deviation was only -50. This great improvement can be attributed to the fact that when $(3d+4s)^84p$ was considered G'_{ps} assumed a much higher value (7038 ± 56 cm^{-1} versus 6571 ± 62 cm^{-1}).

The experimental data for Co I are not sufficient to permit A'', the height of $3d^64s^24p$, to change freely. Thus in the final variation the value of A'' was held fixed at 85220 so that with the final values of the parameters, D'' should approximately equal its original value of 42410. The final parameters in the uniform treatment are given in table 1.

TABLE 1. *Parameters for* Co I $(3d+4s)^84p$ *(in units of* cm^{-1}*)*

Parameter	Initial Value	Final Value
A	39790	39264 ± 122
A'	50800	50677 ± 69
A''	87980	85220 (Fixed)
B	740	833 ± 8
B'	1000	956 ± 6
B''	1260	1079 (Arith. Progress.)
C	3660	3744 ± 63
C'	3770	3875 ± 18
C''	3880	4006 (Arith. Progress.)
$G'_{ds}=G$	1540	1607 ± 33
F_2	170	218 ± 10
F'_2	300	303 ± 7
F''_2	430	388 (Arith. Progress.)
G_1	200	196 ± 9
G'_1	240	199 ± 7
G''_1	280	202 (Arith. Progress.)
$G_3=G'_3=G''_3$	20	14 ± 2
G'_{ps}	7120	7038 ± 56
$\alpha=\alpha'=\alpha''$	85	71 ± 3
$H=H'$	85	72 ± 6
$J=J'$	1180	1245 ± 50
K	2460	2331 ± 55
K'	3352	3223 (Fixed Diff.)
$\zeta_d=\zeta'_d=\zeta''_d$	410	517 ± 17
$\zeta_p=\zeta'_p=\zeta''_p$	200	236 ± 53
rms error		164.2 cm^{-1}

The comparison of the experimental and calculated values of the levels and g-factors obtained from the final least-squares of the uniform treatment is given in table A of the Appendix. The calculated values, percentage compositions, and g-factors of all the 258 predicted levels of $3d^84p+3d^74s4p$ are given in table A. The 25 lowest levels of $3d^64s^24p$, based on $3d^6(^5\mathrm{D})$ are also quoted. However, the latter values as well as those higher levels of $3d^84p+3d^74s4p$ containing significant contributions of $3d^64s^24p$ must be considered as only approximate.

[4] The parameters A, A', G'_{ds}, and G'_{ps} are allowed to change freely. The parameters B, C, F_2, and G_1 are in arithmetic progression. The parameters G_3, α, ζ_d, and ζ_p are kept equal, and for the parameters of the interactions between configurations H' is kept equal to H, J' to J, G to G'_{ds}, and $K'=K+892$ (fixed difference).

[5] See the appendix of this paper for the theoretical term designations.

Of the unclassified odd levels only the levels 1°, 2°, 3°, 7°, 10°, 11°, 12°, 15°, and 23° were included. Besides the 28 unclassified odd levels, the following 13 levels were also neglected in the least-squares:

1. The level $3d^8(^3P)4p$: $y\,^2S_{1/2}$
2. The level $3d^8(^3P)4p$: $x\,^2P_{1/2}$
3. The level $3d^8(^3P)4p$: $w\,^2P_{1/2}$
4. The four levels of $3d^74s(^3D)4p$: $s\,^4D$
5. The level $t\,^2F_{7/2}$:
6. The level $s\,^2F_{5/2}$:
7. The four levels of $v\,^4F$

It is evident from table A that one of the terms $y\,^2S$ and $x\,^2S$ cannot be assigned to a corresponding theoretical term ^2S. The theoretical term ^2S, calculated at 48010, contains contributions with the same assignments as $y\,^2S$ and $x\,^2S$, and the experimental values of the two terms are very close. However, $x\,^2S$ was accepted since the correspondence between the calculated and experimental g-factors is better for x^2S than for y^2S.

The levels of the term $^4P(^3P)^2P$ are calculated at 48966 and 48453. Thus, when the experimental level $x\,^2P_{3/2}$ is assigned to $^4P(^3P)^2P_{3/2}$, the deviation is only -119. However, the level $x\,^2P_{1/2}$, which is given as uncertain in AEL, would yield a deviation of around -800, which is incompatible with the results for the other levels. Furthermore, the level $w\,^2S$, which cannot be assigned to a theoretical level ^2S, fits with a deviation of only -128 when assigned to $^4P(^3P)^2P_{1/2}$. Although the agreement between the experimental and calculated g-factors is not very good here, it should be noted that the experimental g-factor of 1.50 for $w\,^2S$ is given as uncertain in AEL.

The theoretical term ^2P following $^4P(^3P)^2P$ in height, is the term $^2P(^3P)^2P$ to which the levels of $v\,^2P$ correspond. Thus, the experimental levels of $w\,^2P$ cannot be assigned to a theoretical term ^2P. The level $w\,^2P_{3/2}$ is assigned to the previously vacant theoretical level $^2P(^3P)^2D_{3/2}$ yielding a deviation of only -60. The experimental g-factor of 1.099 corresponds to the calculated value of 0.991. The only theoretical level to which $w\,^2P_{1/2}$ could conceivably be assigned is $^2P(^3P)^2S$. However, as the resulting deviation would then be greater than 600, and since the agreement between the experimental g-factor of 1.365 and the calculated g-factor of 1.882 is also very poor, the level $w\,^2P_{1/2}$ was not inserted into the least-squares.

It is immediately evident from table A that the experimental levels of $s\,^4D$ have no corresponding vacant theoretical levels to which they could be assigned.

The levels of the term $A^2D(^3P)^2F$ are calculated at 52491 and 52784. Thus, it is evident that the experimental levels $t\,^2F_{5/2}$ and $s\,^2F_{7/2}$ should be grouped together and assigned to the theoretical term $A^2D(^3P)^2F$. The resulting deviations are 305 and 320 with excellent agreement between the experimental and calculated g-factors of both levels. The two remaining levels $t\,^2F_{7/2}$ and $s\,^2F_{5/2}$, both of which are given as uncertain in AEL, have no corresponding theoretical levels to which they could be assigned.

The experimental levels $v\,^4F$ cannot be assigned to a theoretical term ^4F. Conceivably, the levels $v\,^4F_{3/2,5/2,7/2}$ could be fitted to the theoretical levels $^4P(^1P)^4D_{3/2,5/2,7/2}$ and the level $v\,^4F_{9/2}$ could be assigned to $^2H(^3P)^2H_{9/2}$. Besides the danger of performing changes in term designations for such high levels, it is important to note that in the paper of Russell, King, and Moore [20], these levels are considered as doubtful.

The following table indicates how the nine unclassified odd levels were assigned:

TABLE 2. *Unclassified Odd Levels of* Co I

Level	Assignment	Deviation	Observed g-Factor	Calculated g-Factor
$1^\circ_{7/2}$	$^4P(^3P)^6P_{7/2}$	205	1.40	1.709
$2^\circ_{5/2}$	$^4P(^3P)^6P_{5/2}$	165	1.863	1.866
$3^\circ_{7/2}$	$^2G(^3P)^4H_{7/2}$	−1		0.680
$7^\circ_{5/2}$	$^2P(^3P)^2D_{5/2}$	−218		1.163
$10^\circ_{7/2}$	$A^2D(^3P)^4F_{7/2}$	58	1.260	1.257
$11^\circ_{5/2}$	$A^2D(^3P)^4F_{5/2}$	−7	1.079	1.107
$12^\circ_{3/2}$	$A^2D(^3P)^4F_{3/2}$	87	0.569	0.680
$15^\circ_{7/2}$	$^2H(^3P)^4H_{7/2}$	−48		0.690
$23^\circ_{3/2}$	$A^2D(^3P)^2P_{3/2}$	180	1.353	1.363

The unclassified levels 4°, 5°, 8°, 13°, 14°, 16°, 17°, 18°, 19°, 20°, 21°, and 22° have no corresponding theoretical levels to which they could be assigned.

For the level 6° the J-value is questioned. For J equal to 9/2 the level $6^\circ_{7/2?}$ could be assigned to either $^2H(^3P)^4I_{9/2}$ or $^2H(^3P)^4G_{9/2}$.

The level 9° probably should be assigned to $A^2D(^3P)^4F_{9/2}$ to complete with 10°, 11°, and 12° the term $A^2D(^3P)^4F$. However, unlike the levels 10°, 11°, and 12°, the level 9° is given as uncertain in AEL, and there is no experimental g-factor to confirm this assignment. Furthermore, the levels 10°, 11°, and 12° have combinations with levels of 9 even terms, whereas 9° is based on combinations with the levels of only 2 even terms [20]. Although the level 9° was not included in the least-squares calculations, it is inserted in parentheses adjacent to the calculated value of $A^2D(^3P)^4F_{9/2}$ in table A.

The following changes in assignment were performed:

1. AEL $3d^74s(a\,^5P)4pz\,^4P \longrightarrow (^3P)^4P$
2. $^2G(^3P)^2F \longleftrightarrow (^1D)^2F$
3. AEL $3d^8(^3P)4py\,^4P \longrightarrow {}^2P(^3P)^4P$
4. AEL $3d^74s(^3P)4px\,^4P_{3/2} \longrightarrow (^3P)^4S_{3/2}$
5. AEL $3d^8(^3P)4pv\,^4D_{3/2} \longrightarrow {}^4P(^3P)^4P_{3/2}$
6. AEL $3d^74s(^3P)4py\,^4S_{3/2} \longrightarrow (^3P)^4D_{3/2}$
7. AEL $3d^74s(^3P)4pv\,^2D_{3/2} \longrightarrow (^3P)^2D_{3/2}$
8. AEL $3d^8(^3P)4pw\,^2D_{3/2} \longrightarrow {}^4P(^3P)^2D_{3/2}$
9. AEL $3d^74s(^3P)4py\,^2P \longrightarrow (^3P)^2P$
10. AEL $3d^74s(^3P)4px\,^2S \longrightarrow (^3P)^2S$
11. AEL $v\,^2F_{5/2,7/2} \longrightarrow {}^2H(^3P)^4G_{5/2,7/2}$
12. AEL $3d^8(^3P)4px\,^4S \longrightarrow {}^2P(^3P)^4S$

13. AEL $3d^74s(^3P)4pt\ ^4D \longrightarrow A^2D(^3P)^4D$
14. AEL $w\ ^2S_{1/2} \longrightarrow {}^4P(^3P)^2P_{1/2}$
15. AEL $3d^8(^3P)4px\ ^2P_{3/2} \longrightarrow {}^4P(^3P)^2P_{3/2}$
16. AEL $3d^74s(^3P)4pw\ ^2P_{3/2} \longrightarrow {}^2P(^3P)^2D_{3/2}$
17. $^2H(^3P)^2G \longleftrightarrow (^1G)^2G$
18. AEL $3d^74s(^3H)4px\ ^2H_{9/2,11/2} \longrightarrow {}^2H(^3P)^4H_{9/2,11/2}$

Although in most changes of assignment the theoretical eigenfunctions are mixed strongly, in the changes 1, 2, 3, 9, 10, 12, 13, and 15 the compositions of the theoretical levels contain only small contributions of the experimental assignments (see table A).

The experimental g-factor of $y\ ^4S$ is 1.273. Since the theoretical g-factor of ^4S is 2.000, $y\ ^4S$ could be assigned to a theoretical term ^4S if the latter would have significant contributions of terms with low theoretical g-factors (such as $^4F_{3/2}$, $^2D_{3/2}$). However, this is not so in the present case and thus after several variations it was ascertained that the best agreement in the values and g-factors of the levels $^4P(^3P)^4P$, $(^3P)^4D$ and $(^3P)^4S$ is obtained after performing the changes 4, 5, and 6.

The grouping of the levels of $w\ ^2D$ and $v\ ^2D$ as given in AEL, is incongruous with the calculated values of the levels of $(^3P)w\ ^2D$ and $^4P(^3P)v\ ^2D$. Thus, the changes 7 and 8 were performed.

The levels of $v\ ^2F$ cannot be assigned to a theoretical term ^2F. However, when the two levels of $v\ ^2F$ are assigned to the two lowest levels of $^2H(^3P)^4G$, not only is there excellent agreement between the experimental and calculated values of the levels (for each level the deviation is only -24), but there is also a close correspondence between the experimental and calculated g-factors (the experimental g-factors of 0.619 and 1.173 correspond to the calculated values of 0.619 and 1.008, respectively). This change is indicated by 11.

The changes 14 and 16 were discussed previously.

The change 18 is similar to change 11. Although there is no corresponding theoretical term ^2H to which the levels of $x\ ^2H$ could be assigned, there is excellent agreement between the calculated and experimental values of the levels and g-factors when the levels $x\ ^2H$ are assigned to the theoretical levels $^2H(^3P)^4H_{9/2,11/2}$. To the theoretical level $^2H(^3P)^4H_{7/2}$, the level $15^9_{/2}$ (based on 10 combinations with even levels, [20]), is assigned to yield a deviation of only -48.

Below the limit of the experimental levels inserted, there are 21 theoretical levels with no corresponding experimental levels. The lowest of these is the level $^4P(^3P)^6S$ calculated at 34642.

With very few exceptions the agreement between the experimental and calculated g-factors is excellent.

Appendix

Table A. Observed and Calculated Levels and g-Factors

In the column "Name" the calculated designation of the term is given. Whenever the terms of the parent d^n have different seniorities these are denoted by the letters A and B, the lower calculated term being designated by A. The terms of d^7sp are denoted by $d^7v_1S_1L_1(sp^{1,3}P)SL$. The terms of d^8p are differentiated from those of d^6s^2p by using a star for the latter terms.

The entries in the columns "J", "Obs. Level (cm^{-1})", "Calc. Level (cm^{-1})", "Obs. g-Factor" and "Calc. g-Factor" are self-evident. In the column "Percentage", for each calculated level either the three highest contributions or all those contributions exceeding five percent are given.

Whenever the experimental and calculated term designations differ, the experimental designation is entered in the column "AEL" using the notation of C. E. Moore, [14]. In many instances the exchanges involve complete terms rather than isolated levels. Unless specified otherwise, the entries in the column "AEL" pertain to exchanges in terms.

The column "O–C" gives the difference between the observed and calculated values of the levels.

The entries are in increasing energy of the calculated levels.

TABLE A. *Observed and calculated levels of* Co I $(3d+4s)^84p$

Name	J	Percentage	AEL		Obs. Level (cm^{-1})	Calc. Level (cm^{-1})	O–C	Obs. g-Factor	Calc. g-Factor
			Config.	Desig.					
$^4F(^3P)^6F$	1/2	99	$3d^74s(a\ ^5F)4p$	$z\ ^6F$	25233	25240	−7	−0.622	−0.631
	3/2	95			25041	25061	−20	1.118	1.080
	5/2	$90+7\ ^4F(^3P)^6D$			24733	24775	−42	1.336	1.328
	7/2	$84+12\ ^4F(^3P)^6D$			24326	24397	−71	1.436	1.412
	9/2	$78+18\ ^4F(^3P)^6D$			23856	23961	−105	1.481	1.452
	11/2	97			23612	23635	−23	1.466	1.451
$^4F(^3P)^6D$	1/2	94	$3d^74s(a\ ^5F)4p$	$z\ ^6D$	26250	26404	−154	3.286	3.297
	3/2	91			26063	26210	−147	1.812	1.810
	5/2	$87+6\ ^4F(^3P)^6F$			25740	25881	−141	1.612	1.615
	7/2	$83+11\ ^4F(^3P)^6F$			25269	25407	−138	1.550	1.555
	9/2	$78+17\ ^4F(^3P)^6F$			24628	24770	−142	1.569	1.529

TABLE A. *Observed and calculated levels of* Co I $(3d+4s)^8 4p$—Continued

Name	J	Percentage	AEL		Obs. Level (cm^{-1})	Calc. Level (cm^{-1})	O−C	Obs. g-Factor	Calc. g-Factor
			Config.	Desig.					
$^4F(^3P)^6G$	3/2	97	$3d^74s(a\,^5F)4p$	$z\,^6G$	26598	26425	173	0.006	0.042
	5/2	95			26450	26273	177	0.876	0.882
	7/2	94			26232	26049	183	1.150	1.156
	9/2	94			25938	25749	189	1.281	1.278
	11/2	96			25569	25375	194	1.354	1.344
	13/2	100			25139	24941	198	1.40	1.384
$^4F(^3P)^4F$	3/2	$85+13(^3F)^4F$	$3d^74s(a\,^5F)4p$	$z\,^4F$	29563	29561	2	0.410	0.408
	5/2	$82+13(^3F)^4F$			29216	29217	−1	1.033	1.026
	7/2	$80+13(^3F)^4F$			28777	28779	−2	1.247	1.234
	9/2	$82+15(^3F)\,^4F$			28346	28328	18	1.330	1.331
$^4F(^3P)^4G$	5/2	94	$3d^74s(a\,^5F)4p$	$z\,^4G$	30103	30044	59	0.577	0.583
	7/2	91			29735	29680	55	0.995	0.991
	9/2	90			29270	29219	51	1.175	1.175
	11/2	95			28845	28765	80	1.276	1.273
$^4F(^3P)^4D$	1/2	$65+31(^3F)^4D$	$3d^74s(a\,^5F)4p$	$z\,^4D$	30743	30790	−47	−0.006	0.003
	3/2	$62+33(^3F)^4D$			30444	30482	−38	1.192	1.192
	5/2	$57+36(^3F)^4D$			29949	29969	−20	1.359	1.362
	7/2	$53+42(^3F)\,^4D$			29295	29289	6	1.425	1.425
$^4F(^3P)^2G$	7/2	$41+29(^3F)^4F+11(^3F)^2G$	$3d^74s(b\,^3F)4p$	$z\,^2G$	32733	32850	−117	0.899	0.990
	9/2	$47+29(^3F)^4G+13(^3F)^4F$			31700	31822	−122	1.126	1.121
$^4F(^3P)^2F$	5/2	$71+26(^3F)^2F$	$3d^74s(b\,^3F)4p$	$z\,^2F$	32782	32962	−180	0.870	0.863
	7/2	$66+28(^3F)^2F$			31871	32061	−190	1.177	1.153
$(^3F)^4D$	1/2	$59+36\,^4F(^1P)^4D$			33449	33533	−84	0.012	0.003
	3/2	$56+37\,^4F(^1P)^4D$			33151	33209	−58	1.195	1.193
	5/2	$51+41\,^4F(^1P)^4D$			32654	32680	−26	1.366	1.364
	7/2	$46+45\,^4F(^1P)^4D$			32028	31982	44	1.395	1.416
$(^3F)^4G$	5/2	$52+30(^3F)^4F$			33674	33608	66	0.704	0.777
	7/2	$34+31(^3F)^2G+11(^3F)^4F$			33173	33185	−12	1.039	1.040
	9/2	$53+28(^3F)^2G+8\,^4F(^3P)^2G$			32465	32414	51	1.154	1.171
	11/2	94			32431	32296	135	1.287	1.273
$^4F(^3P)^2D$	3/2	$53+37(^3F)^2D$	$3d^74s(b\,^3F)4p$	$z\,^2D$	34352	34423	−71	0.787	0.781
	5/2	$53+42(^3F)^2D$			33463	33497	−34	1.186	1.198
$(^3F)^4F$	3/2	$67+24\,^4F(^1P)^4F$			34196	34205	−9	0.430	0.430
	5/2	$38+42(^3F)^4G$			33946	33937	9	0.900	0.824
	7/2	$25+33(^3F)^4G+24\,^4F(^3P)^2G$			33467	33445	22	1.155	1.055
	9/2	$51+22\,^4F(^1P)^4F+14\,^4F(^3P)^2G$			32842	32791	51	1.313	1.278
$(^3F)^2G$	7/2	$50+21(^3F)^4G+21\,^4F(^3P)^2G$			34134	34179	−45	0.917	0.921
	9/2	$56+27\,^4F(^3P)^2G+11(^3F)^4G$			33440	33420	20	1.165	1.159
$^4P(^3P)^6S$	5/2	99				34642			1.998
$(^3F)^2F$	5/2	$53+18(^3F)^2D+16\,^4F(^3P)^2F$			36330	36250	80	0.892	0.948
	7/2	$61+25\,^4F(^3P)^2F$			35451	35236	215	1.145	1.144
$(^3F)^2D$	3/2	$53+40\,^4F(^3P)^2D$			36875	36923	−48	0.794	0.805
	5/2	$35+36\,^4F(^3P)^2D$			36092	36049	43	1.186	1.118

TABLE A. *Observed and calculated levels of* Co I $(3d+4s)^8 4p$ – Continued

Name	J	Percentage	AEL		Obs. Level (cm^{-1})	Calc. Level (cm^{-1})	O–C	Obs. g-Factor	Calc. g-Factor
			Config.	Desig.					
$^4P(^3P)^6D$	1/2	94				39184			3.314
	3/2	92				39093			1.846
	5/2	92				38991			1.655
	7/2	92				38902			1.583
	9/2	96				38847			1.555
$^4P(^3P)^4S$	3/2	$74+10(^3P)^4S$	$3d^74s(a\,^5P)4p$	$z\,^4S$	40622	40240	382	2.017	1.918
$^4F(^1P)^4D$	1/2	$62+24(^3P)^4D$	$3d^74s(b\,^3F)4p$	$x\,^4D$	41102	41141	−39	0.026	0.012
	3/2	$62+23(^3P)^4D$			40828	40863	−35	1.240	1.204
	5/2	$63+21(^3P)^4D$			40346	40395	−49	1.370	1.369
	7/2	$65+18(^3P)^4D$			39649	39726	−77	1.428	1.428
$^4P(^3P)^6P$	3/2	$90+6\,^4P(^3P)^4S$				40992			2.291
	5/2	93		2^o	41105	40940	165	1.863	1.866
	7/2	97		1^o	41041	40836	205	1.40	1.709
$^4F(^1P)^4F$	3/2	$61+27\,^2G(^3P)^4F$	$3d^74s(b\,^3F)4p$	$x\,^4F$	42797	42396	401	0.406	0.408
	5/2	$59+24\,^2G(^3P)^4F$			42434	42046	388	1.024	1.052
	7/2	$63+23\,^2G(^3P)^4F$			41918	41571	347	1.248	1.234
	9/2	$66+19\,^2G(^3P)^4F$			41226	40917	309	1.319	1.330
$(^3P)^4P$	1/2	$66+14\,^2P(^3P)^4P+11\,^4P(^3P)^4P$	$3d^74s(a\,^5P)4p$	$z\,^4P$	41970	42048	−78	2.51	2.520
	3/2	$64+12\,^4P(^3P)^4P+9\,^2P(^3P)^4P$			41983	41972	11	1.732	1.665
	5/2	$65+12\,^4P(^3P)^4P+9\,^2P(^3P)^4P$			41969	41932	37	1.627	1.548
$^4F(^1P)^4G$	5/2	93	$3d^74s(b\,^3F)4p$	$x\,^4G$	43200	43350	−150	0.649	0.581
	7/2	92			42811	42962	−151	1.004	0.988
	9/2	93			42269	42439	−170	1.169	1.174
	11/2	95			41529	41747	−218	1.291	1.272
$^2G(^3P)^4H$	7/2	95		3^o	42988	42989	−1		0.680
	9/2	90				42775			0.977
	11/2	92				42632			1.135
	13/2	98				42565			1.229
$(^1D)^2P$	1/2	$42+25(^3P)^2P+7\,^2P(^3P)^2P$			43130	43084	46	0.727	0.846
	3/2	$31+23(^1D)^2D+22\,^4P(^3P)^4D$			43538	43544	−6	1.120	1.175
$^4P(^3P)^4D$	1/2	$75+9\,^2P(^3P)^4D$	$3d^74s(a\,^5P)4p$	$w\,^4D$	43436	43444	−8	0.169	0.101
	3/2	$58+9(^1D)^2D$			43264	43298	−34	1.191	1.186
	5/2	$46+28(^1D)^2F$			43243	43218	25	1.101	1.168
	7/2	$88+3(^1D)^2F$			43399	43346	53	1.334	1.417
$(^1D)^2F$	5/2	$37+36\,^4P(^3P)^4D+10\,^2G(^3P)^2F$	$3d^74s(^3G)4p$	$x\,^2F$	43426	43371	55	1.119	1.108
	7/2	$45+20\,^2G(^3P)^4F+16\,^2G(^3P)^2F$			43555	43602	−47	1.229	1.174
$(^1D)^2D$	3/2	$40+33(^1D)^2P+5(^3P)^2P$			43911	43957	−46	1.127	1.070
	5/2	$52+20\,^2G(^3P)^4F$			43922	44113	−191	1.230	1.147
$^4P(^3P)^2S$	1/2	$61+21(^3P)^2S$	$3d^74s(^3P)4p$	$z\,^2S$	44455	44185	270	2.10	1.908
$^2G(^3P)^4F$	3/2	$68+18\,^4F(^1P)^4F+7(^3F)^4F$	$3d^74s(^3G)4p$	$w\,^4F$	44556	44745	−189	0.415	0.412
	5/2	$29+23\,^2G(^3P)^4G+23(^1D)^2D$			44202	44333	−131	0.950	0.970
	7/2	$39+23(^1D)^2F+11\,^2G(^3P)^4G$			43848	43979	−131	1.197	1.183
	9/2	$71+15\,^4F(^1P)^4F+5(^3F)^4F$			43295	43523	−228	1.295	1.318

TABLE A. *Observed and calculated levels of* Co I $(3d+4s)^8 4p$—Continued

Name	J	Percentage	AEL		Obs. Level (cm^{-1})	Calc. Level (cm^{-1})	O−C	Obs. g-Factor	Calc. g-Factor
			Config.	Desig.					
$^2G(^3P)^4G$	5/2	$69+19^2G(^3P)^4F$	$3d^74s(^3G)4p$	$w\,^4G$	44568	44561	7	0.676	0.703
	7/2	$77+11^2G(^3P)^4F$			44394	44343	51	1.004	1.013
	9/2	$85+5^2G(^3P)^4F$			44183	44100	83	1.163	1.169
	11/2	93			43952:	43851	101	1.279	1.266
$^2P(^3P)^4P$	1/2	$44+40^4P(^1P)^4P$	$3d^8(^3P)4p$	$y\,^4P$	44858	45215	−357	2.371	2.523
	3/2	$37+40^4P(^1P)^4P$			44658	44948	−290	1.674	1.680
	5/2	$33+42^4P(^1P)^4P$			44480	44708	−228	1.557	1.565
$^2G(^3P)^2H$	9/2	87	$3d^74s(^3G)4p$	$x\,^2H$	45111	44988	123	0.897	0.907
	11/2	90			45540	45380	160	1.097	1.091
$(^3P)^2D$	3/2	$72+7(^1D)^2D+6^4P(^3P)^2D$	$3d^74s(^3P)4p$	$v\,^2D$	46186	46017	169	1.218	0.853
	5/2	$70+8^4P(^3P)^2D$	$3d^8(^3P)4p$	$w\,^2D$	45688	45397	291	1.219	1.170
$(^3P)^4S$	3/2	$32+25^4P(^3P)^4S+13(^3P)^2P$	$3d^74s(^3P)4p$	$x\,^4P$	45905	45906	−1	1.674	1.794
$^4P(^3P)^4P$	1/2	$44+22(^3P)^4P+15^2P(^3P)^4P$	$3d^74s(^3P)4p$	$x\,^4P$	45957	45864	93	2.522	2.613
	3/2	$30+18(^3P)^4P+16^2P(^3P)^4P$	$3d^8(^3P)4p$	$v\,^4D$	46260	46151	109	1.508	1.714
	5/2	$30+24^2P(^3P)^4P+16(^3P)^4P$	$3d^74s(^3P)4p$	$x\,^4P$	46003	46168	−165	1.543	1.566
$^2G(^3P)^2G$	7/2	$79+10^2H(^3P)^2G$	$3d^74s(^3G)4p$	$x\,^2G$	45767	45931	−164	0.898	0.896
	9/2	$80+10^2H(^3P)^2G$			46032	46211	−179	1.131	1.113
$(^3P)^4D$	1/2	$27+21A^2D(^3P)^4D+17^2P(^3P)^4D$			46502	46489	13	0.161	0.149
	3/2	$14+16(^3P)^2P+12(^1D)^2P$	$3d^74s(^3P)4p$	$y\,^4S$	46563	46654	−91	1.273	1.200
	5/2	$28+25^2P(^3P)^4D+11^4F(^1P)^4D$			46330	46485	−155	1.365	1.361
	7/2	$44+22^2P(^3P)^4D+11^4F(^1P)^4D$			45971	46229	−258	1.424	1.406
$^4P(^3P)^2D$	3/2	$61+14^2P(^3P)^2D+7(^3P)^4D$	$3d^8(^3P)4p$	$w\,^2D$	46455	46803	−348	0.869	0.893
	5/2	$45+20^2G(^3P)^2F+9(^3P)^4D$	$3d^74s(^3P)4p$	$v\,^2D$	46672	46695	−23	1.233	1.130
$^2G(^3P)^2F$	5/2	$33+22^4P(^3P)^2D+14(^1D)^2F$	$3d^8(^1D)4p$	$w\,^2F$	47129	46944	185	0.858	0.971
	7/2	$36+31^2P(^3P)^4D+11(^1D)^2F$			47225	47062	163	1.229	1.310
$(^3P)^2P$	1/2	$46+30(^1D)^2P+10^4P(^3P)^2P$	$3d^74s(^3P)4p$	$y\,^2P$	47091	47215	−124	0.656	0.671
	3/2	$27+12(^1D)^2P+9(^3P)^4D$			46685	46471	214	1.352	1.394
$^2P(^3P)^4D$	1/2	$37+21(^3P)^2S+20(^3P)^4D$		$u\,^4D$	47905	48010	−105	0.016	0.691
	3/2	$47+18(^3P)^4D+10A^2D(^3P)^4F$			47612	47554	58	1.122	1.105
	5/2	$45+13^4P(^3P)^2D+11(^3P)^4D$			47394	47365	29	1.324	1.319
	7/2	$26+23A^2D(^3P)^4D+21^2G(^3P)^2F$			46873	46806	67	1.352	1.394
$^2H(^3P)^4I$	9/2	94				48081			0.739
	11/2	94				47874			0.968
	13/2	97				47717			1.108
	15/2	100				47613			1.200
$(^3P)^2S$	1/2	$35+26^2P(^3P)^4D+15^4P(^3P)^2S$	$3d^74s(^3P)4p$	$x\,^2S$	48026	48010	16	1.699	1.193
$^2H(^3P)^4G$	5/2	$81+7^2G(^3P)^2F$		$v\,^2F$	48616:	48640	−24	0.619	0.619
	7/2	$84+4^2G(^3P)^2F$		$v\,^2F$	48317	48341	−24	1.173	1.008
	9/2	92				47996			1.171
	11/2	95				47626			1.272

TABLE A. *Observed and calculated levels of* Co I $(3d+4s)^8 4p$—Continued

Name	J	Percentage	AEL		Obs. Level (cm^{-1})	Calc. Level (cm^{-1})	O−C	Obs. g-Factor	Calc. g-Factor
			Config.	Desig.					
$A^2D(^3P)^4D$	1/2	$52+16(^3P)^4D$	$3d^74s(^3P)4p$	$t\,^4D$	48572	48893	−321	0.452	0.198
	3/2	$21+22^2P(^3P)^4S+12(^3P)^4D$			48546	48742	−196	1.050	1.254
	5/2	$52+19(^3P)^4D$			48444	48796	−352	1.340	1.339
	7/2	$51+18(^3P)^4D$			48217	48573	−356	1.211	1.386
$^4P(^3P)^2P$	1/2	$69+12^2P(^3P)^2S+10(^3P)^2P$		$w\,^2S$	48838	48966	−128	1.50:	0.840
	3/2	$40+15^2P(^3P)^4S+11A^2D(^3P)^4D$	$3d^8(^3P)4p$	$x\,^2P$	48334	48453	−119	1.436	1.369
$^2P(^3P)^4S$	3/2	$48+26A^2D(^3P)^4D+8(^3P)^4D$	$3d^8(^3P)4p$	$x\,^4S$	48754	48946	−192	1.728	1.623
$^2P(^3P)^2D$	3/2	$29+34^4P(^3P)^2P+24A^2D(^3P)^4F$	$3d^74s(^3P)4p$	$w\,^2P$	49025	49085	−60	1.099	0.991
	5/2	$32+34A^2D(^3P)^4F+10^2P(^3P)^4D$		7^0	48829	49047	−218		1.163
$A^2D(^3P)^4F$	3/2	$50+15^2P(^3P)^2D+11A^2D(^3P)^2D$		12^0	50105	50018	87	0.569	0.680
	5/2	$43+24^2P(^3P)^2D$		11^0	49847	49854	−7	1.079	1.107
	7/2	$75+6^2P(^3P)^4D$		10^0	49484	49426	58	1.260	1.257
	9/2	98		9^0	(49198:)	49108	(90)		1.333
$^2H(^3P)^2I$	11/2	90				50080			0.936
	13/2	$67+31^2H(^3P)^4H$				50435			1.126
$(^1G)^2H$	9/2	$81+9^2H(^3P)^2H$			50211	50124	87	0.899	0.915
	11/2	$69+17^2H(^3P)^2H$			50376	50389	−13	1.091	1.085
$^2P(^3P)^2S$	1/2	$68+13^4P(^3P)^2P$				50417			1.882
$(^1G)^2G$	7/2	$38+37^2H(^3P)^2G$	$3d^74s(^3H)4p$	$w\,^2G$	50611	50556	55	0.82	0.908
	9/2	$40+38^2H(^3P)^2G$			50593	50616	−23	1.10	1.095
$(^1G)^2F$	5/2	$57+17A^2D(^3P)^2F$			50712	50771	−59	0.905	0.909
	7/2	$60+12A^2D(^3P)^2F+8^2G(^3P)^2F$			50579	50693	−114	1.125	1.120
$^2P(^3P)^2P$	1/2	$71+13A^2D(^3P)^4D$		$v\,^2P$	50945	50972	−27	0.732	0.707
	3/2	$53+15A^2D(^3P)^4D$			50925	50861	64	1.340	1.331
$^2H(^3P)^4H$	7/2	$89+5(^1G)^2G$		15^0	51185	51233	−48		0.690
	9/2	$86+5(^1G)^2G$	$3d^74s(^3H)4p$	$x\,^2H$	50903	51048	−145	0.941	0.982
	11/2	$86+11(^1G)^2H$	$3d^74s(^3H)4p$	$x\,^2H$	50703	50828	−125	1.110	1.128
	13/2	$68+30^2H(^3P)^2I$				50573			1.184
$A^2D(^3P)^4P$	1/2	$66+12^2P(^3P)^4P$	$3d^74s(^3D)4p$	$w\,^4P$	52355	52180	175	2.304	2.414
	3/2	$57+17^2P(^3P)^2P$			52014	51784	230	1.616	1.617
	5/2	$73+13^2P(^3P)^2P$			51160	50950	210	1.578	1.564
$A^2D(^3P)^2F$	5/2	$58+17(^1G)^2F$		$t\,^2F$	52796	52491	305	0.883	0.897
	7/2	$75+11^2G(^3P)^2F$		$s\,^2F$	53104	52784	320	1.136	1.149
$A^2D(^3P)^2D$	3/2	$51+21^2P(^3P)^2D$		$u\,^2D$	53075	52884	191	0.823	0.816
	5/2	$49+18^2P(^3P)^2D$			53196	53964	232	1.206	1.180
$^2H(^3P)^2G$	7/2	$44+30(^1G)^2G+22^2G(^3P)^2G$	$3d^8(^1G)4p$	$v\,^2G$	53374	53288	86	0.888	0.889
	9/2	$44+28(^1G)^2G+24^2G(^3P)^2G$			53276	53214	62	1.124	1.111
$A^2D(^3P)^2P$	1/2	93				53764			0.750
	3/2	87		23^0	54165	53985	180	1.353	1.363

TABLE A. *Observed and calculated levels of* Co I $(3d+4s)^8 4p$ – Continued

Name	J	Percentage	AEL		Obs. Level (cm^{-1})	Calc. Level (cm^{-1})	O–C	Obs. g-Factor	Calc. g-Factor
			Config.	Desig.					
$^2H(^3P)^2H$	9/2	$91+6(^1G)^2H$				54608			0.910
	11/2	$88+6(^1G)^2H$				54821			1.092
$^4P(^1P)^4D$	1/2	$82+10(^5D)^4D^*$				55223			0.094
	3/2	$80+10(^5D)^4D^*$				55057			1.224
	5/2	$81+11(^5D)^4D^*$				54867			1.377
	7/2	$85+12(^5D)^4D^*$				54693			1.427
$^4P(^1P)^4S$	3/2	$58+27(^3P)^4S$				55395			1.961
$^4P(^1P)^4P$	1/2	$70+19(^5D)^4P^*$				55825			2.561
	3/2	$61+17(^5D)^4P^*$				55792			1.729
	5/2	$70+21(^5D)^4P^*$				55421			1.587
$^2G(^1P)^2H$	9/2	93				57733			0.914
	11/2	91				57103			1.088
$(^5D)^6D^*$	1/2	99				58371			3.328
	3/2	99				58244			1.864
	5/2	98				58035			1.655
	7/2	97				57754			1.585
	9/2	99				57426			1.554
$^2G(^1P)^2F$	5/2	$84+4(^1D)^2F$				58878			0.859
	7/2	$80+4(^1D)^2F$				58189			1.138
$^2G(^1P)^2G$	7/2	$74+11(^1G)^2G$				59402			0.892
	9/2	$68+13^2H(^1P)^2G$				58698			1.105
$^2P(^1P)^2P$	1/2	$65+17A^2D(^1P)^2P$				60923			0.776
	3/2	$65+13A^2D(^1P)^2D$				60947			1.231
$(^5D)^6F^*$	1/2	99				61723			−0.659
	3/2	98				61647			1.066
	5/2	98				61517			1.312
	7/2	97				61332			1.394
	9/2	96				61091			1.432
	11/2	100				60812			1.455
$^2P(^1P)^2D$	3/2	$83+6^2P(^1P)^2P$				61733			0.854
	5/2	$79+8A^2D(^1P)^2F$				61014			1.175
$^2F(^3P)^4G$	5/2	94				61635			0.579
	7/2	93				61764			0.990
	9/2	94				61941			1.175
	11/2	95				62174			1.270
$^2F(^3P)^4F$	3/2	94				62192			0.416
	5/2	91				62335			1.035
	7/2	95				62483			1.232
	9/2	$60+27^2H(^1P)^2G$				62848			1.250
$^2H(^1P)^2I$	11/2	96				62729			0.929
	13/2	98				62101			1.077

TABLE A. *Observed and calculated levels of* Co I $(3d+4s)^8 4p$ – Continued

Name	J	Percentage	AEL		Obs. Level (cm^{-1})	Calc. Level (cm^{-1})	O–C	Obs. g-Factor	Calc. g-Factor
			Config.	Desig.					
$^2F(^3P)^4D$	1/2	93				62496			0.002
	3/2	92				62487			1.189
	5/2	89				62485			1.359
	7/2	87				62484			1.436
$^2P(^1P)^2S$	1/2	$70+14\,^2P(^3P)^2P$				62732			1.816
$A^2D(^1P)^2D$	3/2	$69+10\,^2P(^1P)^2P$				63531			0.862
	5/2	$78+8\,^2F(^3P)^2D$				62568			1.186
$^2H(^1P)^2G$	7/2	$60+11(^5D)^4F^*$				63467			0.949
	9/2	$36+31\,^2F(^3P)^4F+17(^5D)^4F^*$				62864			1.221
$(^5D)^6P^*$	3/2	97				63870			2.363
	5/2	98				63447			1.878
	7/2	93				62815			1.697
$A^2D(^1P)^2F$	5/2	$66+16\,^2F(^3P)^2D$				64160			0.970
	7/2	89				63306			1.141
$(^5D)^4F^*$	3/2	93				63975			0.427
	5/2	89				63699			1.054
	7/2	$77+8\,^2H(^1P)^2G$				63330			1.209
	9/2	$77+10\,^2H(^1P)^2G$				62810			1.305
$^2F(^3P)^2D$	3/2	$68+12(^5D)^4D^*$				64398			0.857
	5/2	$49+14(^5D)^4D^*$				64410			1.175
$(^5D)^4D^*$	1/2	$73+9\,^4P(^1P)^4D$				64715			0.055
	3/2	$61+13\,^2F(^3P)^2D$				64573			1.131
	5/2	$53+24\,^2F(^3P)^2D$				64226			1.312
	7/2	$68+7(^5D)^4F^*$				63916			1.415
$^2H(^1P)^2H$	9/2	$78+13\,^2F(^1P)^2G$				64952			0.937
	11/2	90				64391			1.091
$^2F(^3P)^2G$	7/2	$85+10\,^2H(^1P)^2G$				64832			0.890
	9/2	$78+14\,^2H(^1P)^2H$				64886			1.088
$A^2D(^1P)^2P$	1/2	$66+12\,^2P(^3P)^2P$				65449			0.694
	3/2	78				64135			1.347
$^2F(^3P)^2F$	5/2	96				66808			0.859
	7/2	96				66717			1.143
$(^3D)^4P^*$	1/2	$78+20\,^4P(^1P)^4P$				68813			2.662
	3/2	$78+20\,^4P(^1P)^4P$				68540			1.732
	5/2	$77+21\,^4P(^1P)^4P$				68061			1.599
$^2F(^1P)^2G$	7/2	$87+9(^3H)^2G^*$				75095			0.890
	9/2	$87+9(^3H)^2G^*$				75389			1.111
$^2F(^1P)^2D$	3/2	88				75783			0.801
	5/2	$73+15\,^2F(^3P)^2F$				75894			1.143

TABLE A. *Observed and calculated levels of* Co I $(3d+4s)^8 4p$ – Continued

Name	J	Percentage	AEL		Obs. Level (cm^{-1})	Calc. Level (cm^{-1})	O–C	Obs. g-Factor	Calc. g-Factor
			Config.	Desig.					
$^2F(^1P)^2F$	5/2	$75+15^2F(^1P)^2D$				76244			0.915
	7/2	$90+6(^3G)^2F^*$				76512			1.142
$(^1S)^2P$	1/2	$89+9A^2D(^1P)^2D$				76561			0.667
	3/2	$88+10A^2D(^1P)^2D$				76836			1.333
$B^2D(^3P)^4P$	1/2	97				79901			2.664
	3/2	95				79919			1.733
	5/2	96				79977			1.599
$B^2D(^3P)^4F$	3/2	95				80762			0.401
	5/2	95				80885			1.028
	7/2	94				81057			1.237
	9/2	93				81278			1.332
$B^2D(^3P)^2P$	1/2	$65+17B^2D(^3P)^4D+9(A^3P)^4D^*$				84473			0.477
	3/2	$79+12B^2D(^3P)^4D$				84186			1.298
$B^2D(^3P)^2F$	5/2	$75+13B^2D(^3P)^4D$				84381			0.945
	7/2	$75+19B^2D(^3P)^4D$				84408			1.199
$B^2D(^3P)^4D$	1/2	$71+23B^2D(^3P)^2P$				84201			0.171
	3/2	$73+10B^2D(^3P)^2P$				84393			1.183
	5/2	$78+12B^2D(^3P)^2F$				84538			1.297
	7/2	$45+18B^2D(^3P)^2F$				85100			1.387
$B^2D(^3P)^2D$	3/2	96				86758			0.803
	5/2	96				86672			1.200
$B^2D(^1P)^2P$	1/2	$56+32(^3D)^2P^*$				93582			0.669
	3/2	$55+35(^3D)^2P^*$				93960			1.332
$B^2D(^1P)^2F$	5/2	$41+23(^3G)^2F^*+20(^3D)^2F^*$				96929			0.868
	7/2	$42+22(^3D)^2F^*+20(^3G)^2F^*$				96971			1.142
$B^2D(^1P)^2D$	3/2	$49+41(^3D)^2D^*$				98049			0.805
	5/2	$51+36(^3D)^2D^*$				98457			1.199

References

[1] Roth, C., J. Res. Nat. Bur. Stand. (U.S.), **72A** (Phys. and Chem.), No. 5, 505 (1968).
[2] Roth, C., J. Res. Nat. Bur. Stand. (U.S.), **73A** (Phys. and Chem.), No. 2, 125 (1969).
[3] Roth, C., J. Res. Nat. Bur. Stand. (U.S.), **73A** (Phys. and Chem.), No. 2, 159 (1969).
[4] Roth, C., J. Res. Nat. Bur. Stand. (U.S.), **73A** (Phys. and Chem.), No. 6, 599 (1969).
[5] Rohrlich, F., Phys. Rev. **74,** 1381 (1948).
[6] Smith, G., and Siddall, J., J. Opt. Soc. Am. **59,** 419 (1969).
[7] Martin, W., and Sugar, J., J. Opt. Soc. Am. **59,** 1266 (1969).
[8] Wilson, M., J. Phys. B, Ser. 2, **2,** 524 (1969).
[9] Roth, C., J. Res. Nat. Bur. Stand. (U.S.), **73A** (Phys. and Chem.), No. 5, 497 (1969).
[10] Roth, C., J. Res. Nat. Bur. Stand. (U.S.), **74A** (Phys. and Chem.), No. 2, 141 (1970).
[11] Roth, C., J. Res. Nat. Bur. Stand. (U.S.), **74A** (Phys. and Chem.), No. 2, 157 (1970).
[12] Roth, C., J. Res. Nat. Bur. Stand. (U.S.), **74A** (Phys. and Chem.), No. 4, 507 (1970).
[13] Roth, C., J. Res. Nat. Bur. Stand. (U.S.), **74A** (Phys. and Chem.), No. 2, 181 (1970).
[14] Moore, C. E., Atomic energy levels, Nat. Bur. Stand. (U.S.), Circ. 467, Vol. II (1952). Referred to as AEL.
[15] Roth, C., J. Math. Phys. **9,** No. 5, 686 (1968).
[16 Racah, G., Phys. Rev. **62,** 438 (1942).
[17] Racah, G., and Shadmi, Y., Bull. Res. Counc. Israel **8F,** No. 1, 15 (1959).
[18] Ishidzu, T., and Obi, S., J. Phys. Soc. Japan **5,** No. 3, 124 (1950).
[19] Roth, C., J. Math. Phys. **10,** No. 6, 1038 (1969).
[20] Russell, H. N., King, R. B., and Moore, C. E., Phys. Rev. **58,** 407 (1940).

(Paper 74A5–635)

JOURNAL OF RESEARCH of the National Bureau of Standards—A. Physics and Chemistry
Vol. 74A, No. 5, September–October 1970

Odd Configurations in Neutral Nickel (Ni I)*

Charles Roth**

(May 28, 1970)

Experimental levels of the configurations $3d^94p$, $3d^84s4p$ and $3d^95p$ of Ni I were compared with corresponding calculated values. The electrostatic interactions between the configurations $(3d+4s)^94p$ as well as between $3d^84s4p$ and $3d^95p$ were considered explicitly.

For the configurations $(3d+4s)^94p$, 71 experimental levels were fitted by means of 17 free parameters to yield an rms error of 131 cm^{-1}. On fitting 83 levels of the configurations $3d^94p+3d^84s4p+3d^95p$ by means of 25 free parameters an rms error of 147 cm^{-1} was obtained.

Key words: Energy levels; g-factors; interactions between configurations; nickel; $(3d+4s)^94p$; $3d^94p+3d^84s4p+3d^95p$.

1. The Configurations $(3d+4s)^94p$

The configurations $(d+s)^9p$ comprise 92 terms splitting into 212 levels. In AEL [1][1], 27 terms splitting into 66 levels are assigned to the configurations $3d^94p+3d^84s4p$, and in addition, there are 6 unclassified odd levels. As in Co I [7], only the initial values for the parameters[2] B', C', and α', were obtained by linear extrapolation from the results of Sc I–Co I[2–7]. Then,

$$\begin{aligned} B' &= 1040 \\ C' &= 4140 \\ \alpha' &= \ \ 84 \end{aligned} \tag{1}$$

The initial values of the other parameters were taken as the final values of Co I [7].

The initial value for the height of the configuration $3d^84s4p$ can be obtained either from the electrostatic matrices of ^5F or ^5G (they only differ by $4F_2'$). Then from ^5G, we have [1], [8]

$$^5G_{C.G.} = A' - 8B' - 2G'_{ds} - F_2' - G'_{ps} + 12\alpha' = 27900 \tag{2}$$

Hence, from the values of the previously determined parameters

$$A' = 45670 \tag{3}$$

The height of the configuration $3d^94p$ was obtained from the electrostatic matrix of $3d^94p\,^3P$, since the terms ^3P of $3d^84s4p$ are sufficiently high that the interaction with them is not strong.

Then, since

$$3d^94pz\,^3P_{C.G.} = A - 7F_2 = 29330 \tag{4}$$

initially,

$$A = 30870 \tag{5}$$

It should be noted that the above value of A contains the contribution 6α, since the constant matrix of α for d^9p was not put on tape.

The parabola used to find D″ (Co I) [7], extrapolated further gives

$$D''[\text{Ni I}] = 48300 \tag{6}$$

By using the values of B'' and C'' from V I to Co I [3–7] in order to obtain the best straight lines for these parameters, and extrapolating to Ni I

$$\begin{aligned} B'' &= 1190 \\ C'' &= 4190 \end{aligned} \tag{7}$$

Then, from eqs (8) and (9), [5]

$$A'' = 85680 \tag{8}$$

The final values of the parameters obtained in the uniform treatment[3] are given in table 1.

The final value of A'' was fixed at 85060, so that with the new values of the parameters, D'' (Ni I) should approximately equal the original value of 48300.

*An invited paper.

**Present address: Department of Mathematics, McGill University, Montreal 110, Canada.

[1] Figures in brackets indicate the literature references at the end of this paper.

[2] Unprimed parameters refer to the configuration $3d^94p$, primed parameters to $3d^84s4p$, and doubly primed to $3d^74s^24p$.

The numerical values of all levels and parameters are in cm^{-1}.

[3] The parameters A, A', G'_{ds}, and G'_{ps} are allowed to change freely. The parameters B, C, F_2, and G_1 are in arithmetic progression. The parameters G_3, α, ζ_d, and ζ_p are kept equal, and for the parameters of the interactions between configurations H' is kept equal to H, J' to J, G to G'_{ds} and $K' = K + 956$ (fixed difference).

From the values of B', B'', C', and C'' obtained for first spectra investigated previously it was apparent that the approximate differences were:

$$\begin{aligned} B''-B' &= 85 \\ C''-C' &= 100 \end{aligned} \tag{9}$$

These differences were kept fixed in the least-squares calculations.

In order to estimate the effects of the interactions with the configurations $3d^74s^24p$, the configurations $3d^94p+3d^84s4p$ were also considered without $3d^74s^24p$. Although $3d^74s^24p$ is very high, the rms error rose from the present value of 131 to 173, stressing the importance of inserting the interactions with $3d^74s^24p$ explicitly. Although all the levels had higher deviations without $3d^74s^24p$, the level $^3F(^1P)y\,^3G_5$ [4] can be singled out in particular. Whereas in the case of $(3d+4s)^94p$ the deviation for this level was 330, for $3d^94p+3d^84s4p$ the deviation rose to 540. The final parameters for $3d^94p+3d^84s4p$ are given in table 1.

Since it was not possible to perform a variation in the least-squares with A'' free, the calculated values of the levels $3d^74s^24p$ are not significant. The comparison of the experimental and calculated values of the levels and the g-factors of the configurations $3d^84p+3d^74s4p$ are given in table A of the appendix, when these configurations were considered together with $3d^95p$.

2. Ni I $-3d^94p+3d^84s4p+3d^95p$

All the predicted levels of the configuration $3d^95p$ have been observed experimentally. Furthermore, since the configuration $3d^95p$ lies in the middle of the range of observed levels of $3d^84s4p$, it is interesting to investigate the effect of the interaction between $3d^84s4p$ and $3d^95p$. The necessary matrices comprising the configurations d^9p, d^8sp, d^9p' and the interactions d^9p-d^8sp and $d^9p'-d^8sp$ had already been lculated for Cu II [9].

The initial values for the parameters of $3d^94p+3d^84s4p$ were taken as the final values obtained for Ni I $(3d+4s)^94p$.

For $3d^95p$, the initial values of A^*[5] and F_2^* were obtained from the electrostatic matrices of ^3P, ^3D, and ^3F. By using the centers of gravity of the three terms and least-squares to reduce the 3 equations in 2 unknowns to 2 equations in 2 unknowns the solution gives

$$\begin{aligned} A^* &= 49260 \\ F_2^* &= 37 \end{aligned} \tag{10}$$

Since the matrices of J equal to 0 and 4 are of order 1, we obtain from $^3P_0$, $^3F_4$, and (10) initially

$$\begin{aligned} \zeta_d^* &= 640 \\ \zeta_p^* &= 340 \end{aligned} \tag{11}$$

Then, by using the fact that the trace equals the sum of the eigenvalues we obtain from the matrices of J equal to 1 and 3:

$$\begin{aligned} G_1^* &= 95 \\ G_3^* &= 13 \end{aligned} \tag{12}$$

The above initial values were used at first in the diagonalization of $3d^95p$ alone. After two iterations the following values were obtained:

$$\begin{aligned} A^* &= 49470 \pm 43 \\ F_2^* &= 42 \pm 9 \\ G_1^* &= 73 \pm 10 \\ G_3^* &= 0 \text{ (Fixed)} \\ \zeta_d^* &= 531 \pm 36 \\ \zeta_p^* &= 159 \pm 82 \\ \text{rms error} &= 139.4 \text{ cm}^{-1} \end{aligned} \tag{13}$$

The parameter G_3^* was eliminated, since it had a value of -9 ± 9 when left to change freely.

Guided partly by the results of Cu II [9], the initial values for the parameters J^* $(3d^95p-3d^84s4p)$ and K^* $(3d^95p-3d^84s4p)$ were taken to equal about half of the corresponding values of J and K. Then, from table 1

$$\begin{aligned} J^* &= 500 \\ K^* &= 1000 \end{aligned} \tag{14}$$

In the final variation of the least-squares all the 33 terms splitting into 78 levels, which are assigned to $3d^94p+3d^84s4p+3d^95p$ in AEL, were inserted. In addition, 5 unclassified levels were also included. The values of the parameters for the three configurations are given in table 1.

The parameter F_2^* was eliminated since it assumed a small negative value when left to change freely.

The values for the parameters G_3, G_3^*, and ζ_p^* are not meaningful since the standard errors are larger than the numerical values of the parameters.

The values for the parameters J^* and K^* are important since they provide the only information about the strength of the interaction $3d^n5p+3d^{n-1}4s4p$ in the first spectra of the iron group.

The calculated values, percentages compositio and g-factors of all the 114 predicted levels (50 tern of $3d^94p+3d^84s4p+3d^95p$ are given in table (appendix).

The only odd level not included was 3° at 44336.10. An examination of the combinations of the level 3° as given by Russell [10], reveals that this level is based upon combinations with only the two even levels $a\,^3F_3$ and $a\,^3F_4$. From table A it is evident that this level could conceivably be assigned to $^3P(^3P)^5D_4$, yielding a deviation of around 300. However, since it is doubtful whether 3° is a valid level, this assignment was rejected.

[4] For the theoretical term designations see the appendix of this paper.

[5] Starred parameters refer to the configuration $3d^95p$.

TABLE 1. *Final parameters in units of cm^{-1}*

Parameter	$(3d+4s)^9 4p$	$3d^9 4p + 3d^8 4s 4p$	$3d^9 4p + 3d^8 4s 4p + 3d^9 5p$
A	31158 ± 156	30814 ± 218	31016 ± 161
A'	45786 ± 139	45144 ± 167	45352 ± 140
A''	85060 (Fixed)		
A^*			49417 ± 183
B'	1024 ± 7	1017 ± 10	1011 ± 9
B''	1109 (Fixed)		
C'	4187 ± 54	4202 ± 73	4112 ± 66
C''	4287 (Fixed)		
F_2	166 ± 13	148 ± 18	159 ± 15
F_2'	311 ± 7	304 ± 9	315 ± 8
F_2''	456 (Arith. Progress.)		
F_2^*			0 (Fixed)
G_1''	165 ± 9	166 ± 13	163 ± 12
G_1	223 ± 9	240 ± 14	251 ± 13
G_1'	281 (Arith. Progress.)		
G_1^*			41 ± 14
$G_3 = G_3'$	14 ± 4	15 ± 5	15 ± 6
$G_3'' = G_3'$	14 (Equal)		
G_3^*			3 ± 10
G_{ds}'	1626 ± 53	1505 ± 90	1470 ± 81
$G = G_{ds}'$	1626 (Equal)		
G_{ps}'	7027 ± 60	6705 ± 67	6755 ± 55
α'	83 ± 7	81 ± 11	59 ± 11
$\alpha'' = \alpha'$	83 (Equal)		
H	154 ± 33	159 ± 64	174 ± 48
$H' = H$	154 (Equal)		
J	1144 ± 34	693 ± 219	1003 ± 155
$J' = J$	1144 (Equal)		
$J^*(3d^9 5p - 3d^8 4s 4p)$			573 ± 77
K	2072 ± 135	1691 ± 223	2010 ± 162
K'	3028 (Fixed Diff.)		
$K^*(3d^9 5p - 3d^8 4s 4p)$			996 ± 74
ζ_d ζ_d'	603 ± 19	581 ± 26	600 ± 22
$\zeta_d'' = \zeta_d'$	603 (Equal)		
ζ_d^*			596 ± 51
$\zeta_p = \zeta_p'$	255 ± 51	229 ± 62	206 ± 59
$\zeta_p'' = \zeta_p'$	255 (Equal)		
ζ_p^*			51 ± 120
rms error	131.1 cm^{-1}	173.3 cm^{-1}	147.0 cm^{-1}

There were the following changes in assignment:

1. AEL $3d^8 4s(b\,^2D)4py\,^3P_{1,2}$ ⟶ $^1D(^3P)^3D_{1,2}$
2. AEL $3d^8 4s(b\,^2D)4px\,^3D_2$ ⟶ $^1D(^3P)^3F_2$
3. $^3F(^1P)^3D_3$ ⟷ $^1D(^3P)^3F_3$
4. AEL $3d^8 4s(b\,^2D)4py\,^1P$ ⟶ $^1D(^3P)^3P_1$
5. AEL $3d^8 4s(b\,^2D)4px\,^1D$ ⟶ $^1D(^3P)^3P_2$
6. AEL $3d^8 4s(b\,^2D)4px\,^1F$ ⟶ $^3P(^3P)^5D_3$
7. $^3F(^1P)^3F_3$ ⟷ $^3F(^1P)^3G_3$
8. $5p\,^1F$ ⟷ $5p\,^3F_3$
9. $5p\,^3D_2$ ⟷ $5p\,^1D$

The calculated values of the levels $^1D(^3P)^3P_{1,2}$ are, on the average, higher by 1000 than the experimental values of the levels $y\,^3P_{1,2}$. Such high deviations would be completely inconsistent with all the results obtained thus far. However, the experimental levels $y\,^3P_{1,2}$ correspond very closely to the calculated values of the levels $^1D(^3P)^3D_{1,2}$ but there is a very large discrepancy between the experimental g-factor of 1.32 for $y\,^3P_1$ and the calculated g-factor of 0.643 for $^1D(^3P)^3D_1$.

Experimental g-factors for Ni I were obtained by Bakker [11], Marvin and Baragar [12], Dijkstra [13], and Lindsley [14]. For many levels 4 different g-factors were obtained, usually differing from each other by very little. However, the experimental g-factor for $y\,^3P_1$ was obtained only by Lindsley [14]. Furthermore, not only is the value of 1.32 based on one very weak separate line, $b\,^3D_2 - y\,^3P_1$, with only one measurement used to determine this value, but, actually "only the difference of the g's could be determined from the pattern because of overlapping", [14]. Then the average

389-821 O - 70 - 8

g-factor of the better known level, here $b\,^3D_2$, was assumed.

Thus, we felt justified in neglecting the g-factor of 1.32 and performing the first change above, yielding deviations of only 37 and 64.

The experimental level $x\,^3D_2$ at 42954 is then assigned to the previously vacant theoretical level $^1D(^3P)^3F_2$, yielding a deviation of only -22. The experimental g-factor of 0.840 corresponds to the calculated value of 0.744.

The experimental level $x\,^3F_4$ fits very well in height and g-factor to the corresponding calculated values of $^1D(^3P)^3F_4$. However, the experimental level $x\,^3F_3$, whose term designation is questioned by Russell [10], (the question mark is not in the right place in AEL), cannot be assigned to $^1D(^3P)^3F_3$, as the deviation would then be about 900, which is completely incompatible with the deviations of -22 and -10 obtained for the other two levels assigned to $^1D(^3P)^3F$. Thus, as indicated by change 3, the level $w\,^3D_3$ is assigned to $^1D(^3P)^3F_3$ with a resulting deviation of only -54 and excellent agreement between the experimental and calculated g-factors (1.22 vs 1.189). Then the experimental level $x\,^3F_3$ is assigned to the vacant level $^3F(^1P)^3D_3$, yielding a deviation of only -119. The experimental g-factor of 1.24 compares favorably with the calculated value of 1.317.

The calculated values of the terms $^1D(^1P)^1D$ and $^1D(^1P)^1P$ are 58144 and 58832, respectively. Thus, the experimental terms $x\,^1D$ and $y\,^1P$ cannot be fitted to the theoretical terms with the same designations. As indicated by the changes 4 and 5, these two levels are assigned to the vacant levels $^1D(^3P)^3P_{1,2}$ (see change 1). The resulting deviations are only 18 and 0, and there is excellent agreement between the experimental and calculated g-factors (the experimental values of 1.48 and 1.39 correspond to the calculated values of 1.457 and 1.418, respectively).

Similarly, since the calculated value of the term $^1D(^1P)^1F$ is 56358 the experimental term $x\,^1F$ is erroneously designated. Russell, [10], observed that $x\,^1F$ has combinations with the levels of $a\,^3D$, $a\,^3F$ and $a\,^1D$. However, the transition with $a\,^1D$ is questioned and thus, we felt justified in assigning $x\,^1F$ to the only vacant theoretical level with J-value of 3 in that range, i.e., $^3P(^3P)^5D_3$, as indicated by change 6. The resulting deviation is only 47.

When the levels $w\,^3F_3$ and $y\,^3G_3$ were assigned to the theoretical levels with the same term designations, the deviations were -562 and 714, respectively. When these two levels are interchanged the deviations for $w\,^3F_3$ and $y\,^3G_3$ are only -19 and 154, respectively. However, then the experimental values of 0.78 and 1.04 for the g-factors do not agree well with the calculated values of 1.059 and 0.784, respectively. As in the case of $y\,^3P_1$, of the 4 sources of the experimental g-factors of Ni I, the values for $w\,^3F_3$ and $y\,^3G_3$ were obtained only by Lindsley, [14]. The g-factor of 1.04 is based on two lines, one of which is unresolved, and the g-factor of 0.78 is based on only one unresolved line. In *all* cases, the average g-factors for the even levels ($a\,^3F_2$ and $a\,^3F_3$) were *assumed* in order to obtain the g-factor for the odd levels. Thus, as for $y\,^3P_1$, the discrepancies in the g-factors were disregarded, and the exchange 7 performed.

For the exchange 8 it should be noted that the eigenfunctions of $5p\,^1F$ and $5p\,^3F_3$ are mixed strongly. In the configuration $3d^95p$ the coupling is more likely jl than LS which explains the large mixture of LS components.

The last exchange had already been performed when the configuration $3d^95p$ was considered alone. Since the calculated values of the levels $5p\,^1D$ and $5p\,^3D_2$ are 49003 and 50674, respectively, it is evident that the term designations for the two experimental levels $5p\,^3D_2$ at 49185 and $5p\,^1D$ at 50689 should be interchanged.

The eigenfunctions of the levels $^3F(^3P)y^3D_2$ and $^3F(^3P)y\,^3F_2$ are so strongly mixed that it is not meaningful to give one particular term designation to each level.

It should be emphasized that as in previous configurations investigated the parameters were first determined—within small ranges of possible fluctuations—by those levels inserted whose experimental and theoretical term designations coincided. The other levels, with changed assignments, were only inserted later.

The following table gives the assignments of the undesignated levels:

TABLE 2. *Undesignated odd levels of* Ni I

Level	Assignment	Deviation	Obs. g-factor	Calc. g-factor
1°_3	$^3P(^3P)^5P_3$	74	.....	1.633
2°_2	$^3P(^3P)^5P_2$	26	.....	1.796
3°	$(^3P(^3P)^5D_4)$	(336)	.....	(1.294)
4°_2	$^3P(^3P)^5S_2$	-188	.....	1.874
$5^\circ_{2,1}$	$^3P(^3P)^1P_1$	91	.....	1.063
6°_3	$^3P(^3P)^1D_2$	-104	.....	1.030

As explained before, the level 3° was not included in the least-squares, and thus entries pertaining to it are given in parentheses.

For the level 6°, Russell [10], gives 7 combinations with the levels of the 4 even terms $a\,^3P$, $a\,^1D$, $a\,^3F$, and $a\,^3D$. Thus, it is evident that 6° is a valid level, but there is no corresponding experimental level with J-value of 3 to which it can be assigned. An examination of the identified lines of Ni I, [10], reveals that the only transition of the level 6° with an even level of J-value 4 is the weak line $a\,^3F_4-6^\circ$ at 49032. However, *this* line was measured by Shenstone in the spectrum of Ni II, [15]. Then neglecting the above transition, the level 6° can be assigned to $^3P(^3P)^1D$, as indicated above.

Below 54000, (the limit of the experimental data available), there are 10 theoretical levels with no corresponding experimental levels. The lowest of these is the level $^3P(^3P)^5P_1$ at 40695.

As mentioned previously, whenever there is more than one experimental source for the g-factors, the

agreement is usually very good between the various values obtained. The only exceptions are the g-factors of the levels $y\,^3F_2$ and $y\,^3D_2$, which were measured by Lindsley, [14], and Marvin and Baragar, [12]. Lindsley's value of 0.973 for $y\,^3F_2$ is based on 6 separate lines with 14 measurements taken, and his value of 0.859 for $y\,^3D_2$ is also based on 6 separate lines with 19 measurements taken. In only one of these 12 lines is the g-factor for the even level assumed. The experimental values of 0.79 and 1.19 obtained for the g-factors of $y\,^3F_2$ and $y\,^3D_2$ by Marvin and Baragar are based on only two lines in each case. Although for these two levels the g-factors of Marvin and Baragar are quoted in AEL, it seems evident that Lindsley's values are more reliable and should be adopted. This assumption is verified by the calculated g-factors obtained in the present investigation. For the theoretical levels $^3F(^3P)^3F_2$ and $^3F(^3P)^3D_2$, the g-factors of 0.903 and 0.929, respectively, are obtained to which Lindsley's values fit much better than those of Marvin and Baragar.

With the exception of the g-factors for $y\,^3P_1$, $w\,^3F_3$ and $y\,^3G_3$, discussed previously, the agreement between the experimental and calculated g-factors is very good.

The calculated values, percentage compositions and g-factors of all the 114 predicted levels (50 terms) of $3d^94p + 3d^84s4p + 3d^95p$ are given in table A.

It is interesting to note that the rms error of 131 for the configurations $(3d+4s)^94p$ is lower than the present value of 147. The difference between the rms deviations is not so large, since for $(3d+4s)^94p$ there are 17 free parameters for 71 levels yielding an rms deviation of 114, whereas for $3d^94p + 3d^84s4p + 3d^95p$, there are 25 free parameters for 83 levels giving an rms deviation of only 122.

Finally, the rms error of 147 obtained here should be compared with the rms errors of 173 for $3d^94p + 3d^84s4p$ and 139 for $3d^95p$. Since the configuration $3d^95p$ lies within the range of the observed levels of $3d^84s4p$ a greater improvement may have been expected. However, from table A it is apparent that although the eigenfunctions of the levels of $3d^94p$ are mixed considerably, the mixing is mostly among eigenfunctions belonging to $3d^95p$. Only the eigenfunctions of two levels from $3d^84s4p$ comprise contributions of more than 15 percent belonging to $3d^95p$. These are the levels $^1G(^3P)^3F_{2,3}$. Although for $(3d+4s)^94p$ the mean deviation for the levels of $^1G(^3P)^3F$ is only 109, in the present case the mean deviation is reduced to 13.

Appendix

Table A. Observed and Calculated Levels and g-Factors

In the column "Name" the calculated designation of the term is given. The terms of d^8sp are denoted by $d^8v_1S_1L_1\ (sp^{1,3}P)SL$.

The entries in the columns "J", "Obs. Level (cm^{-1})", "Calc. Level (cm^{-1})", "Obs. g-Factor" and "Calc. g-Factor" are self-evident. In the column "Percentage" for each calculated level either the three highest contributions or all those contributions exceeding five percent are given.

Whenever the experimental and calculated term designations differ, the experimental designation is entered in the column "AEL", with the notation of C. E. Moore, [1]. In many instances the exchanges involve complete terms rather than isolated levels. Unless specified otherwise, the entries in the column "AEL" pertain to exchanges in terms.

The column "O−C" gives the difference between the observed and calculated values of the levels.

The entries are in increasing energy of the calculated values.

TABLE A. *Observed and calculated levels of* Ni I $3d^94p + 3d^84s4p + 3d^95p$

Name	J	Percentage	AEL		Obs. Level (cm^{-1})	Calc. Level (cm^{-1})	O−C	Obs. g-Factor	Calc. g-Factor
			Config.	Desig.					
$^3F(^3P)^5D$	0	96	$3d^84s(a\,^4F)4p$	$z\,^5D$	28213	28241	−28		
	1	95			27944	28008	−64	1.486	1.486
	2	94			27415	27551	−136	1.49	1.488
	3	94			26666	26906	−240	1.50	1.492
	4	96			25754	26119	−365	1.51	1.497
$^3F(^3P)^5G$	2	96	$3d^84s(a\,^4F)4p$	$z\,^5G$	29013	28856	157	0.364	0.359
	3	$90+6\,^3F(^3P)^5F$			28578	28473	105	0.945	0.938
	4	$87+8\,^3F(^3P)^5F$			28068	28015	53	1.171	1.165
	5	$88+10\,^3F(^3P)^5F$			27580	27543	37	1.28	1.277
	6	100			27261	27151	110	1.32	1.333
$^3F(^3P)^5F$	1	97	$3d^84s(a\,^4F)4p$	$z\,^5F$	30392	30231	161	0.006	0.020
	2	$72+9(^2D)4p\,^3D+7(^2D)4p\,^1D$			30163	30030	133	0.985	1.012
	3	$84+5\,^3F(^3P)^5G$			29833	29658	175	1.208	1.219
	4	$76+9(^2D)4p\,^3F+8\,^3F(^3P)^5G$			29084	29094	−10	1.288	1.317
	5	$90+8\,^3F(^3P)^5G$			28542	28490	52	1.38	1.386

TABLE A. *Observed and calculated levels of* Ni I $3d^9 4p + 3d^8 4s 4p + 3d^9 5p$ – Continued

Name	J	Percentage	AEL		Obs. Level (cm^{-1})	Calc. Level (cm^{-1})	O–C	Obs. g-Factor	Calc. g-Factor
			Config.	Desig.					
$(^2D)4p\,^3P$	0	96			30192	30183	9		
	1	$87 + 5(^2D)4p\,^3D$			29501	29498	3	1.426	1.420
	2	$91 + 4(^2D)4p\,^3D$			28569	28590	−21	1.485	1.481
$(^2D)4p\,^3F$	2	$72 + 10\,^3F(^3P)^3F + 6(^2D)4p\,^3D$			30619	30655	−36	0.740	0.742
	3	$48 + 27(^2D)4p\,^1F + 8(^2D)4p\,^3D$			29321	29323	−2	1.086	1.087
	4	$79 + 12\,^3F(^3P)^5F + 6\,^3F(^3P)^3F$			29481	29419	62	1.287	1.263
$(^2D)4p\,^3D$	1	$59 + 30\,^3F(^3P)^3D$			30913	30919	−6	0.552	0.564
	2	$28 + 22\,^3F(^3P)^5F + 17(^2D)4p\,^1D$			29888	29893	−5	1.044	1.021
	3	$59 + 24\,^3F(^3P)^3D + 11(^2D)4p\,^1F$			29669	29760	−91	1.300	1.290
$(^2D)4p\,^1F$	3	$52 + 34(^2D)4p^3F$			31031	31021	10	1.048	1.049
$(^2D)4p\,^1D$	2	$61 + 17(^2D)4p\,^3D + 12\,^3F(^3P)^3D$			31442	31418	24	1.060	1.060
$^3F(^3P)^3G$	3	95	$3d^8 4s(a\,^2F)4p$	$z\,^3G$	31786	31765	21	0.761	0.763
	4	91			30980	31061	−81	1.052	1.049
	5	96			30923	30917	6	1.21	1.203
$(^2D)4p\,^1P$	1	95			32982	32983	−1	1.005	1.008
$^3F(^3P)^3F$	2	$49 + 35\,^3F(^3P)^3D$	$3d^8 4s(a\,^2F)4p$	$y\,^3D$	34163	34096	67	0.859	0.903
	3	$43 + 29\,^3F(^3P)^3D$	$3d^8 4s(a\,^2F)4p$	$y\,^3F$	33112	33197	−85	1.193	1.181
	4	86			32973	32994	−21	1.22	1.216
$^3F(^3P)^1G$	4	$72 + 13\,^3F(^3P)^3G + 12\,^3F(^3P)^3F$	$3d^8 4s(a\,^2F)4p$	$z\,^1G$	33590	33619	−29	1.035	1.043
$^3F(^3P)^3D$	1	$69 + 27(^2D)4p\,^3D$	$3d^8 4s(a\,^2F)4p$	$y\,^3D$	34409	34410	−1	0.511	0.507
	2	$31 + 39\,^3F(^3P)^3F + 17(^2D)4p\,^3D$	$3d^8 4s(a\,^2F)4p$	$y\,^3F$	33611	33622	−11	0.973	0.929
	3	$45 + 32\,^3F(^3P)^3F$	$3d^8 4s(a\,^2F)4p$	$y\,^3D$	33501	33511	−10	1.198	1.219
$^3F(^3P)^1F$	3	$84 + 10\,^3F(^3P)^3F$	$3d^8 4s(a\,^2F)4p$	$y\,^1F$	35639	35723	−84	1.013	1.014
$^3F(^3P)^1D$	2	$82 + 8(^2D)4p\,^1D$	$3d^8 4s(a\,^2F)4p$	$y\,^1D$	36601	36480	121	1.013	1.012
$^3P(^3P)^5P$	1	96				40695			2.456
	2	92		2°	40484	40458	26		1.796
	3	$90 + 8\,^1D(^3P)^3D$		1°	40361	40287	74		1.633
$^1D(^3P)^3D$	1	$75 + 10\,^3F(^3P)^3D$	$3d^8 4s(b\,^2D)4p$	$y\,^3P$	42656	42619	37	(1.32)	0.643
	2	$68 + 12\,^3F(^3P)^3D$			42654	42590	64		1.202
	3	$41 + 39\,^3F(^3P)^3D$	$3d^8 4s(b\,^2D)4p$	$x\,^3D$	42621	42418	203		1.354
$^1D(^3P)^3F$	2	$80 + 4\,^3P(^3P)^5D$	$3d^8 4s(b\,^2D)4p$	$x\,^3D$	42954	42976	−22	0.840	0.744
	3	$66 + 20\,^3P(^3P)^5D$	$3d^8 4s(a\,^4F)4p$	$w\,^3D$	42768	42822	−54	1.22	1.189
	4	$53 + 39\,^3P(^3P)^5D$	$3d^8 4s(b\,^2D)4p$	$x\,^3F$	42585	42595	−10	1.35	1.349
$^1D(^3P)^3P$	0	$62 + 32\,^3P(^3P)^3P$				43079			
	1	$59 + 23\,^3P(^3P)^3P + 8\,^1D(^3P)^3D$	$3d^8 4s(b\,^2D)4p$	$y\,^1P$	43464	43464	0	1.39	1.418
	2	$44 + 27\,^3P(^3P)^5D + 12\,^3P(^3P)^3P$	$3d^8 4s(b\,^2D)4p$	$x\,^1D$	43933	43915	18	1.48	1.457

TABLE A. *Observed and calculated levels of* Ni I $3d^94p + 3d^84s4p + 3d^95p$—Continued

Name	J	Percentage	AEL		Obs. Level (cm^{-1})	Calc. Level (cm^{-1})	O−C	Obs. g-Factor	Calc. g-Factor
			Config.	Desig.					
$^3P(^3P)^5D$	0	91				44134			
	1	89				44094			1.485
	2	$56 + 27\,^1D(^3P)^3P$				44061			1.461
	3	$58 + 17\,^1D(^3P)^3D + 11\,^1D(^3P)^3F$	$3d^84s(b\,^2D)4p$	$x\,^1F$	44206	44159	47		1.401
	4	$34 + 30\,^3F(^1P)^3F + 21\,^3F(^1P)^3G$				44000			1.294
$^3F(^1P)^3G$	3	91	$3d^84s(a\,^4F)4p$	$w\,^3F$	44565	44411	154	(1.04)	0.784
	4	$72 + 24\,^3F(^1P)^3F$	$3d^84s(a\,^4F)4p$	$y\,^3G$	44315	44567	−252	1.18	1.289
	5	100			43090	42572	518	1.23	1.200
$^3F(^1P)^3D$	1	$67 + 11\,^3P(^3P)^3D$	$3d^84s(a\,^4F)4p$	$w\,^3D$	45122	45008	114	0.57	0.471
	2	$56 + 15\,^1D(^3P)^3D$			44475	44479	−4	1.16	1.172
	3	$34 + 29\,^1D(^3P)^3D + 16\,^3P(^3P)^5D$	$3d^84s(b\,^2D)4p$	$x\,^3F$	43655	43774	−119	1.24	1.317
$^3F(^1P)^3F$	2	86	$3d^84s(a\,^4F)4p$	$w\,^3F$	45419	45902	−483	0.68	0.668
	3	77	$3d^84s(a\,^4F)4p$	$y\,^3G$	45281	45300	−19	(0.78)	1.059
	4	$36 + 30\,^1D(^3P)^3F + 22\,^3P(^3P)^5D$	$3d^84s(a\,^4F)4p$	$w\,^3F$	43259	43501	−242	1.25	1.112
$^3P(^3P)^3P$	0	$63 + 30\,^1D(^3P)^3P$	$3d^84s(a\,^4P)4p$	$x\,^3P$	47687?	47660	27		
	1	$47 + 19\,^3P(^3P)^3D + 17\,^1D(^3P)^3P$			47208	47254	−46		1.203
	2	$59 + 18\,^3P(^3P)^5S$			46523	46609	−86		1.573
$^3P(^3P)^3D$	1	$66 + 14\,^3P(^3P)^3P$	$3d^84s(a\,^4P)4p$	$v\,^3D$	47425	47448	−23	0.726	0.727
	2	81			47139	47209	−70	1.209	1.170
	3	90			47030	47052	−22	1.331	1.323
$^3P(^3P)^5S$	2	$76 + 9\,^3P(^3P)^3P + 8\,^1D(^3P)^3P$		4°	47329	47517	−188		1.874
$(^2D)5p\,^1F$	3	$56 + 35(^2D)5p\,^3F$	$3d^9(a\,^2D)5p$	$v\,^3F$	48672	48677	−5		1.052
$^3P(^3P)^1P$	1	$83 + 6(^2D)5p\,^1P$		5°	48818	48727	91		1.063
$(^2D)5p\,^1D$	2	$47 + 17(^2D)5p\,^3P + 12\,^3P(^3P)^1D$	$3d^9(a\,^2D)5p$	$u\,^3D$	49185	49003	182		1.123
$^3P(^3P)^1D$	2	$75 + 11(^2D)5p\,^1D$		6°	49033	49137	−104		1.030
$(^2D)5p\,^3P$	0	$91 + 8\,^3P(^3P)^3P$			50139	50159	−20		
	1	$62 + 22(^2D)5p\,^1P + 7\,^3P(^3P)^3P$			49403	49238	165		1.374
	2	$65 + 19(^2D)5p\,^1D + 8\,^3P(^3P)^3P$			48735	48704	31		1.403
$^1G(^3P)^3H$	4	100				49553			0.800
	5	100				49653			1.034
	6	100				49778			1.167
$(^2D)5p\,^3F$	2	$57 + 30\,^1G(^3P)^3F$			50039	49937	102		0.662
	3	$23 + 24(^2D)5p\,^3D + 24(^2D)5p\,^1F$	$3d^9(a\,^2D)5p$	$w\,^1F$	50143	50074	69		1.138
	4	$84 + 13\,^1G(^3P)^3F$			48715	48792	−77		1.251
$^3P(^3P)^3S$	1	98				49928			1.986
$(^2D)5p\,^3D$	1	$80 + 10\,^3F(^1P)^3D$			50851	50929	−78		0.508
	2	$69 + 11(^2D)5p\,^1D + 11\,^3F(^1P)^3D$	$3d^9(a\,^2D)5p$	$w\,^1D$	50689	50674	15		1.130
	3	$59 + 14(^2D)5p\,^1F + 11(^2D)5p\,^3F$			49328	49423	−95		1.223
$(^2D)5p\,^1P$	1	$64 + 26(^2D)5p\,^3P$			50458	50519	−61		1.150

TABLE A. *Observed and calculated levels of* Co I $(3d+4s)^8 4p$—Continued

Name	J	Percentage	AEL		Obs. Level (cm^{-1})	Calc. Level (cm^{-1})	O−C	Obs. g-Factor	Calc. g-Factor
			Config.	Desig.					
$^1G(^3P)^3F$	2	$57+32(^2D)5p\,^3F+6^3F(^1P)^3F$	$3d^84s(a\,^2G)4p$	$u\,^3F$	51344	51337	7		0.662
	3	$61+27(^2D)5p\,^3F+7^3F(^1P)^3F$			51125	51139	−14		1.081
	4	$81+12(^2D)5p\,^3F$			50790	50808	−18		1.246
$^3P(^3P)^1S$	0	99				51726			
$^1G(^3P)^3G$	3	100				54106			0.750
	4	100				54129			1.050
	5	100				54152			1.200
$^1D(^1P)^1F$	3	$87+9^3P(^1P)^3D$				56358			1.034
$^3P(^1P)^3P$	0	93				57919			
	1	$69+21^1D(^1P)^1P$				57337			1.379
	2	$47+44^1D(^1P)^1D$				56671			1.259
$^1D(^1P)^1D$	2	$46+47^3P(^1P)^3P$				58144			1.257
$^1D(^1P)^1P$	1	$66+24^3P(^1P)^3P$				58832			1.140
$^3P(^1P)^3D$	1	95				59750			0.514
	2	95				59533			1.164
	3	$89+8^1D(^1P)^1F$				59274			1.303
$^3P(^1P)^3S$	1	98				62691			1.980
$^1G(^1P)^1H$	5	100				63188			1.000
$^1G(^1P)^1F$	3	93				64652			1.009
$^1G(^1P)^1G$	4	100				67640			1.000
$^1S(^3P)^3P$	0	99				80851			
	1	99				80934			1.500
	2	99				81103			1.500
$^1S(^1P)^1P$	1	99				94586			1.000

References

[1] Moore, C. E., Atomic energy levels, Nat. Bur. Stand. (U.S.), Circ. 467, Vol. II (1952). Referred to as AEL.
[2] Roth, C., J. Res. Nat. Bur. Stand. (U.S.), **73A** (Phys. and Chem.), No. 5, 497 (1969).
[3] Roth, C., J. Res. Nat. Bur. Stand. (U.S.), **74A** (Phys. and Chem.), No. 2, 141 (1970).
[4] Roth, C., J. Res. Nat. Bur. Stand. (U.S.), **74A** (Phys. and Chem.), No. 2, 157 (1970).
[5] Roth, C., J. Res. Nat. Bur. Stand. (U.S.), **74A** (Phys. and Chem.), No. 4, 507 (1970).
[6] Roth, C., J. Res. Nat. Bur. Stand. (U.S.), **74A** (Phys. and Chem.), No. 2, 181 (1970).
[7] Roth, C., J. Res. Nat. Bur. Stand. (U.S.), **74A** (Phys. and Chem.), No. 5, 703 (1970).
[8] Roth, C., J. Math. Phys. **9**, No. 5, 686 (1968).
[9] Roth, C., J. Res. Nat. Bur. Stand. (U.S.), **73A** (Phys. and Chem.), No. 6, 599 (1969).
[10] Russell, H. N., Phys. Rev. **34**, 821 (1929).
[11] Bakker, Proc. Akad. Amsterdam **35**, 82 (1932).
[12] Marvin, H. H., and Baragar, A. E., Phys. Rev. **43**, 973 (1933).
[13] Dijkstra, H., Physica **4**, 81 (1937).
[14] Lindsley, C. H., J. Opt. Soc. Am. **32**, 94 (1942).
[15] Shenstone, A. G., Phys. Rev. **30**, 255 (1927).

(Paper 74A5–636)

JOURNAL OF RESEARCH of the National Bureau of Standards – A. Physics and Chemistry
Vol. 74A, No. 5, September–October 1970

Electron-Spin Resonance Study of an Alkaline Solution of Copper(II) Oxalate–*meso*-Tartrate Complex (The Somogyi Reagent) and Related Complexes

Alexander J. Fatiadi

Institute for Materials Research, National Bureau of Standards, Washington, D.C. 20234

(February 27, 1970)

Electron-spin resonance (e.s.r.) studies of the structure of four reagents commonly used in the carbohydrate field, namely, the Somogyi reagent, the Fehling reagent, the Benedict reagent, and the Reeves reagent, in frozen aqueous solution at 77 K, gave definite indications of dimer in the Fehling reagent only; the Benedict reagent contains a relatively low concentration of dimer as compared to monomer. The presence of an "extra" peak at 3.245 kgauss in the e.s.r. spectrum of the Somogyi reagent at 25 °C may be associated with a paramagnetic, superoxide, ion-ligand O_2^-; at 77 K, extra peaks were observed for the Somogyi, Fehling, and Benedict reagents.

Key words: Alkaline; complex; copper, e.s.r.; ligand; paramagnetic; reagent; superoxide; spectra; structure.

1. Introduction

Despite considerable work on determination of the structure of coordination complexes [1–4],[1] there are practically no reports on the structure of the blue complex present in the Somogyi reagent. From early work on determination of the structure of the blue complex present in the related Fehling solution [5], the presence of an ionized species in the complex was indicated, and a five-membered, copper-chelate ring was proposed; the latter was also favored by Cotton and Wilkinson [6].

In an e.s.r. and magnetic-susceptibility study of five copper compounds of D-tartaric acid, Ablov and co-workers [7] proposed a polymeric, chain-type structure for copper D-tartrate trihydrate; however, x-ray analysis of the related vanadyl tartrates showed a binuclear structure [3, 4]. The work of Lefebvre [8] on the composition of copper(II) citrate chelates indicates that they have a monomeric or dimeric structure, depending on pH and pCu; recent studies on this subject [9–11] have been interpreted as showing the existence, at pH 11 or higher, of a dimer in which two Cu^{2+} ions are separated by ~0.31 nm.

In general, the e.s.r. spectrum of monomeric species ($\Delta M = 1$, $g \sim 2$ region) in frozen aqueous solution (at 77 K) of Cu(II) complexes shows a characteristic, single, intense, perpendicular component, ($g_\perp$) and less-intense, four-line, parallel components ($g_\parallel$); the spectrum of the complex can thus be characterized by its anisotropic features associated with $g_\perp$, $g_\parallel$ and $A_\perp$, $A_\parallel$ components [2].

A typical e.s.r. spectrum of the Cu(II) complex in aqueous solution at room temperature shows a four-line, asymmetric pattern due to coupling of an unpaired electron of copper with the nuclear spin of the ^{63}Cu and ^{65}Cu nuclei ($I_{Cu} = \frac{3}{2}$); ^{63}Cu and ^{65}Cu have similar nuclear moments [1]. However, e.s.r. spectra of inorganic cupric salts (for example, $CuCl_2$, $Cu(NO_3)_2$, or $CuSO_4$) in aqueous solution show only a one-line pattern [12] that readily changes to a four-line spectrum on addition of a base (complex formation).

Recent advances, particularly in the application of modern polarography [9, 10], conductivity measurements [13], and, especially, low-field e.s.r. spectrometry [9, 11, 14, 15] provide tools for structural studies of coordination complexes. For copper or vanadyl complexes of a dimer having $\Delta M = 2$ transitions, an e.s.r. low-field peak is observed [9, 11, 14, 15] at about $H_0/2$ or 1.6 kG ($g \sim 4$), whereas a monomer structure ($\Delta M = 1$ transitions) shows a peak at $g \sim 2$ (H_0/3.3 kG).

2. Experimental Procedure

Ultraviolet and visible spectra were recorded with a Beckman DK–2 or Cary 14 spectrophotometer. Electron-spin resonance spectra were recorded with a Varian Model 4500 EPR spectrometer[2] with 100-kHz field-modulation and detection, operating at ~9.2

[1] Figures in brackets indicate the literature references at the end of this paper.

[2] Certain commercial instruments are mentioned in this paper; this does not imply recommendation or endorsement by the National Bureau of Standards.

and ~9.5 GHz. The klystron frequency was measured with a transfer oscillator and frequency counter. The magnetic field was measured by a proton gaussmeter monitored by the same frequency counter. All spectra were recorded in duplicate or triplicate, and the measurements were averaged. Replicate readings for the frequency-counter meter agreed within ±3 percent.

The solutions were examined in a Varian Model V-4548 aqueous-solution sample-cell at various temperatures (25 to 60 °C) and at 77 K. A measured volume of the inosose solution was introduced directly into a cell by means of a microsyringe equipped with a long needle to facilitate mixing. The inosose solution and the reagents were prepared according to the published procedures indicated in the text.

2.1. Magnetic Parameters [16, 17][3]

For the e.s.r. calculations, the following equations were employed, where g_{cal} is the g value calculated from the spectrum, ν_κ = klystron frequency, and ν_p = proton frequency; $g_{cal} = 3041.9\ \nu_\kappa/\nu_p$; Δ (gauss) $= (\nu_p - \nu_{p'}) \times 2.3486 \times 10^{-4}$. A (in cm^{-1}) $= g_{cal} - 4669 \times 10^{-4} \times \Delta$ (in gauss) where there is a separation between peaks. In spectra of liquids (at 25 °C), g_m is defined as the middle point of the hyperfine lines of the spectrum. For spectra of crystalline materials (at 25 °C or 77 K), identification of $g_{||}$ and $g_\perp$ was similar to that in the literature [16, 18]. Calculated g_m values for the solution at 25 °C were in approximate agreement with that calculated by the use of the relationship $g_m = (2g_\perp + g_{||})/3$ [18].

3. Results and Discussion

3.1. Structure of the Alkaline Copper(II) Oxalate–*meso*-Tartrate Complex (the Somogyi Reagent) and Related Complexes

Figure 1 shows, for four reagents important in the carbohydrate field, the complete e.s.r. spectra (1.0 to 3.5 kG) of supercooled (77 K), polycrystalline samples of the Cu(II) complexes from aqueous solutions. The reagents studied are: the Somogyi reagent [A, alkaline solution of copper(II) oxalate–*meso*-tartrate complex [19, 20]], the Fehling reagent [B, alkaline copper(II) *meso*-tartrate complex [21]], the Reeves reagent [C, copper(II) tetraamine hydrate complex [22], and the Benedict reagent [D, alkaline copper(II) citrate complex [21]]. Of these spectra, B and, in part, D (fig. 1) have low-field absorption (1.0–2.0 kG region), suggesting the presence of dimeric as well as monomeric species, whereas A and C lack this feature.

The Cu(II) complexes present in *the Somogyi reagent* (in the polycrystalline state at 77 K and at room temperature) can be envisaged as an equilibrium mixture of *meso*-tartrate–oxalate monomeric species (a, b, and c), with the following as possible structures for the monomeric anions: [4]

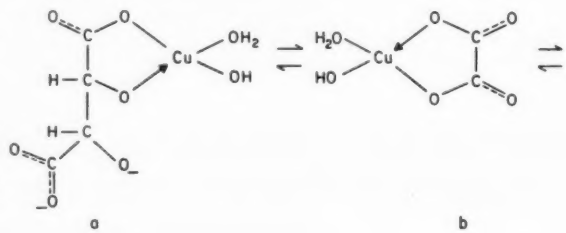

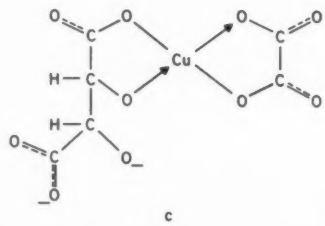

FORMULA I

Evidence is now presented, for the first time,[5] for the existence of a dimer of the Cu(II) tartrate complex of *the Fehling reagent* at 77 K; a polynuclear, complex structure for this reagent had been suggested without proof [22, 23]. The low-field lines (1.6 kG) of the e.s.r. spectrum of the frozen Fehling solution (B, fig. 1) may be associated with the $\Delta M = 2$ transitions[6] of a Cu^{2+}–Cu^{2+} ion pair, as has been suggested for other complexes [14, 17]. Hence, the evidence strongly suggests the existence of a dimer in the Fehling solution at 77 K. A possible structure for a dimer present in the Fehling reagent is depicted, where *a'* and *c'* are *meso*-tartrate hydroxyl-carboxylate ligands that bridge [25] the $Cu^{2+}(OH)^-$–$Cu^{2+}(OH)^-$ ion-pair *b'* to give five-membered, chelate rings (a strongly alkaline reagent facilitates the ionization of the hydroxyl groups of *meso*-tartaric acid). The e.s.r. spectrum of the Fehling reagent at *room temperature* did not show the low-field absorption as observed elsewhere for Cu(II) sulfosalicyclic acid dimer [11].

The e.s.r. spectrum of *the Benedict reagent* at 77 K (spectrum D, fig. 2) shows much broader, weaker, low-field absorption at 1.5 to 2.0 kG; it may also indicate the presence of a dimer. Indications of dimer in Cu(II) citrate complex at different pH's have been found [9, 11]. This sort of existence of dimers is lacking in the Somogyi reagent (A) and *the Reeves reagent* (C).[7]

[3] See refs. [2] and [17] for a discussion of the magnetic parameters $g_{||}$, $g_\perp$, $A_{||}$, and $A_\perp$, and the transitions for metal complexes, $\Delta M = 1$ and $\Delta M = 2$ for monomer and dimer structures, respectively.

[4] The coordination number of Cu(II) complexes in solution is larger than that of such complexes in the solid state; consequently, an aqueous Cu(II) *meso*-tartrate–oxalate complex may contain two water ligands that provide a maximum coordination number of six.

[5] After completion of this work, Chasteen, N. D. and Belford, R. L., [*J. Inorg. Chem.*, **9**, 169 (1970)] described the e.s.r. spectra of alkaline Cu(II) D, DL, and meso-tartrates; the authors found a binuclear copper complex with the racemic or DL-tartrate only. The Fehling reagent used in this study was prepared from a commercial Rochelle salt, a mixture of potassium-sodium-*meso* and D-tartrates.

[6] Reference [24] describes application of high-field e.s.r. spectrometry (H_0 3.6–4.0 kG) to a study of transitions $\Delta M = 2$; the paper discusses a dimer structure for Cu(II) propionate monohydrate, for which a seven-line spectrum was observed.

[7] The Reeves reagent has proved to be a useful tool in conformational analysis [26, 27]; see also, refs. [28, 29], describing other possible structures for Cu(II)–tetraamine complexes $[Cu(NH_3)_4 \cdot (H_2O)_2]^{2+}$.

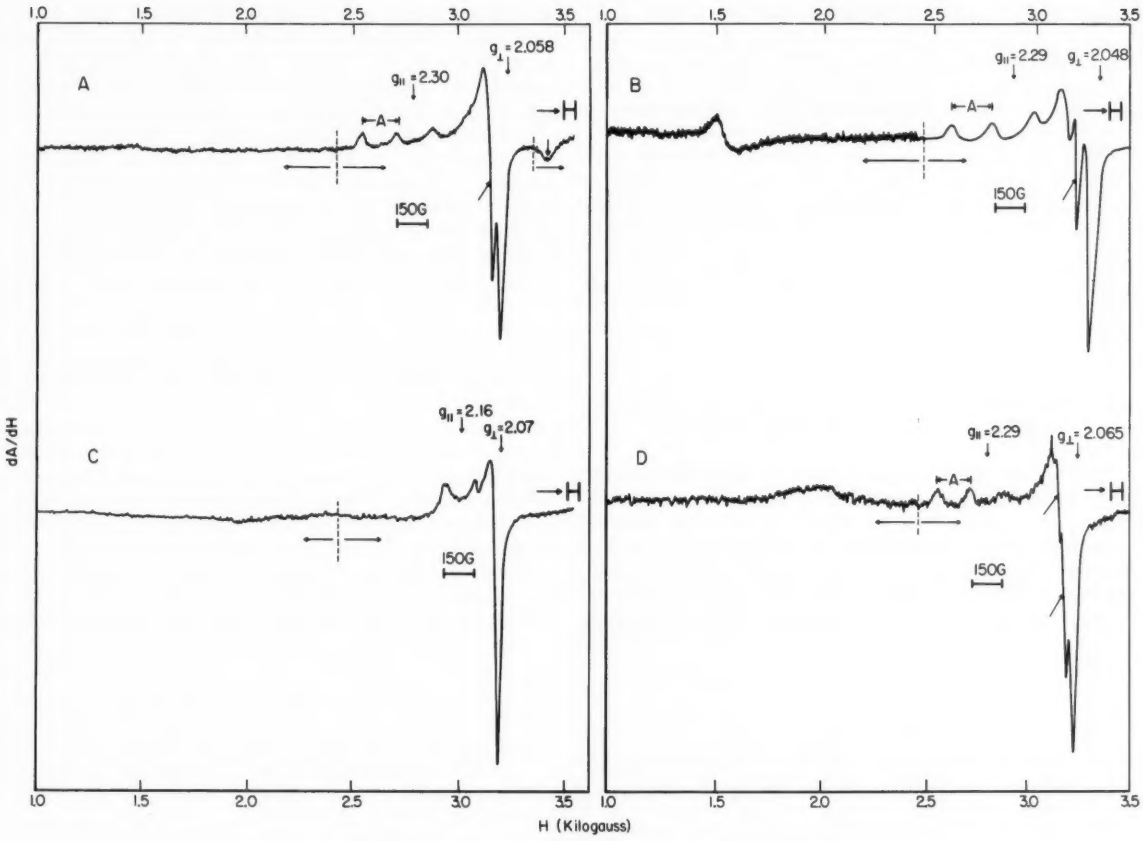

FIGURE 1. *E.s.r. spectra of frozen (77 K) aqueous alkaline solutions of* Cu(II) *complexes: spectrum A, meso-tartrate–oxalate (the Somogyi reagent); B,* meso*-tartrate (the Fehling reagent); C, citrate (the Benedict reagent); and D, tetraamine hydrate (cuprammonium, the Reeves reagent). All four low-field e.s.r. spectra on the left side of the dotted line were recorded at somewhat greater field-modulation amplitude than the spectra for the g ~2 region. A signal at 3.46 kG (spectrum A) was obtained at the same field-modulation amplitude as that used for the low-field spectrum.*

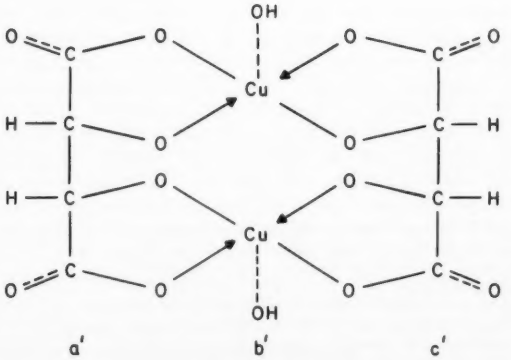

FORMULA 2

The hyperfine structure in the e.s.r. spectrum of the freshly prepared Benedict reagent *at room temperature* slowly disappears as the reagent ages, although the oxidizing power remains. For example, a three-year-old reagent showed only a one-line e.s.r. spectrum having width $\Delta = 19.3$ gauss and $g_m = 2.091$; the associated structural changes remain unexplained.

Some overlap is observed in all four of the e.s.r. spectra of figure 1. Spectrum C is highly atypical and does not show the four components. The magnetic parameters for the monomeric species are given in table 1; the table also shows the coupling constants (a_{Cu}) found for the Cu(II) complexes of the four reagents in solution (at room temperature).

TABLE 1. *Magnetic parameters*[a] *for the Cu(II) complexes of the Somogyi (A), Fehling (B), Reeves (C), and Benedict (D) Reagents at 77 K, and the coupling constants* a_{Cu} *for the reagents at* 25 °C

Reagent	$g_\perp$	$g_\parallel$	$A_\parallel$ ($cm^{-1} \times 10^{-4}$)	a_{Cu} (gauss)
A	2.058 ± 0.003	2.302 ± 0.005	164 ± 10	[b] 67 ± 1
B	2.048 ± 0.004	2.294 ± 0.003	188 ± 10	[c] 68 ± 2
C	2.072 ± 0.001	.....	.....	[d] 80 ± 3
D	2.065 ± 0.003	2.291 ± 0.002	165 ± 5	[e] 47 ± 2

[a] Indicated limits of error for the $g_\perp$, $A_\parallel$ and a_{Cu} values are based on repeatability of measurements of reference points in the spectra.
[b] For spectrum E, figure 3.
[c] For spectrum Y, figure 2.
[d] For spectrum A–1, figure 2.
[e] For spectrum B–1, figure 2.

3.2. The Nature of Complexing Ligands (*meso*-Tartrate and Oxalate) in the Somogyi Reagent

The results of a recent kinetic study [30] indicate that, in order to achieve stability in solution for complexes of Cu(II), it is necessary to have at least a bidentate donor coordinated to the metal ion. In the Somogyi reagent, the bidentate ligands are the organic anions oxalate and *meso*-tartrate; the former, because of its structure, provides a continuous pathway between the metal ions of conjugated π bonds that allows electron exchange to occur about a hundred times faster than do the others [31]. However, as will be shown, the complexing power (ability) of the oxalate anion present in the Somogyi reagent is far below that of the *meso*-tartrate anion present.

In order to obtain more information about the monomer relationship of the oxalate and *meso*-tartrate ligands present in *the Somogyi reagent*, the e.s.r. spectrum of an aqueous solution of each at room temperature was separately studied. It was found that, when potassium–sodium *meso*-tartrate was omitted from the reagent (all other constituents unchanged), a blue solution was obtained having the prominent e.s.r. spectrum depicted in T, figure 2; however, soon after preparation of the solution, crystallization of a bluish white copper oxalate complex started, and this proceeded continuously for several days. The shape of the e.s.r. spectrum of the solid (E–1, fig. 2) suggests a magnetically dilute sample that could have a polycrystalline structure. The solid decomposes on recrystallization from water, but is stable when recrystallized from basic solution. It was also observed that addition of reagent containing potassium–sodium *meso*-tartrate (U, fig. 2) to the oxalate solution keeps the copper oxalate complex in solution. This result indicates that,

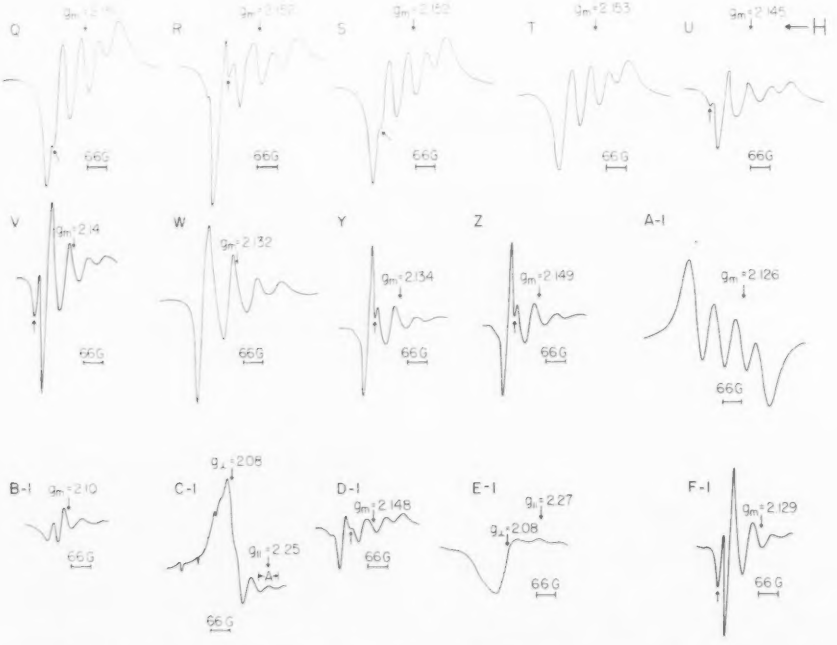

FIGURE 2. *E.s.r. spectra of selected* Cu(II) *complexes at 25* °C: *spectrum Q, the Somogyi reagent in which copper sulfate was added as the last constituent; R, the Somogyi reagent containing* ^{65}Cu *isotope; S, the Somogyi reagent containing* ^{63}Cu *isotope; T, the Somogyi reagent containing oxalate ligand only; U, the Somogyi reagent containing tartrate ligand only; V, the Fehling reagent in ~ 200mM sodium carbonate; W, the Fehling reagent in ~ 50mM sodium hydroxide; Y, freshly prepared Fehling reagent; Z, the Somogyi reagent in deuterium oxide; A–1, the Reeves reagent; B–1, the Benedict reagent; C–1, the freeze-dried solid from the Somogyi reagent; D–1, solid G–1 dissolved in deoxygenated water; E–1, the solid from the oxalate solution T; F–1, the Fehling reagent in deuterium oxide.*

in the Somogyi solution, the Cu(II) oxalate complex cannot long exist in solution in the absence of a more powerful complexing agent, namely, the *meso*-tartrate anion, but that the latter (alone) can exist. The Cu(II) *meso*-tartrate complex (U, fig. 2) has about one tenth the derivative peak-height of the Cu(II) oxalate complex (T, fig. 3). The e.s.r. spectrum of the Somogyi reagent prepared in deuterium oxide (Z, fig. 2) was difficult to reproduce. Sometimes, it was similar to that for the aqueous solution (for example, spectrum R, fig. 2), and sometimes it was identical with that of the Fehling reagent prepared in deuterium oxide (F−1, fig. 2).

3.3. The Nature of the Extra Lines Observed in the E.S.R. Spectra of the Somogyi and Related Reagents

Various workers [9, 32] have observed the presence of extra lines, in addition to four transitions, in a variety of Cu(II) complexes. Recently, Baines and coworkers [33] observed a multilined e.s.r. spectrum for Cu(II) complexes in frozen sodium hydroxide and in a frozen sodium hydroxide-cellulose system. The authors [33] explained the extra paramagnetic species observed as being due to trapped electrons that subsequently formed radicals; however, these are very reactive species that could not be observed at room temperature [34–43].

The e.s.r. spectrum of the Somogyi reagent at room temperature (E, fig. 2) shows an extra line at about 3.245 kG ($g=2.068$, indicated by the arrow, E) and this signal slowly increased in magnitude with the "aging" of the reagent caused by exposure to daylight. On freezing, the extra line seems to shift reversibly toward the $g_\perp$ line ($g=2.072$; see arrow in A, fig. 1).

A similar reversible shift on cooling was also observed for the Fehling reagent; the extra line observed at 77 K (indicated by the arrow in B, fig. 1) shifted on warming the sample to room temperature (Y, fig. 2), and this spectrum was identical with that of freshly prepared Fehling reagent. The similarity between spectra E (fig. 3) and Y (fig. 2) is also evident.

Examination of the e.s.r. spectrum Q may lead to confusion regarding the extra line for the ^{63}Cu isotope, as a slight difference in the nuclear spins of ^{63}Cu and ^{65}Cu isotopes has been deduced from spectra by the use of Kivelson's method [44, 45]. To eliminate this remote possibility of confusion regarding the extra line for the ^{63}Cu isotope, separate Somogyi reagents containing ^{65}Cu and ^{63}Cu isotopes, respectively, were prepared, and their e.s.r. spectra were examined (spectra R and S in fig. 2 for ^{65}Cu and ^{63}Cu, respectively). From the position of their strongest peaks (at about 3.277 kG for ^{63}Cu, and 3.270 kG for ^{65}Cu, as compared to 3.275 kG for the Somogyi reagent prepared from the natural-abundance mixture of ^{65}Cu and ^{63}Cu), it was concluded that the extra peak in spectrum Q does *not* arise from ^{63}Cu, which would be difficult to observe under ordinary conditions [1, 44]. The extra peak was also observed in the spectrum of the Somogyi reagent prepared from the ^{65}Cu and ^{63}Cu isotopes, respectively, and measured at 77 K.

a. Effect of pH of the Solution

Study of the extra lines observed in the e.s.r. spectra of the Somogyi and related reagents at room temperature was approached from several different angles. The possibility that the extra line in the e.s.r. spectrum of the Somogyi reagent arises from a labile, paramagnetic ligand of the Cu(II) complex received support from several pertinent observations: (1) the position and intensity of the extra line was found to be pH-dependent (see fig. 3); (2) the line decreased in size, and finally disappeared, on successive treatment with a reducing compound, namely, inosose (fig. 4, see arrows); and (3) it was lessened in size by bubbling nitrogen through the solution or by using deoxygenated water to prepare the reagent (see spectra C−1 and D−1, fig. 2). Moreover, as already mentioned, this extra line had a tendency to (a) increase in intensity and shift to higher field on "aging" by exposure to daylight or by slight warming, (b) decrease in intensity when kept in the dark, and (c) be somewhat dependent on the order of mixing of the components.

The possibility that the extra line was due to impurity in the reagents was eliminated. A typical e.s.r. spectrum of the Somogyi reagent (E, fig. 3) showed an extra line at about 3.245 kG (see arrow). This reagent was successively titrated with an aqueous base (50 to 200 m*M* sodium hydroxide), and the change in the shape of the e.s.r. spectrum was monitored. Spectrum G (fig. 3) was obtained at about pH 10.1 (range 9.6 to 10.3); it showed a decrease in intensity of the extra peak (see arrow); at pH 10.9 (range 10.6 to 11.0), the peak appeared as a shoulder (spectrum I, arrow); at pH 11.5 (range 11.2 to 12.1), it shifted to higher field (K, arrow). A further addition of base, to pH 13.2 (range 13.0 to 14.0), produced an increase in intensity of the peak (F, arrow), and, at 100 m*M* in base, the extra line reached the maximum intensity (H, arrow), resembling the spectrum of the Somogyi reagent containing Cu(II) tartrate only (U, fig. 2).

Also, treatment of the Somogyi reagent with aqueous acetic acid (1 *M*) caused shift of the original extra line. At pH 8.8 (range 8.3 to 8.9), the line appeared as a shoulder at the strongest peak (J, fig. 3, arrow), and, at pH 7.6 (range 7.5 to 7.8), it disappeared completely and irreversibly, to give a four-line, asymmetric, e.s.r. pattern (L, fig. 3) typical of Cu(II) complex [1]. This spectrum resembles that of the Somogyi reagent containing, as the organic ligand, oxalate only (T, fig. 2); further addition of acetic acid to the probe caused liberation of iodine that interfered with the measurements. However, when the Somogyi reagent, prepared without potassium iodide or iodate, was neutralized to about pH 6 (1 *M* hydrochloric acid), the e.s.r. spectrum obtained showed a one-line pattern, similar to that for neutral cupric salts [12].

The results of the foregoing experiments definitely prove the lability and pH-dependence of the "extra" paramagnetic species present in the Somogyi reagent; they also indicate the basic character of the species that could not exist below pH 8.0. As judged from the shape of the e.s.r. spectra (H, L, fig. 3, and T, U,

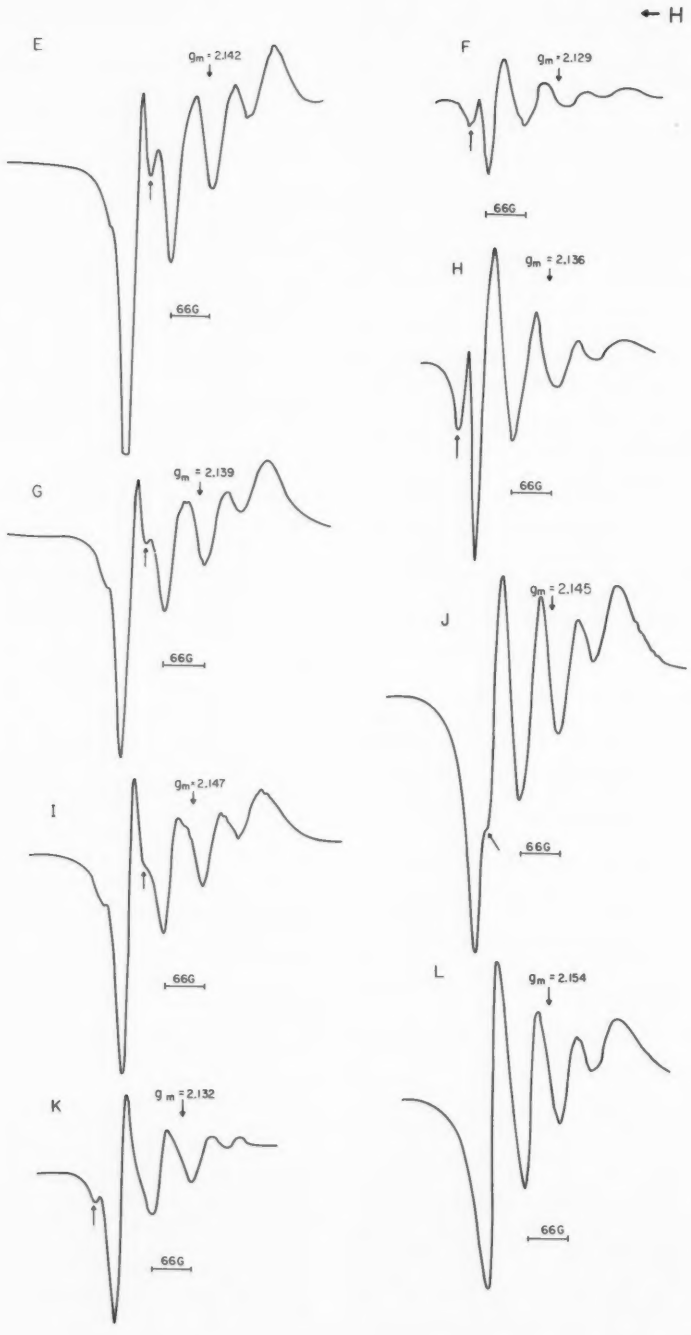

FIGURE 3. *E.s.r. spectra of the Somogyi reagent at 25 °C, at various pH's: E, pH 9.4; G, ~ 10.1 (range 9.6 to 10.3); I, ~ 10.9 (range 10.6 to 11.00); K, ~ 11.5 (range 11.2 to 12.1); F, ~ 13.2 (range 13.0 to 14.0); H, ~* 100mM *sodium hydroxide; J, pH ~ 8.8 (range 8.3 to 8.9); and L, ~ 7.6 (range 7.5 to 7.8).*

fig. 2) at the lower pH, Cu(II) oxalate complex appears to be a preponderant component of the Somogyi reagent; and, at higher pH, the equilibrium apparently favors Cu(II) tartrate complex as the major component.

An analogous pH-dependence was observed for the Fehling reagent; the original, high-field peak in Y (arrow, fig. 2) shifted to below the strongest peak when the reagent was prepared in 200 m*M* sodium carbonate solution (V, fig. 2, arrow). This line was not visible in 50 m*M* sodium hydroxide solution, apparently due to overlapping with the strongest peak (spectrum W); moreover, it shifted when the solution was prepared in deuterium oxide (F−1, fig. 2, arrow).

b. Effects of Absorbed Oxygen and Reductants

The influence of absorbed oxygen on the position of the extra line for the Somogyi reagent was demonstrated by the following experiment. An aliquot of the Somogyi reagent was freeze-dried to give a paramagnetic solid having the e.s.r. spectrum shown in C−1 (fig. 2); the spectrum was somewhat different from those reported [46] for cupric sulfate pentahydrate. Dissolution of this solid in deoxygenated water [8] under nitrogen gave the Somogyi reagent that had an e.s.r. spectrum (D−1, fig. 2) showing an extra, high-field peak that was considerably lessened (arrow) in comparison with the usual solution spectra (E, fig. 3) or (M, fig. 4).

The influence of the reductant [for example, an inosose (pentahydroxycyclohexanone) [47] or ascorbic acid] on the shape of the e.s.r. spectrum of the Somogyi reagent is shown in figure 4. This experiment may be used for demonstrating that the extra line observed in the e.s.r. spectrum of the Somogyi reagent is the first (among all of the transitions) to respond to treatment with the inosose. Figure 4 shows that a gradual decrease in intensity of the extra lines occurs, until they disappear completely (P, fig. 4, arrow) as a consequence of gradual addition of the inosose to the reagent (see arrows in M, N, O, and P, fig. 4). This experiment indicates the existence of the superoxide type of component in *the Somogyi reagent*, and only a paramagnetic species of such a type is able to show the observed sensitivity toward inosose (or any other reductant).

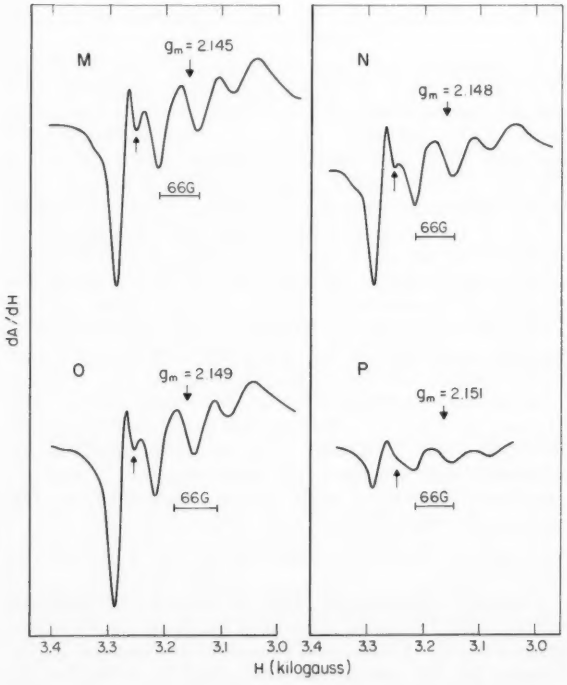

FIGURE 4. *E.s.r. spectral changes after titration of the Somogyi reagent (~0.4 ml) with* 1m*M inosose: spectrum* M, *the Somogyi reagent before titration (25°); O, after mixing with ~0.1 ml of* 1 m*M inosose (25°); N, after mixing with ~ 0.2 ml (55°); P, after mixing with ~0.4 ml (55°).*

[8] Distilled water was refluxed with potassium permanganate, and the distillate was cooled under a bubble-stream of purified nitrogen.

c. New Possible Ligands in the Somogyi Reagent and the Fehling Reagent

Careful examination of the results in the preceding experiments indicates existence, in the Somogyi reagent, of the superoxide anions O_2^{2-} and $\dot{O}_2^-$ in equilibrium with the excess of hydroxyl ions present in the reagent. The concentration of the paramagnetic oxygen-carrying ligand (for example, $\dot{O}_2^-$ in the Somogyi reagent) is rather small, as judged from the low width and magnitude of the extra derivative peak.

Consequently, the structure proposed for the Somogyi and the Fehling reagent should contain new parts, involving the active-oxygen ligands a″ and b″, for monomeric and dimeric species, respectively.

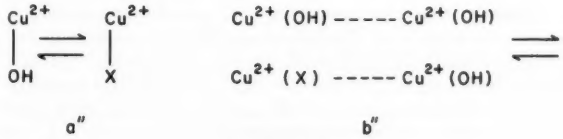

FORMULA 3

where $X = O_2^{2-} \rightleftarrows \dot{O}_2^- \rightleftarrows O_2 \rightleftarrows OH^-$. The components O_2^-, and O_2 are known [48] to be paramagnetic, and one line can be expected in their e.s.r. spectra. To the above equilibrium ($O_2^{2-} \rightleftarrows \dot{O}_2^- \rightleftarrows O_2 \rightleftarrows OH^-$) can be added the contribution from the electron-rich organic ligand (such as R—O^- with any hydroxy compound or hydroxy carboxylic acid). For example, the observed shift of the extra line for the Fehling reagent in the different basic media (spectra V, W, Y, fig. 2) may be partially explained as due to a change in conformation of the coordinated tartrate ligand [49, 50]; furthermore, the presence of the extra line is frequently noted in spectra of Cu(II) complexes containing hydroxyl or hydroxy carboxylic groups.

One possible source of the active-oxygen-containing

species that could possibly arise in the alkaline Somogyi reagent is shown in the following reactions:

$$OH^- + O_2 \xrightarrow{\text{catalyst}} \cdot OH + \dot{O}_2^-$$

$$OH^- + \dot{O}_2^- \longrightarrow \cdot OH + O_2^{2-}$$

$$2 \cdot OH \longrightarrow H_2O_2$$

The energy required for the first two reaction-sequences to occur can be supplied by photons [51], or another species equivalent to paramagnetic $\dot{O}_2^-$ can be formed by the reaction of a semidone radical (R′, see below) with O_2: $R' + O_2 \rightarrow R'O_2$. The catalyst that could possibly initiate this reaction sequence could be Cu^{2+} ion, photon [51] (colored Somogyi solution, 690–700 nm) with the possible excitation of *d* electrons [52],[9] an indirect influence of the hydrated electron [43], or a trace proportion of the semidone type of radical derived from *meso*-tartaric acid or any hydroxy carboxylic acid. The paramagnetic products would then be stabilized in equilibrium, in an anion vacancy (OH^- ligands), after all transitory species (such as $\cdot OH$ radicals) had been decomposed.

Calculation of the *g* values possible arising from the paramagnetic superoxide ions ($\dot{O}_2^-$) observed in the frozen solutions at 77 K (see fig. 1) gave the following values: for *the Somogyi reagent* (A, arrow next to $g_\perp$ line), $g = 2.072$, and the presence of another, unknown, extra line at 3.459 kG with $g = 1.912$ (A, arrow far right) was observed; for *the Fehling reagent*, $g = 2.054$ (B, indicated by the arrow); and for *the Benedict reagent*, $g = 2.068$ and $g = 2.074$ (D, arrows). These values are roughly comparable to the assigned *g* values of mononegatively charged oxygen ions, $g(O^-) = 2.06$, obtained [39, 40] on radiolysis of strongly alkaline ices at 77 K, or $g(\dot{O}_2^-) = 2.089$ at 77 K [Ref. 40, p. 156].

Taking into consideration the chemistry and the catalytic ability of Cu(II) in oxidation–reduction reactions involving molecular oxygen in enzymic [54, 55] and nonenzymic systems [56–58], or in ligand-transfer [59] or electron-transfer [60] oxidations, the idea that Cu(II) complex may contain active oxygen, either as an addition, π-electron-bonded, ethylene type of complex [49, 61, 62]

$$\underset{\downarrow}{\ddot{O}{=}O} \text{ or as an anion ligand } \underset{|}{\ddot{O}_+{=}\ddot{O}}, (\dot{\underset{\cdot}{O}}_2^-), \text{ seems possible.}$$
$$\text{Cu(II)} \qquad\qquad \text{Cu(II)}$$

In the first example, in the CuO_2—Cu (π-electron-bonded complex), the molecule will be diamagnetic, the spins being completely coupled in the metal–metal bond [49, 61, 62, 63]. Analogous oxygen-containing complexes have been reported for a series of transition metals, such as iridium [63–65], platinum [66], cobalt [53, 67, 68], and others [69].

In the second case, in which the active oxygen in the (Cu(II)) complex is present as an anion ($\dot{O}_2^-$), for example in $(CuO_2)^{2+}$ or in $(CuO_2Cu)^{2+}$ cations, the spin in the oxygen anion remains uncoupled, and, in the e.s.r. spectrum, these complexes would be expected to give one extra line, in addition to four others. The existence of such peroxo or superoxo complexes has been proposed for certain phenolases [70–72] and for certain metallo-proteins, such as hemoglobin, that was able to carry molecular oxygen [63, 73], or combine with it in certain electron-transfer processes, for example, in the two-step transfer mechanism proposed for oxidase, laccase, and other enzymes [74].

For example, beginning with a diamagnetic Cu(II)–oxygen adduct *c* (π-complex), an electron transfer in an alkaline solution may involve an oxygen bridge; as a result, an ionic superoxo complex *d* containing a paramagnetic ligand $\dot{O}_2^-$ (or a peroxo nonparamagnetic ligand O_2^{2-}) could be formed. This transfer can be visualized as follows:

$$\underset{\substack{c \\ \pi\text{-complex}}}{\text{Cu(II)—O}_2(\uparrow\downarrow)\text{—Cu(II)}} \leftrightarrow \underset{\substack{\text{Cu(II)}(\downarrow)\text{—}O_2^{2-}\text{—Cu(II)}(\uparrow) \\ d \\ \text{ionic superoxo complex.}}}{\text{Cu(II)}(\downarrow)\text{—}\dot{O}_2^-(\uparrow)\text{—Cu(I)}}$$

In addition to these adducts containing either molecular oxygen or an superoxo type of group, and the old oxidants manganese dioxide and lead dioxide, there have recently been discovered germainum peroxide [75], the specific oxidant nickel peroxide [76–78], the perferryl cation FeO_2^{2+}, [79] and the Cu^{2+}—hydrogen peroxide complex (CuO_2H^+) [80].

All of the evidence presented here indicates the existence of the superoxo type of ligand in the Cu(II) complex in both the Somogyi and the Fehling reagent at room temperature and in the polycrystalline state at 77 K. However, the possibility is not excluded that a certain proportion of the extra lines observed in the e.s.r. spectra of the Somogyi reagent, the Fehling reagent, and, particularly, the Benedict reagent (see arrows, fig. 1) at 77 K may be due to the perpendicular features from ^{63}Cu and ^{65}Cu isotopes modified by quadrupole interaction, but their separation may be obscured by overlap with features derived from the superoxide ion.

I thank colleagues at NBS: T. Murphy for samples of ^{63}Cu and ^{65}Cu salts, N. Adams for the e.s.r. measurements, R. E. Florin for a useful discussion, R. S. Tipson for his encouragement, and R. Schaffer for his support.

4. References

[1] Lewis, W. B., and Morgan, L. O., in Transition Metal Chemistry, **4**, 82–90, R. L. Carlin, Ed. (M. Bekker, New York, 1968).

[2] Kokoszka, G. F., and Gordon, G., in Technique of Inorganic Chemistry, **7**, 188–198, H. B. Jonassen and A. Weissberger, Eds. (Interscience Publishers, New York, 1968).

[9] In analogy to electron transfer with an ion pair [52] ($Fe^{3+}OH^- \xrightarrow{h\nu} Fe^{2+} + \cdot OH$), the following reaction is also feasible [53]: $Cu^{2+}OH^- \xrightarrow{h\nu} Cu^{2+} + \cdot OH$.

[3] Forrest, J. G., and Prout, C. K., J. Chem. Soc. (A) **(1967)** 1312.
[4] Chasteen, N. D., Belford, R. L., and Paul, I. C., Inorg. Chem. **8,** 408 (1969).
[5] Sidgwich, N. V., The Chemical Elements and Their Compounds, pp. 168–170 (Oxford Univ. Press, Oxford, England, 1951).
[6] Cotton, F. A., and Wilkinson, G., Advanced Inorganic Chemistry, p. 157 (Interscience Publishers, 2nd edition, 1966).
[7] Ablov, A. V., Popovich, G. A., and Suntsov, E. V., J. Structur. Chem. **9,** 861 (1968).
[8] Lefebvre, J., J. Chem. Phys. **54,** 581 (1957).
[9] Dunhill, R. H., Pilbrow, J. R., and Smith, T. D., J. Chem. Phys. **45,** 1474 (1966).
[10] Rajan, K. S., and Martell, A. E., J. Inorg. Nucl. Chem. **29,** 463 (1967).
[11] Boss, J. F., Dunhill, R. H., Pilbrow, J. R., Strivastave, R. C., and Smith, T. D., J. Chem. Soc. (A) **(1969)** 94.
[12] Fujuwara, S. and Hayashi, H., J. Chem. Phys. **43,** 23 (1965).
[13] Howe, A., and Fensham, P. J., Quart. Rev. **21,** 507 (1967).
[14] Belford, R. L., Chasteen, N. D., So, H., and Tapscott, R. E., J. Amer. Chem. Soc. **91,** 4675 (1969).
[15] Hitchman, M. A., and Belford, R. L., in T. F. Yen, Editors, Electron Spin Resonance Spectrum of Metal Complexes (Plenum Publishing Co., New York, N.Y., 1969, chapter 7).
[16] Carrington, A., and McLachlan, A. D., Introduction to Magnetic Resonance, pp. xix, 4, 72, 99, 132, and 157 (Harper and Row, New York, 1967).
[17] Atkins, P. W., and Symons, M. C. R., The Structure of Inorganic Radicals (Elsevier Publishing Co., New York, 1967, chapter 5).
[18] McCarvey, B. R., J. Phys. Chem. **60,** 71 (1956).
[19] Somogyi, M., J. Biol. Chem. **70,** 599.
[20] Schaffer, P. A., and Somogyi, M., J. Biol. Chem. **100,** 695 (1933).
[21] Shriner, R. L., Fuson, R. C., and Curtin, D. Y., The Systematic Identification of Organic Compounds, 4th Edition, pp. 102–103 (John Wiley & Sons, New York, 1956).
[22] Ref. [6], pp. 905–907.
[23] Dunlop, J. H., Evans, D. F., Gilland, R. D., and Wilkinson, G., J. Chem. Soc. (A) **(1966)** 1260.
[24] Kokoszka, G. F., Linzer, M., and Gordon, G., Inorg. Chem. **7,** 1730 (1968).
[25] Rossotti, F. J. C., in Modern Coordination Chemistry, Principles and Methods, p. 68, J. Lewis and R. G. Wilkins, Eds. (Interscience Publishers, New York, 1960).
[26] Bukhari, S. T. K., Guthrie, R. D., Scott, A. I., and Wrixon, A. D., Chem. Commun. **1968,** 1580.
[27] Bukhari, S. T. K., Guthrie, R. D., Scott, A. I., and Wrixon, A. D., J. Chem. Soc. (C) **1969,** 1073.
[28] Gustafson, R., and Martell, A., J. Amer. Chem. Soc. **81,** 525 (1959).
[29] Countney, R., Gustafson, R., Chaberek, S., and Martell, A., J. Amer. Chem. Soc. **81,** 519 (1959).
[30] Martell, A. E., in Reactions of Coordinated Ligands and Homogeneous Catalysis, D. H. Busch, Ed. (Amer. Chem. Soc. Monograph, Washington, D.C., 1963, p. 161).
[31] Ref. 6, p. 181.
[32] Gershmann, H. R., and Swalen, J. D., J. Chem. Phys. **36,** 3221 (1962).
[33] Bains, M. S., Hinojosa, O., and Arthur Jr., J. C., Carbohyd. Res. **6,** 233 (1968).
[34] Walker, D. C., Quart. Rev. **21,** 79 (1967).
[35] Anbar, M., Quart. Rev. **22,** 578 (1968).
[36] Rich, R., Periodic Correlations, p. 110 (W. A. Benjamin, Inc., New York, 1965).
[37] Hart, E. J., Accounts Chem. Res. **2,** 161 (1969).
[38] Blandamer, M. L., Shields, L., and Symons, M. C. R., Nature **199,** 902 (1963).
[39] Schulte-Frohlinde, D., and Eiber, K., Z. Naturforsch., **17a,** 445 (1962); **18a,** 199 (1963).
[40] Ayscough, P. B., Electron Spin Resonance in Chemistry, pp. 356–360 (Methuen and Co., London, 1967).
[41] Thomas, J. K., Gordon, S., and Hart, E. J., J. Phys. Chem. **68,** 1524 (1964).
[42] Kevan, L., J. Amer. Chem. Soc. **87,** 1481 (1965).
[43] Anbar, M., Advan. Phys. Org. Chem. **7,** 115 (1969).
[44] Kivelson, D., J. Chem. Phys. **45,** 1324 (1966).
[45] Solozhenkin, P. M. and Kopitsya, N. I., J. Structur. Chem. **8,** 470 (1967).
[46] Bergen, W., and Kossler, H. J., Naturwissenschaften **47,** 424 (1960).
[47] Posternak, T., Biochem. Prepn. **2,** 57 (1952).
[48] Ref. 6, p. 375.
[49] Sargeson, A. M., in Ref. [1], Vol. 6, p. 303.
[50] Jones, M. M., Mechanisms of Inorganic Reactions, Adv. Chem. Ser. **48,** 153–162 (1965).
[51] Roy, R. R., and Reed, R. D., Interactions of Photones and Leptones with Matter, pp. 174–224, and 240 (Academic Press, New York, 1968).
[52] J. A. Sartos, Ref. 25, p. 175.
[53] Tl'ykewich, L. A., and Shagisultanova, Khim. Vysok. Energi **3,** 207 (1969).
[54] Frieden, E., Osaki, S., and Kobayashi, H., J. Chem. Physiol. **49,** 213 (1965).
[55] Lontie, R., and Witters, R., in The Biochemistry of Copper, p. 455, J. Plisach, P. Aisen, and W. E. Blumberry, Eds. (Academic Press, New York, 1966).
[56] Basolo, F., and Pearson, R. G., Mechanisms of Inorganic Reactions, p. 500 (John Wiley & Sons, New York, 1967).
[57] Vogt, L. H., Jr., Wirt, J. G., and Finkbeiner, H. L., J. Org. Chem. **34,** 273 (1969).
[58] Scott, G., Atmospheric Oxidation and Antioxidants, pp. 41, 88, 91, 334, and 341 (Elsevier Publishing Co., New York, 1965).
[59] Kochi, J. K., and Mog, D. M., J. Amer. Chem. Soc. **87,** 522 (1965).
[60] Kornblum, N., Michel, R. E., and Kerber, R. C., J. Amer. Chem. Soc. **88,** 5662 (1966).
[61] Ref. 6, p. 368.
[62] Chem. Eng. News **48,** 30 (1970).
[63] Bayer, E., and Schretzmann, P., in Structures and Bonding, 2, 240, C. K. Torgensen, J. B. Neilands, B. S. Nyholm, D. Reinen, and R. J. P. Williams, Eds. (Springer-Verlag, New York, 1967).
[64] Vaska, L., Science **140,** 809 (1963).
[65] LaPlace, J., and Ibers, J. A., J. Amer. Chem. Soc. **87,** 2581 (1965).
[66] Kashiwagi, T., Yasuoka, N., Kasai, N., Kakudo, M., Takahashi, S., and Hagihara, N., Chem. Commun. **1969,** 473.
[67] Simplicio, J., and Wilkins, R. G., J. Amer. Chem. Soc. **91,** 1325 (1969).
[68] Calligaris, M., Nardin, G., and Randaccio, L., Chem. Commun. **1969,** 763.
[69] Ref. 63, pp. 190–242.
[70] Kertesz, D., Zito, R., and Chiretti, F., in Oxygenases, p. 52, O. Hayaishi, Ed. (Academic Press, London, 1962).
[71] Orgel, L., in T. K. King, H. S. Mason, and M. Morrison (Eds.), Oxidases and Related Redox Systems, p. 110 (John Wiley & Sons, New York, 1956).
[72] Manwell, C., in Oxygen in Animal Organisms, p. 5, F. Dickens and E. Neil Eds (Pergamon Press, Oxford, 1964).
[73] Gray, R. D., J. Amer. Chem. Soc. **91,** 56 (1969).
[74] Wuthrich, K., Helv. Chim. Acta **49,** 1400 (1969).
[75] Dannely, R. L., and Farrant, G. C., J. Org. Chem. **34,** 2428 (1969).
[76] Nakagawa, K., Konaka, R., and Nakata, T., J. Org. Chem. **27,** 1597 (1962).
[77] Konaka, R., Terabe, S., and Kuruma, K., J. Org. Chem. **34,** 1335 (1969).
[78] Fieser, L. F., and Fieser, M., Reagents for Organic Synthesis p. 731, (John Wiley, New York, 1967).
[79] George, P., J. Chem. Soc. **1954,** 4349.
[80] Stewart, R., Oxidation Mechanisms, p. 159 (W. A. Benjamin, Inc., New York, 1964).

(Paper 74A5–637)

JOURNAL OF RESEARCH of the National Bureau of Standards—A. Physics and Chemistry
Vol. 74A, No. 5, September–October 1970

Publications of the National Bureau of Standards*

Selected Abstracts

American National Standard, Radiological safety in the design and operation of particle accelerators, *Nat. Bur. Stand. (U.S.), Handb. 107, 22 pages (June 1970) 30 cents, SD Catalog No. C13.11:107.*

Key words: Accelerator design; accelerator operation; health physics; particle accelerators; radiation measurements; radiation protection; standard.

This American National Standard provides the basic considerations essential to the safe operation of a particle accelerator. It applies principally to particle accelerators with primary energies less than 100 MeV. It considers the characteristics of and controls for radiations as they affect accelerator design, operating procedures, and exposure evaluation. The section on radiation protection design criteria includes radiation shielding considerations and the use of safety systems. Operational health physics requirements are treated extensively, and radiation measurements are discussed in terms of the types of radiation that may be produced and proper techniques for monitoring. The final section, on dose assessment, includes basic exposure considerations such as maximum permissible dose and dose equivalent.

Armstrong, G. T., **Hydrogen fluoride and the thermochemistry of fluorine,** *Nat. Bur. Stand. (U.S.), Tech. Note 513, 21 pages (Feb. 1970), 30 cents, SD Catalog No. C13.46:513.*

Key words: Fluorides; fluorine dissociation energy; fluorine thermochemistry; heats of formation; hydrofluoric acid; hydrogen fluoride.

The thermochemistry of hydrogen fluoride is reviewed. The principal emphasis is on the experimental basis of the heats of formation of HF(g) and of HF(aq). Data from flame calorimetry in which HF(g) and HF(aq) are formed, evidence from processes involving other fluorine compounds, and some evidence from spectroscopic and photo-dissociation studies are brought together.

Becker, E. D., Ferretti, J. A., Farrar, T. C., **Driven equilibrium Fourier transform spectroscopy. A new method for nuclear magnetic resonance signal enhancement,** *J. Am. Chem. Soc.* **91,** *7784–7785 (1969).*

Key words: Driven-equilibrium; Fourier-transform; high resolution; nuclear magnetic resonance.

A new method using a high-resolution pulsed NMR spectrometer is described by which the equilibrium magnetization of nuclei with long T_1 may be restored rapidly in order to take full advantage of the Fourier transform technique.

Bender, P. L., Alley, C. O., Currie, D. G., Dicke, R. J., Faller, J. B., **Some implications for physics and geophysics of laser range measurements from earth to a lunar retro-reflector** *(Proc. Conf. NATO Advanced Study Institute, University of Newcastle, Upon Tyne, England, Mar.–Apr. 1967), Chapter in The Application of Modern Physics to the Earth and Planetary Interiors, S. K. Runcorn, ed., pp. 523–530 (John Wiley & Sons Inc., London, England, 1969).*

Key words: Astronomy; continental drift; geophysics; gravity; laser; lunar; moon.

The technique of high-accuracy laser range measurements to an optical retro-reflector package on the moon is discussed. The information which can be obtained by this method about the hypotheses of continental drift and ocean floor spreading and about the motion of the pole is described. A method for checking on the constancy of the gravitional constant is also given. The accuracy with which information on all of these questions can be obtained from lunar range measurements is higher than for any other methods which have been suggested.

Benson, S. W., O'Neal, H. E., **Kinetic data on gas phase unimolecular reactions,** *Nat. Bur. Stand. (U.S.), Nat. Stand. Ref. Data Ser. 21, 645 pages (Feb. 1970) $7.00, SD Catalog No. C13.48:21.*

Key words: Arrhenius parameters; chemical kinetics; critical review data; gas phase; mechanisms; molecular reactions; rate constants; reaction rates.

Available rate data on thermally induced, unimolecular, homogeneous gas phase reactions of molecules and free radicals have been reviewed and critically evaluated. Introductory discussion is given of theory and assumptions used in compiling the selected data. Mechanisms of reaction are discussed. The major portion (537 out of 617 pages) of the work presents selected data, with references, in the form of data sheets (one to two pages per molecule). Preferred values are indicated and discussed.

Brenner, A., Sligh, J. L., **Electrodeless electrolysis,** *J. Electrochem. Soc.* **117,** *No. 5, 602–608 (May 1970).*

Key words: Electrodeless electrolysis; electrolysis; electrolysis of electron beam electrolysis; electrolysis of glass; fused salts; glow discharge.

Solid ionic conductors and fused salts were electrolyzed without contact of solid electrical leads. The current was carried to the materials to be electrolyzed either by means of electrons emitted by a hot filament or by a glow discharge. The materials were made the separating wall between the anode and cathode compartments of an apparatus constructed of glass or fused silica.
Electrolysis of glass produced a white opaque material which did not seem to differ chemically from the original glass. Dendrites of several metals were obtained in the glow electrolysis of fused salts. The latter process resembled conventional electrolysis with metal electrodes and was not similar to the glow discharge electrolysis of aqueous electrolytes.

Brown, D. W., Wall, L. A., **Glass transition temperatures of several fluorine-containing polymers,** *J. Polymer Sci.: Part A–2,* **7,** *601–608 (1969).*

Key words: Fluorine-containing polymers; fluorine-containing styrene; glass temperature; high pressure; perfluoro-α, ω-dienes; perfluoro-α-olefins.

The glass-transition temperatures, *Tg*, of several fluorine-containing polymers were determined by use of the Differential Scanning

389-821 O - 70 - 9

Calorimeter. Values between −3 and 230 °C were obtained. In polymers of α-olefins, *Tg* increases with the fluorine content of the backbone and the length of the *n*-perfluoroalkyl branch. In styrene polymers *Tg* also is higher if the backbone contains fluorine but nearly the same *Tg*'s are found for polymers with phenyl and pentafluorophenyl groups. Saturated polymers of perfluoro-α, ω-dienes have lower *Tg*'s than polyperfluoro-α-olefins. *Tg*'s of chloroperfluoropolymers are higher than those of perfluoropolymers. Polyperfluoropentadiene-1,3 has the lowest *Tg* of the polymers examined. Polyperfluoropentadiene-1,3 forms by 1,4-addition.

Bullis, W. M., Editor, **Methods of measurement for semiconductor materials, process control, and devices. Quarterly report July 1 to September 30, 1969,** *Nat. Bur. Stand. (U.S.), Tech. Note 520, 69 pages (Mar. 1970), 65 cents, SD Catalog No. C13.46:520.*

Key words: Alpha detectors; aluminum wire; carrier lifetime; die attachment; electrical properties; epitaxial silicon; gamma detectors; germanium; gold-doped silicon; indium antimonide; metallization; methods of measurement; microelectronics; microwave devices; nuclear radiation detectors; resistivity; semiconductor devices; semiconductor materials; semiconductor process control; silicon; thermal resistance; thermographic measurements; ultrasonic microphone; wire bonds.

This quarterly progress report, fifth of a series, describes NBS activities directed toward the development of methods of measurement for semiconductor materials, process control, and devices. Principal emphasis is placed on measurement of resistivity, carrier lifetime, and electrical inhomogeneities in semiconductor crystals; evaluation of wire bonds; and measurement of thermal properties of semiconductor devices. Other tasks involve study of infrared measurement methods, deep-lying impurities in InSb, and gold in silicon; establishment of a processing facility; evaluation of aluminum metallization and wafer die attachment; review of NASA measurement methods; and measurement of Hall effect in semiconductor crystals, second breakdown in transistors, and properties of microwave devices. Related projects on silicon nuclear radiation detectors and specification of germanium are also described. Supplementary data concerning staff, committee activities, technical services, and publications are included as appendixes. Laboratory procedures for use and calibration of a capacitor microphone to measure vibration amplitude of the tool tip of an ultrasonic wire bonder are also described in a separate appendix.

Bullough, R., Simmons, J. A., **On the deformation of an imperfect solid,** *Chapter 5 in Physics of Strength and Plasticity, A. S. Argon, ed., pp. 47–63 (Massachusetts Institute of Technology Press, Cambridge, Mass., 1969).*

Key words: Continuity equations; continuous distribution of dislocations; defect measures; deformations of connections; deformations of tensors; dislocations; imperfect continuum; non-linear elasticity; non-linear strain measures; point defects.

A new formalism is presented for treating the non-linear aspects of the elastic theory of continuous distributions of dislocations and point defects. The concept of deformations of tensors and connections associated with an imperfect continuum is introduced and used to obtain relevant continuity equations together with expressions for the charge of defect content without invoking either "non-Euclidean spaces or anholonomic coordinates." Attention is drawn to the fact that the ordinarily used Cauchy strain is a generally invalid strain measure and the theory is therefore developed using both the correct Green strain and other appropriate strain measures. The correct defect measure is the Cauchy torsion tensor shown to be, in general, independent of the analogous Green torsion tensor which occurs in the continuity equation for the Green strain. The consequent difficulties are discussed and procedures for solving two new types of non-linear defect problems are given.

Caswell, R. S., Danos, M., **On the accuracy of the adiabatic separation method,** *J. Math. Phys.* **11,** *No. 2, 349–354 (Feb. 1970).*

Key words: Adiabatic approximation; adiabatic separation method; coupled oscillators; matrix diagonalization; nuclear collective model.

Numerical experiments, performed for a model of two strongly coupled oscillators, indicate that the adiabatic separation method yields accurate results even where the condition of adiabaticity is violated to a very high degree, except in those cases where two levels are degenerate in the adiabatic approximation. An accurate solution for those cases can be obtained by diagonalizing the 2×2 Hamiltonian submatrix built on the two degenerate adiabatic states. It is conjectured that the adiabatic separation method can be expected quite generally to yield highly accurate results at least for states belonging to the discrete spectrum.

Christ, B. W., **On the mechanism of interstitial-impurity-induced cross-slip in iron deformed near 175 °K,** *Acta Met.* **17,** *No. 10, 1317 1321 (Oct. 1969).*

Key words: Cross slip; ductility; interstitial impurity; iron; nitrogen; yield stress.

A mechanism is proposed whereby the elastic dipole distortion of stationary interstitial impurity atoms in lattice solution can promote nucleation and stabilization of double-kink-size dislocation segments on cross-slip planes. Stress relaxation accompanying interstitial-impurity-induced cross-slip can account for the experimental observations that small atom fractions of nitrogen in lattice solution in iron deformed around 175 °K decrease yield and flow stresses and increase ductility.

Christ, B. W., Gamble, R. P., Smith, G. V., **On the distinction between alloy softening due to nitrogen and nickel in dilute lattice solution in iron,** *Script. Met.* **3,** *No. 8, 521–530 (Aug. 1969).*

Key words: Alloy softening; elastic; electronic; Fe-N alloys; Fe-Ni alloys; flow stress; lower yield stress; mobile dislocation density; Peierls stress.

Alloy softening (AS) is the decrease in yield and flow stresses of iron and other b.c.c. metals which accompanies increasing quantities of solute in lattice solution, within critical ranges of solute concentration and temperature. This note is a comparison of existing alloy softening data on Fe-N and Fe-Ni. Whereas AS in each alloy system is due to a reduction in the thermal component of stress, the basic cause of the reduction is different in each system. This is inferred from differences in the concentration and temperature dependence of AS for each alloy system. AS in Fe-N is attributed to an increase in mobile dislocation density during yielding and flow, as compared with that of hydrogen-purified iron, arising from the mechanism of interstitial-impurity-induced cross-slip. AS in Fe-Ni is attributed to a systematic reduction in the Peierls stress of iron with increasing Ni. Whereas AS in Fe-N is primarily of elastic origin, AS in Fe-Ni is primarily of electronic origin.

Cohen, M. I., Casella, R. C., Blunt, R. F., Forman, R. A., **Lattice absorption in strontium titanate,** *Phys. Rev.* **186,** *No. 3, 834–838 (Oct. 15, 1969).*

Key words: Brillouin zone; critical points; infrared; optical absorption; phonons; selection rules; strontium titanate.

The optical absorption spectrum of $SrTiO_3$ is presented over the energy range 0.05 eV to 0.3 eV, well below the fundamental edge. Nine absorption bands are observed. We interpret all but one of them as being due to multi-phonon creation processes. The sole exception is a band at 0.068 eV which we attribute to a single-phonon process. Selection rules for simultaneous creation of either two or three phonons are obtained in dipole approximation, at selected critical points in the Brillouin zone. The observed bands are assigned using these rules together with the experimental phonon dispersion curves of Cowley and other published values for the higher energy branches obtained at specific points in the zone by other techniques.

Colwell, J. H., Mangum, B. W., Thornton, D. D., Wright, J. C., Moos, H. W., **Low-temperature magnetic properties of $DyPO_4$: An ideal three-dimensional Ising antiferromagnet,** *Phys. Rev. Letters* **23,** *No. 21, 1245–1247 (Nov. 24, 1969).*

Key words: Antiferromagnet; $DyPO_4$; exchange interaction; Ising; magnetic; three-dimensional Ising antiferromagnetic.

We have measured the magnetic susceptibility and heat capacity of $DyPO_4$ at low temperatures and compared our results with the exact series expansions based on the three-dimensional Ising model for the diamond lattice. There is excellent agreement between experiment and theory.

Coxon, B., **The synthesis, equilibration, and conformation of diastereoisomeric 1,2-*o*-isopropylidene-3,5-*o*-(methoxymethylidene)-6-*o*-*p*-tolysulfonyl-α-D-glucofuranoses. Conformational evidence from a nuclear Overhauser effect,** *Carbohydrate Res.* **12,** *313–334 (May 15, 1970).*

Key words: Conformations; equilibration; glucofuranoses; interaction energies; NMR spectroscopy; nuclear Overhauser effect.

The diastereoisomers of 1,2-*o*-isopropylidene-3,5-*o*-(methoxymethylidene)-6-*o*-*p*-tolylsulfonyl-α-D-glucofuranoses have been prepared by the reaction of 1,2-*o*-isopropylidene-6-*o*-*p*-tolylsulfonyl-α-D-glucofuranose with trimethyl orthoformate. Equilibration reactions of the diastereoisomers have been studied quantitatively by NMR spectroscopy. The resulting thermodynamic data allow a decision as to the diastereoisomer that is stabilized by intramolecular dipole–dipole interactions, which, when used in conjunction with conformational evidence from vicinal coupling-constants obtained by a computed spectrum analysis, indicated the configuration of the new asymmetric carbon atom.
Evidence for a favored orientation of the methoxyl group in one of the diastereoisomers was obtained from nuclear Overhauser experiments. Van der Waals interaction energies have been calculated for the conformations assigned to the diastereoisomers and for the possible conformations of the closely related 1,2:3,5-di-*o*-benzylidene-α-D-glucofuranose derivatives.

Demtroder, W., McClintock, M., Zare, R. N., **Spectroscopy of Na_2 using laser-induced fluorescence,** *J. Chem. Phys.* **51,** *No. 12, 5495–5508 (Dec. 1969).*

Key words: Alkali dimers; laser-induced fluorescence; molecular fluorescence; molecular spectroscopy; Na_2; resonance fluorescence.

The argon ion laser lines at 4658, 4727, 4880, 4965, 5017 and 5145 Å are each found to excite one or more resonance fluorescence series of the $Na_2(X^1\Sigma_g^+ - B^1\Pi_u)$ blue-green band system. Altogether, nineteen different fluorescence progressions have been identified and assigned v, J quantum numbers. The absolute wavenumbers of many of these emission lines have been measured interferometrically using a Fabry-Perot etalon crossed with a Bass-Kessler type spectrograph. A revised set of spectroscopic constants has been determined for both the upper and lower states which reproduce the observed term energies to better than 0.1 cm^{-1} on the average. Using these improved spectroscopic, data potential curves have been constructed for the B and X states of Na_2 by the Rydberg-Klein-Rees method. These potential curves are used in turn to compute Franck-Condon factors for the Na_2B-X band system.

Dickens, B., Brown, W. E., **The crystal structure of calcium carbonate hexahydrate at $\sim -120°$,** *Inorg. Chem.* **9,** *No. 3, 480–486 (Mar. 1970).*

Key words: Calcium phosphate; calcium phosphate-calcium silicate solid solution; calcium phosphosilicates; calcium silicates; crystal structures; glaserite; hydroxyapatite; single crystal x-ray diffraction.

The crystal structure of $Ca_5(PO_4)_2SiO_4$ (silico-carnotite) has been determined from 3358 x-ray deffraction data collected by a counter method and has been refined to $R = 0.045$. The unit cell parameters are $a = 6.737(1)$ Å, $b = 15.508(2)$ Å and $c = 10.132(1)$ Å at 24 °C and the space-group is Pnma with $z = 4$. The observed density is 3.06, the calculated density is 3.03 $g \cdot cm^{-3}$. The crystal contains about 2.5% V_2O_5 as an impurity. The structure has some relationship to the structure of $Ca_5(PO_4)_3OH$, the predominant inorganic phase in the human body, and suggests that the $Ca_5(PO_4)_2OH$ type structure may not be stable without some of the OH positions being filled. $Ca_5(PO_4)_2SiO_4$ is more closely related to $K_3Na(SO_4)_2$ (glaserite); the relationship requires systematic cation vacancies in $Ca_5(PO_4)_2SiO_4$. Cation vacancies in the glaserite-type structure have been postulated for solid solutions between Ca_2SiO_4 and $Ca_3(PO_4)_2$ and between $Ca_3(PO_4)_2$ and $CaNaPO_4$.

Evenson, K. M., Wells, J. S., Matarrese, L. M., Elwell, L. B., **Absolute frequency measurements of the 28- and 78-μm cw water vapor laser lines,** *Appl. Phys. Letters* **16.** *No. 4, 159–161 (Feb. 15, 1970).*

Key words: Laser frequency measurement; 10.7 and 3.8 THz frequency measurement; 28 and 78 micron water vapor laser.

Frequencies of the 28 and 78 micron CW water vapor laser lines were found to be 10.718065 ± 0.000002 THz and 3.821769 ± 0.000002 THz by beating each of these radiations with the 337 and 373 radiation from an HCN laser in a metal on metal point contact diode. The frequencies of the HCN laser were in turn measured by beating the 337 micron radiation with 74 GHz radiation and by measuring the 337 to 373 difference.

Frederikse, H. P. R., **The electronic band structure of strontium titanate: Theory and experiment** *(Proc. Conf. International Advanced Study Institute: Electronic Structures in Solids, Chania, Crete, Greece, June 30–July 14, 1968), Chapter in Electronic Structures in Solids, pp. 259–269 (Plenum Press, New York, N.Y., 1969).*

Key words: Electronic bandstructure; oxides; semiconductors; strontium titanate; transition metal compounds; transport measurements.

The approach used for calculating the electronic energy bands of $SrTiO_3$ is indicated. A number of experiments designed to test the result of this calculation is discussed. Among these are both transport measurements and optical investigations.

Frederikse, H. P. R., **Superconducting semiconductors** *(Proc. Conf. International Advanced Study Institute: Electronic Structures in Solids, Chania, Crete, Greece, June 30–July 14, 1968), Chapter in Electronic Structures in Solids, pp. 270–282 (Plenum Press Inc., New York, N.Y., 1969).*

Key words: Semiconductors; solid state; strontium titanate; superconducting semiconductors.

The application of the BCS theory to multi-valley semiconductors as carried out by M. L. Cohen is described. The optimum conditions for finding superconductivity in semiconductors are listed. Application of these ideas to $SrTiO_3$ and the experiments concerned with superconductivity in this compound are discussed. Other examples are mentioned.

Freeman, D. H., Goldstein, S., Schmucker, G., **Homogeneous sulfonation of styrene-divinylbenzene copolymers with oleum in organic solvents,** *Israel J. Chem.* **7,** *No. 6, 741–749 (1969).*

Key words: Cation exchangers; ion exchangers; oleum; sulfonation.

In order to obtain homogeneously sulfonated cation exchangers, the copolymers were sulfonated by oleum in a mixture of methylene-chloride and nitromethane. The influences of the chemical interaction and of the diffusion process on the kinetic behavior of these systems were investigated, and it was shown that raising the temperature of the sulfonation mixture markedly increases the chemical reaction rate, while the effect on the diffusion is small. A curve-fitting technique was used for the interpretation of the degree-of-sulfonation-vs.-time curves. These investigations served as guidelines for the subsequent preparation of homogeneous highly sulfonated copolymers.

Furukawa, G. T., Saba, W. G., Sweger, D. M., Plumb, H. H., **Normal boiling point and triple point temperatures of neon,** *Metrologia* **6,** *No. 1, 35–37 (Jan. 1970).*

Key words: Boiling point; neon; triple point.

The normal boiling point and triple point temperatures and the triple point pressure of neon were found to be 27.096 ± 0.001 K and 24.553 ± 0.001 K and $4332 \pm 13 N/m^2$ (325.02 ± 0.10 mm Hg (0 °C)), respectively. (The temperatures are in terms of the NBS–1955 provisional temperature scale. The figures after the ± symbol

indicate estimated uncertainties.) The triple point pressure is in accord with the more recent values, but the normal boiling point and triple point temperatures deviate significantly from those of previous investigators.

Gadzuk, J. W., **Resonance transmission in electron emission from surfaces with adsorbed atoms,** *Surface Sci.* **18,** *193–203 (1969).*

Key words: Adsorption; electron emission; reflection resonance; transmission resonance.

Recent work on the effects of resonance tunneling through virtual bound states of adsorbed atoms on metal surfaces in field emission is extended to treat possible resonance transmission effects over adsorbed atoms in thermionic, auger, and photoelectron emission. The resonance effects are illustrated through exact calculations on model potentials for the metal and adsorbed atom. Shortcomings of the pseudopotential formulation of wave interference phenomenon are indicated. The transmission and transmission enhancement functions are calculated for an electron coming from within the metal which then crosses the combined potential of the metal surface and the adsorbed atom. Resonance in the transmission, similar to Ramsauer peaks, are predicted for suitable choices of model potential parameters which may be reasonable approximations to the parameters describing alkali atoms adsorbed on metal surfaces.

Guildner, L. A., Stimson, H. F., Edsinger, R. E., Anderson, R. L., **An accurate mercury manometer for the NBS gas thermometer,** *Metrologia* **6,** *No. 1, 1–18 (Jan. 1970).*

Key words: Capacitance; diaphragm pressure transducer; environment; meniscus characteristics; mercury manometer; pressure; pressure regulator; vacuum joints; vacuum valves; wring tests.

A mercury manometer using capacitance sensing of meniscus positions has been refined to give an accuracy within 2 parts in 10^6 of the pressure in the range from 1×10^4 to 1.3×10^5 N/m^2. The determination of pressure ratios is accurate within 1.5 parts in 10^6 for pressures in the same range.

Haller, W., Blackburn, D. H., Wagstaff, F. E., Charles, R. J., **Metastable immiscibility surface in the system Na_2O-B_2O_3-SiO_2,** *J. Am. Ceram. Soc.* **53,** *No. 1, 34–39 (1970).*

Key words: B_2O_3-Na_2O-SiO_2; glass; immiscibility; melts; microheterogeneities; Na_2O-B_2O_3-SiO_2; SiO_2-B_2O_3-Na_2O.

Opalescence and clearing techniques have been used to determine the metastable immiscibility surface for sodium borosilicate solutions. These results indicate that a three-liquid region, which may or may not be metastable to two-liquid regions, underlies the immiscibility surface.

Heinrich, K. F. J., **Advances in the matallurgical application of electron probe microanalysis,** *Proc. Conf. 5th International Congress on X-ray Optics and Microanalysis, Tubingen, Germany, Sept. 9–14, 1968, G. Mollebstedt and K. H. Gaukler, eds., pp. 415–423 (Springer-Verlag Publ. Co., Berline, Germany, Dec. 1969).*

Key words: Applications; electron probe; metallurgy; microanalysis; spectrometry; x-rays.

Electron probe microanalysis is widely used in the investigation of phenomena of general metallurgical interest as well as in the study of specific materials and processes. New devices for x-ray detection, and automatic data collection, increase the usefulness of the microprobe for such applications. Besides the well-known methods for qualitative and quantitative electron probe analysis, the instrument can also be used advantageously for quantitative metallography and related techniques.

Heinrich, K. F. J., **Electron and ion microprobe analysis** *(Proc. 10th Symp. Electron, Ion, and Laser Beam Technology, Gaithersburg, Md., May 21–23, 1969), Chapter in Record of the 10th Symposium on Electron, Ion, and Laser Beam Technology, L. Martin, ed., pp. 353–360 (San Francisco Press, San Francisco, Calif., 1969).*

Key words: Electron microprobe; ion microprobe; mass spectrography; microanalysis; scanning electron microscopy; x-rays.

This review covers the principles and development of electron probe microanalysis, with particular emphasis on recent developments. The double function of the instrument as a spectrograph and as a microscope is considered. The salient characteristics of the ion beam microprobe are also indicated.

Heinrich, K. F. J., Yakowitz, H., **Propagation of errors in correction models for quantitative electron probe microanalysis,** *Proc. Conf. 5th International Congress on X-ray Optics and Microanalysis, Tubingen, Germany, Sept. 9–14, 1968, G. Mollebstedt and K. H. Gaukler, eds., pp. 151–159 (Springer-Verlag Publ. Co., Berlin, Germany, Dec. 1969).*

Key words: Absorption of x-rays; atomic number effects; error propagation; fluorescence; microprobe analysis; quantitative analysis.

Lack of appropriate standards frequently forces the analyst to use elemental standards. The usefulness of correction models is limited by the accuracy to which the input parameters are known. Uncertainties in presumably known quantities (mass absorption, coefficients, fluorescence yield, mean ionization potentials, etc.) are in many cases the limiting factors. The resulting analytical errors can be minimized by judicious choice of experimental conditions. This paper will give examples involving the corrections for absorption, fluorescence by characteristic lines, and atomic number effects.

Heinrich, K. F. J., Yakowitz, H., **Quantitative electron probe microanalysis: Uncertainty in the atomic number correction,** *Mikrochim. Acta* **7,** *No. 1, 123–134 (Jan.* 1970).

Key words: Atomic number correction; Bethe's Law; electron backscatter; error propagation; mean ionization potential; microprobe analysis.

The atomic number effect in quantitative electron probe microanalysis has been considered from the point of view of error propagation. The results indicate that the chief causes of analysis uncertainty are poorly known electron backscattering factors and mean ionization potential values. Operating variables such as working voltage or x-ray take-off angle cannot be manipulated so as to reduce the effect of the uncertainties. However, the overall analysis uncertainty remains nearly constant over the entire range of working voltages practical for microanalysis.

Hellwig, H., **Hydrogen spin exchange frequency shifts,** *Nat. Bur. Stand. (U.S.), Tech. Note 387, 13 pages (March 1970), 30 cents, SD Catalog No. C13.45:387.*

Key words: Frequency pulling; hydrogen beam tube; hydrogen maser; maser tuning; spin exchange.

Frequency shifts due to hydrogen spin exchange collisions are discussed for the hydrogen maser and the hydrogen storage beam tube. The combined effects of spin exchange and cavity pulling in the hydrogen maser are evaluated with emphasis on frequency errors introduced by standard tuning procedures. It is found that an automatic cavity tuning system based on a variation of the linewidth does not introduce a frequency error. In contrast, manual tuning procedures based on an interpolation of measurements at different cavity settings do not yield a perfect compensation of spin exchange effects. However, the frequency error becomes only significant at unnecessarily large cavity offsets.
The smallness of the spin exchange shifts and the near-absence of cavity pulling in a hydrogen storage beam tube are expected to permit a determination of spin exchange shifts by varying the beam intensity with a precision adequate for stability and accuracy figures of 10^{-14} or better.

Henderson, B., Stokowski, S. E., Ensign, T. C., **Luminescence from *F* centers in calcium oxide,** *Phys. Rev.* **183,** *No. 3, 826–831 (July* 15, 1969).

Key words: Calcium oxide; color centres; *F*-centres; luminescence; optical absorption; radiative lifetimes.

This paper reports data on the luminescence spectra associated with F^- and F^+-centres in calcium oxide. Irradiation in the F-band excites emission bands at 500 nm and 627 nm, which we identify with the transitions $^1P \rightarrow {}^1S$ and $^3P \rightarrow {}^1S$ respectively of the F-centre. Radiative lifetime measurements are consistent with this assignment. It is suggested that the weakness of the 500 nm band relative to the 627 nm band is due to competition between the $^1P \rightarrow {}^1S$ transition and a radiationless decay from the $^1P \rightarrow {}^3P$-level. At 4 K well-resolved fine structure is observed on the high energy side of both the 627.0 nm band and the 369.7 nm (F^+-band) band. For both bands the phonon assisted structure can be reconstructed using only three vibrational modes.

Hilten, J. S., **Accelerometer calibration with the earth's field dynamic calibrator,** *Nat. Bur. Stand. (U.S.), Tech. Note 517, 30 pages (Mar. 1970), 35 cents, SD Catalog No. C13.46:517.*

Key words: Accelerometer; air bearings; calibrator, accelerometer; dynamic; earth's field; InterAgency Transducer Project; low frequency; rotational frequency response; transducer.

This paper describes a simple device for the precise dynamic calibration of certain accelerometers at low frequencies. Calibration of an accelerometer is achieved by rotating the instrument in the earth's gravitational field at a number of constant rotational speeds.

Hosler, W. R., Frederikse, H. P. R., **Magnetoresistive effects in $KTaO_3$,** *Solid State Commun.* **7,** *1443–1449 (1969).*

Key words: Band structure; magnetoresistance; perovskites; potassium tantalate.

The magnetoresistance of semiconducting $KTaO_3$ has been investigated. Low field results indicate that the bottom of the conduction band consists of 3 or 6 ellipsoids along the ⟨100⟩ crystalline axes, similar to the energy band model predicted (and experimentally confirmed) for $SrTiO_3$. Contrary to expectations the high field magnetoresistance did *not* show Shubnikov-de Haas oscillations.

Kasen, M. B., **Grain boundary resistivity of aluminum,** *Phil. Mag.* **21,** *No. 171, 599–610 (Mar. 1970).*

Key words: Aluminum; electrical resistivity; grain boundaries; recrystallization; solute segregation; super-purity metals.

Residual resistivity at 4 K has been studied as a function of grain boundary area per unit volume in aluminum of two differing purities. A positive correlation between residual resistivity and boundary area was observed above a minimum boundary area per unit volume. The resistivity attributable to the presence of grain boundaries was found to reflect both the defect structure of the boundaries and the solute redistribution due to boundary segregation. Elimination of the solute effect yielded a specific boundary resistivity of $1.35 \pm 0.5 \times 10^{-12}$ ohm-cm^2 for pure boundaries. Evidence of a purification effect due to grain boundary segregation was noted.

Kaufman, V., Humphreys, C. J., **Accurate energy levels and calculated wavelengths of ^{86}Kr I,** *J. Opt. Soc. Am.* **59,** *No. 12, 1614–1628 (Dec. 1969).*

Key words: Calculated wavelengths; energy levels; krypton 86; standard wavelengths.

A total of 235 spectral lines of ^{86}Kr I has been measured interferometrically during the past decade. Some have been measured in only one laboratory while others have been measured in as many as twelve. On the whole, the agreement is good, but some discrepancies appear. For this work almost all of the wavelengths have been averaged and used for the determination of a best set of energy-level values for this isotope of krypton. Forty-seven even and sixty-six odd levels have been calculated by the method of least squares with uncertainties ranging from ± 0.0001 to ± 0.0016 cm^{-1}. These interferometrically-determined levels have, in turn, been used to calculate a completely consistent set of wavelengths which are preferable to any single set of measurements or averages of measurements of ^{86}Kr I. The list of 537 lines contains only those transitions which have been observed from krypton sources in the spectral region 3300 to 40,700 Å. With the exception of a number of weak lines and some close pairs, the final list of wavelengths warrants consideration for adoption as secondary standards.

Kieffer, L. J., **Low-energy electron-collision cross-section data. Part I: Ionization, dissociation, vibrational excitation,** *Atomic Data* **1,** *19–89 (1969).*

Key words: Atom; cross section; electron; molecule.

Graphical displays of selected experimental data on cross sections as functions of electron energy are presented for some 60 targets important in aeronomy, astrophysics, and plasma physics. The processes covered are ionization, dissociation, and vibrational excitation. Criteria for data selection are discussed. The literature available up to September, 1968, has been searched.

Klein, R., Scheer, M. D., **Addition of oxygen atoms to olefins at low temperature. IV. Rearrangements,** *J. Phys. Chem.* **74,** *No. 3, 613–616 (Feb. 5, 1970).*

Key words: Atoms; oxygen; low temperature; oxygen atoms; straight chain olefins.

Rearrangements in the $O(^3P)$ atom addition to internal, straight-chain olefins involve, as one of the processes, internal rotations resulting in configurational changes. Symmetrical *cis*-olefins at 90 K were found to show greater stereospecificity in the oxygen atom addition reaction as the chain length was increased. Rearrangements involving migration of alkyl groups and localization of oxygen on one of the carbon atoms of the olefinic pair occur in a concerted manner. This was shown from the reactions of 3-ethyl-e-methyl-2-pentene and two of its isomers. Clearly, independent rates cannot be associated with migrating alkyl groups, and additional factors, other than electron density, determine the position of addition of the oxygen atom.

Klose, J. Z., **Transition probabilities and mean lives of the $3s_2$ laser level in neon I,** *Phys. Rev.* **188,** *No. 1, 45–49 (Dec. 5, 1969).*

Key words: Atomic lifetimes; atomic spectra; atomic transition probabilities; laser; neon.

The mean life of the $3s_2$ (Paschen notation) laser level in Ne I has been measured for a series of pressures in the range of 3 to 11 μm of Hg using a method of delayed coincidence. The lifetime values, obtained by means of the $3s_2 \rightarrow 2p_4$ (6328 Å) transition, show an increase in magnitude with increasing pressure. This pressure dependence was interpreted as being due to the imprisonment of the 600.04 Å spectral line emitted in the transition of the $3s_2$ level to the ground state. The Holstein theory of the imprisonment of resonance radiation was applied to the analysis of the lifetime vs. pressure data to yield the following results: $A_{600} = 1.8 \pm 0.5 \times 10^7$ sec^{-1}, $\Sigma' A = (\Sigma A - A600) = 1.76 \pm 0.10 \times 10^7$ sec^{-1}, and lifetimes of 28 ± 4 and 57 ± 3 nsec for the low-pressure and high-pressure limits respectively. The error limits are obtained from the maximum estimated errors in the measured lifetimes and the measured pressures. Experimental results of other workers along with theoretical values calculated under various assumptions are presented for comparison with the results of the present work.

Kokoszka, G. F., Brinckman, F. E., **Electron paramagnetic resonance studies of phosphorus-containing reactive intermediates,** *J. Am. Chem. Soc.* **92,** *No. 5, 1199–1205* (1970).

Key words: EPR; free radicals; irradiation; low-temperature reaction; methylchlorophosphines; phosphorus halides.

Several novel phosphorus-containing radicals have been produced by photolytic methods at $-196°$ C and characterized by EPR spectrometry. In additon to the formation of PCl_2 [$A(P) = 92$ MHz; $g = 2.018$] in neat parent PCl_3, a secondary reaction has been observed which yields PCl_4 [$A(P) = 3398$ MHz; $A'(Cl) = 175$ MHz; $A''(Cl) = 21$ MHz; $g = 2.013$]. Appropriate modification of the parent matrix by either co-condensation of inert diluent (Xe) or possibly reactive materials (PF_3, $SnCl_4$) results in useful additional

spectral information. Thus in PF_3:PCl_3 (1:10) the full anisotropy of PCl_2 is revealed [$A_{||}(P) = 753$ MHz; $A_{\perp}(P) = 78$ MHz; $A_{||}(Cl) = 41.5$ MHz; $A_{\perp}(Cl \approx 0$ MHz; $g_{||} = 2.001 + g_{\perp} = 2.021$].
In contrast to neat PCl_3, irradiation of Xe:PCl_3 (9:1) results in formation of PCl_4, presumably from inhibition of $Cl + PCl_3 \rightarrow PCl_4$ by competitive Cl recombination. Irradiation of $SnCl_4$:PCl_3 (6:1) results in formation both of PCl_2 and PCl_4.
Several related organophosphines were also irradiated, but only with CH_3PCl_2 was evidence obtained suggesting formation of a four-coordinate radical similar to PCl_4 [$A(P) = 3015$ MHz; $g = 2.000$]. In al cases, however, EPR data are consistent with bond scission of the ternary phosphine to produce PCl_2-like fragments.

Krauss, M., Mielczarek, S. R., **Minima in generalized oscillator strengths: C_2H_4,** *J. Chem. Phys.* **51,** *No. 12, 5241–5243 (Dec. 15, 1969).*

Key words: C_2H_4; cross section; configurational mixing; differential; electron impact; excitation; oscillator strength.

A characteristic of electron impact excitation of low-lying Rydberg states is a minimum in the generalized oscillator strength as a function of K, the momentum transfer. This characteristic is used as a probe of the Rydberg character of four transitions in C_2H_4. Three, the $^1A_g \rightarrow {}^1B_{2u}(\pi \rightarrow 3s)$, $^1A_g \rightarrow {}^1B_{2u}(\pi \rightarrow 3p_z - 3p_z)$, and $^1A_g \rightarrow {}^1B_{2u}(\pi \rightarrow 4s)$, transitions have long been identified as Rydberg and are found to exhibit the characteristic minimum. A fourth transition, $^1A_g \rightarrow {}^1B_{1u}(\pi \rightarrow \pi^*)$, is normally termed a valence excitation and a theoretical calculation using Hartee-Fock molecular orbitals had predicted no minimum. For an energy loss of 8.0 eV, which is identified with the valence transition, a definite minimum is observed. Speculation on the source of this anomaly centers on a type of valence-Rydberg configurational mixing which can occur in many molecules. It is suggested that the presence or absence of minima in generalized oscillator strength curves be used to probe this aspect of the character of the excited state.

Lafferty, W. J., Maki, A. G., Coyle, T. D., **High resolution infrared spectrum and structure of diborane,** *J. Mol. Spectr.* **33,** *No. 2, 345–367 (1970).*

Key words: Bond angles; boron-boron bond length; boron hydrogen bond lenghts; diborane; high resolution; infrared spectrum; molecular structure; rotational constants.

The two infrared active terminal B–H stretching bands, ν_8 and ν_{16}, of $^{10}B_2H_6$ and $^{11}B_2H_6$ have been studied with a resolution of 0.04–0.05 cm^{-1}. The following ground state rotational constants have been obtained: for $^{10}B_2H_6$, $A_0 = 2.65550 \pm 0.00056$ cm^{-1}, $B_0 = 0.642190 \pm 0.000080$ cm^{-1}, and $C_0 = 0.587372 \pm 0.000066$ cm^{-1}; for $^{11}B_2H_6$, $A_0 = 2.65569 \pm 0.00026$ cm^{-1}, $B_0 = 0.606463 \pm 0.000068$ cm^{-1} and $C_0 = 0.557279 \pm 0.000056$ cm^{-1}. These constants have been used to derive the following structural parameters; B $\cdots$ B $= 1.762 \pm 0.0026$ *A*, B–$H_t = 1.200_5 \pm 0.0036$ *A*, B–$H_b = 1.320_4 \pm 0.0010$ *A*, $\angle H_tBH_t = 121.0 \pm .6°$ and $\angle H_bBH_b = 96.2 \pm .2°$. (All errors cited are twice standard errors). Upper state constants are reported.

Lang, S. B., Rice, L. H., Shaw, S. A., **Pyroelectric effect in barium titanate ceramic,** *J. Appl. Phys.* **40,** *No. 11, 4335–4340 (Oct. 1969).*

Key words: Barium titanate; ceramics; ferroelectricity; phase transitions; pyroelectricity; spontaneous polarization.

The pyroelectric coefficient (at constant stress) of a 95 percent $BaTiO_3$, 5 percent $CaTiO_3$ ceramic composition (Clevite Ceramic B) was measured over the temperature range from 4.9 to 400 °K. Extrema in the pyroelectric coefficient were observed at the rhombohedral-orthorhombic transition point (150 to 170 °K), the orthohombic-tetragonal transition point (240 to 260 °K), and the tetragonal-cubic transition point (Curie point, at 387 °K). The pyroelectric coefficient showed no anomalous behavior below 150 °K. A spontaneous polarization curve derived from the pyroelectric results is compared with published single-crystal measurements. A model for ceramic polarization suggests that domain switching at phase transitions is biased by electrical interactions arising from space charges and by mechanical interactions resulting from internal strains.

Lechner, R. E., Rowe, J. M., Sköld, K., Rush, J. J., **Study of molecular reorientation in solid neopentane by quasielastic neutron scattering,** *J. Chem. Phys. Letters* **4,** *No. 7, 444–448 (Dec. 15, 1969).*

Key words: Activation energy; cold neutron; constant; correlation time; diffusion molecular reorientation; neopentane; neutron scattering; plastic crystal; quasielastic.

Results of cold neutron scattering by plastic neopentane at several temperatures are presented. The measured quasielastic peak widths are compared with calculations for two simple models of molecular reorientation. An activation energy for reorientation of 0.88 ± 0.11 kcal/mole (3680 J/mole) is derived.

Lide, D. R., Jr., **Determination of anharmonic potential constants in linear XYZ molecules,** *J. Mol. Spectr.* **33,** *No. 3, 448–459 (Mar. 1970).*

Key words: Anharmonic constants; Fermi resonance; linear molecules; vibrational potential function; vibration-rotation interactions.

A method for determining the anharmonic potential constants k_{122}, k_{322}, and k_{2222} of linear triatomic molecules is formulated. The calculation makes use of experimental rotational constants B_v and vibrational term values G_v of low-lying vibrational levels. The anharmonic (Fermi) interactions among the triad (10^00), (02^00), (00^01) are treated explicitly, but otherwise the calculation is based on the usual second-order theory. The method is applied to four molecules for which sufficiently accurate experimental data are available: N_2O, ClCN, BrCN, and OCS. The internal consistency of the calculation is not very satisfactory, which suggests that higher order terms in the vibration-rotation Hamiltonian cannot be neglected. However, a set of anharmonic constants is obtained for each molecule which is felt to be more reliable than those previously published.

McAlister, A. J., **Calculation of the soft X-ray K-emission and absorption spectra of metallic Li,** *Phys. Rev.* **186,** *No. 3, 595–599 (Oct. 15, 1969).*

Key words: Absorption spectrum; band calculation; emission spectra; K-spectra; lithium; transition probability.

In an attempt to account for the premature peaking of the Li K-emission spectrum, detailed augmented plane wave calculations were performed for metallic Li, at many general points in the Brillouin zone as well as symmetry points. Wave functions were extracted, and the one electron K-emission and absorption transition densities evaluated. The screening arguments so commonly invoked were not employed. No early peaking was found in the emission density. Various spectral broadening mechanisms were assessed. A good fit to the experimental data was obtained by including available estimates of K-state broadening by the phonon field. At present, there is no basis for claiming uniqueness for this agreement.

McClintock, M., Demtroder, W., Zare, R. N., **Level crossing studies of Na_2 using laser-induced fluorescence,** *J. Chem. Phys.* **51,** *No. 12, 5509–5521 (Dec. 1969).*

Key words: Laser-induced fluorescence; laser molecular level crossing; level crossing; molecular fluorescence; molecular spectroscopy; Na_2.

The technique of using laser excitation to study level crossings in molecules has been developed and used to determine the radiative lifetime of an excited state of Na_2. Optical detection of level crossing in the $v' = 10$, $J' = 12$ level of the $B^1\Pi_u$ electronic state of Na_2, excited by the 4765 Å argon ion laser line, has resulted in a precise measurement of the product $g\tau = 3.80 \times 10^{-11}$ sec, corresponding to a magnetic field halfwidth of 1498 ± 45 G. If the g value is calculated assuming Hund's coupling case (*a*), the radiative lifetime is determined to be $\tau = 5.93 \pm 0.18 \times 10^{-9}$ sec. The influence of molecular hyperfine structure on this measurement is discussed and is found in general to contribute little uncertainty to the value of the radiative lifetime, provided the rotational angular momentum is much larger

than the nuclear spin and/or provided the hyperfine interaction is much smaller than the natural width of the excited state.

Manning, J. R., **Cross terms in the thermodynamic diffusion equations for multicomponent alloys,** *Met Trans. AIME* **1,** *499–505 (Feb. 1970).*

Key words: Alloys; cross terms; diffusion; multicomponent alloys; random alloys; thermodynamic equations.

The kinetic equations for the atom fluxes in a multicomponent alloy are derived in terms of atomic driving forces for a random alloy model. In this model, the contribution of each atom flux from the vacancy wind effect is directly proportional to the vacancy flux. The kinetic equations allow the L_{ik} coefficients to be identified. The cross terms relating the flux of species i to the chemical potential gradients of other species k are found to be non-zero. Neglecting the cross terms can lead to serious inaccuracies since these terms can have an appreciable effect on the atom fluxes and can lead to negative intrinsic diffusion coefficients even in ideal systems. The L_{ik} in an n-component system depend on the n tracer diffusion coefficients. In this respect, it still is possible to express the n atom fluxes in terms of only n coefficients.

Marsden, C. P., Cowan, R. Y., **Tabulation of data on semiconductor amplifiers and oscillators at microwave frequencies,** *Nat. Bur. Stand. (U.S.), Tech. Note 518, 66 pages (Feb. 1970), 65 cents, SD Catalog No. C13.46:518.*

Key words: Amplifiers; basic characteristics; microwave; oscillators; solid-state.

This tabulation in cludes some of the basic characteristics of semiconductor microwave devices, specifically amplifiers and oscillators of foreign and domestic origin.

Mazur, J., **Higher order Markov chains and statistical thermodynamics of linear polymers,** *Chapter 6 in Markov Chains and Monte-Carlo Calculations in Polymer Science, G. G. Lowry, ed., pp. 153–185 (Marcel Dekker, Inc., New York, N.Y., 1970).*

Key words: Linear polymers; Markov chains; order-disorder transitions; random variables; restricted chains; Theta point; transition probabilities; volume exclusion.

The general theory of Markov chains is presented as it applies to linear polymer chains. The polymer chain is considered here as a linear sequence of consecutive events, upon which short-range intra-chain interactions are superimposed. The statistical and thermodynamic properties of these chains are obtained from the chain partition function, which is derived by the methods of averaging functions over the chains of random variables. The partition function and its various derivatives are calculated in terms of the eigenvalues and the eigenvectors of the matrices of the transition probabilities. In the various applications of the matrix method to the conformational properties of the linear polymer chains, the matrix of transition probabilities can be subsequently reduced by similarity transformations. The theory of Markov chains is applied, in particular, to the following problems: 1) The theory of the theta (ideal) point for lattice-simulated chains with short-range interactions, 2) Volume exclusion problems for Markov chains and 3) Cooperative phenomena in linear polymers and the conditions for order-disorder transitions in self-interacting chains.

Milligan, D. E., Jacox, M. E., **Infrared and ultraviolet spectra of the products of the vacuum-ultraviolet photolysis of silane isolated in an argon matrix,** *J. Chem. Phys.* **52,** *No. 5, 2594–2608 (Mar. 1, 1970).*

Key words: Disilane; free radical; infrared spectrum; matrix isolation; Si_2; SiH; SiH_2; SiH_3; silane; ultraviolet spectrum; vacuum-ultraviolet photolysis.

The vacuum-ultraviolet photolysis of silane and of the various deuterosilanes isolated in an argon matrix at 4° or at 14° K leads to the production of several reactive species. Infrared and ultraviolet spectroscopic evidence is presented indicating that Si_2, SiH, SiH_2, and SiH_3 are stabilized in these experiments. A previously unobserved transition of Si_2, tentatively identified as the $D(^3H)-X(^3\Sigma^-)$ transition, is reported. Observation of the bending vibration absorption of SiH_2 at 1008 cm^{-1} has confirmed that the lower state of the previously observed electronic transition of singlet SiH_2 is the ground state of this species. The stretching vibrations of SiH_2 have also been observed near 2000 cm^{-1}. Infrared absorptions at 925, 996, 1955, and 1999 cm^{-1} have been tantatively assigned to SiH_3. The removal of one or more H atoms from SiH_4 leads to an appreciable lengthening of the remaining Si-H bonds. Disilane and incompletely characterized products of its photolysis contribute significantly to the infrared spectra observed at 14° K.

Nargolwalla, S. S., LaFleur, P. D., **Characterization of standard reference materials for industry and research by neutron activation analysis,** *Proc. American Nuclear Society Topical Meeting, San Juan, Puerto Rico, May 4–6, 1969, pp. 183–186 (1969).*

Key words: Neutron generator activation analysis; organometallics; oxygen; standard reference materials; steels.

Described herein are examples which demonstrate the use of a low-cost neutron generator facility for materials characterization in the steel and oil industries. Analytical results for oxygen in steels and for the metallic component in a number of organometallic oil additives are given. The accuracy of these results is indicated by the close agreement of the activation data with that obtained by conventional and will proven chemical methods. These applications illustrate the utilization of small accelerators as reliable analytical tools for certification of standard materials useful for industrial and research needs.

Paabo, M., Bates, R. G., **Dissociation constant of protonated 2,2-*bis*(hydroxymethyl)-2,2′,2″-nitrilotriethanol (*bis-tris*) and related thermodynamic functions from 0 to 50°,** *J. Phys. Chem.* **74,** *No. 4, 702–705 (Feb. 19, 1970).*

Key words: Acidity; *bis-tris;* 2,2-*bis*(hydroxymethyl)-2,2′,2″-nitrilotriethanol; buffer solutions; dissociation constant; ionization constant; *pH*; *pK*; thermodynamics.

The acidic dissociation constant of protonated 2,2-*bis*(hydroxymethyl)-2,2′,2″-nitrilotriethanol ("*bis-tris*") has been determined at 11 temperatures from 0 to 50 °C by emf measurements of hydrogen-silver chloride cells without liquid junction. At 25 °C, pK_a is 6.483, and consequently buffer solutions of the base and its hydrochloride are useful for *pH* control in the region *pH* 5.5 to 7.5. The values of pK_a over the temperature range studied are given as a function of the thermodynamic temperature (T) by the equation

$$pK_a = 1287.855/T + 2.7905 - 0.00210396T.$$

Standard thermodynamic functions for the acidic dissociation process have been derived. At 25 °C, $\Delta H° = 28{,}238$ J mol^{-1}, $\Delta S° = -29.4$ J K^{-1} mol^{-1}, and $\Delta C_p° = 24$ J K^{-1} mol^{-1}. Conventional pa_H values for five equimolal buffer solutions composed of *bis-tris* and its hydrochloride have been calculated.

Paule, R. C., Mandel, J., **Standard reference materials: Analysis of interlaboratory measurements on the vapor pressure of gold (certification of standard reference material 745),** *Nat. Bur. Stand. (U.S.), Spec. Publ. 260–19, 21 pages (Jan. 1970), 30 cents, SD Catalog No. C13.10:260–19.*

Key words: Components of error (within- and between-laboratories); gold; heats of sublimation (second and third law); interlaboratory measurements; standard errors; standard reference materials; vapor pressure.

A detailed statistical analysis has been made of results obtained from a series of interlaboratory measurements on the vapor pressure of gold. The gold Standard Reference Material 745 which was used for the measurements has been certified over the pressure range 10^{-8} to 10^{-3} atm. The temperature range corresponding to these pressures is 1300–2100 K. The gold heat of sublimation at 298 K and the associated standard error were found to be $87{,}720 \pm 210$ cal/mol ($367{,}040 \pm 900$ J/mol). Estimates of uncertainty have been calculated for the certified temperature-pressure values as well as

for the uncertainties expected from a typical single laboratory's measurements. The statistical analysis has also been made for both the second and third law methods, and for the within- and between-laboratory components of error. Several notable differences in second and third law errors are observed.

Penner, S., **Beam handling techniques for electron linear accelerators,** *Nat. Bur. Stand. (U.S.), Tech. Note, 522, 21 pages (Apr. 1970), 30 cents, SD Catalog No. C13.46:522.*

Key words: Beam handling; beam optics; beam transport; electron linear accelerator; instrumentation for electron beams; linac.

The design of beam transport systems for electron linear accelerators intended for nuclear physics research is discussed. The subjects covered include beam optics, diagnostics and control of electron beams, and problems of handling high power beams.

Penner, S., **Experimental techniques for electron scattering investigations,** *Nat. Bur. Stand. (U.S.) Tech. Note 523, 46 pages (Apr. 1970), 50 cents, SD Catalog No. C13.46:523.*

Key words: Background; current monitoring; detector ladders; electron scattering; experimental techniques; line-shape fitting; on-line computer systems; radiative tails; resolution; spectrometer design.

Modern experimental techniques for high energy electron scattering are discussed. Subjects included are: high resolution spectrometer design, the energy loss spectrometer concept, detector ladder systems, beam current monitoring techniques, suppression and measurement of background, the use of on-line computer systems, theoretical considerations and the analysis of data, and 180° scattering.

Powell, C. J., **Analysis of optical- and inelastic-electron-scattering data. II. Application to Al,** *J. Opt. Soc. Am.* **60,** *No. 1, 78–93 (Jan. 1970).*

Key words: Complex dielectric constant; electron-energy-loss; electronic band structure; infrared; least-squares fit to optical data; optical constants; reflectance; ultraviolet; visible.

Optical and electron energy-loss data for aluminum between 0.04 and 72 eV have been critically analyzed and used to test the validity of models for $\epsilon(\omega)$, the complex frequency-dependent dielectric constant. Experimental data and models for $\epsilon(\omega)$ can be effectively compared using a non-linear least-squares computer program and, at least in simple cases, the model parameters have physical significance. Though aluminum has been widely regarded as a relatively ideal "free-electron" metal, it has been found that a Drude model for $\epsilon(\omega)$ does not adequately describe the observed data. Deviations from the Drude model have been interpreted in terms of the effects of interband electronic transitions and a significant *L*-shell contribution to the real part of $\epsilon(\omega)$ between 10 and 72 eV. From a fit of reflectance data between 0.2 and 12 eV it has been possible to derive parameters describing the interband-transition contribution $\epsilon^{(b)}(\omega)$ to $\epsilon(\omega)$. The imaginary part of $\epsilon^{(b)}(\omega)$ does not differ significantly from calculations based on the aluminum band structure.

Powell, C. J., **Analysis of optical- and inelastic-electron-scattering data. III. Reflectance data for beryllium, germanium, antimony, and bismuth,** *J. Opt. Soc. Am.* **60,** *No. 2, 214–220 (Feb. 1970).*

Key words: Antimony; beryllium; bismuth; complex dielectric constant; germanium; least-squares fit to reflectance; optical constants; reflectance.

A procedure is described for simultaneously fitting reflectance data obtained for various photon energies and angles of incidence using a simple physical model for $\epsilon(\omega)$, the complex frequency-dependent dielectric constant. The mutual consistency of the model and of the experimental data is tested, within the accuracy of each measurement. As an example of the technique, reflectance data in the vacuum ultraviolet obtained by Toots, Fowler and Marton for Be, Ge, Sb and Bi have been satisfactorily fitted. The model parameters have been used to derive the optical constants n and k (in satisfactory agreement with conventional determinations) and can be readily related to other relevant experimental results or theoretical calculations of $\epsilon(\omega)$ if these are available.

Powell, F. X., Johnson, D. R., **Microwave detection of $H_2^{18}O$,** *Phys. Rev. Letters* **24,** *No. 12, 637 (Mar. 23, 1970).*

Key words: Astrophysical; emission; galactic distribution of isotopes; $H_2^{18}O$; microwave absorption; rotational transition.

Laboratory detection of a microwave absorption in $H_2^{18}O$ near 5.33 cm is reported. This observed signal has been assigned to a pure rotational transition between the 6_{16} and 5_{23} levels in the ground vibrational state of $H_2^{18}O$. Signals from these same two rotational levels for $H_2^{16}O$ have been detected in emission from several sources in the galaxy.

Rogers, E. E., Abramowitz, S., Jacox, M. E., Milligan, D. E., **Matrix-isolation studies of the infrared spectra of the free radicals CCl_3 and CBr_3,** *J. Chem. Phys.* **52,** *No. 5, 2198–2204 (Mar. 1, 1970).*

Key words: Bromoform; CBr_3; CCl_3; carbon tetrabromide; carbon tetrachloride; chloroform; infrared spectrum; lithium atoms; matrix isolation; vacuum-ultraviolet photolysis.

CCl_3 has been stabilized both by the reaction of lithium atoms with CCl_4 in an argon matrix at 20° K and by the vacuum-ultraviolet photolysis of $HCCl_3$ or of $DCCl_3$ in an argon or a nitrogen matrix at 14° K. The analogous techniques have been found to lead to the stabilization of CBr_3. The product spectra obtained in the lithium-atom experiments are considerably simpler than those obtained in the previous studies of the reaction of lithium atoms with matrix-isolated CX_4. In the vacuum-ultraviolet photolysis experiments, $DCCl_2$, $HCBr_2$, and CBr_2 have also been observed. The absorption frequencies and contours obtained for ν_3 of CCl_3 and of CBr_3 are independent of the method used to produce these species, suggesting that lithium atoms and their reaction products do not appreciably perturb the degenerate stretching mode of either CCl_3 or CBr_3. Despite yields of these species comparable to those previously reported, absorptions at 674 and at 582 cm^{-1}, previously attributed to ν_1 of CCl_3 and CBr_3, respectively, are completely missing from the present experiments. No other absorption attributable to ν_1 of either species has been detected. It is concluded that a pyramidal (C_{3v}) structure for CCl_3 and for CBr_3 has not been established.

Roth, R. S. Stephenson, N. C., **Chemical and structural investigations in the Ta_2O_5-WO_3 system,** *(Proc. Institute for Advanced Study on the Chemistry of Extended Defects in Non-Metallic Solids, Scottsdale, Arizona, April 16–26, 1969), Chapter in The Chemistry of Extended Defects in Non-Metallic Solids, L. Eyring and M. O'Keeffee, ed., pp. 167–182 (North-Holland Publ. Co., Amsterdam, The Netherlands, 1970).*

Key words: Crystal structure; non-stoichiometry; order oxygen vacancies; tantalum oxide; tantulum tungsten system.

Crystal structures have been determined for the compounds $Ta_{22}W_4O_{67}$, $Ta_{30}W_2O_{81}$, $Ta_{74}W_2O_{191}$, and Ta_2O_5. These compounds are stable phases in the Ta_2O_5-WO_3 system and have unit-cells which are based, respectively, on 13, 8, 19 and 11 UO_3-type subcell units. Metal atoms are either octahedrally coordinated to six oxygen atoms or else surrounded by seven oxygen atoms in the form of a pentagonal bipyramid.
On the basis of these structures a building-block scheme is developed which enables the *ideal*, or undistorted, structure to be predicted for any member of the hundreds of compounds which form a continuous series of structures in the region Ta_2O_5–$11Ta_2O_5 \cdot 4WO_3$. Anionic packing distortions occur in the *ideal* structures. In the *real* structures these distortions are minimized by a reduction in the coordination number of *some* seven-coordinated metal atoms. These atoms form distortion-sheets throughout the structure. The importance and distribution of these distortion-sheets is discussed.

Ruegg, F. C., Spijkerman, J. J., DeVoe, J. R., **A Mössbauer spectrometer for the structural analysis of materials,** *(Proc. Symp. Radioisotope Instruments in Industry and Geophysics, Warsaw, Poland, Oct. 18–22, 1965), Chapter in Radioisotope Instru-*

ments in Industry and Geophysics I, 325–335 (International Atomic Energy Agency, Vienna, Austria, May 1966).

Key words: Mössbauer; spectrometer; structural analysis; materials.

A Mössbauer Spectrometer has been designed to provide high precision Mössbauer spectra. The instrument uses two electromechanical transducers, one driver and one sensor, in a feedback loop which incorporates an operational amplifier and a power amplifier. The transducer system is coupled to the scaler input of a multichannel analyzer. A high degree of synchronization between the channel number (which represents units of velocity) and the actual velocity produced by the transducer is obtained by using the analogue voltage of the channel number as the input to the electromechanical system. By advancing sequentially the channel number as a linear function of time, a motion of constant acceleration is produced. Gamma rays from the radiation detector proportional counter or NaI(Tl) are then energy selected by a single channel pulse height analyzer and these pulses are presented to the multiscaler input. The spectrometer can be used to accept high counting rates by using a units scaler with a ten megahertz response.
The spectrometer can be used with a variety of auxiliary equipment such as to measure spectra at low temperature or high pressure.
The linearity of the spectrometer is found to be within ± 0.1% relative standard deviation with the use of voltage-to-frequency converter which is connected between the sensing transducer and the multiscaler input to the analyzer.
Some applications of the spectrometer for the analysis of materials will be discussed.

Schroeder, L. W., **Infrared and Raman spectra of $ClHCl^-$ and $BrHBr^-$ ions in $CsCl{\cdot}k/3H_3OHCl_2$ and $CsBr{\cdot}1/3H_3OHBr_2$,** *J. Chem. Phys.* **52,** *No. 4, 1972–1978 (Feb. 1970).*

Key words: $ClHCl^-$ ion; $BrHBr^-$ ion; environmental effects; infrared spectra; Raman spectra; symmetrical.

Infrared and Raman studies of $CsCl{\cdot}1/3H_3OHCl_2$ and $CsBr{\cdot}1/3HOHBr_2$ have been conducted in the 50 to 4000 cm^{-1} region. The spectra show the bands expected for the oxonium ion plus bands due to the XHX^- ion. The XHX^- ions are in a symmetrical environment and a consistent interpretation of the spectra suggests that the XHX^- ions have a centrosymmetric structure in these salts.

Sieck, L. W., Searles, S. K., Ausloos, P., **High-pressure photoionization mass spectrometry. I. Unimolecular and bimolecular reactions of $C_4H_8^+$ from cyclobutane,** *J. Am. Chem. Soc.* **91,** *No. 27, 7627–7634 (Dec. 31, 1969).*

Key words: Cyclobutane; ion-molecule reactions; mass spectrometry; photoionization; reaction kinetics; vapor phase.

Various mixtures of cyclobutane with cyclohexane, methylcyclopentane, 2-methylpentane, and cyclopentane have been selectively photolyzed at either 1236 Å (10.0 eV) or 1165 Å (10.6 eV) in a mass spectrometer designed to provide specific information concerning thermal ion-molecule reactions occurring in the gas phase. The modes of reaction, as well as the total reactivity found for $C_4H_8^+$ from cyclobutane in mixtures with the various hydrocarbons have been compared with those determined for $1-C_4H_8^+$ and $2-C_4H_8^+$ ions produced by photoionization of the appropriate butene at 10.0 eV. Evaluation of these data, including the charge exchange pattern for $C_4H_8^+$ established by the addition of compounds with various ionization potentials (NO, trimethylamine, cyclohexane, etc.), indicate the $C_4H_8^+$ ion from cyclobutane is non-cyclic and that the probability for isomerization to a $1-C_4H_8^+$ ion structure is approximately 0.2. The reaction cyclo-$C_6H_{12}^+ + \square \rightarrow C_6H_{12} + C_4H_8^+$, where cyclo-$C_6H_{12}^+$ is produced by photoionization of cyclohexane at 10.0 eV, has also been found. The interesting feature of this process is that charge exchange is exothermic only if $C_4H_8^+$ acquires a butene ion structure during the lifetime of the collision complex.

Simpson, J. A., **Electron impact spectroscopy,** *(Proc. 10th Symp. on Electron, Ion & Laser Beam Technology, Gaithersburg, Md., May 21–23, 1969), Chapter in Record of 10th Symposium, Electron, Ion, and Laser Beam Technology, L. Marton, ed., pp. 345–352 (San Francisco Press, San Francisco, Calif., 1969).*

Key words: Chemical analysis; electron impact spectrometer; uv absorption.

Recent developments in electron spectrometer design have made the application of inelastic electron scattering measurements to gas analysis competitive with other techniques. The energy distribution of electrons of an initially monoenergetic electron beam after an encounter with a gas target, the loss spectrum, contains the optical absorption spectrum of the gas. This absorption data extends from the extreme vacuum ultraviolet into the visible with an energy resolution comparable to a 1/2 meter optical grating spectrometer. Its response is linear with concentration over a very wide range and contains between 10^3 and 10^4 resolution widths. This spectrum by revealing the valence energy states of the gas is the most intrinsic possible "fingerprint" of the atom or molecule. An instrument has been built to explore the potentialities of this method. The instrument is described and its performance as a trace analyzer for air pollution studies discussed.

Snelleman, W., **The measurement and calculation of flame temperature,** *Chapter 7 in Flame Emission and Atomic Absorption Spectrometry I, 213–239 (Marcel Dekker, Inc., New York, N.Y., 1969).*

Key words: Equilibrium; flame-calculations; flame-composition; flame temperature; line-reversal.

The concept of thermo-dynamic equilibrium and temperature is briefly described and the deviations from this equilibrium that occur in actual flame gases are discussed. The various methods of measuring flame temperatures are considered, with special attention to the method of line-reversal as to systematic and random errors. Next a description is given of the calculation of flame temperatures (with some examples) and finally a comparison is made between calculated and measured flame temperatures.

Swartz, J. C., Swartzendruber, L. J., Bennett, L. H., Watson, R. E., **Nuclear magnetic resonance of ^{57}Fe in the paramagnetic alloys $TiFe_{1-x}Co_x$,** *Phys. Rev.* **1,** *No. 1, 146–152 (Jan. 1, 1970).*

Key words: Electronic structure; ^{57}Fe; Knight shift; nuclear magnetic resonance; nuclear moment; TiFe.

Nuclear magnetic resonances of ^{57}Fe in isotopically enirched specimens of TiFe and $TiFe_{0.8}Co_{0.2}$ are reported. The Knight shift of iron in TiFe is $+(1.29 \pm 0.02)\%$ at room temperature and $+(1.34 \pm 0.03)\%$ at 77 K and its estimated uncertainty. Similar values are obtained for iron in $TiFe_{0.8}Co_{0.2}$. These data supplement the NMR information on the pseudobinary series $TiFe_{1-x}Co_x$. Assuming the intrinsic paramagnetism of this series is essentially that reported by DeSavage and Goff, the NMR results on the three constituents of $TiFe_{1-x}Co_x$ suggest (1) *s–d* admixture in the wave function character at the Fermi surface for the (Fe, Co) sublattice, (2) greater *s* admixture at an iron site than at a cobalt site, and (3) a nuclear moment of cobalt closer to that of Freeman, Murray and Richards than to that more recently determined by Walstedt, Wernick and Jaccarino. Mössbauer effect results give $K = (0 \pm 1)\%$ for dilute Fe in Ti. NMR of Ti in TiCo and Fe in enriched $FeCl_3$ is also reported.

Venable, W. H., Jr., **Effects upon radiant intensity measurements due to scattering by optical elements,** *Appl. Opt.* **9,** *No. 3, 609–615 (Mar. 1970).*

Key words: Instrument function; iterative computation; nitrogen arc; radiance; radiant sources; scattering.

Measurements to determine the radiance of one portion of a nonuniform source can be strongly influenced by radiation from other portions of the source scattered by the optical system used to transmit the radiation to the detector. Conditions under which such scattering is important and procedures to correct for it are discussed. An illustration is provided from measurements made on a nitrogen arc source.

Wall, L. A., Flynn, J. H., Straus, S., **Rates of molecular vaporization of organic plasticizers,** *Polymer Eng. Sci.* **10,** *No. 1, 19–23 (Jan. 1970).*

Key words: Energy of vaporization; internal energies of vaporization; molecular vaporization; organic plasticizers; plasticizers; solubility parameters.

The kinetics of the molecular vaporaization process of 21 plasticizers were investigated in detail. By both isothermal and nonisothermal weight loss methods it was evident that 11 were quite pure single compounds while 10 were clearly mixtures of compounds. For the single component species internal energies, for vaporization and rates of volatilization are obtained from the kinetic data. The internal energies of vaporization are about ½ or less of values one can estimate from solubility parameters estimated by the additive factor method of Small. Thus solubility parameters based on our experimental energies of vaporization are low by about 30%. From this and other work on linear *n*-alkanes it is concluded that in the molecular vaporization process, the large organic molecules studied evaporate approximately as spheres and hence low values for the energy of vaporization are obtained. Consequently the difference between our experimental energy and that estimated from solubility parameters is the energy for extending the molecule in a vacuum environment.

Weiss, A. W., **Superposition of configurations and atomic oscillator strengths—boron isoelectronic sequence,** *Phys. Rev.* **188,** *No. 1, 119–130 (Dec. 5, 1969).*

Key words: Energy levels; oscillator strengths; superposition of configurations; wave functions.

Oscillator strengths have been computed for transitions between a number of low-lying levels in B I and Ne VI. The wavefunctions were computed by the method of superposition of configurations, utilizing the pseudonatural orbital technique to accelerate convergence. The asymptotic, large-Z limiting *f*-values were also computed, using the nuclear charge perturbation expansion. Together with previous theoretical data from C II, these results have been used to make a graphical study of the *f*-value behavior for these transitions along the isoelectronic sequence. Comparisons were made between experiment and the predictions of the Hartree-Fock and charge expansion methods as well as the present calculations. Finally these theoretical curves were used to predict individual *f*-values for each member of the sequence through $Z = 15$(P XI).

White, H. J., Jr., **Absorption of cationic surfactants by cellulosic substrates,** *Chapter 9 in Cationic Surfactants* **4,** *311–340 (Marcel Dekker, Inc., New York, N.Y., 1970).*

Key words: Absorption; adsorption; cationic surfactants; cellulosic materials; review.

The physical chemistry of the interaction of cationic surfactants with cellulosic substrates is reviewed.

Wiederhorn, S. M., Moses, R. L., Bean, B. L., **Plastic deformation and the fracture surface energy of sodium chloride,** *J. Am. Ceram. Soc.* **53,** *No. 1, 18–23 (Jan. 21, 1970).*

Key words: Cleavage; fracture; fracture energy; plastic deformation; sodium chloride; surface energy.

This paper presents a correlation between plastic deformation at crack tips in sodium chloride and the measured value of the fracture surface energy. It is shown that plastic deformation can either aid or hinder crack growth depending on the mode of deformation at the crack tip. If plane stress deformation occurs, crack motion is hindered by step formation, dislocation generation and plastic blunting of the crack tip. If plane strain deformation occurs, crack motion is aided by stress fields that arise from the deformation. The specific surface free energy of sodium chloride, {100} plane, is estimated to lie between 0.3 and 0.37 J/m².

Wims, A. M., Sengers, J. V., McIntyre, D., Shereshefsky, J., **Interfacial tension of 3-methylpentane-nitroethane near the critical point,** *J. Chem. Phys.* **52,** *No. 6, 3042–3049 (Mar. 15, 1970).*

Key words: Binary liquid mixtures; capillary rise; coexistence curve; critical phenomena; 3-methylpentane; nitroethane; surface tension.

Experimental data are reported for the capillary rise of the interface between the two liquid phases of 3-methylpentane-nitroethane as a function of temperature. The data are interpreted in terms of a power law currently proposed for the behavior of the interfacial tension near the critical point. The results seem to indicate that for 3-methylpentane-nitroethane the region of asymptotic behavior is limited to rather small values of $\Delta T^* = (T_c - T)/T_c$. For $\Delta T^* \geq 10^{-2}$ Sugden's parameter a^2 can be represented by a power law $a^2 = A^2 \Delta T^{*\varphi}$ with a classical value $\varphi = 1.00 \pm 0.01$ over an appreciable temperature range. A comparison is made with the behavior of the surface tension of simple one-component liquids near the gas-liquid critical point.

Young, K. F., Frederikse, H. P. R., **Temperature and pressure dependence of dielectric constant of cadmium fluoride,** *J. Appl. Phys.* **40,** *No. 8, 3115–3118 (July 1969).*

Key words: Cadmium fluoride; dielectric constant; pressure dependence; temperature dependence.

The temperature and pressure dependence of the dielectric constant ϵ' of CdF_2 has been measured for $T = 4$–300 K (at atmospheric pressure) and $P = 1$–2000 bar (at room temperature). The frequency dependence of the real and imaginary part (ϵ' and ϵ'') has been investigated up to 100 MHz.

Other NBS Publications

J. Res. Nat. Bur. Stand. (U.S.), 74B (Math. Sci.), No. 3 (July–Sept. 1970), SD Catalog No. C13.22/sec. B:74/3.

Hecke basis theorems for groups of genus O. M. I. Knopp and J. R. Smart.
The distribution of eigenvalues of covariance matrices of residuals in analysis of variance. J. Mandel.
Expansions with coefficient algorithms for time domain responses of skin effect lossy coaxial cables. R. D. Holt.
Derivatives of the Grüneisen and Einstein functions, A. Cezairliyan.
Selecting nonlinear transformations for the evaluation of improper integrals. T. A. Atchison.
On the spheroidal functions. D. R. Rhodes.
Automatic computing methods for special functions. I. A. Stegun and R. Zucker.
Publications of the National Bureau of Standards.

J. Res. Nat. Bur. Stand. (U.S.), 74C (Engr. and Instr.), Nos. 1 and 2 (Jan.–June 1970), SD Catalog No. C13.22/sec. C:74/1 & 2.

Production of near-perfect interferograms of variable visibility. J. B. Saunders.
Locked nuclear quadrupole resonance spectrometer for pressure measurements. R. C. Frisch and D. L. VanderHart.
Precise continuous optical attenuator. G. Ruffino.
An A–C resistance thermometer bridge. R. D. Cutkosky.
On the flow induced by a Maxwell-Chartoff rheometer. E. A. Kearsley.
Mechanical compliance measurements of single-edge-notch tension specimens. M. J. Orloski.
Effect of notch geometry and temperature on the creep-rupture behavior of a titanium alloy. W. D. Jenkins and W. A. Willard.
Publications of the National Bureau of Standards.

Adams, J. W., Jarvis, S., Jr., Current distribution in barretters and its application to microwave power measurements, IEEE Trans. Micro. Theory Tech. **MTT-17,** No. 10, 778–785 (Oct. 1969).
Baker, M. A., 1964 exposure test of porcelain enamels on alunimum three year inspection, Nat. Bur. Stand. (U.S.), Bldg. Sci. Ser. **29,** 13 pages (Apr. 1970), 25 cents, SD Catalog No. C13.29/2:29.
Balcom, M. M., Influence of red and blue pre-adaptation on hue matching of purple samples, J. Opt. Soc. Am. **60,** No. 1, 118–121 (Jan. 1970).
Ballard, D. B., Yakowitz, H., Investigation of secondary cracks from the failed Point Pleasant, West Virginia, Bridge, Proc. Third Annual Scanning Electron Microscope Symp., April 1970, pp. 321–328 (Illinois Institute of Technology, Research Institute, Chicago, Illinois, 1970).

Bennett, L. H., Comments on "Fe and Ni hyperfine fields in Ni_3Fe," Phys. Rev. **188,** No. 2, 1048 (Dec. 10, 1969).

Berger, M. J., Seltzer, S. M., Penetration of electrons and associated bremsstrahlung through aluminum targets, Chapter in Protection Against Space Radiation, NASA SP–169, pp. 285–322 (National Aeronautics and Space Administration, Greenbelt, Md., 1968).

Birky, M. M., Simultaneous recording of near-field and far-field patterns of lasers, Appl. Opt. **8,** No. 11, 2249–2253 (Nov. 1969).

Blake, R. W., Language of performance, an NBS project, Mater. Res. Std. **9,** No. 3, 11–14 (Mar. 1969).

Bowman, R. R., Quantifying hazardous electromagnetic fields: practical considerations, Nat. Bur. Stand. (U.S.), Tech. Note 389, 15 pages (Apr. 1970), 30 cents, SD Catalog No. C13.46:389.

Brady, E. L., The National Standard Reference Data System, Mater. Res. Std. **9,** No. 10, 19–21 (Oct. 1969).

Branscomb, L. M., Truth in packaging of scientific information, Meas. Data **3,** No. 5, 104–105 (Sept.–Oct. 1969).

Brauer, G. M., Termini, D. J., Burns, C. L., Characterization of components of dental materials and components of tooth structure by differential thermal analysis, J. Dental Res. **49,** No. 1, 100–110 (Feb. 1970).

Bullis, W. M., Editor, Methods of measurement for semiconductor materials, process control, and devices, Quarterly Report October 1 to December 31, 1969, Nat. Bur. Stand. (U.S.), Tech. Note 527, 60 pages (May 1970) 60 cents, SD Catalog No. C13.46:527.

Coyle, T. D., Silica, Kirk-Othmer Encyclopedia of Chemical Technology, 2d Ed., **18,** 46–61 (1969).

Currie, L. A., Indirect estimation of component variability in chemical and physical systems, Anal. Chem. **41,** No. 14, 2051–2054 (Dec. 1969).

Cuthill, J. R., A soft X-ray spectrometer with improved drive, Rev. Sci. Instr. **41,** No. 3, 422–423 (Mar. 1970).

Diamond, J. J., Editor, Bibliography on the high temperature chemistry and physics of materials. October, November, December 1969, Nat. Bur. Stand. (U.S.), Spec. Publ. 315–4, 85 pages (Jan. 1970), 75 cents, SD Catalog No. C13.10:315–4.

Diamond, J. J., Editor, Bibliography on the high temperature chemistry and physics of materials, January, Feburary, March 1970, Nat. Bur. Stand. (U.S.), Spec. Publ. 315–5, 82 pages (Apr. 1970) 75 cents, SD Catalog No. C13.10:315–5.

DiMarzio, E. A., Guttman, C. M., Separation by flow, Macromolecules **3,** No. 2, 131–146 (Mar.–Apr. 1970).

Durst, R. A., Fluoride microelectrode–fabrication and characteristics, Anal. Chem. **41,** No. 14, 2089–2090 (Dec. 1969).

Ederer, D. L., Computer analysis of resonance profiles by the method of least squares, Appl. Opt. **8,** No. 11, 2315–2325 (Nov. 1969).

Eick, J. D., Caul, H. J., Hegdahl, T., Dickson, G., Chemical composition of dental gold casting alloy and dental wrought gold alloys, J. Dental Res. **48,** No. 6, 1284–1289 (Nov.–Dec. 1969).

Eisele, J. W., Types and sizes of forms for one-way concrete joist construction, Nat. Bur. Stand. (U.S.), Prod. Stand. 16–69, 16 pages (June 1970), 10 cents, SD Catalog No. C13.20/2:16–69.

Eisenhart, C., Anniversaries in 1970 of interest to statisticians, Am. Stat. **24,** No. 1, 25–68 (Feb. 1970).

Engen, G. F., An evaluation of the "back-to-back" method of measuring adaptor efficiency, IEEE Trans. Instr. Meas. **IM–19,** No. 1, 18–22 (Feb. 1970).

Evenson, K. M., Wells, J. S., Matarrese, L. M., Absolute frequency measurements of the CO_2 cw laser at 28 THz (10.6 μm), Appl. Phys. Letters **16,** No. 6, 251–253 (Mar. 15, 1970).

Faison, T. K., Jr., Davis, J. C., Achenbach, P. R., Performance of louvered devices as air mixers, Nat. Bur. Stand. (U.S.), Bldg. Sci. Ser. 27, 22 pages (Mar. 1970) 30 cents, SD Catalog No. C13.29/2:27.

Fatiadi, A. J., Conversion of certain cyclic phenylhydrazino derivatives into phenylazo compounds with periodic acid, J. Org. Chem. **35,** No. 3, 831–833 (Mar. 1970).

Fatiadi, A. J., Preparation of inositol hexasulfate, Carbohydrate Res. **12,** 293–296 (1970).

Feldman, A., Horowitz, D., Refractive index of cuprous chloride, J. Opt. Soc. Am. **59,** No. 11, 1406–1408 (Nov. 1969).

The Flammable Fabrics Program, 1968–1969. U.S. Department of Commerce report of activities under the Flammable Fabrics Act, 1968–1969, Nat. Bur. Stand. (U.S.), Tech. Note 525, 84 pages (Apr. 1970), 75 cents, SD Catalog No. C13.46:525.

Franklin, A. D., Bennett, H. S., Editors, ARPA–NBS program of research on high temperature materials and laser materials. Reporting period January 1 to June 30, 1969, Nat. Bur. Stand. (U.S.), Tech. Note 514, 98 pages (Jan. 1970), $1.00, SD Catalog No. C13.46:514.

Freeman, D. H., Currie, L. A., Kuehner, E. C., Dixon, H. D., Paulson, R. A., Development and characterization of ion-exchange bead microstandards, Anal. Chem. **42,** No. 2, 203–209 (Feb. 1970).

Gadzuk, J. W., Resonance tunneling through impurity states in metal-insulator-metal junctions, J. Appl. Phys. **41,** No. 1, 286–291 (Jan. 1970).

Graminski, E. L., The stress-strain behavior of accelerated and naturally aged papers, Tappi **53,** No. 3, 406–410 (Mar. 1970).

Green, J. A. S., Mengelberg, H. D., Yolken, H. T., Oxide growth on copper and alpha-brasses in aqueous ammonia, J. Electrochem. Soc. **117,** No. 4, 433–437 (Apr. 1970).

Greenfeld, S. H., Warner, E. R., Reinhart, H. W., Bibliographies on fabric flammability. Part 1. Wearing apparel; Part 2. Fabrics used on beds; Part 3. Carpets and rugs, Nat. Bur. Stand. (U.S.), Tech. Note 498, 36 pages (Feb. 1970), 40 cents, SD Catalog No. C13.46:498.

Gross, D., Natrella, M. G., Interlaboratory comparison of the potential heat method, Am. Soc. Testing Mater. Spec. Tech. Pulb. 464, Fire Test Performance, pp. 127–152 (1970).

Haber, S., Sequences of numbers that are approximately completely equidistributed, J. Assoc. Computing Mach. **17,** No. 2, 269–272 (Apr. 1970).

Handy, L. B., Brinckman, F. E., Chemistry of the methoxyfluorotungsten (VI) series, Chem. Commun. pp. 214–215 (1970).

Harvey, J. L., Brenner, F. C., Tire use survey. The physical condition, use, and performance of passenger car tires in the United States of America, Nat. Bur. Stand. (U.S.), Tech. Note 528, 59 pages (May 1970), 60 cents, SD Catalog No. C13.46:528.

Heinrich, K. F. J., Fiori, C., Yakowitz, H., Image-formation technique for scanning electron microscopy and electron probe microanalysis, Science **167,** 1129–1131 (Feb. 20, 1970).

Horn, W. A., Optimal networks joining in points in the plane (Proc. IVth International Symp. The Theory of Traffic Flow, Karlsruhe, Germany, June 18–20, 1968), Chapter in Strassenbau und Strassenverkehrstechnik 86, W. Leutzbach and P. Baron, Ed., pp. 160–166 (Bundesminister fur Verkehr, Germany, 1969).

Hummer, D. G., Observatory Report–Joint Institute for Laboratory Astrophysics of the National Bureau of Standards and the University of Colorado, Bull, Am. Astron. Soc. **2,** No. 1, 59–65 (1970).

Ireland, C. T., Ku, H. H., Kullback, S., Symmetry and marginal homogeneity of an $r \times r$ contingency table, J. Am. Statist. Assoc. **64,** 1323–1341 (Dec. 1969).

Jones, M. C., Far infrared absorption in liquefied gases, Nat. Bur. Stand. (U.S.), Tech. Note 390, 39 pages (April 1970), 50 cents, SD Catalog No. C13:46:390.

Jones, R. N., Huntley, L. E., A precision, high frequency calibration facility for coaxial capacitance standards, Nat. Bur. Stand. (U.S.), Tech. Note 386, 27 pages (March 1970), 35 cents, SD Catalog No. C13.46:386.

Kilgore, S. B., Electronic circuit breaker for motor load protection, Rev. Sci. Instr. **41,** No. 1, 40–41 (Jan. 1970).

Kose, V. E., Sullivan, D. B., Influence of external noise on microwave-induced Josephson steps, J. Appl. Phys. **41,** No. 1, 169–174 (Jan. 1970).

Kostkowski, H. J., Erminy, D. C., Hattenburg, A. T., High-accuracy spectral radiance calibration of tungsten-strip lamps, Chapter 4 in Advances in Geophysics **14,** 111–127 (Academic Press, Inc., New York, N.Y., 1970).

Kuriyama, M., The dynamical scattering amplitude of an imperfect crystal, Acta Cryst. **A26,** No. 6, 56–59 (Jan. 1970).

Kushner, L. M., Are there standards? (Proc. National Safety Congress Conf., Chicago, Ill., Oct. 28, 1969), National Safety Congress Trans,, Civic Leadership **6,** 12–16 (1969).

Larson, W., Desch, R. F., Gillard, B. F., Further analysis of the off-null versus power ratio method of attenuation measurement, IEEE Trans. Microwave Theory Tech. **MTT–18,** No. 2, 112–113 (Feb. 1970).

Latanision, R. M., On the dislocation distribution near the surface of lightly deformed copper single crystals, Scripta Met. **3,** No. 7, 465–470 (July 1969).

Lawton, R. A., Allred, C. M., Hudson, P. A., A wide-range CW measurement technique, IEEE Trans. Instr. Meas. **IM–19,** No. 1, 28–34 (Feb. 1970).

Lutz, G. J., Editor, Determination of the light elements in metals: A bibliography of activation analysis papers, Nat. Bur. Stand.

(U.S.), Tech. Note 524, 66 pages (May 1970), 75 cents, SD Catalog No. C13.46:524.

Lutz, G. J., Determination of oxygen in sodium by photon activation analysis, Anal. Chem. **42,** No. 4, 531–532 (Apr. 1970).

Lutz, G. J., Editor, Forensic science: A bibliography of activation analysis papers, Nat. Bur. Stand. (U.S.), Tech. Note 519, 47 pages (Mar. 1970), 50 cents, SD Catalog No. C13.46:519.

Lutz, G. J., Boreni, R. J., Maddock, R. S., Meinke, W. W., Editors, Activation Analysis: A bibliography, Nat. Bur. Stand. (U.S.), Tech. Note 467, Part 1, Addendum 1, 176 pages (Dec. 1969) and Part 2, Appendices, Revision 1, Nat. Bur. Stand. (U.S.), Tech. Note 467, 264 pages (Dec. 1969), $8.50 per set of 3 volumes, sold in sets only. Part 1 of September 1968 accompanies these sets, SD Catalog No. C13.46:467.

McCrackin, F. L., Analyses and corrections of instrumental errors in ellipsometry, J. Opt. Soc. Am. **60,** No. 1, 57–63 (Jan. 1970).

McLaughlin, W. L., Photographic film dosimeters, Chapter in Manual on Radiation Dosimetry, N. W. Holm and R. J. Berry, Ed., pp. 387–394 (Marcel Dekker, Inc., New York, N.Y., 1970).

McLaughlin, W. L., Radiochromic dye-cyanide dosimeters, Chapter in Manual on Radiation Dosimetry, N. W. Holm and R. J. Berry, Ed., pp. 377–385 (Marcel Dekker, Inc., New York, N.Y., 1970). 1970).

McLaughlin, W. L., Hussmann, E. K., The measurement of electron and gamma-ray dose distributions in various media (Proc. Symp. Utilization of Large Radiation Sources and Accelerators in Industrial Processing, Munich, Germany, Aug. 18–22, 1969), Chapter in Large Radiation Sources for Industrial Processes, IAEA–SM–123/43, pp. 579–590 (International Atomic Energy Agency, Vienna, Austria, 1969).

Mackay, D. R., American Softwood Lumber Standard, Nat. Bur. Stand. (U.S.), Prod. Stand. 20–70, 26 pages (Jan. 1970), 35 cents, SD Catalog No. C13.20/2:20–70.

Mahler, R. J., Nominal $\Delta m = \pm 1, 2, 3, 4, 5$ magnetic nuclear transition probabilities in ruby, Phys. Rev. **188,** No. 2, 584–590 (Dec. 1969).

Messina, C. G., Hilsenrath, J., Edit-insertion programs for automatic typesetting of computer printout, Nat. Bur. Stand. (U.S.), Tech. Note 500, 50 pages (Apr. 1970), 60 cents, SD Catalog No. C13.46:500.

Meyerson, M. R., Friedman, L., Giles, P. M., Dimensional stability of a 12% nickel maraging steel at ambient temperatures, Trans. ASM **62,** No. 3, 809–812 (Sept. 1969).

Miles, B. M., Wiese, W. L., Bibliography on atomic transition probabilities, January 1916 through June 1969, Nat. Bur. Stand. (U.S.), Spec. Publ. 320, 111 pages (Feb. 1970) (Supersedes NBS Misc. Publ. 278 and Supplement), $1.25, SD Catalog No. C13.10:320.

Mosburg, E. R., Jr., A new probe configuration for plasma diagnostics, J. Appl. Phys. **40,** No. 13, 5290–5300 (Dec. 1969).-

Mosburg, E. R., Jr., Periodic potential probe configuration for plasma diagnostics, J. Appl. Phys. **40,** No. 13, 5290–5300 (Dec. 1969).

Mozer, B., Price, D. L., Keating, D. T., Meister, H., Incoherent neutron scattering from liquid and solid CuNi, Physics Letters **30A,** No. 3, 206–207 (Oct. 6, 1969).

Nargolwalla, S. S., Crambes, M. R., Suddueth, J. E., Photon self-adsorption corrections for the minimization of systematic errors in 14-MeV neutron activation analysis, Anal. Chim. Acta. **49,** No. 3, 425–436 (Mar. 1970).

Newman, M., Isometric circles of congruence groups, Am. J. Math. **XCI,** No. 3, 648–656 (July 1969).

Newman, M., A table of the first factor for prime cyclotomic fields, Math. Compt. **24,** No. 109, 215–219 (Jan. 1970).

Ohashi, M., Paffenbarger, G. C., Some flow characteristics at 37 °C of ternary wax mixtures that may have possible dental uses, J. Nihon Univ. School Dentistry **11,** No. 3, 109–208 (Sept. 1969).

Paabo, M., Bates, R. G., Deuterium isotope effects and the dissociation of deuteriophosphoric acid from 5 to 50°, J. Phys. Chem. **74,** No. 4, 706–710 (Feb. 19, 1970).

Philo, H. A., Technical Standards Coordinator, Polyethylene (PE) plastic pipe (SDR), Nat. Bur. Stand. (U.S.), Prod. Stand. 11–69, 14 pages (Mar. 1970), 15 cents, SD Catalog No. C13.20/2:11–69. (Supersedes Commercial Standard CS 255–63.)

Philo, H. A., Technical Standards Coordinator, Polyethylene (PE) plastic pipe (schedule 40—inside diameter dimensions), Nat. Bur. Stand. (U.S.), Prod. Stand. 10–69, 14 pages (Mar. 1970), 15 cents. SD Catalog. No. C13.20/2:10–69. (Supersedes Commercial Standard CS 197–60.)

Philo, H. A., Technical Standards Coordinator, Polyethylene (PE) plastic pipe (schedules 40 and 80—outside diameter dimensions), Nat. Bur. Stand. (U.S.), Prod. Stand. 12–69, 14 pages (Mar. 1970), 15 cents, SD Catalog No. C13.20/2:12–69.

Photonuclear data index, January 1965 through January 1970, Nat. Bur. Stand. (U.S.), Spec. Publ. 322, 86 pages (May 1970), 75 cents, SD Catalog No. C13.10:322 (Supersedes Supplement 1 to Miscellaneous Publication 277).

Pizer, R. S., Spinner, S., An apparatus for determining the actual footprint area of tires, Mater. Res. Std. **10,** No. 2, 20–23 (Feb. 1970).

Potzick, J., Low-frequency sine-wave oscillator, EEE **18,** No. 3, 130 (Mactier Publishing Corp., Mar. 1970).

Reader, J., Epstein, G. L., Revised $4p^5\ {}^2P^\circ_{1/2,3/2}$ splitting of Yv, J. Opt. Soc. Am. **60,** No. 1, 140 (Jan. 1970).

Romanoff, M., Corrosion evaluation of steel test piles exposed to permafrost soils, Proc. National Association of Corrosion Engineers 25th Conf., Houston, Texas, March 10–14, 1969, pp. 6–13 (National Association of Corrosion Engineers, Houston, Texas, 1970).

Romanoff, M., Performance of steel pilings in soils, Proc. National Assoc. of Corrosion Engineers 25th Conf., Houston, Texas, March 10–14, 1969, pp. 14–22 (National Association of Corrosion Engineers, Houston, Texas, 1970).

Santoro, A., Mighell, A. D., Determination of reduced cells, Acta. Cryst. **A26,** No. 6, 124–127 (Jan. 1970).

Schwerdtfeger, W. J., Corrosion rates of metals, alloys, and galvanic couples as measured by polarization techniques, Mater. Res. Std. **10,** No. 3, 22–28 (Mar. 1970).

Screw-thread standards for federal services. Part I. Unified UNJ unified miniature screw threads, Nat. Bur. Stand. (U.S.), Handb. 28, 237 pages (Dec. 1969), $2.00, SD Catalog No. C13.11:28. (Superseding H28 (1957) Part I and that applicable to Part I in the 1963 Supplement to H28.)

Shields, W. R., Editor, Analytical Mass Spectrometry Section: Summary of activities July 1968 to June 1969, Nat. Bur. Stand. (U.S.), Tech. Note 506, 55 pages (May 1970), 55 cents, SD Catalog No. C13.46:506.

Skolnik, H., Tauber, S. J., Introduction to the symposium on management and operation of information groups and centers, J. Chem. Doc. **9,** No. 4, 195 (Nov. 1969).

Snediker, D. K., The Mossbauer effect of Sn^{119} in palladium-rich palladium–tin solid solutions (Proc. 2d Symp. Mossbauer Effect Methodology, New York, N.Y., Jan. 25, 1966), Chapter in Mossbauer Effect Methodology **2,** 161–170 (Jan. 1966).

Snelleman, W., Menis, O., Rains, T. C., Yee, K. W., Cook, H. D., Flame emission spectrometry with repetitive optical scanning in the derivative mode, Anal. Chem. **42,** No. 3, 394–398 (Mar. 1970).

Stevens, M. E., Automatic indexing: A state-of-the-art report, Nat. Bur. Stand. (U.S.), Monogr. 91, 290 pages (Mar. 1970), $2.25, SD Catalog No. C13.44:91. (Reissued with additions and corrections February 1970).

Stevens, M. E., Research and development in the computer and information sciences. 1. Information acquisition, sensing, and input: A selective literature review, Nat. Bur. Stand. (U.S.), Monogr. 113 Vol. 1, 170 pages (Mar. 1970), $1.50, SD Catalog No. C13.44:113/Vol. 1.

Stevens, M. E., Research and development in the computer and information sciences. 2. Processing, storage, and output requirements in information processing systems: A selective literature review, Nat. Bur. Stand. (U.S.) Monogr. 113 Vol. 2, 125 pages (May 1970), $1.25, SD Catalog No. C13.44:113/Vol. 2.

Swiggard, E. M., Clabaugh, W. S., Preparation of barium titanate semiconductors containing controlled amounts of neodymium, Am. Ceram. Soc. Bull. **45,** No. 9, 777–781 (Sept. 1966).

Technical Highlights of the National Bureau of Standards, Annual Report, Fiscal Year 1969, Nat. Bur. Stand. (U.S.), Spec. Publ. 325, 243 pages (Mar. 1970), SD Catalog No. C13.10:325.

Tighe, N. J., Kreglo, J. R., Jr., Electron microscopy of periclase brick, J. Am. Ceram. Soc. **49,** No. 2, 188–192 (Feb. 7, 1970).

Utech, H. P., Growing crystals in space, Proc. Conf. Manufacturing Technology Unique to Zero Gravity Environment, George C. Marshall Space Flight Center, Nov. 1, 1968, Huntsville, Alabama, pp. 197–214 (National Aeronautics and Space Administration, Greenbelt, Md., 1969).

Waclawski, B. J., Hughey, L. R., Adsorption of water vapor on polycrystalline tungsten, Surface Sci. **19,** 464–468 (1970).

Wacker, P. F., Quantifying hazardous microwave fields: Analysis, Nat. Bur. Stand. (U.S.), Tech. Note 391, 19 pages (Apr. 1970), 30 cents, SD Catalog No. C13.46:391.

Wells, J. S., Evenson, K. M., A new LEPR spectrometer, Rev. Sci. Instr. **41,** No. 2, 226–227 (Feb. 1970).

West, E. D., Jennings, D. A., Power measurement of large laser beams with a small dual-cone calorimeter, Rev. Sci. Instr. **41,** No. 1, 142 (Jan. 1970).

Wilson, W. K., Discussion of paper "New Approaches to Preservation," by Richard D. Smith, Library Quart. **40,** No. 1, 171–175 (Jan. 1970).

Wilson, W. K., Record papers and their preservation, Chemistry **43,** No. 3, 8–12 (Mar. 1970).

**Publications for which a price is indicated are available by purchase from the Superintendent of Documents, U.S. Government Printing Office, Washington, D.C. 20402 (foreign postage, one-fourth additional). The NBS non-periodical series are also available from the Clearinghouse for Federal Scientific and Technical Information, Springfield, Va. 22151. Reprints from outside journals and the NBS Journal of Research may often by obtained directly from the authors.*

U. S. GOVERNMENT PRINTING OFFICE : 1970 OL - 389-821

JnrnA OCT 46129
UNIVERSITY MICROFILMS INC
ATTN SERIALS SECTION
300 NORTH ZEEB RD
ANN ARBOR MICH 48106

UNITED STATES
GOVERNMENT PRINTING
DIVISION OF PUBLIC DOCUMENTS
WASHINGTON, D.C. 20402

OFFICIAL BUSINESS
PENALTY FOR PRIVATE USE, $300

POSTAGE AND FEES PAID
U.S GOVERNMENT PRINTING OFFICE

JOURNAL OF RESEARCH of the National Bureau of Standards
A. Physics and Chemistry

Vol. 74A, No. 5 Sept.–Oct. 1970

Contents

Page

Heat capacity and thermodynamic properties of α-beryllium nitride, Be_3N_2, from 20 to 315 K. George T. Furukawa and Martin L. Reilly. 617

Heat capacity and thermodynamic properties of lithium hexafluoroaluminate, Li_3AlF_6, from 15 to 380 K. George T. Furukawa, William G. Saba, and James C. Ford. 631

Thermodynamics of hydrochloric acid in 80 weight percent 2-methoxyethanol and 20 weight percent water from 10 to 50 °C. Harry P. Thun, Bert R. Staples, and Roger G. Bates. 641

Vapor pressure and heat of sublimation of platinum. E. R. Plante, A. B. Sessoms, and K. R. Fitch. 647

Thermophysical properties of methane: Virial coefficients, vapor and melting pressures. Robert D. Goodwin. 655

Specific heats, C_v, of compressed liquid and gaseous fluorine. Rolf Prydz and Robert D. Goodwin. 661

Acidic dissociation of diprotonated piperazine in methanol-water solvents from 10 to 40 °C. Maya Paabo and Roger G. Bates. 667

Thermal conductivity standard reference materials from 4 to 300 K. I. Armco iron: Including apparatus description and error analysis. J. G. Hust, Robert L. Powell, and D. H. Weitzel. 673

Mössbauer spectrometer calibration using TiFe. L. J. Swartzendruber and L. H. Bennett. 691

Energies of $1snl$ ($l \geq 3$) configurations in He^4 I as calculated from polarization theory. W. C. Martin. 699

A theoretical investigation of the configurations $(3d+4s)^6 4p$ in neutral cobalt (Co I). Charles Roth. 703

Odd configurations in neutral nickel (Ni I). Charles Roth. 711

Electron-spin resonance study of an alkaline solution of copper (II) oxalate–*meso*-tartrate complex (the Somogyi reagent) and related complexes. Alexander J. Fatiadi. 723

Publications of the National Bureau of Standards. 733

Library of Congress Catalog Card Number: 62–37059

For sale by the Superintendent of Documents, U.S. Government Printing Office, Washington, D.C. 20402. (Order by SD Catalog No. C 13.22/sec.A:74/5). Single copy price varies. This issue $1.75. Subscription price $9.50 a year; $2.25 additional for foreign mailing.

UNITED STATES GOVERNMENT PRINTING OFFICE, WASHINGTON : 1970

KUM